# Novel System Approach for a mm-range Precision Indoor Positioning System

# Neuartiger Systemansatz für ein Innenpositionierungssystem mit Präzision im mm-Bereich

vom
Fachbereich Elektrotechnik und Informationstechnik
der Technischen Universität Kaiserslautern
zur Verleihung des akademischen Grades eines

**Doktor der Ingenieurwissenschaften (Dr. -Ing.)**

genehmigte Dissertation

von
M. Sc. Renhai Xiong
geb. in FUJIAN (Volksrepublik China)

**D 386**

Tag der mündlichen Prüfung : 04.11.2020
Dekan des Fachbereichs: Prof. Dr.-Ing. Ralph Urbansky

Promotionskommission
Vorsitzender: Prof. Dr.-Ing. N. Wehn
Besichterstattende: Prof. Dr.-Ing. Steven Liu
Prof. Dr.-Ing. Stefan van Waasen

# Acknowledgements

# ABSTRACT

Indoor positioning system (IPS) is becoming more and more popular in recent years in industrial, scientific and medical areas. The rapidly growing demand of accurate position information attracts much attention and effort in developing various kinds of positioning systems that are characterized by parameters like accuracy, robustness, latency, cost, etc. These systems have been successfully used in many applications such as automation in manufacturing, patient tracking in hospital, action detection for human-machine interacting and so on.

The different performance requirements in various applications lead to existence of greatly diverse technologies, which can be categorized into two groups: inertial positioning (involving momentum sensors embedded on the object device to be located) and external sensing (geometry estimation based on signal measurement). In positioning systems based on external sensing, the input signal used for locating refers to many sources, such as visual or infrared signal in optical methods, sound or ultra-sound in acoustic methods and radio frequency based methods.

This dissertation gives a recapitulative survey of a number of existence popular solutions for indoor positioning systems. Basic principles of individual technologies are demonstrated and discussed. By comparing the performances like accuracy, robustness, cost, etc., a comprehensive review of the properties of each technologies is presented, which concludes a guidance for designing a location sensing systems for indoor applications. This thesis will lately focus on presenting the development of a high precision IPS prototype system based on RF signal from the concept aspect to the implementation up to evaluation. Developing phases related to this work include positioning scenario, involved technologies, hardware development, algorithms development, firmware generation, prototype evaluation, etc..

The developed prototype is a narrow band RF system, and it is suitable for a flexible frequency selection in UHF (300MHz~3GHz) and SHF (3GHz~30GHz) bands, enabling this technology to meet broad service preferences. The fundamental of the proposed system classified itself as a hyperbolic position fix system, which estimates a location by solving non-linear equations derived from time difference of arrival (TDoA) measurements. As the positioning accuracy largely depends on the temporal resolution of the signal acquisition, a dedicated RF front-end system is developed to achieve a time resolution in range of multiple pico seconds down to less than 1 pico second. On the algorithms aspect, two processing units: TDoA estimator and the Hyperbolic equations solver construct the digital signal processing system. In order to implement a real-time positioning system, the processing system is implemented on a FPGA platform. Corresponding firmware is generated from the algorithms modeled in MATLAB/Simulink, using the high level synthesis (HLS) tool HDL Coder. The prototype system is evaluated and an accuracy of better than 1 cm is achieved. A better performance is potential feasible by manipulating some of the controlling conditions such as ADC sampling rate, ADC resolution, interpolation process, higher frequency, more stable antenna, etc. Although the proposed system is initially dedicated to indoor applications, it could also be a competitive candidate for an outdoor positioning service.

# KURZFASSUNG

Indoor-Positionierungssysteme (IPS) erfreuen sich in den letzten Jahren steigender Beliebtheit in industriellen, wissenschaftlichen und medizinischen Bereichen. Die schnell wachsende Nachfrage nach genauen Positionsinformationen generiert viel Aufmerksamkeit und treibt die Entwicklung verschiedener Arten von Positionierungssystemen voran, die durch Parameter wie Genauigkeit, Robustheit, Latenz, Kosten, usw. gekennzeichnet sind. Diese Systeme wurden erfolgreich in vielen Anwendungen eingesetzt, wie z.B.: Automatisierung in der Fertigung, Patientenverfolgung im Krankenhaus, Handlungserkennung für Mensch-Maschine-Interaktion und so weiter.

Die unterschiedlichen Leistungsanforderungen in verschiedenen Anwendungen führen zu bestehenden, vielfältigen Technologien, die in zwei Gruppen eingeteilt werden können: Inertialpositionierung (mit Beschleunigungs-Sensoren, die auf dem zu lokalisierenden Objektgerät eingebaut sind) und externe Erfassung (Geometrie-Schätzung basierend auf Signalmessung). In Positionssystemen, die auf der externen Erfassung basieren, bezieht sich das Eingangssignal, das für die Lokalisierung verwendet wird, auf viele Modalitäten, wie z. B. visuelles oder infrarotes Signal in optischen Methoden, Ton oder Ultraschall in akustischen Methoden und hochfrequenzbasierte Verfahren.

Diese Dissertation gibt einen rekapitulativen Überblick über eine Reihe von bestehenden populären Lösungen für Indoor-Positionierungssysteme. Grundprinzipien einzelner Technologien werden demonstriert und diskutiert. Durch den Vergleich von Kennwerten in den Bereichen Genauigkeit, Robustheit, Kosten usw., wird eine umfassende Überprüfung der Eigenschaften der einzelnen Technologien vorgestellt, die eine Anleitung zur Gestaltung eines Standortmesssystems für Innenanwendungen abschließt. Im zweiten Teil dieser Dissertation wird die Entwicklung eines hochpräzisen IPS-Prototyp-Systems auf der Grundlage von HF-Signalen von der Konzeptphase bis hin zur Umsetzung vorgestellt. Die Entwicklungsphasen im Zuge dieser Arbeit umfassen: Positionierungsszenario, beteiligte Technologien, Hardware-Entwicklung, Algorithmen-Entwicklung, Firmware-Generierung, Prototyp-Bewertung, usw.

Der entwickelte Prototyp ist ein Schmalband-RF-System und eignet sich für eine flexible Frequenzauswahl in UHF (300MHz $\sim$ 3GHz) und SHF (3GHz $\sim$ 30GHz) -Bändern, so dass diese Technologie breite Service-Anforderungen erfüllen kann. Die Grundlagen des vorgeschlagenen Systems klassifizieren es als hyperbolisches Positionsfixiersystem, das eine Position durch Lösen von nichtlinearen Gleichungen aus der Zeitdifferenz der Signalsankunft (TDoA) schätzt. Da die Positioniergenauigkeit weitgehend von der zeitlichen Auflösung der Signalerfassung abhängt, wurde ein dediziertes RF-Front-End-System entwickelt, um eine zeitliche Auflösung im Pico-Sekunden-Bereich oder sogar im Sub-Pico-Sekunden-Bereich zu erreichen. Auf der Algorithmen-Seite umfasst das digitale Signalverarbeitungssystem zwei Verarbeitungseinheiten: den TDoA-Schätzer und der hyperbolische Gleichungslöser. Um eine Echtzeit-Positionierung zu erreichen, wurde das Verarbeitungssystem auf einer FPGA-Plattform implementiert. Entsprechende Firmware wird aus den in MATLAB / Simulink modellierten Algorithmen mit dem High-Level-Synthese- (HLS) -Tool HDL Coder generiert. Das Prototypsystem wird ausgewertet und eine Genauigkeit besser als 1 cm erreicht. Eine bessere Leistung ist möglich durch Optimierung der steuern Bedingungen wie ADC-Abtastrate, ADC-Auflösung, In-

terpolationsprozess, höhere Frequenz, stabilere Antenne, usw. Das vorgeschlagene System ist zunächst für Indoor-Anwendungen ausgelegt, kann aber auch zu einem wettbewerbsfähigen Kandidaten für einen Outdoor-Positionierung Service weiterentwickelt werden.

**ABSTRACT**
**KURZFASSUNG**

# Contents

# List of Figures

# List of Tables

# 1. Introduction

The history of voyage reflects the history of navigation. In the early stage, sailors used traditional practice, geometry, astronomy, or special instruments to determine directions and their locations. These navigational tools include compass, nautical charts, astrolabe, sextant, etc. In the modern era however, these tools have been largely replaced by electronic and technological equivalents especially after the invention of computers, which were usually originally motivated by military intention. Radar [3], Long Range Navigation (LORAN) [4], Gyro-compass [5] and the most famous satellite based global positioning system (GPS) [6] are among those. The GPS is the first satellite based system that has a global coverage. It was launched by the U.S. Department of Defense in 1973 for use by the United States military and became fully operational in 1995. A GPS receiver compares the time of broadcast encoded in the transmission of three or four different satellites, thereby measuring the time-of-flight (ToF) to each satellite, allowing a continual fix to be generated in real time using trilateration. Multiple global navigation satellite systems (GNSS) beside GPS such as GLONASS in Russia, Galileo in Europe and BeiDou in China are developed and have been partially or fully providing the worldwide navigating service with meter-range positioning accuracy for civilian applications.

The navigation technologies in context are conventionally with respect to outdoors navigating purpose, however a system that could give a precise positioning service indoors has drawn significant attention by the huge scale of applications, with the help of development of computing technologies in the past decades. It is relatively new under investigation which started from approximate middle 90's last century. Unfortunately, a satellite based GNSS is able to realize a global coverage, fails to locate an object within an indoor environment or lead to severe deterioration of position accuracy. GNSS signal suffers from gross distortion in the indoor case due to fading, multi-path distortion and attenuation. The complexity and material characteristics of a building cause the distortion by reflecting, diffracting, scattering of the GNSS signal when it propagates into the building. Comparing to the outdoor case, there are more short delay multi-path components indoors, which leads to severely degraded pseudo-range estimation. Furthermore, there is no standard model for an indoor positioning, as environments significantly differ from case to case. On the other hand, a typical requirement of an Indoor Positioning System (IPS) is high accuracy which in many cases should be within range of 1 meter or even millimeter, depending on the specific applications. These obstacles make the GNSS not a suitable candidate for indoor usage.

Many alternatives have been researched and applied to IPS systems. There are three categorization methods: location of signal sources, positioning signal type or positioning principle. They can be classified into two groups: inertial positioning system and external sensing positioning systems, regarding the source of signals. Those who determine the location by using inertial sensors such as accelerometers or gyroscopes belong to the first class, where the signal generation and signal sensing happen internally. Candidates from the other group determine the position by analyzing external signals, and can be categorized based on positioning media includes optical, radio frequency, magnetic and acoustic systems. An optical system usually means a system built up by cameras [7, 8]. The position is determined by processing the image frames of the object. An object can be a specific part like head of a person or fiducial marker attached onto it. Classification could also be made by measurements, e.g. Angle of Arrival (AoA), Time of Arrival

**Table 1.1:** Overview of indoor positioning technologies [1]

| Technology | Typical Accuracy | Typical Coverage (m) | Typical Measuring Principle | Typical Application |
|---|---|---|---|---|
| Cameras | $0.1mm - dm$ | $1 - 10$ | angle measurements from images | metrology, robot navigation |
| Infrared | $cm - m$ | $1 - 5$ | thermal imaging, active beacons | people detection, tracking |
| Tactile & Polar Systems | $m - mm$ | $3 - 2000$ | mechanical, interferometry | automotive, metrology |
| Sound | cm | $2 - 10$ | distances from time of arrival | hospitals, tracking |
| WLAN / WiFi | m | $20 - 50$ | fingerprinting | pedestrian navigation, LBS |
| RFID | $dm - m$ | $1 - 50$ | proximity detection, fingerprinting | pedestrian navigation |
| Ultra Wideband | $cm - m$ | $1 - 50$ | body reflection, time of arrival | robotics, automation |
| High Sensitive GNSS | 10 m | global | parallel correlation, assistant GPS | location based services |
| Pseudolites | $cm - dm$ | $10 - 1000$ | carrier phase ranging | GNSS challenged pit mines |
| Other Radio Frequencies | m | $10 - 1000$ | fingerprinting, proximity | person tracking |
| Inertial Navigation | 1 % | $10 - 100$ | dead reckoning | pedestrian navigation |
| Magnetic Systems | $mm - cm$ | $1 - 20$ | fingerprinting and ranging | hospitals, mines |
| Infrastructure Systems | $cm - m$ | building | fingerprinting, capacitance | ambient assisted living |

(ToA), Time Difference of Arrival (TDoA), Received Signal Strength Indicator (RSSI), etc. Each of these technologies has its own advantages and disadvantages with respect to performance, system complexity, cost and so on.

Table 1.1 compares 13 different IPS technologies by evaluating the performance like accuracy, application range, positioning principle, cost etc. [1]. This table also briefly lists some popular IPS applications, including metrology, robot navigation which requires very high positioning accuracy, and those who could be less accurate but require a greater coverage like person tracking in a building or location based services.

IPS systems can be applied in almost all areas, such as medical, logistic, safety, science, gaming, industry, etc. Two different types of positioning mechanisms summarize the applications for indoor positioning systems: active systems and passive systems. They are categorized by the location where the positioning computation is implemented. An active system means that the target device determines its position internally. Most location based services belong to this kind, for example person guiding in a shopping mall or in a museum, commercially relevant information or public transportation service. On the contrary, a passive indoor positioning device does not have to be aware of its position, instead, a centralized station will carry out the positioning computation. This kind of IPS is actually a monitoring system. Patient monitoring in medical care facility,

locating a fireman in a building, arbitration of a goal in the field, motion tracking along with many others are passive IPS systems.

## 1.1. Motivation

In recent years, as the improvement of the automation technology and intelligent systems in commercial, industry, education and science areas, indoor positioning systems have become increasingly popular [9]. Unlike a GNSS system, there isn't a standard framework in developing an indoor positioning system due to the extreme complexity and diversity of indoor environments. Several technologies have been reported in literature for indoor positioning systems such as Vision [7, 8, 10, 11, 12], Infrared [13, 14, 15], Ultrasound [16, 17, 18, 19, 20], Wi-Fi [21, 22, 23, 24, 25, 26, 27], RFID [28, 29, 30, 31, 32], Bluetooth [33, 34, 35, 36], UWB [37, 38, 39, 40, 41], etc. Each of them assumes a specific infrastructure, environment, and usually also the application oriented performance. For instance, the system proposed in [22] is developed using Received Signal Strength (RSS) from Wireless Local Area Network (WLAN) Access Points (APs). Example experiments were carried out on a $30m \times 46m$ area of a building floor, involving 26 APs and achieved an accuracy of better than 2 meters.

This work is motivated to develop a high accuracy indoor positioning system. It is expected to achieve a millimeter-range positioning accuracy. The referred works either have low accuracy or could not work without line of sight condition. Technologies based on Wifi, Bluetooth or RFID could only reach meter-range accuracy. Methods using light, no matter visible or invisible, fail to function in non-line of sight situations. This work can be applied to the wide span indoor applications that rely on accurate positioning. They include but are not limited to the examples:

**Tracking**
Patients and medical equipments tracking in hospitals give the possibility of efficient emergency detection and provides an intelligent solution in medical resource management. Even a precise robotic surgery assistant becomes realistic. Object tracking inside a building can be an indoor navigator for personnel like visitors in a shopping mall or precise guidance for automatic forklift truck in a factory. Localizing authorized persons in high-security areas or locating and recovery of lost or stolen properties. Location sensing provides the internet of things (IoT) the precise location of a thing, both in time and space. The smart house for example where all the elements within the house can be virtually connected and communicate with each other, and the IPS enhances this system to a higher level with object tracking of either the people or equipments like a robot vacuum cleaner.

**Motion Capturing**
The most popular example is entertainment, including video games that require the interaction between players and the host machine, sport analysis for training by analyzing the motion of the sport player or a object like a football, etc.. It can also be used in an ambient assistant living system, assisting the senior people by monitoring their activity and trigger an emergency alarm when an abnormal motion is detected. Animated films with the help of motion capturing have already been applied for a long time.

Table 1.2 summarizes general requirements for typical indoor positioning systems. The actual user requirements are determined by the specific applications. The development of an indoor positioning system is initiated by setting goals in terms of criterion. Together with Table 1.1 which gives an overview of the existing IPS technologies and performance comparison, an attempt is made to figure out a comprehensive guideline for developing an IPS that meets the requirements from a vast diversity of applications by comparing the performances such accuracy, coverage, positioning principle, etc.

**Table 1.2:** List of typical user requirements for indoor positioning systems

| Criteria | Criteria Description |
|---|---|
| Accuracy | Estimation error to the ground truth |
| Coverage | Applicable environment size |
| Potability | Size of mobile device |
| Update rate | Object position update rate |
| Operation time | Time to run out of battery |
| Installation complexity | Fundamental infrastructure |
| Latency | Time to determine the position |
| Cost | Price per unit |
| Capacity | Number of targets can be simultaneously traced |
| Reliability | Robustness in complicated indoor environment |
| Adaptivity | Freedom in using frequencies, media, positioning technologies and dynamic environments, etc. |

This work focuses on describing a newly developed indoor positioning system, which achieves the performance of high accuracy, high update rate, low cost, low latency, high adaptivity, etc.

## 1.2. Objective and Challenges

This work is intended to develop a high precision positioning system for vast applications in tracking and motion capturing within an indoor environment. Objective is initiated and the challenges that could obstruct these goals are discussed.

**Objective**
A complete solution including the hardware system and the signal processing system are expected from this work. Three key goals should be accomplished. First, a thorough review of the potential technologies on indoor positioning. Second, proposal of a guideline for developing an IPS, covering phases of application case study, positioning strategy, hardware and signal processing scenario, etc. Third, development of a mm precision indoor positioning system based on multilateral technology is the focus of this work.

**Challenges**
The major challenge in developing an indoor positioning system based on multilateral technologies is to accurately measuring the distances information, which correspondingly requires a high temporal resolution in the data acquisition part. Conventionally, high speed ADCs are necessary for achieving a desirable time resolution. But GHz

sampling rate ADCs are too expensive and energy hungry, making it not suitable for usual applications. A customized RF front-end is developed to overcome the limitation by introducing a sub-sampling RF architecture, with the cost of extended measurement duration. This dissertation describes a configurable solution for different accuracy requirements from diverse of applications, either improving the accuracy or increasing the position update rate.

The multi-path and Non-Line-of-Sight (NLoS) propagation are two major contributors for indoor positioning error. The multi-path effect could cause the inaccurate ToA/TDoA estimation, due to the signal distortion. The influence of multi-path can be suppressed by deploying a system with high frequency and some modulation schemes. But using a higher frequency would in return degrade the performance in NLoS condition. In Non-Line-of-Sight condition, the signal either could not be detected or a reflected signal is detected instead. Some redundant Beacons could be necessary to ensure a Line-of-Sight (LoS) propagation is available. Another effective way to mitigate multi-path is averaging over time with an appropriate motion filter.

The complicated and impractically measurable Phase Center Variation (PCV) of the antennas is also a problematic issue strangling the attempt in achieving a mm positioning precision. Due to the nature of RF antenna, its phase center (considered as the point where the signal is radiated or collected) is not a static point. The Antenna Phase Center (APC) does not coincide with the antenna physical (geometrical) center and varies with the frequency and incident angle of the incoming signal. This effect makes the reference receivers (beacons) no longer fixed as expected, thus lead to positioning error. Instead of introducing certain phase center offset cancellation antenna array or a post-processing procedure which are out of the scope of this work, the narrow band dipole antenna with relative small PCV is used in our system.

It is also challenging to accurately measure the locations of reference receivers (beacons). As they are prerequisites for solving the positioning equations, measurements error could degrade the accuracy.

## 1.3. Contribution of this Work

This work presents a novel indoor positioning system with millimeter-range precision [42]. It is a RF-based system, implementing the TDoA technology. It achieves a better performance compared to referred RF-based work. The low cost custom hardware also make this system more competitive than the optic-based systems, and it works in NLoS condition. Contributions of this work include the following major aspects: design, producing, evaluation of the hardware system; development of positioning algorithms and firmware; system prototyping and evaluation.

**Hardware**
In order to accomplish the objective, a carefully designed hardware system is required. The positioning strategy is to developed a RF-based TDoA system, which is explained lately in subsection 3.1.3. Then the key components of this system should at least include RF transmitters, RF receivers and a digital signal processing unit. The basic function of the receiver is to produce a time stretched version of the received periodic RF-signal. A newly developed RF front-end implements signal pre-amplification, fil-

tering , frequency conversion with a sub-sampling mixer, Automatic Gain Controlling (AGC) and baseband signal filtering. This customized module is composed by two individual circuit boards: preamplifier and filtering stage, signal stretch stage. The first stage works as a channel selector and amplify the interested frequency using multiple stages Low Noise Amplifier (LNA). Meanwhile, a directional power coupler is introduced for power detection and is further fed into the AGC block on the second stage, where a sub-sampling mixer is implemented. The second stage realizes a quasi time stretch [43] operation. It stretches the modulated UHF/SHF signal to a low frequency without using a conventional mixer, feeding the ADC board and further into the Digital Signal Processing (DSP) unit. The AGC of this design enlarge the dynamic range by 40 dB, which in another word results in an effective positioning range increment of more 100 times.

This dissertation describes the following design procedure of the hardware: circuit simulation in Advance Design System (ADS), high frequency module simulation in ANSYS HFSS, PCB layout design in Altium Designer, hardware test and evaluation. Results and developing considerations for each phase are presented.

**Algorithms**

Because the applied technology in this system is based on TDoA information, the signal processing includes two key process: TDoA Estimation, Hyperbolic Positioning Algorithm (Figure 1.1). The basic idea of the developed algorithm is to extract the TDoA information and to estimate the location based on this information by trilateration principle. The algorithms development starts with the TDoA estimation. In order to estimate the TDoA, a set of raw signal processing algorithms is required, including the baseline compensation, event arbitrator, normalizer, filter, ambiguity eliminator, etc. A Kalman filter is introduced as the last stage to improve the estimation performance.
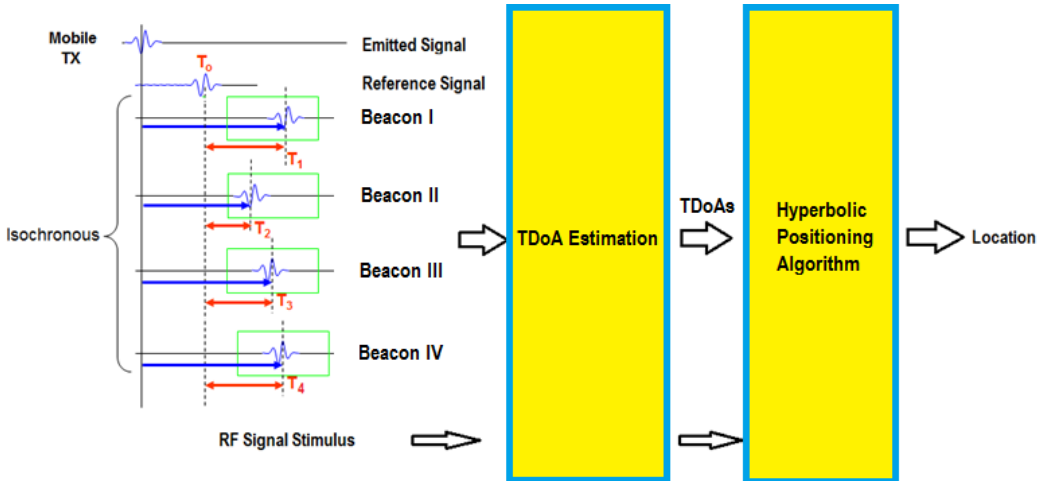


**Figure 1.1:** Simplified signal processing chain

A numerical algorithm based on the Newton-Raphson method is proposed for solving hyperbolic non-linear equations to determine the 3D coordinate of the mobile device. Initiative position estimation converges within 7 iterations, with an error of less than 100 ppm. Subsequent estimations require only 3 iterations to achieve the similar accuracy by substituting the initial guess with previous estimation. This dissertation presents a

simulink model where the iteration length can be dynamically configured during processing, reducing the computation complexity on demand.

As Previously mentioned, the complete processing system is firstly modeled in MATLAB/Simulink environment. The high level synthesis tool HDL Coder is involved in firmware generation from the Simulink model. Simulation results are provided, including the co-simulation which concludes the identical functionality of the algorithm model and the firmware model. This dissertation describes a complete design flow of the IPS signal processing system from modeling to FPGA implementation. Merits and drawbacks of the development environment is discussed and some appropriate suggestions are summarized.

**Sytem Evaluation**

Performance evaluation for each individual component of the system, including the two stages customized PCB boards and the positioning algorithm model is provided. Measurements of the 1D ranging and 3D positioning were separately carried out and evaluated. The 1D test in an anechoic chamber was taken in order to understand the influence of some parameters such as cables and the antennas, which gives a deep insight on potentials for further improvement. A Root Mean Square Error (RMSE) of 0.807cm is achieved in a complicated office/Lab environment, with a variance of $0.197cm^2$. The goals listed in Table 1.3 are fully accomplished.

The proposed system provides a high degree of flexibility in frequency usage, ranging from hundreds of MHz to tens of GHz. It implements a narrow-band RF architecture and shows a strong immunity to neighbor bands interference and could even reject high in-band noise. Moreover, it can be adapted to varies coverage applications from meters up to tens of kilo-meters. The high adaptivity and narrow-band property make this system to be a competitive player in IPS market, promoted by its low cost, and robustness high accuracy.

This work also demonstrates the influence of the PCV on the positioning accuracy. Two type antennas are evaluated, the wide-band antenna and the dipole antenna. A comprehensive analysis of the PCV behavior of the dipole antenna is presented. The simulated matched well with the experimental result and proved that the PCV dominates the error in 1D ranging, thus further degrades the accuracy in 3D positioning.

Geometry dilution of precision (GDOP) effect caused by the distribution of the references nodes is observed and analyzed in the prototype system evaluation, giving a hint for further improvement.

It must be noted that, although this system was initially developed for indoor applications, it can be used outdoors and provide a superior performance to indoors condition, because there are much less short multi-path components than in indoor environment.

## 1.4. Dissertation Structure

The dissertation is structured in the following way. This introduction is followed by an overview of the general background and related work on indoor positioning systems in Chapter 2. It describes the existing technologies by investigating the positioning

signals, principles and algorithms. Chapter 3 presents the development methodology of the proposed local positioning system, including the technical aspect of the hardware architecture and the signal processing system involved in the system. The simulation and measurement of the customized RF front-end, the development of the positioning algorithms are demonstrated. Chapter 4 describes the prototyping and evaluation of the underlying technologies. Performance evaluation of the proposed system is presented. 1D and 3D test are carried out and correspondingly the results are analyzed Chapter 5 concludes the contributions, challenges and key positioning error sources. Chapter 6 closes the dissertation with suggestions on possible future developments based on this work.

## 2. State-of-the-Art Indoor Positioning Technologies

Indoor positioning systems have been investigated for decades. Previous surveys addressed a large scale of related technologies in diverse perspectives, including performance, positioning signal measurement, mathematical modeling and limitations [44, 45, 46, 47, 48]. Comparison between different technologies in literature presents the developers a comprehensive start point for their specific applications. As described in context, the existing technologies can be grouped into two categories: inertial positioning (involving momentum sensors embedded on the object device to be located) and external sensing (geometry estimation based on signal measurement).

**Inertial Positioning**
This sort of system involves the usage of momentum sensors embedded on the mobile device. The position is determined by monitoring the motion of the target object. Continuous and accurate measurement of velocity, acceleration or orientation is the essential information to ensure the positioning performance. As the position computation relies only on the historical estimations and measurements, the error is cumulative and would finally fail in meeting the accuracy requirement. Rather than in positioning, inertial systems are more popular in motion detection or used as an enhancement for an external sensing positioning system.

**External Sensing**
In contrast with the inertial positioning system, this approach determines the location by measuring the signal propagation between the target node and the reference nodes. There is variety of information which can be extracted from the incident signal for positioning, such as Angle of Arrival (AoA), Time of Arrival (ToA), Time Difference of Arrival (TDoA), Received Signal Strength Indicator (RSSI), etc. A crucial precondition is that the coordinates of the reference nodes should be known, location fixed or precisely predicable. The determination of the position doesn't require knowledge of historical estimation but can depend only on the current measurements. This makes a more reliable solution, making the external sensing method dominating the location system market.

With the advantages of applicability and reliability, the external sensing system became the preferred system approach in developing a mm-range precision indoor positioning system. This chapter describes the related work by discussing three fundamental considerations of an IPS: positioning signal, positioning principle and positioning algorithm. Section 2.1 gives an overview of possible signals that can be used in a location system. Section 2.2 goes further into the various of positioning principles, comparing their pros and cons. Section 2.3 presents some existing algorithms developed for localization.

### 2.1. Positioning Signal

All systems described in this work are wireless, which means the signals involved can propagate in the space without introducing cables. This property encourages a large freedom in using various signals. They can be categorized into four groups: optical signal, acoustic signal, magnetic field and radio frequency. Each of these leads to a distinctive hardware implementation. The characteristics of different signal types also determine their potential in performance in terms of accuracy, coverage, robustness,

cost, etc.

### 2.1.1. Optical Signal

The optical signals deployed in existing positioning systems include visible light and infrared radiation.

**Visible Light**

Visible light is the part of the EM spectrum with a wavelength between 380 nm and 760 nm ($400 - 790$ terahertz) which can be detected by the human eye. It comprises only a tiny fraction of the entire electromagnetic radiation spectrum. There are many sources of visible light, either being nature or artificial. When venturing outside, a vast majority of the light visible to humans is emitted from the sun, which also produces many other frequencies of radiation that do not fall into the visible range. Many biological organisms are capable of emitting visible light, such as the familiar lightning bugs ("fireflies") and more exotic glows from the sea. Inside, we are exposed to visible light that originates from artificial sources, such as fire, fluorescent and incandescent tungsten device, LED, Laser, etc..

Various photon detectors have been invented to measure the kinetic energy of the photoelectrons, including vacuum phototube, photomultiplier tube, photodiode, charge-coupled device (CCD), Complementary metaloxidesemiconductor (CMOS) sensors, etc.

Information like intensity and propagation direction can be estimated, with the usage of photo detectors. Additionally, modern technologies also enable the measurement of distance, with a single range imaging camera [49, 50]. A camera-based IPS only works in condition of line-of-sight (LoS), as the light propagates in a straight line and can only be seen by detectors when no obstacles block in between. This shortcoming in return results in a perfectly high angular resolution, thus provides a high positioning precision. Researchs on IPS using visible light have achieved an accuracy levels between tens of $\mu$m and dm [7, 8, 10, 11, 12, 51].

**Infrared Radiation**

Infrared is an invisible (to the human eye) electromagnetic radiation with frequency ranging from 300 GHz to 430 THz, extending from the nominal red edge of the visible spectrum. The primary source of infrared radiation is heat or thermal radiation. This is the radiation produced by the motion of atoms and molecules in an object. The higher the temperature, the more the atoms and molecules move and the more infrared radiation they produce. Artificial sources such as IR laser, IR LED can emit light in the infrared range of the electromagnetic radiation spectrum, resulting from the so called electro-luminescence effect.

Infrared radiation is light just like visible light because they have similar properties. But due to the long wavelength, infrared radiation is less scattered and offers better transmission through various media. There are two main types of IR detectors: thermal detectors and photodetectors. Thermal detectors use the infrared energy as heat and their photo sensitivity is independent of the wavelength. Photodetectors in contrast convert light signals that hit the detector material into voltage or current (same as

visible light photodetector), depending on the wavelength or photon's energy.

Infrared object tracking systems based on high resolution infrared sensors are able to detect artificial IR light sources with sub-mm precision [52] but should be under LoS condition and is sensitive to ambient interference. Systems based on active beacons [53, 54] or those using natural radiation [55] usually provide meters positioning precision and can be used for rough locating applications.

### 2.1.2. Acoustic Signal

In contrast to an optical signal, radio frequency or magnetic field, which can be classified as electromagnetic wave, an acoustic signal refers to the mechanical wave transmitted through a medium by pressure oscillation. This pressure is initiated by a speaker or some other mechanical device that creates a series of pulses of energy that, in turn, cause air molecules to vibrate. The acoustic signal can be further categorized into audible sound, ultrasound and infrasound distinguished by the location in spectrum.

**Audible Sound**
The sound frequencies ranging from 20 Hz to 20 KHz is audible to the average human, as the vibrations reach a listener's ear with sufficient energy to cause pressure on the eardrum. Audible sound has been investigated for localization purpose [56, 57]. Speaker and microphone are involved as acoustic signal transmitter and receiver respectively.

**Ulrasound**
Ultrasound refers to the sound waves with frequencies higher than 20 KHz, the upper limit of audible sound. But it is audible to some animals such as bats, dolphins and whales. They are able to emit ultrasound and use it for locating prey and obstacles [58]. Many ultrasonic-based systems were developed to detect objects and measure distances [16, 17, 18, 19, 20], where even sub-centimeter precision can be achieved. Artificially, the ultrasound is generated or detected by using an ultrasonic transducer that converts an electrical signal into ultrasound or vice versa. It typically refers to piezoelectric transducers or capacitive transducers.

**Infrasound**
The sound with frequency of less than 20 Hz is known as infrasound, which is also the lower limit of human hearing. The sources include wind turbulence, earthquake, snow avalanche, vehicle, industrial facilities, air conditioning system, etc. Infrasound can travel great distances from hundreds to thousands kilometers with little attenuation, due to its low frequency. Technologies are developed to detect and localize events that generate infrasound, like earthquake, explosion, avalanche and so on [59, 60, 61, 62].

All sound signals are mechanical waves of pressure which propagate through compressible media such as air, water or solid. During their propagation, waves can be reflected, refracted, or attenuated by the medium. Three properties are most concerned for a sound-based positioning: propagation speed in the air, attenuation, NLoS propagating capability.

Comparing to the propagation speed of electromagnetic wave in air (299,702,534 m/s), the sound propagates far slower (331.4 m/s). The penetration capability and low speed

eases the development a high accuracy positioning system with low cost, loose synchronization requirement, function in NLoS condition. The drawbacks of relative low speed are the non-negligible Doppler shift and lower update rate. Moreover, the speed of sound depends on environmental factors such as temperature, humidity, and atmospheric pressure. Although temperature sensors can be used to compensate the variations of speed of sound due to temperature, other environmental factors and the finite resolution in temperature measurements can result in the actual speed being different from that used for position estimation. The existing multi-path propagation and ambient noises make the development of reliable sound-based positioning systems at cm level or better remain a challenge.

### 2.1.3. Magnetic Field

Magnetism is one of the most ancient methods in navigating. Using the compass for open-seas navigation started from the 15th century. The associated magnetic field is the magnetic effect caused by electrons' motion or magnetic materials, where electrons spin to produce directional field. Figure 2.1 shows some examples of magnetic field sources. The Earth itself is a giant magnet, sourcing from circulating electric currents within the molten metallic core.
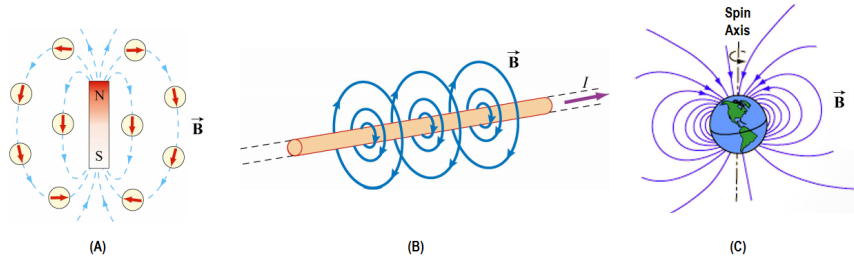


**Figure 2.1:** Examples of magnetic field source, bar magnet (A), wire carrying current (B), the earth (C).

A magnetic field is mathematically described as a vector field. It exerts a force on particles in the field due to the Lorentz force, which attracts or repels other objects. The term magnetic flux $\phi$ is introduced to describe the amount of these force lines passing through an area and can be formulated as:

$$\phi = \int_S \mathbf{B} \bullet d\mathbf{A} \tag{2.1}$$

Where $\mathbf{B}$ represents the flux density vector measured in T and $\mathbf{A}$ describes the cross-sectional area. Four properties of magnetic field are found: Magnetic field lines never cross; The density of field lines indicates the strength of the field; Magnetic field lines always make closed loops and will continue inside a magnetic material; Magnetic field is directional. Whereas there are two properties we can measure from a magnetic field vector: the strength and direction. The direction is easy to measure by lining up a magnetic compass with the field. The strength on the other hand can be measured by magnetometers which exploit the force an electron feels as it moves through a magnetic field [63] or by measuring the giant magnetoresistance (GMR) [64, 65] in thin-film structures composed of alternating ferromagnetic and non-magnetic conductive layers. Many other technologies have been deployed for magnetic sensing, including Hall effect

sensor, magneto-diode, magneto-transistor, AMR magnetometer, magnetic tunnel junction magnetometer, magneto-optical sensor, Electron Tunneling based MEMS sensor, MEMS compass, etc.

Many investigations have been carried out for indoor positioning using either ambient or artificial magnetic field and meter-level precision or better was achieved [66, 67, 68, 69]. All magnetic-based positioning systems in literature involve the measurements of the strength and the direction of the magnetic field. Compared to the light and radio methods, a significant advantage of this type of system is that the artificially generated magnetic field is not affected by most obstacles, hence multi-path or NLoS errors can be neglected. However, it suffers from fluctuations due to the presence of magnetic field anomalies arisen by natural and artificial sources [70]. Furthermore, moving objects containing ferromagnetic materials and electronic devices may affect the magnetic field.

### 2.1.4. Radio Frequency

Any electromagnetic wave frequencies that lie in the range extending from around 3 kHz to 300 GHz is defined as Radio Frequency (RF).

A RF signal is the result of oscillating electric and magnetic fields that move as an energy force in wave form through space. It can be produced by both natural and artificial sources. Natural sources like the sun, the earth and the ionosphere all emit low level RF fields. Artificial sources of RF are mainly used for telecommunication purposes. Radio and television broadcasting, mobile phones and satellite communications all produce RF. Other sources of RF fields include microwave ovens, radar, industrial heaters and sealers, and various medical applications.

The RF spectrum range is further splitted into sub bands as listed in Table 2.1. Transmission systems work in the RF spectrum range including analogue radio, aircraft navigation, marine radio, amateur radio, TV broadcasting, mobile networks and satellite systems.

| Frequency Range | Description | Abbreviation |
|---|---|---|
| $3kHz \sim 30kHz$ | very low frequency | VLF |
| $30kHz \sim 300kHz$ | low frequency | LF |
| $300kHz \sim 3MHz$ | medium frequency | MF |
| $3MHz \sim 30MHz$ | high frequency | HF |
| $30MHz \sim 300MHz$ | very high frequency | VHF |
| $300MHz \sim 3GHz$ | ultra high frequency | UHF |
| $3GHz \sim 30GHz$ | super high frequency | SHF |
| $30GHz \sim 300GHz$ | extremely high frequency | EHF |

**Table 2.1:** Information from different measurements used for positioning.

RF-based indoor positioning systems utilize the propagation of Radio Frequency (RF) signals. The system is composed of transmitter nodes and receiver nodes. The link between these nodes includes the origin transmitting antenna, propagation medium (the air), and the destination receiving antenna. The simplest form of Friis transmission equation describes the radio propagation in free space:

$$\frac{P_r}{P_t} = G_t G_r (\frac{\lambda}{4\pi R})^2 \tag{2.2}$$

Where $G_t$ and $G_r$ represent the antenna gains on the transmitter and the receiver respectively. $P_t$ is the output power to the transmitting antenna and $P_r$ is the input power of the receiver antenna. $R$ defines the distance between two antennas.

But this is an ideal model that is inaccurate for ordinary terrestrial condition, where RF signals generally propagate between the transmitting antenna and the receiving antenna in the following patterns: line-of-sight (LoS, direct propagation), refraction, or reflection (NLoS, multipath). Dominant propagation characteristics vary with the frequency (or wavelength) of the transmitted signal involved. Metals and fluids tend to be highly reflective surfaces for electromagnetic waves and thus influence the path of propagation, resulting in multipath fading, especially significant in urban or indoor environments. In multipath conditions, both the direct and reflected signals are present at the antenna. What's worse, in some situations, the direct signal may be obstructed or greatly attenuated to a level well below that of the received multipath signal. These effects make the multipath phenomenon the most problematic obstacle in developing a high precision indoor positioning system. A careful site selection, better antenna design, multipath reduction algorithms, special receiver hardware implementation and other methods have been investigated for the multipath influence mitigation.

Nevertheless, the suitability in NLoS propagation, low cost hardware and relatively easy development encourage a huge amount of engineers and resources on developing RF-based positioning system. Three kinds of information can be in principle used for determining the location: signal strength, angle of arrival and time of arrival. Technologies using Radar, GNSS, Wifi, Bluetooth, RFID, FM Radio, UWB, ZigBee, etc. have been able to achieve accuracy ranging from centimeter to meter, with various coverages. [45, 51]

## 2.2. Positioning Principle

There is no universal model to characterize the indoor environment [9], due to the localized and dynamic nature of each individual circumstance. This complexity and unpredictability result in fragmented indoor positioning technologies to meet diverse requirements, such as accuracy, update rate, latency, cost etc. Several commercial systems have been developed using different signals in context. Then what information can be extracted from those signals for positioning? There are three fundamental measurements of a propagating wireless signal that can be carried out: intensity, propagation direction, time information. These measurements determine three primary positioning principles: single strength-based, angulation-based and time-based. This section discusses each of these methods. The position estimation based on aforementioned measurements signal strength and time involves the triangulation positioning scenario (Figure 2.2). Figure 2.2(A) assumes the distances from the target to the fixed access points $AP_i$ are estimated, then each of this distance defines a circle in 2D or a sphere in 3D, surrounding $AP_i$. Intersection of these circles or spheres determines the target's location. Figure 2.2(B) assumes the distance differences from the target to the pairwise fixed access points $AP_i$ are estimated, then each distance differences defines a hyperbola in 2D or a

hyperboloid in 3D. Intersection of these curves or surfaces gives the positioning solution.
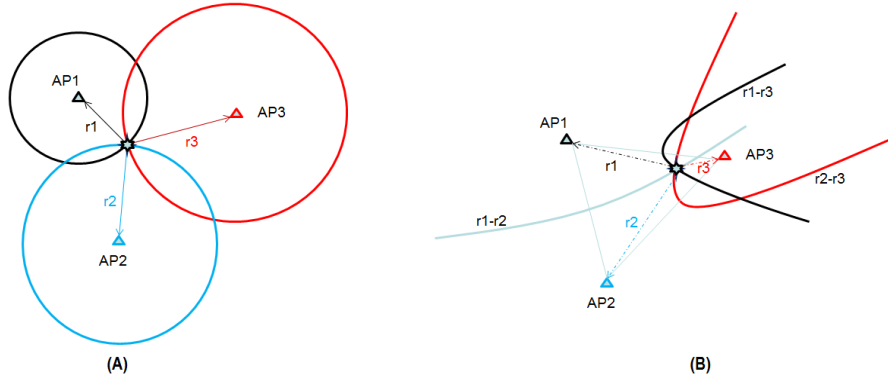


**Figure 2.2:** Concept of triangulation positioning, using distance information (A) and distance difference information (B).

### 2.2.1. Signal Strength-based Method

Received signal strength (RSS) is a measurement of the power level detected by the receiver. With the knowledge of received signal strength and the path loss model, the distance can be estimated in an ideal noise-free condition. One of the factors influencing RSS values obtained by a wireless device is the distance between emitter and receiver, the further the signal propagates, the lower the signal strength. Generally, sound, radiation, magnetic and light source from a point source propagates spherically, the energy is distributed over the ever-increasing surface diameter of the wave front surface (Inverse Square Law, Figure 2.3).
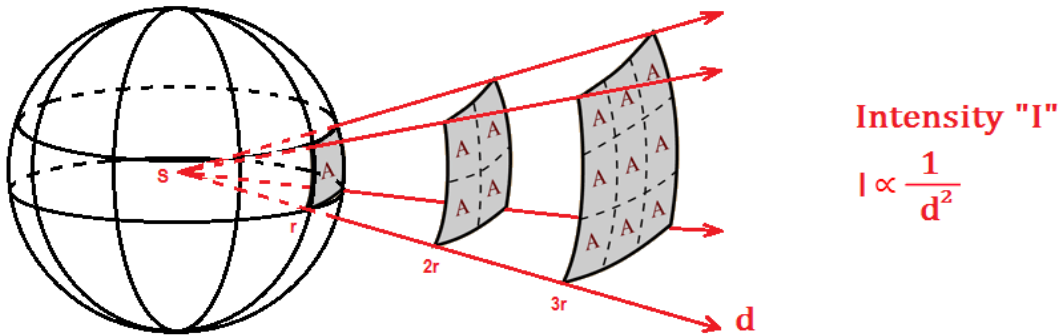


**Figure 2.3:** Field intensity is inversely proportional to the square of the distance from the source in free field.

It concludes that for every doubling of the distance from the source in a free field situation, the signal intensity will diminish by 6 decibels. The accuracy depends on the suitability of the propagation models used for the actual propagation conditions. The multi-path and the shadowing effect can be modeled with Rayleigh or Rician decaying model [71] for RF systems. Many researches attempted to model the RF propagation in an multi-path-rich environment [72, 73, 74, 75, 76, 77]. But there is no universal model

for the vastly diverse indoor environments. Recapitulatively, the signal attenuation, caused by the propagation distance, is known as path loss, and the intensity is modeled to be inversely proportional to the distance between the emitter and the receiver raised to a certain exponent known as path loss factor. An average pass loss factor $\bar{P}_{loss}$ for signal propagating from the location at distance $d_0$ to the location at distance $d$ can be summarized as:

$$\bar{P}_{loss}(d_0 \to d) \propto (\frac{d}{d_0})^n \tag{2.3}$$

Where the exponent $n$ indicates the power decaying speed, depending the exact environment. $n$ equals to 2, obeying the Inverse Square Law when signal propagates in free space, otherwise, it is greater than 2. The pass loss law of signal strength used for indoor localization can be formulated as:

$$RSS = RSS_0 - 10nlog\|p - p_0\| + e \tag{2.4}$$

where RSS is the detected power by the receiver located at $p$, and $RSS_0$ refers to the signal intensity at the reference position $p_0$. $e$ is the induced error.

An offline calibration and real time adjustment are usually necessary for obtaining a promising performance. Fingerprinting is one method to use RSS for positioning, where the vector of the RSS values at a point is called the location fingerprint of that point. The basic idea is to build a map of fingerprints that are empirically obtained by taking exhaustive RSS measurements. Position estimation is determined by matching online measurements with the best position in a database that approaches the percomputed fingerprint [45, 78]. The maximum likelihood is evaluated for the matching process. The system searches for the most probable combination of RSS values and determines the closest position, according to the fingerprint map. The more the collected RSS information at each position, the more accurate the fingerprint data can guarantee.

RADAR [79] is one of the first positioning systems, making use of RSS. The advantage of RSS-based positioning system is the simplicity of implementation and its low cost. It can be built on many existing infrastructures such as cellular network [80], WLAN [81, 82, 83], Bluetooth [84, 85, 86]. The widely spread smart phone can be used as the mobile device, thus it requires almost no extra hardware. Li proposed an visible light based positioning system using RSS with a small scale hardware [87].

The RF RSS-based method is commonly used in low accuracy applications, because the accuracy is significantly impacted by multi-path effect especially the short delay components. Additionally, objects such as doors, furniture, and people are even more problematic, as they can affect the signal strength dynamically and randomly. Magnetic field on the other hand shows more robustness for implementing a RSS-based system. Joerg and Abdelmoumen proposed a system based on artificial fields, which is free of NLoS error and multi-path effects and achieved an accuracy of a few centimeters in short range $(< 10m)$ [68].

### 2.2.2. Angulation-based Method

The propagation direction of the wireless signal is also used in many positioning systems to locate the object. By measuring the angle of arrival (AoA) of the incident signal at multiple anchor units, the target's location can be determined as the intersection of directions lines (Figure 2.4). This method reduces the hardware infrastructure, comparing to other methods, as no time synchronization is needed. Only 2 measurement nodes for 2D positioning, while minimum 3 nodes are required for 3D. In principle, the AoA mechanism could be introduced in any systems, involving any listed signals in context. This adaptability provides the developers a high flexibility in hardware implementation and scenarios optimization. However, when the target object to be located is far away, the precision of non-light systems degrade significantly, due to the geometric dilution [88].
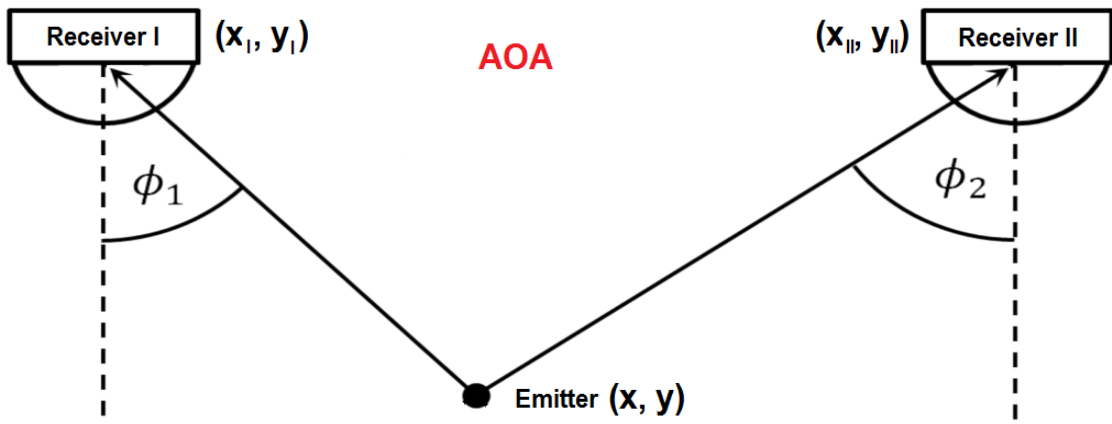


**Figure 2.4:** Localization by angle of arrival.

**Optical Systems**
The biggest advantage of implementing an optical positioning system is the straight propagation nature of light, enabling a precise AoA estimation. Cameras are able to capture the object features with a high update rate. Centimeter or even sub-millimeter accuracy can be achieved by optical systems [89, 52]. However, the shortcoming of AoA method in optical system is also obvious: it fails in NLoS condition, due to the straight propagation nature again.

**Acoustic Systems**
A low cost microphone array is capable to locate the sound source [90]. The acoustic signal processing is much easier comparing to the image processing where resource hungry processors are usually required. The key disadvantage of this method is the sensitivity to ambient interference, sourcing from multi-path fading in the complicated indoor environment. Moreover, positioning quality degrades as the mobile target moves farther from the measuring units.

**RF Systems**
Estimation of AoA in RF-based positioning system can be accomplished either with directional antennas or with an array of antennas (Figure 2.5) [91, 92, 93]. The angle $\theta$ can be computed by estimation of the propagation delays at different antenna elements.

$$\theta = \arccos(\frac{\Delta d_{ij}}{(j-i)*d}) \qquad (2.5)$$

Where $\Delta d_{ij}$ refers to the propagation range difference which can be derived by multiplying the propagation delay with the speed. $d$ is the space between neighboring antenna elements.
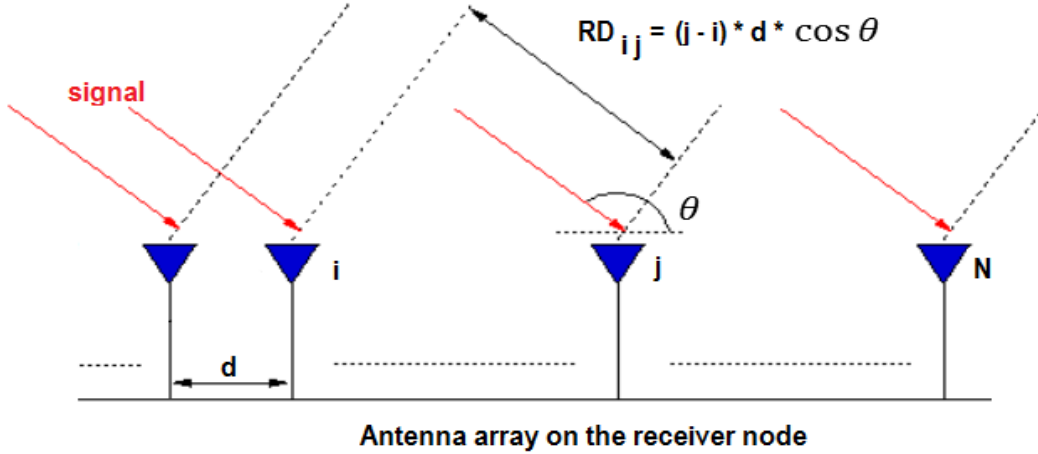


**Figure 2.5:** Angle estimation using antenna array.

For narrow-band RF systems, time differences can be represented as phase shifts. Therefore, the combinations of the phase shifted of signals arrives at different antennas can be measured for AoA estimation. However, for wideband systems, time delays of received signals should be involved instead, due to the large span of phase differences for a wideband signal [94].

### 2.2.3. Time-based Method

The third category is time-based positioning. It refers to these three measurements: time of arrival (ToA), round trip time (RTT) and time difference of arrival (TDoA). (Figure 2.6). The ToA and RTT measurements only involve two nodes, while the TDoA measurement involves three nodes.

**ToA**
The signal propagation time from the emitter to the receiver is directly proportional to the distance. The distance between two nodes can be derived by multiplying the signal travel time with the propagation speed. Many RF positioning systems, such as GPS [6] and Loran-C [4], are based on ToA measurements.

The Measurement of ToA requires a precise synchronization between emitter and receiver. Generally, it is more challenging to implement synchronization in a RF system than in a acoustic system, due to the much higher propagating speed. For acoustic-based positioning systems, a radio signal is usually involved for synchronization purpose and
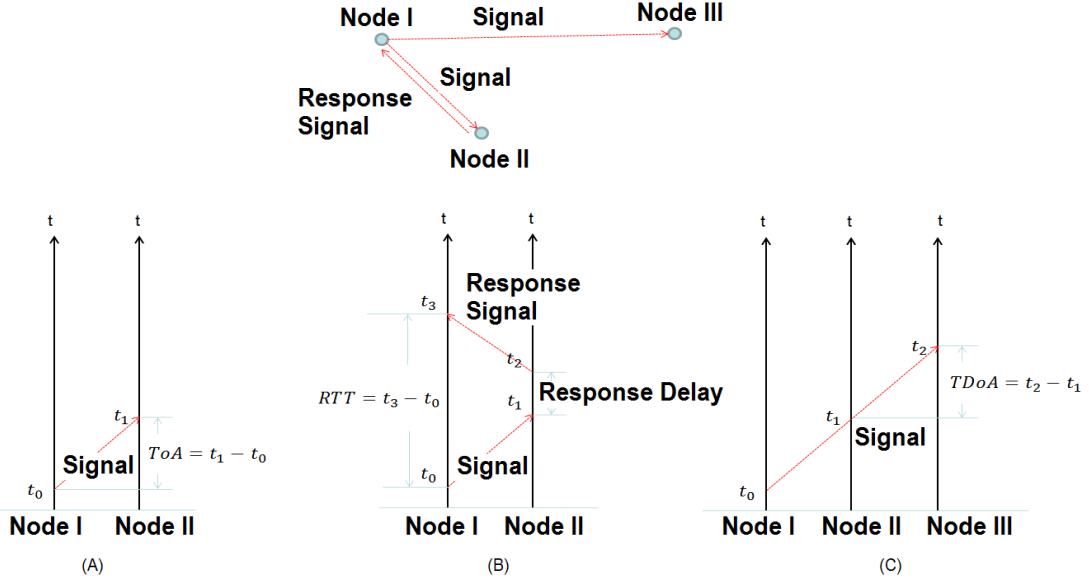
**Figure 2.6:** Time measurements: time of arrival (ToA) (A), round trip time (RTT) (B), time difference of arrival (TDoA) (C).

the sound signal is used for ranging [95]. Some semiconductor imagers can do ranging without synchronization between nodes by measuring the time of flight of the light [96, 97, 98].

In a ToA positioning system, the measured ToAs are defined as $ToA_i$. A set of ranges (Cartesian distance) between the target node and the $i_{th}$ anchor node: $d_i$ can be computed:

$$d_i = \parallel P - P_i \parallel = ToA_i * v + e_i \tag{2.6}$$

where $P$ represents the target location and $P_i$ are the known coordinates of the anchor nodes. $v$ is the signal propagation speed and $e_i$ refers to the inaccuracy caused by all kind of process noises and measurement error.

**RTT**
RTT refers the duration from the signal emission on the first node to the moment of receiving the acknowledge signal sent by the second node. It includes the internal delay within the node which answers with an acknowledgment And in a RTT-based positioning system, the measured RTTs are defined as $RTT_i$, then a sets of range (Cartesian distance) between the target node and the $i_{th}$ anchor node: $d_i$ can be computed:

$$d_i = \parallel P - P_i \parallel = \frac{RTT_i - TD_i}{2} * v + e_i \tag{2.7}$$

where $TD_i$ refers to the response delay in the $i_{th}$ node. A calibration of these delays is critical in developing a RTT-based positioning system. Frequently, the RTT measurements are used to estimate the ToA, with a priori knowledge of the response delay.

**TDoA**

Comparing to a the ToA system where the transmitter-to-receiver synchronization is necessary, the TDoA measurement on the contrary only need a synchronization between the anchor nodes. This advantage reduces the implementation complexity and cost as well. With the foreknowledge of signal propagation velocity, the range differences $\Delta d_{ij}$ from the target device to the anchor nodes $i$ and $j$ can be derived:

$$\Delta d_{ij} = \| P - P_i \| - \| P - P_j \| = (TDoA_{ij}) * v + e_{ij} \tag{2.8}$$

Where $e_{ij}$ refers to the inaccuracy caused by process noises and measurement errors on anchor nodes $i$ and $j$.

The range difference with two anchor nodes located at the foci defines a hyperboloid (Figure 2.7 (A)), where the target location can be at any position on the surface. A minimum of three range difference measurements is required, in order to estimate the 3D location by computing the intersection of three hyperboloids (Figure 2.7 (B)). Consequently, the TDoA-based system is also known as hyperbolic positioning system.
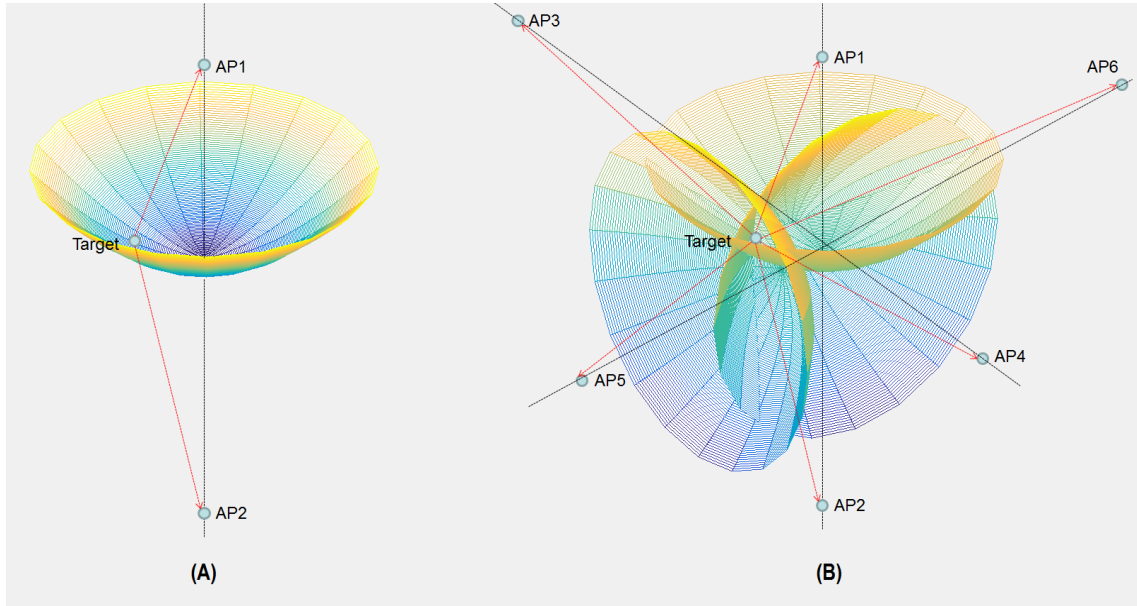


**Figure 2.7:** The range difference to pairwise access points (anchor nodes) defines a hyperboloid (A) and intersection of three hyperboloids derives the 3D location (B).

### 2.2.4. Summary

Each individual method has its limitation. The signal strength fluctuates unpredictably in complex indoor environment, which degrades the accuracy in RSS range-based positioning system. The angular resolution in AoA method depends on antenna configuration. Temporal methods such as ToA, RTT and TDoA rely on synchronization and event estimator. These fundamental limitations imply a high dependency of accuracy on the system implementation. A common obstacle for all these measurements is the measurement inaccuracy caused by non-line-of-sight (NLoS) propagation. Higher positioning accuracy can be achieved in the presence of non-line-of-sight (NLoS) by using hybrid positioning schemes that use combinations of available ToA, TDoA and AoA

measurements to solve the location [99], such as RSS/AoA [100, 101, 99], ToA/AoA [102, 103, 104] and TDoA/AoA [105, 106, 107].

Furthermore, all types signals presented in section 2.1 can be involved in a time-based system. Each has its pros and cons. Sound systems have the simplest implementation but are sensitive to ambient noise and have lower update rates. Optical systems have the highest precision but are limited to LoS propagation and require more computation effort. RF systems are a moderate method, lower cost compared to camera systems and more robustness compared to sound systems, coming with meter down to millimeter precision can be achieved by specific infrastructure hardware.

## 2.3. Positioning Algorithms

This section focuses on describing the mathematical perspectives of the positioning systems, attempting to provide a comprehensive overview of existing positioning algorithms. The study starts from the assumption of a specific indoor positioning system infrastructure, constructed by multiple access points (APs) located at known positions and a mobile device (MD) the object to be tracked. On the signal processing aspect, the positioning can either be carried out on a central station or locally on the mobile device, referring to the passive system and active system respectively. In a passive system, the design of mobile device is significantly simplified and can have a long battery life, as no computation effort is required. But the system capacity is limited by the frequency resource. The active system on the contrary allows unlimited amount of mobile devices, because the target device works as signal receiver and computes its position locally similar to GNSS systems.

The determination of the MD coordinate is only possible when sufficient signal measurements are obtained. These information can be any kind of the measurements discussed in previous sections: RSS, AoA, ToA, RTT or TDoA. It can also involve a combination of two or multiple sorts of measurement to achieve an enhanced performance.

Some notations are clarified as follows:
$p$: real coordinate of the mobile device (MD);
$\hat{p}$: position estimation of the mobile device (MD);
$p_i$: coordinates of the access points (APs).

A general relationship between the estimated MD position $\hat{p}$, the measurements $\{m_n\}$ and the known AP locations $\{p_i\}$ can be formulated as:

$$m_n = \mathbf{h}(\hat{p}; p_i) + e_n \tag{2.9}$$

$i = 1, ... N_{AP}$ and $n = 1, ... N_m$, where $N_{AP}$ and $N_m$ refer to the amount of AP and the amount of measurements respectively. The transfer function $\mathbf{h}$ reflects relationship between the positions and the measurement quantities. The error $e$ includes the process error, the measurement error and the signal processing error. The process error comes from the signal distortion due to the multipath fading and the shadowing effect. The error follows a distribution $p_e(e)$ which can be used to evaluate the accuracy performance of the system. As Gaussian distribution can be motivated by asymptotic arguments or the central limit theorem [108], the error is assumed to follow the gaussian distribution:

$$p_e(e) = N(\mu, \sigma^2) = \frac{1}{\sigma\sqrt{2\pi}} e^{-\frac{1}{2}(\frac{e-\mu}{\sigma})^2} \tag{2.10}$$

The measurement has a mean error of $\mu$ and a variance of $\sigma^2$. In a LoS situation, the mean error $\mu = 0$, thus $p_e(e) = N(0, \sigma^2)$. For a error vector $\mathbf{e}$, the error distribution in LoS condition follows:

$$P_e(\mathbf{e}) = N(0, \sigma^2 \mathbf{I}_n) \tag{2.11}$$

Table 2.2 summarizes the information that can be derived from the measurements for positioning, including the geometric information such as range and angle, or the digital summary like fingerprint.

| Measurement | Description | Information for positioning |
|---|---|---|
| RSS | Signal strength | Range: $r_i = \|\hat{p} - p_i\| + e_i$ (power loss model) or Fingerprint: $\{RSS_i\}$ |
| ToA/RTT | Time of arrival/ round trip time of arrival | Range: $r_i = \|\hat{p} - p_i\| + e_i$ (propagation model) |
| TDoA | Time difference of arrival | Range Difference: $\Delta r_{ij} = \|\hat{p} - p_i\| - \|\hat{p} - p_j\| + e_{ij}$ (propagation model) |
| AoA | Angle of arrival | Angle: $\alpha_i = \arccos(\vec{\hat{p}} \cdot \vec{p_i}) + e_i$ (geometric model) |

**Table 2.2:** Information from different measurements used for positioning.

**Regression Model**
Based on the relationship in formula 2.9, the positioning system can be modelled as a regression process:

$$\mathbf{m} \approx \mathbf{h}(\hat{p}; p_i) \tag{2.12}$$

i) The geometry location as unknown parameters: $\hat{p}$, with length of $K$, corresponding to $(\hat{x}, \hat{y})$ for 2D positioning and $(\hat{x}, \hat{y}, \hat{z})$ for 3D positioning.
ii) The known AP locations as independent variables: $p_i$, with size of $N \times 3$, i.e. $N$ nodes with 3D coordinate.
iii) The observed measurements as dependent variables: $\mathbf{m} = \{m_n\}$, with length of $N_m$.

Carrying out regression analysis requires specification of the function $\mathbf{h}$. And the form of this function is based on knowledge about the relationship between $m_n$ and $p_i$ that is determined geometrically or by Fingerprinting. In order to approach the position estimation $\hat{p}$, there should be enough amount of measurements available, i.e. $N_m > K$

(length of vector $\hat{p}$) for solving a non-linear function $\mathbf{h}$.

**Model Analysis**
The error in formula 2.9 implies the distance of the measurements and the estimation $\mathbf{h}(\hat{p}; p_i)$. In other words, the optimum position estimation is achieved by minimizing the error. A standard approach in analyzing the system model is using the least squares (LS) method, in terms of non-linear least squares (NLLS) for solving a non-linear model. "Least squares" means that the estimation minimizes the sum of the squares of the errors made in the results of every single equation in 2.16:

$$\hat{p} = \arg min \sum_{n=1}^{N_m} (m_n - \mathbf{h}(\hat{p}; p_i))^2 \tag{2.13}$$

An example of a model is the positioning system based on ToA measurements, referring to Table 2.2:

$$\hat{p} = \arg min \sum_{m=1}^{N_m} (r_m - \|\hat{p} - p_i\|)^2 \tag{2.14}$$

where $r_m$ denotes the distances between targets and access nodes.
The formula (2.13) describes a regular non-linear least squares regression where measurement errors all have the same variance. In case that assumption is not true, it is appropriate to use a weighted fit:

$$\hat{p} = \arg min \sum_{n=1}^{N_m} \mathbf{W}(m_n - \mathbf{h}(\hat{p}; p_i))^2 \tag{2.15}$$

where $\mathbf{W}$ is a diagonal weight matrix, which is the reciprocal of error variance-covariance matrix $\Sigma = Cov(\mathbf{e})$ of the measurements:

$$\mathbf{W} = \Sigma^{-1} \tag{2.16}$$

The weighted non-linear least squares is also called cost function:

$$\mathbf{e} = (m_n - \mathbf{h}(\hat{p}; p_i))^T \Sigma^{-1} (m_n - \mathbf{h}(\hat{p}; p_i)) \tag{2.17}$$

minimizing the cost function yields the position estimation:

$$\hat{p} = \arg min(\mathbf{e}) \tag{2.18}$$

If the error probability distribution $f_e$ is known, the maximum likelihood (ML) estimator can be used to find the optimal solution by maximize the joint probability, according to Bayes' theorem:

$$\hat{p} = \arg\max \prod_{n=1}^{N_m} f(m_n|\hat{p}) \tag{2.19}$$

where $f(m_n|\hat{p})$ is the probability distribution function of measurements $m_n$ conditioned on position $p$, which is also the likelihood function for $p$. And the product $\prod_{n=1}^{N_m} f(m_n|\hat{p})$ explain a collection of statistically independent measurements, thus the likelihood function factors into a product of individual likelihood functions.

Rewrite formula 2.19 in logarithm form for convenience:

$$\hat{p} = \arg\max \sum_{n=1}^{N_m} \ln f(m_n|\hat{p}) \tag{2.20}$$

where the likelihood function product can be represented with the sum of individual log-likelihood $\sum_{n=1}^{N_m} \ln f(m_n|\hat{p})$, whose derivative is often easier to be computed than the derivative of a product.

As the maximum likelihood is equivalent to achieve a minimum error, it can be represented as minimizing the error:

$$\hat{p} = \arg\min \sum_{n=1}^{N_m} \ln f_e(m_n - \mathbf{h}(\hat{p}; p_i)) \tag{2.21}$$

**Optimization Criteria**
The model analysis results in finding an optimization solution for one of the underlined criteria: non-linear least squares (NLS), weighted non-linear least squares (WNLS), maximum likelihood (ML) or gaussian maximum likelihood (GML) [109] (Table 2.2). The desired solution is determined by either minimizing the least squares cost function or maximizing the likelihood function.

| Optimization Criteria | Description | Criteria Formulation |
|---|---|---|
| NLS | Non-linear Least Squares | $V_{NLS}(p) = (\mathbf{m} - \mathbf{h}(p; p_i))^2 = (\mathbf{m} - \mathbf{h}(p; p_i)^T)(\mathbf{m} - \mathbf{h}(p; p_i))$ |
| WNLS | Weighted Non-linear Least Squares | $V_{WNLS}(p) = (\mathbf{m} - \mathbf{h}(p; p_i))^T \Sigma^{-1}(\mathbf{m} - \mathbf{h}(p; p_i))$ |
| ML | Maximum Likelihood | $V_{ML}(p) = \ln f_e(\mathbf{m} - \mathbf{h}(p; p_i))$ |
| GML | Gaussian Maximum Likelihood | $V_{GML}(p) = (\mathbf{m} - \mathbf{h}(p; p_i))^T \Sigma^{-1}(\mathbf{m} - \mathbf{h}(p; p_i)) + \ln det(\Sigma(p))$ |

**Table 2.3:** Position can be estimated by optimizing one of these criteria: NLS, WNLS, ML or GML.

Each of these methods is suitable for a specific stochastic condition, w.r.t the error distribution characteristics. Optimizing the 2-norm NLS criteria is the best approach, if the errors are independent, identically distributed Gaussian variables, with $f_e = N(0, \rho_e \mathbf{I})$. Otherwise when the errors variance have a dependency on geometry location or variable

over time, the NLS should be weighted accordingly by involving the error covariance matrix $Cov(\mathbf{e}) = \Sigma$. The ML approach provides an efficient estimator, with a given error probability distribution $f_e$. In the special case of a Gaussian error distribution with position-dependent covariance $f_e = \Sigma(p)$ , the GML is prefered, similar to the WNLS, but with the term $\ln det(\Sigma(p))$.

**Root Mean Square Error (RMSE)**
In order to evaluate the performance of the positional accuracy, the root mean square error (RMSE) is frequently invloved, it describes the difference between estimation and ground truth:

$$RMSE = \sqrt{E[\|\hat{p} - p\|^2]} \tag{2.22}$$

Where the operation $E$ calculates the mean value. The RMSE equals to the standard variance of the error, when the estimator is unbiased.

**Cramer-Rao Lower Bound (CRLB)**
The $CRLB$ expressed the lower bound on the variance (or covariance matrix) of any unbiased parameter estimation [110]. It is the theoretical limits for the positioning accuracy. The bound states that the variance of any unbiased estimator is not less than the inverse of the Fisher Information Matrix (FIM) $I(p)$:

$$I(p) = -E[\frac{\partial^2}{\partial p^2} \sum_{n=1}^{N_m} \ln f(m_n|p)] \tag{2.23}$$

$$\tag{2.24}$$

This formula determines the Fischer information as the second order derivative of the natural logarithm of the likelihood function with respect to the parameter $p$.
Then the CRLB is expressed as:

$$E[(\hat{p} - p)(\hat{p} - p)^T] \geq CRLB = \frac{1}{I(p)} \tag{2.25}$$

This comparison of matrices implies a definite condition:

$$(E[(\hat{p} - p)(\hat{p} - p)^T])_{ii} \geq CRLB_{ii} \tag{2.26}$$

In practice, the RMSE of position estimation is determined as the euclidean distance, so the following relation is always true:

$$RMSE^2 = E[\|\hat{p} - p\|^2] \geq tr(cov(\hat{p})) \geq tr(CRLB) \tag{2.27}$$

In a 3D positioning system, the deterministic parameter is the 3 elements vector $p(x, y, z)$ to be estimated from measurements $m_n$. Then the FIM is a $3 \times 3$ matrix:

$$I(p) = \begin{bmatrix} I_{xx} & I_{xy} & I_{xz} \\ I_{xy} & I_{yy} & I_{yz} \\ I_{xz} & I_{yz} & I_{zz} \end{bmatrix} \tag{2.28}$$

With the matrix element at row $r$, column $c$:

$$I_{rc} = -E[\frac{\partial^2}{\partial p_r \partial p_c} \sum_{n=1}^{N_m} \ln f(m_n|p)] \tag{2.29}$$

The variance of the spatial position is then bounded as:

$$var(\hat{x}) \geq \frac{1}{det(I(p))}(I_{yy}I_{zz} - I_{yz}^2) \tag{2.30}$$

$$var(\hat{y}) \geq \frac{1}{det(I(p))}(I_{xx}I_{zz} - I_{xz}^2) \tag{2.31}$$

$$var(\hat{z}) \geq \frac{1}{det(I(p))}(I_{xx}I_{yy} - I_{xy}^2) \tag{2.32}$$

where $det(I(p))$ is the determinant of the matrix. If the estimator is unbiased, then $RMSE^2 = var$:

$$RMSE^2(\hat{x}) = var(\hat{x}) \geq \frac{1}{det(I(p))}(I_{yy}I_{zz} - I_{yz}^2) \tag{2.33}$$

$$RMSE^2(\hat{y}) = var(\hat{y}) \geq \frac{1}{det(I(p))}(I_{xx}I_{zz} - I_{xz}^2) \tag{2.34}$$

$$RMSE^2(\hat{z}) = var(\hat{z}) \geq \frac{1}{det(I(p))}(I_{xx}I_{yy} - I_{xy}^2) \tag{2.35}$$

The impact on the CRLB is dependent on the likelihood function. In practice, different measurement techniques, signal property, signal to noise ratio, effective bandwidth, propagation model and infrastructure geometry lead to different CRLBs. A promising IPS solution is based on a well-designed hardware architecture that is capable of achieving the measurement as accurate as possible.

Next section covers several existing algorithms dedicated to solve the likelihood function/non-linear least squares equations derived from range-based system, i.e. RSS (power loss model-based)/ToA/RTT/TDoA systems. These algorithms are grouped into two categories: analytical algorithms and numerical algorithms.

### 2.3.1. Analytical Algorithms

An analytical algorithm is intended to derive a explicit expression for the parameters. With some assumptions or simplifications, non-linear least-squares positioning equations can be solved analytically, which are extensively documented in literature. The solver is simplified when the APs are arranged linearly. Abel and Smith [111] provide an explicit solution that can achieve the CRLB in the limit of small estimation errors.

Hahn [112] provides an efficient estimator for localizing a distant noisy target. In the situations where APs are placed arbitrarily, finding the solution is more difficult due the non-linearity of the equations. Fand [113] presented an exact solution when the number of measurements is equal to the number of unknown parameters, limited by discarding extra measurements which can be used for accuracy improvement. Chaffee and Abel [114], Bancroft [115] and Chan [116] exploited the quadratic character to get a relatively simple algebraic solution. These methods, however lead to solution ambiguity in computing the square root.

The analytical method for a range-based positioning system is motivated by the capability of accurate measurements. In this case, a set of equations established algebraically are directly used to derive the geolocation. For demonstration simplicity, the following discussion is dedicated for 2D range-based positioning system.

**RSS/ToA/RTT System**
A ToA/RTT based system determine the distances from the APs to the MD by multiplying the one way signal travel time measurements $\Delta t_i$ with the propagation speed $v$:

$$r_i = \Delta t_i * v + e_i \tag{2.36}$$

where $r_i$ is the range between $AP_i$ and the MD, with error $e_i$. In a range-based system by measuring RSS, the $r_i$ is determined based on the introduced propagation model.

Assume the coordinates of three APs, one MD and its estimation as: $p_1(0,0)$, $p_2(x_2, y_2)$, $p_3(x_3, y_3)$, $p(x, y)$, $\hat{p}(\hat{x}, \hat{y})$. The geometry relation is given as:

$$r_i = \|p - p_i\| + e_i \tag{2.37}$$

The relation without the term $e_i$ determines a the ranges estimation $\hat{r}_i$:

$$\hat{r}_i = \Delta t_i * v \tag{2.38}$$
$$\hat{r}_i = \|\hat{p} - p_i\| \tag{2.39}$$

squaring both sides of (2.39):

$$\hat{r_1}^2 = \hat{x}^2 + \hat{y}^2 \tag{2.40}$$
$$\hat{r_2}^2 = (\hat{x} - x_2)^2 + (\hat{y} - y_2)^2 \tag{2.41}$$
$$\hat{r_3}^2 = (\hat{x} - x_3)^2 + (\hat{y} - y_3)^2 \tag{2.42}$$

subtracting (2.40) from (2.41) and (2.42) respectively:

$$\hat{r_2}^2 - \hat{r_1}^2 = x_2^2 - 2x_2\hat{x} + y_2^2 - 2y_2\hat{y} \tag{2.43}$$
$$\hat{r_3}^2 - \hat{r_1}^2 = x_3^2 - 2x_3\hat{x} + y_3^2 - 2y_3\hat{y} \tag{2.44}$$

the position $(x, y)$ can be estimated by solving the matricial form:

$$\mathbf{H}\hat{p} = \mathbf{C} \tag{2.45}$$

where

$$\mathbf{H} = \begin{bmatrix} x_2 & y_2 \\ x_3 & y_3 \end{bmatrix} ; \hat{p} = \begin{bmatrix} \hat{x} \\ \hat{y} \end{bmatrix} ; \mathbf{C} = \frac{1}{2} \begin{bmatrix} x_2^2 + y_2^2 - \hat{r_2}^2 + \hat{r_1}^2 \\ x_3^2 + y_3^2 - \hat{r_3}^2 + \hat{r_1}^2 \end{bmatrix} \tag{2.46}$$

when more measurements are available, the eq. 2.45 is still valid with:

$$\mathbf{H} = \begin{bmatrix} x_2 & y_2 \\ x_3 & y_3 \\ \vdots & \vdots \end{bmatrix} ; \mathbf{C} = \frac{1}{2} \begin{bmatrix} x_2^2 + y_2^2 - \hat{r_2}^2 + \hat{r_1}^2 \\ x_3^2 + y_3^2 - \hat{r_3}^2 + \hat{r_1}^2 \\ \vdots \end{bmatrix} \tag{2.47}$$

The least squares solution of eq. (2.45) is found by the pseudoinverse:

$$\hat{p} = (\mathbf{H}^T \mathbf{H})^{-1} \mathbf{H}^T \mathbf{C} \tag{2.48}$$

When the error $e_i$ follows a zero-mean Gaussian distribution $f_e = N(0, \Sigma)$, with the covariance matrix error $Cov(\mathbf{e}) = \Sigma_2$, the solution for (2.45) can be improved by solving the WNLS problem with the weight matrix $\Sigma_2^{-1}$ [47]:

$$\hat{p} = (\mathbf{H}^T \Sigma_2^{-1} \mathbf{H})^{-1} \mathbf{H}^T \Sigma_2^{-1} \mathbf{C} \tag{2.49}$$

**TDoA System**
Different from the range-based method in the RSS, ToA or RTT system where the range estimation involves two nodes, the TDoA system uses the time difference measurement that is a quantity determined from 3 nodes. The range difference $r_{ij}$ is computed by multiplying the signal propagation speed with the difference of propagation time between $AP_i$ to $MD$ and $AP_j$ to $MD$:

$$r_{ij} = r_i - r_j = \Delta t_{ij} * v + e_{ij} \tag{2.50}$$

similarly, the estimation $r_{ij}$:

$$\hat{r_{ij}} = \Delta t_{ij} * v = \hat{r_i} - \hat{r_j} \tag{2.51}$$

As $\hat{r_2} = \hat{r_2} - \hat{r_1} + \hat{r_1} = \hat{r_{21}} + \hat{r_1}$ substituting the term $\hat{r_2}^2$ in (2.43) with $(\hat{r_{21}} + \hat{r_1})^2$, we get:

$$(\hat{r_{21}} + \hat{r_1})^2 = x_2^2 - 2x_2\hat{x} + y_2^2 - 2y_2\hat{y} + \hat{r_1}^2 \tag{2.52}$$

$$-x_2\hat{x} - y_2\hat{y} = \hat{r_{21}}\hat{r_1} + \frac{1}{2}(\hat{r_{21}}^2 - x_2^2 - y_2^2) \tag{2.53}$$

similarly, from (2.44), we get:

$$(\hat{r_{31}} + \hat{r_1})^2 = x_3^2 - 2x_3\hat{x} + y_3^2 - 2y_3\hat{y} + \hat{r_1}^2 \tag{2.54}$$

$$-x_3\hat{x} - y_3\hat{y} = \hat{r_{31}}\hat{r_1} + \frac{1}{2}(\hat{r_{31}}^2 - x_3^2 - y_3^2) \tag{2.55}$$

rewriting eq. (2.53) and (2.55) in matricial form:

$$\mathbf{H}\hat{p} = r_1\mathbf{C} + \mathbf{D} \tag{2.56}$$

where

$$\mathbf{H} = \begin{bmatrix} x_2 & y_2 \\ x_3 & y_3 \end{bmatrix}; \hat{p} = \begin{bmatrix} \hat{x} \\ \hat{y} \end{bmatrix}; \mathbf{C} = \begin{bmatrix} -\hat{r_{21}} \\ -\hat{r_{31}} \end{bmatrix}; \mathbf{D} = \frac{1}{2}\begin{bmatrix} x_2^2 + y_2^2 - \hat{r}_{21}^2 \\ x_3^2 + y_3^2 - \hat{r}_{31}^2 \end{bmatrix} \tag{2.57}$$

The solution for eq. (2.56) yields to:

$$\hat{p} = r_1\mathbf{H}^{-1}\mathbf{C} + \mathbf{H}^{-1}\mathbf{D} \tag{2.58}$$

Then the position $(x, y)$ can be estimated by solving eq. (2.40) and (2.58).

Again, when more measurements are available, the eq. (2.56) also holds with:

$$\mathbf{H} = \begin{bmatrix} x_2 & y_2 \\ x_3 & y_3 \\ \vdots & \vdots \end{bmatrix}; \mathbf{C} = \begin{bmatrix} -\hat{r_{21}} \\ -\hat{r_{31}} \\ \vdots \end{bmatrix}; \mathbf{D} = \frac{1}{2}\begin{bmatrix} x_2^2 + y_2^2 - \hat{r}_{21}^2 \\ x_3^2 + y_3^2 - \hat{r}_{31}^2 \\ \vdots \end{bmatrix} \tag{2.59}$$

Assuming a similar error possibility distribution function as previously discussed in the RSS/ToA/RTT system, the corresponding intermediate solution is derived as:

$$\hat{p} = (\mathbf{H}^T\Sigma_2^{-1}\mathbf{H})^{-1}\mathbf{H}^T\Sigma_2^{-1}(r_1\mathbf{C} + \mathbf{D}) \tag{2.60}$$

The position $(x, y)$ can be estimated by solving eq. (2.40) and (2.60).

The analytical methods provide a closed form solution, but they are not strict least-squares solutions to the used equations, since the relation between the non-linear term and the unknown parameters is not rigorously exploited.

### 2.3.2. Numerical algorithms

In the general case, there is no closed-form solution to a non-linear least squares problem. Rather than attempting to find the exact solution, numerical algorithms are used to find the estimation $\hat{p}$ that minimizes the error, i.e. a numerical solution of approximation. There is a vast literature on this topic that covers a number of standard approaches for constructing numerical solutions. Those general approaches are called numerical

methods, such as the Newton's method and the Levenberg-Marquardt method.

There are $m$ non-linear functions on $n$ unknown parameters $\mathbf{x}$: $f : \mathbf{R}^n \mapsto \mathbf{R}^m$, with $m \geq n$. The non-linear least squares problems can be modeled as minimizing the object function or cost function $\mathbf{F}(\mathbf{x})$:

$$\hat{\mathbf{x}} = argmin_{\mathbf{x}}\mathbf{F}(\mathbf{x}) \tag{2.61}$$

where

$$\mathbf{F}(\mathbf{x}) = \sum_{i=1}^{m}(f_i(\mathbf{x}))^2 = \mathbf{f}(\mathbf{x})^T\mathbf{f}(\mathbf{x}) \tag{2.62}$$

It has the same form as eq. (2.15), generated from geometry relation for a corresponding positioning system. $f_i(\mathbf{x})$ is the residual function, reflecting the estimation error.

Several definitions have to be clarified before describing the methods. Assume that the object function $\mathbf{F}(\mathbf{x})$ is differentiable and has continuous second partial derivatives. Then we have the Taylor expansion [117]:

$$\mathbf{f}(\mathbf{x+h}) = \mathbf{f}(\mathbf{x}) + \mathbf{J}(\mathbf{x})\mathbf{h} + O(\|\mathbf{h}\|^2) \tag{2.63}$$

where $\mathbf{J}$ is a $m \times n$ Jacobian matrix:

$$\mathbf{J}_{ij}(\mathbf{x}) = \frac{\partial f_i}{\partial x_j}(\mathbf{x}) = \begin{bmatrix} \frac{\partial f_1}{\partial x_1}(\mathbf{x}) & \cdots & \frac{\partial f_1}{\partial x_n}(\mathbf{x}) \\ \vdots & \ddots & \vdots \\ \frac{\partial f_m}{\partial x_1}(\mathbf{x}) & \cdots & \frac{\partial f_m}{\partial x_n}(\mathbf{x}) \end{bmatrix}; \tag{2.64}$$

The gradient of the cost function:

$$\mathbf{F}'(\mathbf{x}) = \begin{bmatrix} \frac{\partial \mathbf{F}}{\partial x_1}(\mathbf{x}) \\ \vdots \\ \frac{\partial \mathbf{F}}{\partial x_n}(\mathbf{x}) \end{bmatrix} = 2\begin{bmatrix} \sum_{i=1}^{m} f_i(\mathbf{x})\frac{\partial f_i}{\partial x_1}(\mathbf{x}) \\ \vdots \\ \sum_{i=1}^{m} f_i(\mathbf{x})\frac{\partial f_i}{\partial x_n}(\mathbf{x}) \end{bmatrix} = 2\mathbf{J}(\mathbf{x})^T\mathbf{f}(\mathbf{x}) \tag{2.65}$$

Further, the Hessian matrix of the cost function can be derived as:

$$\mathbf{F}''(\mathbf{x}) = \begin{bmatrix} \frac{\partial f_1}{\partial x_1^2}(\mathbf{x}) & \frac{\partial f_1}{\partial x_1 \partial x_2}(\mathbf{x}) & \cdots & \frac{\partial f_1}{\partial x_1 \partial x_n}(\mathbf{x}) \\ \frac{\partial f_1}{\partial x_2 \partial x_1}(\mathbf{x}) & \frac{\partial f_1}{\partial x_2^2}(\mathbf{x}) & \cdots & \frac{\partial f_1}{\partial x_2 \partial x_n}(\mathbf{x}) \\ \vdots & \vdots & \ddots & \vdots \\ \frac{\partial f_m}{\partial x_n \partial x_1}(\mathbf{x}) & \frac{\partial f_1}{\partial x_n \partial x_2}(\mathbf{x}) & \cdots & \frac{\partial f_1}{\partial x_n^2}(\mathbf{x}) \end{bmatrix} = 2(\mathbf{J}(\mathbf{x})^T\mathbf{J}(\mathbf{x}) + \sum_{i=1}^{m} f_i(\mathbf{x})\mathbf{f}_i''(\mathbf{x})) \tag{2.66}$$

Since the cost function $\mathbf{F}$ is a sum of non-linear equations $\mathbf{f}(\mathbf{x})$, which is assumed to be differentiable, the cost function itself is also differentiable:

$$\mathbf{F(x+h)} = \mathbf{F(x)} + \mathbf{h}^T \mathbf{F'(x)} + \mathbf{h}^T \mathbf{F''(x)h} + O(\|\mathbf{h}\|^3) \tag{2.67}$$

The sufficient condition for the cost function has a local minimizer at position $\mathbf{x}^*$:

1) zero gradient: $\mathbf{F'(x^*)} = 0$ .
2) positive definite $2^{nd}$ partial derivative: Hessian matrix $\mathbf{F''(x^*)}$ is positive definite, i.e. scalar $\mathbf{z}^T \mathbf{F''(x^*)z}$ is positive for any non-zero scalar column vector $\mathbf{z}$.

All methods for non-linear optimization are iterative: from an initial guess $\mathbf{x}_0$ as the start point to gradually converge to the final solution $\hat{\mathbf{x}}$:

**Iterative Procedure**

**begin**
  **Initiation**: $k := 0; \mathbf{x}_k := \mathbf{x}_0$;
  **Condition**: if **criteria** is met
          then $\hat{\mathbf{x}} := \mathbf{x}_k$, go to **end**
          else go to **Update**
  **Update**: compute h$_k$;
          $\mathbf{x}_{k+1} := \mathbf{x}_k + \mathbf{h}_k$;
          $k := k + 1$;
          go to **Condition**
**end**

The choice of the update term $\mathbf{h}_k$ leads to different iterative methods. The **criteria** defines the condition for ending the iteration and yields the estimation $\hat{\mathbf{x}}$:

$\|\mathbf{h}_k\|$ is sufficiently small: $\|\mathbf{h}_k\| \leq \delta$
or
maximum iteration is reached $k < k_{max}$

The convergence rate is used to describe the efficiency of different iterative algorithms, distinguished by the speed the error is decreasing in each step of the iteration (Table 2.3).

| Convergence pattern | Error decreasing rate |
|---|---|
| Linear Convergence | $\|\mathbf{e}_{k+1}\| \leq \beta \|\mathbf{e}_k\|$, when $\mathbf{e}_k$ is small; $0 < \beta < 1$ |
| Superlinear convergence | $\|\mathbf{e}_{k+1}\| / \|\mathbf{e}_k\|$, for $k \to \infty$ |
| Quadratic convergence | $\|\mathbf{e}_{k+1}\| = O(\|\mathbf{e}_k\|^2)$, when $\mathbf{e}_k$ is small |

**Table 2.4:** Different convergence rate of iterative methods.

Many approaches approximate parameters by iteratively descending the objective function:

$$\mathbf{F(x}_{k+1}) < \mathbf{F(x}_k) \tag{2.68}$$

The parameter update in an iterative descent procedure follows the descent direction $\mathbf{h}_d$:

$$\mathbf{x}_{k+1} := \mathbf{x}_k + \mathbf{h}_k := \mathbf{x}_k + \alpha\mathbf{h}_d \qquad (2.69)$$

where the positive scalar $\alpha$ describes how fast the x will go in the direction $\mathbf{h}_d$. $\mathbf{h}_k$ denotes the update increment. The term $\alpha\mathbf{h}_d$ distinguishes different descent methods. The first order Taylor expansion of the updated function is:

$$\mathbf{F}(\mathbf{x}_k + \alpha\mathbf{h}_d) = \mathbf{F}(\mathbf{x}_k) + \alpha\mathbf{h}_d^T\mathbf{F}'(\mathbf{x}_k) + O(\alpha^2\mathbf{h}_d^T\mathbf{h}_d) \qquad (2.70)$$

We assume a small increment, i.e. $\alpha$ is sufficient small that leads to $O(\alpha^2\mathbf{h}_d^T\mathbf{h}_d) \approx 0$, then we have:

$$\mathbf{F}(\mathbf{x}_k + \alpha\mathbf{h}_d) \approx \mathbf{F}(\mathbf{x}_k) + \alpha\mathbf{h}_d^T\mathbf{F}'(\mathbf{x}_k) \qquad (2.71)$$

In order to have the function descending (eq. 2.71) at $\mathbf{x}_k$, the second term on the right side should be negative:

$$\alpha\mathbf{h}_d^T\mathbf{F}'(\mathbf{x}_k) < 0 \qquad (2.72)$$

This section describes some of the iterative descent algorithms, including the Steepest Descent method, the Newton-Raphson method, the Restricted Descent Method, the Gauss-Newton method, the Levenberg-Marguardt method and the Powell's Dog Leg method. The solution is updated iteratively from an initial guess, until a sufficiently accurate value or the defined maximum iteration is reached. The descending condition (2.72) ensures the convergence towards a minimizer, although there might be multiple minimizers and the found one could be a local minimizer and also not necessarily the closest one to the initial guess.

**Steepest Descent Method**
The Steepest Descent method is also known as gradient method, since the descent direction is opposite to the gradient:

$$\mathbf{h}_d = -\mathbf{F}'(\mathbf{x}_k) \qquad (2.73)$$

thus

$$\mathbf{x}_{k+1} := \mathbf{x}_k + \mathbf{h}_k := \mathbf{x}_k - \alpha\mathbf{F}'(\mathbf{x}_k) \qquad (2.74)$$

The motivation of this direction decision is that the objective function descends fastest in the opposite gradient direction at $\mathbf{x}_k$. Further, the scalar factor $\alpha$ is selected by linear search method by minimizing the updated function [118]:

$$\alpha_{exact} = argmin\mathbf{F}(\mathbf{x}_k + \alpha\mathbf{h}_d); \qquad \alpha > 0 \qquad (2.75)$$

this is also applied to other descent methods in literature to determine the step length, i.e. the exact factor $\alpha$ is chosen to minimize the objective function or its approximation.

The parameter update in Steepest Descent method only involves the first order partial derivative of the objective function, which leads to the advantage of low computation complexity. This method faces the risk of failing to find the minimizer with exact line search in case of $\mathbf{F}'(\mathbf{x}_{k+1})$ being orthogonal to $\mathbf{F}'(\mathbf{x}_k)$. Some function has a narrow curved valley which contains the minimum. The bottom of the valley is very flat. The problem of using steepest descent method to estimate the minimum is that the optimization is zig-zagging [119, 120] slowly with small step sizes towards the minimum, because of the curved flat valley. Another drawback is the slow linear convergence, thus in many cases, this method is used as the initial stage in a hybrid iterative process, where the final stage introduces a faster convergence method like the Newton-Raphson method.

**Newton-Raphson Method**
Replace the gradient in eq. (2.73) with the product of the inverse of Jacobean matrix and the observation functions:

$$\mathbf{h}_d = -\mathbf{J}(\mathbf{x})^{-1}\mathbf{f}(\mathbf{x}) \tag{2.76}$$

Assume the scalar factor $\alpha = 1$. Eq. (2.74) can be rewritten as:

$$\mathbf{x}_{k+1} = \mathbf{x}_k - \mathbf{J}(\mathbf{x})_k^{-1}\mathbf{f}(\mathbf{x}_k) \tag{2.77}$$

This method is called Newton-Raphson method.

To derive this method, recall the Taylor expansion:

$$\mathbf{f}(\mathbf{x}+\mathbf{h}) = \mathbf{f}(\mathbf{x}) + \mathbf{J}(\mathbf{x})\mathbf{h} + O(\|\mathbf{h}\|^2) \tag{2.78}$$

ignore the term $O(\|\mathbf{h}\|^2)$, with sufficient small $\|\mathbf{h}\|^2$, and let $\mathbf{f}(\mathbf{x}+\mathbf{h}) = 0$. Then we get:

$$\mathbf{f}(\mathbf{x}) = -\mathbf{J}(\mathbf{x})\mathbf{h} \tag{2.79}$$

and the descent direction $\mathbf{h}$:

$$\mathbf{h} = -\mathbf{J}(\mathbf{x})^{-1}\mathbf{f}(\mathbf{x}) \tag{2.80}$$

The Newton-Raphson method approximates the root of the non-linear functions $\mathbf{f}(\mathbf{x})$ by iteratively searching the root of its tangent at $\mathbf{x}_k$. But this tangent method requires functions based on accurate measurements. Otherwise, the NLLS optimization is preferred. Fortunately, the quadratic convergence makes the Newton-Raphson method a very efficient solution for the NLLS problem $\mathbf{F}(\mathbf{x})$, for which the update term:

$$\mathbf{h}_k = -\mathbf{F}''(\mathbf{x}_k)^{-1}\mathbf{F}'(\mathbf{x}_k) \tag{2.81}$$

eq. (2.81) can be derived from the derivative of the Taylor expansion of $\mathbf{F}(\mathbf{x})$:

$$\mathbf{F}'(\mathbf{x}_k + \mathbf{h}_k) = \mathbf{F}'(\mathbf{x}_k) + \mathbf{F}''(\mathbf{x}_k)\mathbf{h}_k + O(\|\mathbf{h}_k)\|) \tag{2.82}$$

When $\mathbf{h}_k$ is sufficiently small:

$$\mathbf{F}'(\mathbf{x}_k + \mathbf{h}_k) \approx \mathbf{F}'(\mathbf{x}_k) + \mathbf{F}''(\mathbf{x}_k)\mathbf{h}_k \tag{2.83}$$

assuming a stationary point at $\mathbf{x}_{k+1}$, i.e. $\mathbf{F}'(\mathbf{x}_k + \mathbf{h}_k) = 0$, we get:

$$\mathbf{F}''(\mathbf{x}_k)\mathbf{h}_k = -\mathbf{F}'(\mathbf{x}_k) \tag{2.84}$$

this yields eq. (2.81). If the Hessian matrix is proved to be positive definite and the descending condition (eq. 2.72) is met, the stationary point is a minimizer. Newton-Raphson method is very suitable in the final stage of a hybrid iteration algorithm, since it is derived based on the assumption that the current position is located within a region close to the stationary point. Furthermore, it has a quadratic convergence.

**Restricted Descent Method**
The motivation of so called Restricted Descent method is to figure out a measure which ensures that the determined update term $\mathbf{h}_k$ is sufficiently small to meet the approximation of the Taylor expansion:

$$\mathbf{F}(\mathbf{x}_k + \mathbf{h}_k) = \mathbf{F}(\mathbf{x}_k) + \mathbf{h}_k^T \mathbf{F}'(\mathbf{x}_k) + \mathbf{h}_k^T \mathbf{F}''(\mathbf{x}_k)\mathbf{h}_k + O(\|\mathbf{h}_k)\|^3) \tag{2.85}$$
$$\approx \mathbf{F}(\mathbf{x}_k) + \mathbf{h}_k^T \mathbf{F}'(\mathbf{x}_k) + \mathbf{h}_k^T \mathbf{F}''(\mathbf{x}_k)\mathbf{h}_k \tag{2.86}$$

In order to ignore the fourth term of the expansion $O(\|\mathbf{h}_k)\|^3)$, $\mathbf{h}_k$ should be constrained. There are two solutions for this purpose. The first one is setting a trust region $\mathbf{A}_h$ for the $\mathbf{h}_k$ update and the trust region itself should be also updated accordingly to ensure the descending condition:

$$\|\mathbf{h}_k\| < \mathbf{A}_h \tag{2.87}$$

The second is to update $\mathbf{h}_k$ by adding a damping adjustment $\gamma\mathbf{I}$:

$$\mathbf{h}_k = -(\mathbf{F}''(\mathbf{x}_k) + \gamma\mathbf{I})^{-1}\mathbf{F}'(\mathbf{x}_k) \tag{2.88}$$

where the damping factor $\gamma$ is a non-negative scalar.

Both measures are dedicated to meet the descending condition, i.e. $\mathbf{F}(\mathbf{x}_{k+1}) < \mathbf{F}(\mathbf{x}_k)$. The update of the trust region $\mathbf{A}_h$ and damping factor $\gamma$ depend on the ratio of the increment to the approximated increment of the objective function:

$$r = \frac{\mathbf{h}_k^T \mathbf{F}'(\mathbf{x}_k) + \mathbf{h}_k^T \mathbf{F}''(\mathbf{x}_k)\mathbf{h}_k + O(\|\mathbf{h}_k\|^3)}{\mathbf{h}_k^T \mathbf{F}'(\mathbf{x}_k) + \mathbf{h}_k^T \mathbf{F}''(\mathbf{x}_k)\mathbf{h}_k} \tag{2.89}$$

If $r$ is too large, it means a large $O(\|\mathbf{h}_k\|)\|^3$, the trust region should be increased or the damping factor should be reduced and vice versa. In the case $\gamma = 0$, the damping method is identical to the Newton-Raphson method. On the contrast, it is a Steepest Descent method when $\gamma$ is very large, with a step factor $\alpha = \frac{1}{\gamma}$.

**Gauss-Newton Method**
The derivation of the Gauss-Newton Method start with the observation functions $\mathbf{f(x)}$. Recall the Taylor expansion:

$$\mathbf{f(x+h)} = \mathbf{f(x)} + \mathbf{J(x)h} + O(\|\mathbf{h}\|^2) \tag{2.90}$$

$$\tag{2.91}$$

For sufficiently small $\mathbf{h}$, we get the linear approximation $\mathbf{l(h)}$ on $\mathbf{h}$:

$$\mathbf{f(x+h)} \approx \mathbf{l(h)} = \mathbf{f(x)} + \mathbf{J(x)h} \tag{2.92}$$

thus the approximation of the objective function $\mathbf{F(x)}$ as $\mathbf{L(h)}$:

$$\mathbf{F(x+h)} = \sum \mathbf{f(x)}^T \mathbf{f(x)} \tag{2.93}$$

$$\approx \mathbf{L(h)} \tag{2.94}$$

$$= \mathbf{l(h)}^T \mathbf{l(h)} \tag{2.95}$$

$$= \mathbf{f(x)}^T \mathbf{f(x)} + 2\mathbf{h}^T \mathbf{J(x)}^T \mathbf{f(x)} + \mathbf{h}^T \mathbf{J(x)}^T \mathbf{J(x)h} \tag{2.96}$$

$$= \mathbf{F(x)} + 2\mathbf{h}^T \mathbf{J(x)}^T \mathbf{f(x)} + \mathbf{h}^T \mathbf{J(x)}^T \mathbf{J(x)h} \tag{2.97}$$

The gradient of $\mathbf{L(h)}$ is:

$$\mathbf{L(h)}' = \mathbf{(h)} = (\mathbf{l(h)}^T \mathbf{l(h)})' = \mathbf{J(x)}^T \mathbf{f(x)} + \mathbf{J(x)}^T \mathbf{J(x)h} \tag{2.98}$$

and the second order derivative:

$$\mathbf{L(h)}'' = (\mathbf{L(h)}')' = \mathbf{J(x)}^T \mathbf{J(x)} \tag{2.99}$$

Assume a stationary point $x*$ for $\mathbf{L(h)}$:

$$\mathbf{H}'(0) = \mathbf{J(x)}^T \mathbf{f(x)} + \mathbf{J(x)}^T \mathbf{J(x)h} = 0 \tag{2.100}$$

the update term $\mathbf{h}$ can be yielded from:

$$\mathbf{J(x)}^T \mathbf{J(x)h} = -\mathbf{J(x)}^T \mathbf{f(x)} \tag{2.101}$$

refer to the approximation of the Taylor expansion for small $\mathbf{h}$:

$$\mathbf{F(x + h)} = \mathbf{F(x)} + \mathbf{h}^T \mathbf{F}'(\mathbf{x}) + O(\|\mathbf{h}\|)\|^2) \tag{2.102}$$

$$\approx \mathbf{F(x)} + \mathbf{h}^T \mathbf{F}'(\mathbf{x}) \tag{2.103}$$

refer to eq. (2.100) we have the second term:

$$\mathbf{h}^T \mathbf{F}'(\mathbf{x}) = \mathbf{J}(\mathbf{x})^T \mathbf{f}(\mathbf{x}) = -\mathbf{h}^T \mathbf{J}(\mathbf{x})^T \mathbf{J}(\mathbf{x})\mathbf{h} < 0 \qquad (2.104)$$

This implies the descent condition $\mathbf{F}(\mathbf{x}_{k+1}) < \mathbf{F}(\mathbf{x}_k)$ is met.

Convergence of the Gauss-Newton method depends on the values of the functions $\mathbf{f(x)}$ at the stationary point, i.e. the smaller the values, the faster it converges. This method generally converges linearly, but in the case of zero value of $\mathbf{f(x)}$ at stationary point, it has quadratic convergence as in Newton-Raphson method.

**Levenberg-Marquardt Method**
The Levenberg-Marquardt method is a restricted Gauss-Newton method, with the non-negative damping factor $\gamma$. The stationary condition can be adjusted from eq. (2.100), which yields:

$$\mathbf{J}(\mathbf{x})^T \mathbf{f}(\mathbf{x}) + (\mathbf{J}(\mathbf{x})^T \mathbf{J}(\mathbf{x}) + \gamma \mathbf{I})\mathbf{h} = 0 \qquad (2.105)$$

The damping factor has effects on the update direction and convergence rate. A positive value ensures a descent direction as in the Gauss-Newton method. Its selection determines an iteration process which alternates between Gauss-Newton method and the Steepest Descent method. A general idea is to choose a large $\gamma$ when the current position is far from the solution, otherwise, a small $\gamma$ is a better choice for iteration when then position is very close to the solution to achieve quadratic convergence.

**Powell's Dog Leg Method**
This method combines the Gauss-Newton and the Steepest Descent, with a constrained update step using trust region. Assume the Gauss-Newton step $\mathbf{h}_{gn}$, the Steepest Descent direction $\mathbf{h}_{sd}$, the Dog Leg step $\mathbf{h}_{dl}$ and a trust region $\Delta$. The proposed update scenario is:

---

**Powell's Dog Leg Method**

**begin**
    **Steps Computation**: Gauss-Newton Step $\mathbf{h}_{gn}$; Steepest Descent step $\mathbf{h}_{sd} = \alpha \mathbf{h}_d$;
    **Condition**: if $\|\mathbf{h}_{gn}\| \le \Delta$
                $a = 1, \, b = 0, \, c = 0$;
          else if $\|\alpha \mathbf{h}_{sd}\| \ge \Delta$
                $a = 0, \, b = 1, \, c = 0$
          else
                $a = 0, \, b = 1, \, c = arg_c(\|b\alpha \mathbf{h}_{sd} + c(\mathbf{h}_{gn} - \alpha \mathbf{h}_{sd})\| = \Delta)$
    **Update**: $\mathbf{h}_{dl} := a\mathbf{h}_{gn} + b\alpha \mathbf{h}_{sd} + c(\mathbf{h}_{gn} - \alpha \mathbf{h}_{sd})$
**end**

---

The update of the trust region $\Delta$ is similar to the Restricted Descent method. It is considerably better than the Levenberg-Marquardt method for solving NLLS problems. But it also has the disadvantage of slow linear convergence.

### 2.3.3. Summary

The Steepest Descent method has the least computation complexity but with linear convergence, and it might have the Zigzag problem in the case of an elliptically contoured objective function. The Newton-Raphson method on the contrary has the fastest quadratic convergence, but the computation complexity is much higher in solving a NLLS problem. It is an attractive candidate when the measurement is accurate enough that a approximation of the observation equations is much simpler. The Restricted Descent methods have comparable computation complexity as the Newton-Raphson method but with conditional quadratic convergence. The last three methods have a moderate complexity in computation and linear convergence, among which the Dog Leg method is considered superior to others in solving NLLS problems. A hybrid method is commonly considered to either achieve faster or reliable convergence.

## 2.4. Existing Indoor Positioning Systems

The previous sections demonstrate the basics for indoor positioning system in three aspects: signal, principle and algorithms. Related work in the literature implemented various of technologies. An attempt to describe all these systems is not possible, but some representative examples are presented instead to draw an image of the variety of solutions.

Four famous systems are described in this section: the IRIS system, the Cricket system, the RADAR system and PAL605 UWB system. These examples cover three different positioning signal types. The IRIS system is an optical system based on infrared, the Cricket system introduce both RF signal and ultrasound, the RADAR system and the PAL605 UWB system use RF signal with different frequency range.

**IRIS-LPS**
The first example is an optical system. The IRIS-LPS (Infrared Indoor Scout) [121] locate the objects using infrared. Basic components in this system include a number of IR emitting tags and a stationary mounted stereo camera. The stereo camera consists of two USB cameras with 120 degree lenses mounted 20 cm from each other. The cameras measure AoA of light emitted from the tags, and this is used to triangulate the tags. The light results in a bright spot in the image, and the size and the density of the spot is used to determine distance. The stereo camera is connected to a PC which decompresses the images and performs the real-time image processing. For determination of system accuracy it was installed in a lecture hall. The camera was mounted in front of the blackboard, three metres above the floor, covering a room of $15m \times 9m$. The tag itself consists of one LED with a narrow angle of 20 degrees and range over 10 metres. An exposure time of 2 millisecond is enough for the camera to detect the signal. Reflected infrared interference is excluded by using a mask image during signal processing. The accuracy decreases with increasing distance and angle from the camera and was about 8 cm in near range and 16 cm when covering a room of about 100 $m^2$.

In an demonstration application the users wore headsets with eight IR diodes mounted on top of it, each covering 45 degrees in order to get a greater total coverage, as smaller angle gives better range. Increasing the number of tags (up to about 100) does not have a significant impact on processing time, since the sampling rate remains constant with an increasing number of tags. The two USB cameras are not synchronized and therefore

do not take pictures at exactly the same time, resulting in additional error to track fast motions. A major disadvantage of IR optical systems is that a LoS signal propagation from sender to receiver is required. This system proposed the solution by placing the emitting diodes on the head, which however still limits its application where no obstacle exists. IRIS-IPS can currently only locate the static object with acceptable accuracy. Improvement is necessary for tracking moving objects.

**Cricket**

Compared to IR signal, Ultrasound does not require line of sight between tags and the detector. The Cricket system [90] was developed by researchers from MIT by using ultrasound as the positioning signal. It is actually not a pure acoustic system. RF signal is used as the time stamp for ultrasound time of flight (ToF) measurement and the communication is also done by RF module.

The infrastructure system consists of multiple beacons as transmitters placed on walls and/or ceilings. Cricket listeners are attached onto mobile devices for positioning. The beacon and listener hardware are identical, but running different softwares. The beacons periodically broadcast ultrasonic pulse and their position information on a RF channel simultaneously. Because RF travels about $10^6$ times faster than ultrasound, the listener can then use the time difference of arrival between the start of the RF signal and the corresponding ultrasonic pulse to estimate its distance from the beacon. This is how Cricket solve the problem with synchronizing the beacons and the listeners. The listener provides the location information of the beacon and the associated distance to the host device through an API, and the listener or host device infers its position from such information from multiple beacons.

Since the Cricket beacons broadcast their location information, It has to be given to them in advance when deploying the system. Configuring spatial information in the beacons is easy, while measuring accurate position coordinates is cumbersome. Continuous tracking of objects is harder because a listener hears only one beacon at a time, and updating the position thus takes longer time and is more complex. The update rate would not be high due to the slow propagation speed of ultrasound. Cricket also needs a distributed beacon scheduling scheme to avoid RF and ultrasound collisions at the listeners. Additionally, the power consumption of the Cricket units is high due to sound mechanics, which should draw attention in deploying a practical power supply strategy.

The radios run at a frequency of 433 MHz. With the default transmit power level and antennas, they provide a range of about 30 meters indoors when there are no obstacles. The maximum ultrasound range is 10.5 meters when the listener and the beacon are facing each other and there are no obstacles between them. Cricket can be as accurate as between 1 and 3 cm in real deployments.

**RADAR**

RADAR [79] is an indoor positioning system developed by researchers from Microsoft Research based on RF technology. The development of RADAR was motivated by breaking the limitation of earlier systems: requirement of a specialized infrastructure. Alternatively, this approach makes use of existing RF wireless local area networks (WLANs) to provide accurate localization service. Thus the costs of the positioning system can be dramatically reduced by simplifying the hardware development. It should be noted that RADARs goal is the opposite of the network heterogeneity design goal of

Cricket in the previous section. RADAR eliminates the need for such extra infrastructure but requires the knowledge of location information of WLAN devices for position determination.

WLAN stations in the RADAR system are positioned in a way to provide overlapping coverage. They are enhanced to broadcast beacons periodically. Beacon signal strengths detected by mobile WLAN equipped receivers can be used to estimate the distances for trilateration positioning. Determination of location by RADAR is based on radio fingerprint database that maps measured signal strengths to position coordinates.

RADAR has been deployed in an area of 980 $m^2$ with over 50 rooms, covered by three base stations. The accuracy is about 2-3 meters. It could also use a radio propagation model for distance estimation, but with a degraded accuracy about 4.3 meters.

The accuracy can be improved by using the past position estimation for continuously tracking. With the knowledge of previous position, measurements with large deviations can be discarded. This method is proper based on the assumption of slow motion. The aliasing problem, that two locations that are physically far apart are close to each other in signal strength, can be solved using this technique. The aliasing problem may arise if for example there is an obstruction between a receiver and a base station that are close to each other, while there is no obstruction between the base station and a receiver that is farther away. However, the RADAR system like many other fingerprinting methods would have the performance degraded, since the environment change could violate the available RSSI to position mapping. Another limitation of the RADAR system is that it does not take advantages of the existing WLAN infrastructure in indoor environments.

The Radar system represents the signal strength of an access point at a location by a scalar value, for example, the mean value, and use non-probabilistic approaches to estimate the user location. On the other hand, probabilistic techniques like the Horus system [122] store information about the signal strength distributions from the access points in the radio map and use probabilistic techniques to estimate the user location. It achieves an accuracy performance of better than 60 cm. The Ubicarse system [123] further improves the accuracy of a WLAN-based IPS to 39 cm by involving MIMO antennas and motion sensors.

**PAL650 UWB System**
In order to deal with the fast fading of multi-path propagation, which make the most problematic challenges for positioning indoors, the ultra wide band (UWB) RF signal is introduced. The wide band system dramatically improves the resolution in time measurement compared to narrow band system, offering distinct advantages in precision time-of-flight measurement, multi-path immunity for leading edge detection. An example of an UWB positioning system is the PAL650 system [124], which has been commercially available and used for tracking service in hospitals, factories and military facilities.

The infrastructure of this system consists of a set of active UWB tags, UWB receivers, and a centralized processing unit. One of these UWB tags is used as reference node. Three or more receivers are placed at known positions within or around the area to be monitored. At startup the system is calibrated by monitoring data from the reference node which is placed at a known location. The tags produce bursts of short-pulse RF emissions once every second, and the time difference of arrival (TDoA) of the bursts

are measured at the various receivers and sent back to the central unit for position computation. The tags consume approximately 90 $\mu$W for broadcasting UWB pulses, thus tags powered by one 3V 1Ah Lithium cell battery could work for approximately 4 years. The range of an indoor environments is typically 60 meters. Between several walls, an absolute positioning precision of better than 30 cm is routinely achieved. The system works like many other RF-based systems in NLoS situation but has reduced accuracy.

In recent years, commercially available UWB positioning systems like Ubisense [125], Bespoon [126] and Decawave became very popular. By implementing a two-way ranging (TWR) time-of-flight (ToF) measurements, the Pozyx [127] system based on Decawave [128] achieves a ranging precision of 10 cm .

**Summary**
In this section, 4 existing location systems were basically given, covering three different positioning signals: infrared, ultrasound and radio frequency. Corresponding positioning principle and example implementation are described. Performance and challenges are briefly discussed to show a comprehensive view of individual technology. The next chapter focuses on presenting the methodology in developing the indoor positioning system as base of this work. The complete design procedure of the proposed system is described.

# 3. Research Methodology

This chapter demonstrates the development of a high precision indoor positioning system (Figure 3.1). It starts from formulating the system strategy by setting the requirements, discussing the challenges and proposing the underling system scenario. The developed system is further demonstrated in two sections: system hardware and signal processing system. The first section provides the detailed procedure of the hardware development, including the introduction of the architecture of the hardware system, the involved components and especially the design of the customized RF front-end. The signal processing system section presents the involved key algorithms of the proposed IPS system.



**Figure 3.1:** Work flow of developing the methodology.

## 3.1. System Strategy

Related work in literature has proposed a number of technologies to develop indoor position systems that meet diverse application requirements. Therefore the strategy formulation is initiated by prescribing the requirements of our objective system in terms of performance, such as accuracy, coverage, update rate, cost and so on. Once the list of parameters to capture the requirements is derived, the subsequent challenges need to be thoroughly studied and an appropriate system scenario allocated to deal with these challenges and to fulfill the predefined requirements. The determined scenario decides three essential issues, i.e. signal, principle and algorithm, which lead to specific system architecture and hardware implementation.

### 3.1.1. Requirement Analysis

It is important to state requirement parameters for figuring out suitable technologies. Generally, the derivation of user requirements is accomplished by firstly investigating the potential user groups, thus to determine their associated services. For instance, the robotics control of a production line in a factory require high accuracy in range of $mm \sim cm$ or better, while the latency in sport analysis is a more important criteria and personnel navigation in a shopping mall might be more interested in large capacity. The issue can be concluded by answering the question "**Where** to apply the system for **whom/what**, providing what **service**". Table 3.1 gives the high level requirements of some example applications.

| Example Application | Where | Whom/What | Service |
|---|---|---|---|
| Sport Analysis | Gym | Personal | Tracking |
| Intelligent Warehouse | Warehouse | Forklift Truck | Tracking |
| Shopping Mall Navigation | Shopping Mall | Customers | Indoor Navigation |

**Table 3.1:** High level requirements for example applications.

Evaluation of the high level requirements determine an explicit form of parameters. Table 1.2 in Chapter 1 gives a list of most concerned parameters for a positioning system.

It is clear that the intended system is an indoor application, thus the system will be applied to many indoor environments such as office, shopping mall, factory, warehouse, hospital etc. The object expected to be tracked or provided positioning service can be a robot, a forklift truck, personnel or any moving item. Limited by the indoor space, an object's motion wouldn't be as fast as many movements outdoors like a driving car. For example, personnel navigated in a shopping mall moves normally less than 5 km/h, forklift trucks drive at a speed of less than 20 km/h, etc.. On the other hand, the physical nature of indoor environments implies a relative small region compared to the outdoor application which typically covers kilometers size or even global, the indoor positioning in contrast only requires functionality within meters, tens of meters or maximum multiple hundred meters in some special cases. Furthermore, indoor positioning usually demands higher accuracy compared to outdoor applications.

An adequate definition of requirements comes from the thorough study of the potential applications, aiming at accomplishing the expected performance with limited budget and/or acceptable complexity. It is impractical to set up these requirements freely, due to the large number of criteria which need to be compromised by weighting one against others. The list of different parameters in Figure 3.2 can be used as a general basis for the system assessment.

There is no straightforward method to identify the exact system requirements for a particular application. Additionally, not every parameter in the list is considered critical in an application. As a matter of fact, only some of the listed parameters are explicitly stated as hard requirements, which need to be fulfilled to ensure the expected functionality.

**Figure 3.2:** List of most concerned requirements of an indoor positioning system.

In order to demonstrate the derivation of the parameters, an example application is given for discussion: sport analysis in the gym. The basic ideal of this application is to track the motion of a person in a gym for sport analysis. The parts of the body like arms and legs are to be accurately tracked for purposes like training, medical treatment or scientific research. Firstly, the coverage requirement can be easily set according to the gym space, i.e. the positioning signal should be detected within the gym, thus it can be quantified as "> 10 m", assuming a gym with maximum conversation distance of 10 m. Secondly, arms and legs are to be tracked in this application, which leads to an accuracy requirement comparable to the size of corresponding body parts. The accuracy is accordingly defined as "< 1 cm". Thirdly, another concerned property of sport analysis is speed. The associated requirements include latency and update rate. Latency is a most demanding requirement for a real-time tracking system. It implies the delay between the time of event and when it is available to the user. The record of human footspeed was 44.72 km/h (12.4 m/s or 27.8 mph), seen during the final 100 meters sprint of the World Championships in Berlin on August 16th, 2009 by Usain Bolt. For indoor sport analysis, we set the up limit of the motion to be half of the record, i.e. around 22 km/h. The developed system should compute the position within the duration of a position change of 1 cm, which means a latency of less than 1.64 ms (without implementing a predictive model). Another criteria related to speed is the update rate. Higher update rate indicates more precise tracking, resulting a smoother trajectory. With a update rate of 50Hz, the track is maximally spaced by 12 cm, assuming the motion speed of 22 km/h. Additionally, the system should be able to work in NLoS situation, because the body part might be blocked during movement.

Table 3.3 summarizes some of the requirement parameters that our developed system is expected to accomplish. Other function irrelevant criteria listed in table 3.2 are not considered as hard requirements however could be evaluated during performance analysis of the prototype implementation.

| Criteria | Criteria Description | Goal Value |
|---|---|---|
| Accuracy | Estimation Error | < 1 cm |
| Coverage | Applicable environment size | > 10 m |
| Update rate | Object position update rate | > 50 Hz |
| Latency | Time to determine the position | < 1.64 ms |
| NLoS Positoning | Positioning capability during NLoS situation | Yes |

**Table 3.2:** Design requirements for the developed system

### 3.1.2. Challenges Analysis

Key problematic issues forming the bottleneck in precise positioning indoors are sourced from the complicated indoor environment and the limited hardware solutions. Typical indoor environments like an office, a laboratory or a warehouse are usually equipped with many furnitures, instruments or any obstacles that cause several challenges for positioning: multipath interference, Non-Line-of-Sight (NLoS) situation, attenuation and scattering, dynamic environment, limited hardware resource, high requirement for positioning precision.

**Multipath Interference**

For those systems based on RF signal, the enclosed and furnished indoor environment provides plenty of reflection sources, which induce sever multipath effects (Figure 3.3). The small scale fading caused by multipath time delay spread is a characteristic of radio propagation resulting from the presence of reflectors and scatterers that cause multiple versions of the transmitted signal to arrive at the receiver, each distorted in amplitude, phase and angle of arrival.
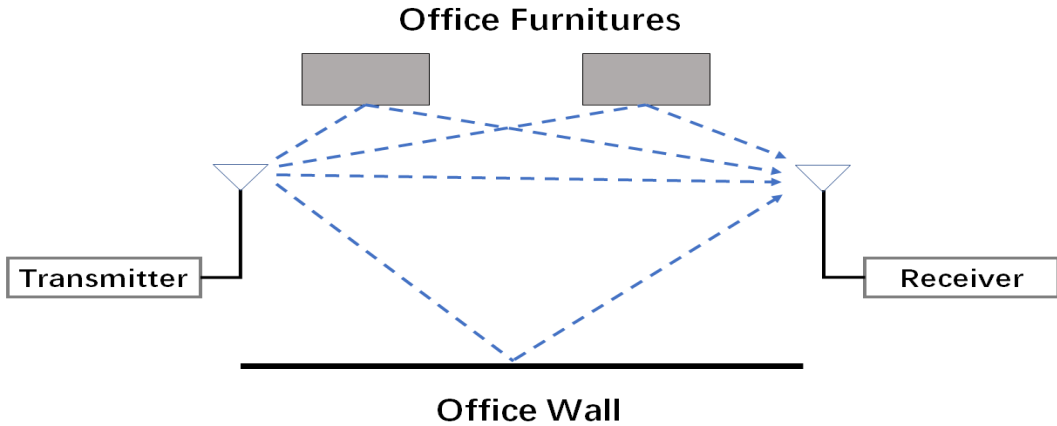


**Figure 3.3:** Multipath propagation in an indoor environment.

The receiving antenna collects many different rays from different directions, producing a rapidly fluctuating RF signal.

**Non-Line-of-Sight (NLoS) Propagation**

The the line-of-sight (LoS) path between transmitter and receiver may be obstructed, especially in case of dense multipath propagation environments, which are full of obstacles, walls, and other objects. A LoS path, also called a direct path (DP), is a straight line path that connects the transmitter and the receiver. Without the presence of the LoS

path, the transmitted signal could only reach the receiver through penetrated, reflected, diffracted, or scattered paths called non-line-of-sight (NLoS) paths.
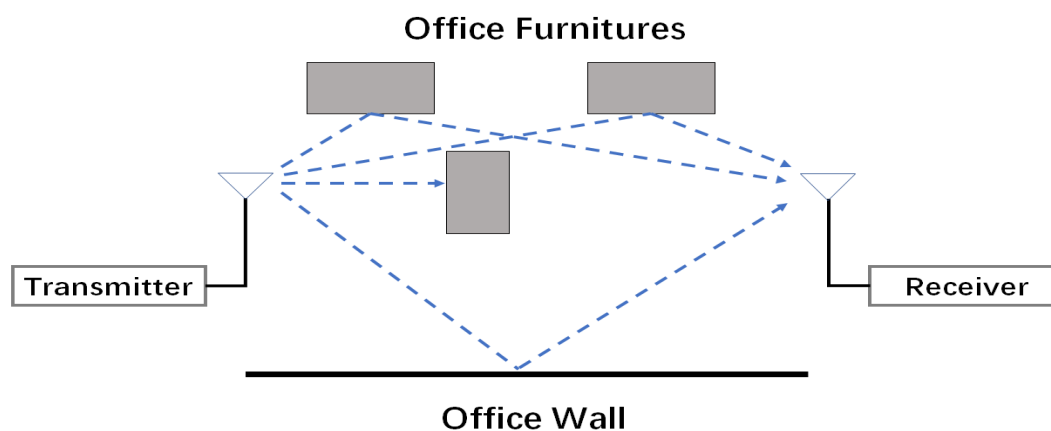


**Figure 3.4:** Line of sight signal is blocked by some obstacle.

However, if the innermost Fresnel zone is not completely obstructed, the receiver could actually detect the LoS signal but partially deflected.

**Attenuation and Scattering**
The strength of waves decreases with distance between transmitter and receiver. Based on certain propagation models, the attenuation can be used to determine the distance. However, in indoor environments with many obstructions, distance estimation using attenuation is usually less accurate than by time measurement, and the signal scattering worsens the accuracy in addition.

**Dynamic Environment**
The presence of moving objects like a person and a robot in motion may cause fast temporal changes of the environment. This dynamic behaviour makes the signal strength measurement less reliable and might also lead to presence of NLoS propagation.

**Limited Hardware Resource**
The implementation of the designed system involves the usage of various hardwares, including commercial standard components and customized modules. Each hardware is expected to accomplish a specific function, e.g. signal preprocessing, computation, communication, etc. Selection of these components severely depends on the underlying positioning technologies. Compromises are frequently made between cost, complexity, performance, etc., while ensuring the functionality of the system. In many cases, some special technique requirements could not be met by any of the existing standard modules. Thus developers have to design their own hardware instead of attempting to obtain them from the market. The limitation of available components make it challenging to develop a customized hardware. For example, the sampling rate of analog-to-digital chip might not be high enough, the sensitivity of the receiver might be too low and so on.

**Higher Precision Requirement**
Accurate position measurement is a critical requirement for indoor positioning techniques. Compared to the positioning outdoors, sensing location in indoor environments

requires a higher precision (typically in range of sub-meter, centimeter or even milimeter) and is a more challenging task in part because various objects reflect and disperse signals.

### 3.1.3. System Scenario

This section describes the procedure of determining an appropriate positioning technology. The proposed system scenario aims to figure out three essential issues discussed in chapter 2: positioning signal, positioning principle and positioning algorithms.

**Positioning Signal**
The existing technologies that have been reported involve four different positioning signals, i.e. Optical, Radio Frequency, Magnetic Field and Acoustic Signal. Based on some performance matrices comparisons of these technologies are summarized in Table 3.3.

| Comparison of different technologies for IPS | | | | | |
|---|---|---|---|---|---|
| | Optical System | Acoustic System | RF System | Magnetic System | |
| Typical Coverage [m] | $1-10$ | $2 \sim 10$ | $1 \sim$ 'global' | $1 \sim 5$ | $5 \sim 300$ |
| Typical Accuracy | 0.1mm $\sim$ m | cm $\sim$ m | cm $\sim$ m | mm $\sim$ cm | dm $\sim$ m |
| Update Rate | high | low | high | high | high |
| NLoS Positioning | no | yes | yes | yes | yes |
| Cost | high | medium /low | medium /low | high | medium /low |

**Table 3.3:** Comparison of different technologies for indoor positioning system.

The RF-based system turns out to be a suitable option to meet the requirements listed in Table 3.2.

The RF system in context covers a set of technologies that can be distinguished either by frequency allocation or by specific wireless communication standard. Some well known technologies like WLAN, ZigBee, Bluetooth, Radar, UWB, Cellular Networks, Pseudolites, etc. have been long investigated. Generally, wider bandwidth results in more accurate positioning. This is based on the foundation that the wider bandwidth signal could achieve a higher temporal resolution compared to the narrow band system.

Table 3.4 compares the accuracy and coverage performance of some popular RF-based indoor positioning technologies. The pseudolite system and the UWB system perform superior to other approaches on the aspect of accuracy. However, there are some fundamental issues that limit further improvement of a pseudolite system. These include the legality of transmitting on GPS frequencies (L1/L2 bands) and the limited multipath mitigation offered by GPS positioning codes (C/A codes). Other problems inherent to all pseudolite systems such as near-far effect and synchronization complicates the design and deployment of such systems and places limits on its operational effectiveness [132]. The UWB technology achieves the highest accuracy among all the listed candi-

| Comparison of different RF-based technologies for IPS | | | | |
|---|---|---|---|---|
| | Frequency | Typical Accuracy | Typical Coverage | References |
| RFID | 125KHz $\sim$ 134.2KHz, 13.56MHz, 860MHz $\sim$ 960MHz, 2.45GHz | 15cm $\sim$ 3m | 1m $\sim$ 50m | [28, 29, 30, 31, 32] |
| Pseudolite | 1GHz, 1.57GHz, 2.4GHz | 2cm $\sim$ 10cm | 3m $\sim$ 50km | [129, 130, 131] |
| Wifi | 2.4GHz band, 5.8GHz Band | 1m $\sim$ 30m | 20m $\sim$ 50m | [21, 22, 23, 24, 25, 26, 27] |
| Bluetooth | 2.4GHz band | 5m $\sim$ 100m | 20m $\sim$ 50m | [33, 34, 35, 36] |
| UWB | 3.1GHz $\sim$ 10.6GHz | 1cm $\sim$ 1.5m | 1m $\sim$ 100m | [37, 38, 39, 40, 41] |

**Table 3.4:** Comparison of different RF-based technologies for indoor positioning system.

dates, since it has a bandwidth of greater than 500 MHz. The main concern regarding UWB technology is the potential interference that they could cause to existing RF systems in the frequency domain as well as to specific critical wireless systems that provide an important public service. Thus the usage of UWB has to be compliant with local regulations (ETSI, FCC etc.). For example, the FCC Part 15.209 rules limit the emissions for intentional radiators to $50\mu$V/m measured at a distance of 3 meters in a 1MHz bandwidth for frequencies greater than 960MHz. This corresponds to an emitted power spectral density of -41.3dBm/MHz. The low power emission limits the coverage or requires a complicated high sensitive receiver design. Typical UWB-based systems which realized the centimeter accuracy work promisingly within a range of less than 10 meter. The detection of the UWB signal require a long data acquisition duration, which results in a low position update rate typically less than 25 Hz [133, 134, 135].

Based on the previous considerations, the development of a narrow band RF system is thought to be an appropriate approach, using UHF within the license-free ISM band. The UHF signal is capable of providing an excellent temporal resolution and the narrow bandwidth minimizes the possible interference to existing frequency users. The high allowed effective radiated power (ERP) relaxes the RF link loss budget and reduces the hardware complexity. It makes the system more robust by improving the signal-to-noise ratio (SNR) and increasing the dynamic range.

**Positioning Principle**

The functionality of an IPS is accomplished based on sensing the positioning signal. And the interested information carried by the signal can be classified into two categories intensity and time, as demonstrated previously in chapter 2. All these either signal strength based measurements or time based measurements lead to diverse positioning principles, including RSS (progation model, fingerprinting), AoA, ToA, RTT and TDoA.
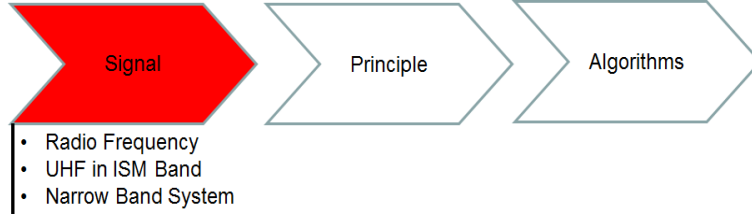
**Figure 3.5:** Radio frequency is chosen as the positioning signal for the IPS.

Firstly, the RSS-based methods measure the received signals strength from/to several reference nodes. The RSSI information is either used to estimate the distance using certain propagation model or used to map the fingerprint that was calibrated in advance. However, the inaccurate propagation model and severe multipath interference in the indoor environment result in meter-level positioning error, which makes it not suitable for the target system. Secondly, the AoA-based approaches determine the position by intersection of several signal propagation direction lines. An optical system could perform the best accurate positioning by AoA method, since the propagation of light is strictly a line. But when it is applied in an RF system, the signal reflections turns to be a problematic issue degrading the angle estimation. Additionally, the requirement of LoS transmission also excludes the AoA method from our options. Thirdly, ToA systems rely on precise propagation time measurements. The harsh requirement on precise synchronization between all the transmitters and receivers is difficult and expensive. Moreover, clock jitter is an important factor that affects the accuracy of the ToA estimation because clock synchronization is needed between the nodes to estimate the time of arrival accurately. In contrast, although no synchronization between the transmitters and receivers required in RTT methods, it is difficult for the measuring unit to know the exact delay/processing time caused by the responder. 1 ns error in time estimation leads to 30cm error in range. The last one is the TDoA-based system which measures the delta in time between the signal's transmission time, thus estimates the position by computing the intersection of hyperbolas. Compared to ToA approach, it doesn't require synchronization between transmitters and receivers, but only between reference nodes instead. TDoA is a more effective solution as there is no synchronization between the target nodes and the reference nodes when the reference nodes are synchronized among themselves [136, 137, 138]. A comparison is summarized in the table 3.5.

The ToA and TDoA methods have higher accuracy compared to other systems [139]. Related study shows an identical theoretical lower bound of positioning accuracy by using TDoA method and ToA method [140]. The TDoA method requires processing of more information, compared to ToA method. But the system architecture of a TDoA system is much less complex than that of a ToA system due to the eased synchronization requirement. Thus the TDoA solution was proposed for IPS implementation.

**Positioning Algorithms**
Hyperbolic positioning is accomplished in two stages. The first stage involves estimation of the TDoAs of the signal from a source, between pairs of receivers by using time delay estimation techniques. In the second stage, the estimated TDoAs are transformed into range difference between reference nodes, resulting in a set of non-linear hyperbolic equations. Thus the key processing phases involved in a TDoA-based indoor positioning system include the TDoA estimation and the Hyperbolic equations solver.

| Methods | RSS | AoA | ToA | RTT | TDoA |
|---|---|---|---|---|---|
| Measurements | Signal strength | Signal propagation direction | Signal propagation time | Signal propagation time | Difference of signal propagation time |
| Position Fix | Trilateration or fingerprinting | Intersection of direction lines | Intesection of spheres | Intesection of spheres | Intersection of hyperbolas |
| NLoS Positioning | yes | no | yes | yes | yes |
| Synchronization Requirement | no | no | Snychronization bewteen senders and receivers | no | Synchronization between reference nodes |
| Accuracy | m | dm $\sim$ m | cm $\sim$ m | m | cm $\sim$ m |
| Disadvantage | Channel inconsistency | Complicated antenna array | Relative clock drift | Fluctuation of delay/processing time | Computation complexity |

**Table 3.5:** Comparison of different RF-based technologies for indoor positioning system.
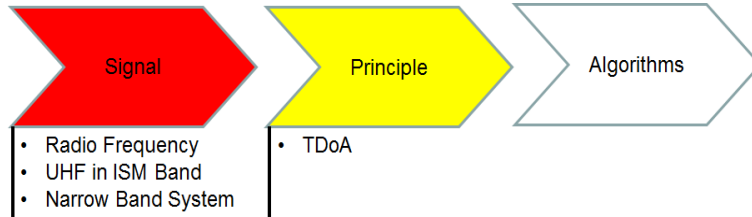


**Figure 3.6:** The proposed positioning system is based on the TDoA technology.

## I. TDoA Estimator

The literature review chapter discusses the technical background of a hyperbolic positioning system, like Loran-C and many other well known systems. The essential task for achieving high positioning precision is an accurate delay estimation, specifically, the TDoA estimation. Several existing methods are investigated in [141] to extract TDoA information from radio signals. Some of the possible candidates include peak detection, leading edge detection, envelope detection, cross correlation detection and use of template waveforms.

## • Leading Edge Detection (Threshold Detection)

Times, at which a certain defined threshold is met by arriving edges of received signals within respective cycle, are noted. The difference of these times is termed as TDoA. Let $t_1$ be the time at which threshold is crossed by first received signal and $t_2$ be the time at which second received signal reaches the threshold then $TDoA = t_2 - t_1$.

## • Peak Detection Methods

Estimation of peak position has huge impact on accuracy of estimated position. Some peak detection methods have been reported in literature including Iterative Peak Subtraction, Matched Filter (MF), Leading Edge Detection, First Peak Detection and Received Signal Strength [2]. Table 3.6 compares the listed peak detection methods.

| Peak/Edge Detection Methods | | | |
|---|---|---|---|
| Algorithm | RMSE(mm) | Max Error(mm) | Min Error(mm) |
| Received Signal Strength | 44.9 | 234 | 1.01 |
| Matched Filter | 89.2 | 421 | 3.38 |
| First Peak | 4.85 | 10.7 | 0 |
| Iterative Peak Subtraction | 9.27 | 53.0 | .182 |
| Leading Edge | 0.920 | 4.9619.4 | 0.121 |

**Table 3.6:** Simulation results of positioning (3D) error using peak detection and leading edge detection algorithms[2].

Let $t_{p_1}$ be time at which the highest peak of first received signal exists and $t_{p_2}$ be the time at which the highest peak of second received signal exists. Then the time difference of arrival is measured as:

$TDoA = t_{p_1}$ - $t_{p_2}$

**• Envelope and Threshold Detection**
An envelope is obtained for each received signal using half wave rectification and low pass filtering. Threshold detection is applied to these envelopes to find the time difference of arrival. Let $t_{ET_1}$ be the time at which threshold is met on envelope of the first received signal and $t_{ET_2}$ be the time at which the envelope of the second received signal achieves the threshold then:

$TDoA = t_{ET_1}$ - $t_{ET_2}$

**• Threshold+Cross Correlation Detection**
A certain window length also called correlation window is selected using the threshold method. Applying cross correlation on long signals will require high computational complexity. Time index of correlation peak gives time difference of arrival of two signals.

**Summary**
In a dense multi-path environment, the earlier the signal feature (leading edge or peak) extracted the more precise the moment of arrival detected, thus a more accurate TDoA estimation could be achieved. On this basis, the leading edge would perform the best as depicted in the Table 3.6. However, the leading edge method severely depend on the effective bandwidth and is sensitive to the amplitude interference, damping and attenuation. The first peak approach on the contrast is more reliable than the leading edge method. We developed a TDoA estimator based on the first peak approach, together with a threshold crossover arbitrator for rough event detection.

**II. Hyperbolic Equations Solver**
The hyperbolic positioning system estimates the target position by finding the intersection point of two or more hyperbolas formed by range differences of multiple anchor nodes from the target [142]. At least three anchor nodes are required to resolve a 2D position in a hyperbolic positioning system, while minimum four nodes are necessary for 3D. Once the TDoA estimates have been obtained, they are converted to range differences by multiplying them with the signal propagation speed. These range differences can be converted into hyperbolic equations. As these equations are non-linear, solving them is not a trivial operation. Many non-linear equation solver have been studied in

chapter 2.

Let the $\bar{p}(x, y, z)$ be the target position and $\bar{q}(x_i, y_i, z_i)$ be the $i^{th}$ anchor node position then range between $\bar{p}(x, y, z)$ and $\bar{q}(x_i, y_i, z_i)$ can be given as:

$$\|\bar{p}(x, y, z) - \bar{q}(x_i, y_i, z_i)\| = (t_i - t_0) \times v + e_i \tag{3.1}$$

Where $\|\bar{p}(x, y, z) - \bar{q}(x_i, y_i, z_i)\| = \sqrt{(x - x_i)^2 + (y - y_i)^2 + (z - z_i)^2}$

$i = 1, 2, 3, .....N$

$N$ is Total number of anchors, $t_i$ is time of arrival at anchor node i, $t_0$ is the start of the transmission from target node, $v$ is the speed of the transmitting signal and the N is the total number of anchors. $e_i$ represents the overall error due to the process and measurement. Assuming an ignorable $e_i$, the range between target and $j_{th}$ anchor node is given as:

$$\|\bar{p}(x, y, z) - \bar{q}(x_j, y_j, z_j)\| = (t_j - t_0) \times v \tag{3.2}$$

The distance difference between the target to the pairwise anchor nodes can be derived:

$$\|\bar{p}(x, y, z) - \bar{q}(x_i, y_i, z_i)\| - \|\bar{p}(x, y, z) - \bar{q}(x_j, y_j, z_j)\| = (t_i - t_j) \times v \tag{3.3}$$

$$\|\bar{p}(x, y, z) - \bar{q}(x_i, y_i, z_i)\| - \|\bar{p}(x, y, z) - \bar{q}(x_j, y_j, z_j)\| = TDoA_{ij} \times v \tag{3.4}$$

$$\sqrt{(x - x_i)^2 + (y - y_i)^2 + (z - z_i)^2} - \sqrt{(x - x_j)^2 + (y - y_j)^2 + (z - z_j)^2} = TDoA_{ij} \times v \tag{3.5}$$

Many algorithms have been investigated in Chapter 2 to solve the non-linear equations (3.5), including the analytical and the numerical approaches. Solving non-linear equations analytically leads to great computation complexity. Among the referred numerical methods, the Newton-Raphson method is an efficient and light algorithm to estimate the position on the basis of ignorable TDoA error.
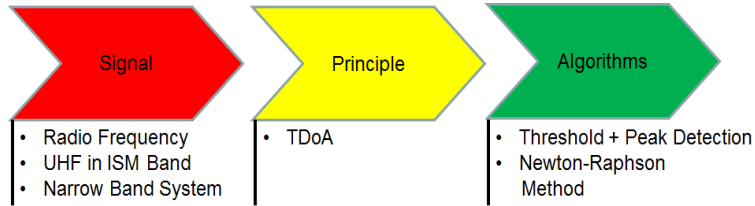


**Figure 3.7:** The processing unit implements the peak detection for TDoA estimation and Newton-Raphson method to solve the hyperbolic equations.

## 3.2. System Hardware

As illustrated in the first part of the strategy section, we proposed a narrow band RF system in UHF range of the ISM band. The hardware development section details the design of the system hardware, including brief introduction of some commercial components and design procedures of the customized RF front-end. A specific hardware architecture is demonstrated, which details the fundamental system structure and design of the customized RF front-end. The circuit design procedure of the customized front-end, including the circuit simulation, elements selection and PCB fabrication is described in detail. PCB measurements for individual modules and the completed design are also presented.

This section introduces the system architecture and hardware design. It deploys a RF receiver network within an indoor environment. In this system, all receivers in the network are synchronized by the same clock source via cables. A high-performance, low additive phase noise LVCMOS clock buffer is involved to replicate multiple clock signals from the common source. No synchronization between target and receiver is required. The customized receiver front-end is fabricated on a 4 layer stack PCB with material FR-4. It works as the interface between the RF antenna and the data acquisition board (FMC108). At least 4 receivers are necessary for 3D positioning by hyperbolic position fix method.
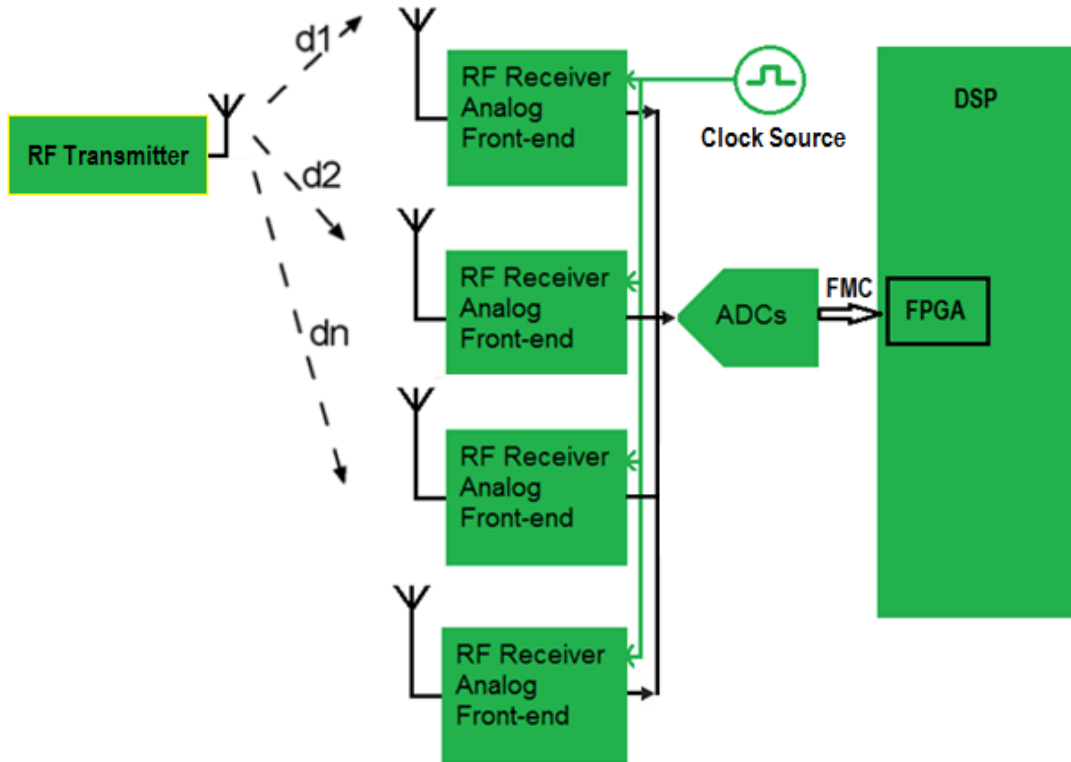


**Figure 3.8:** Signal chain of the proposed system, multi-channel receivers are required to determine the coordinate of the transmitter.

The proposed system consists of the transmitter section and the receiver section. The RF signal generator is introduced to generated the positioning signal in the interested frequency with OOK modulation. The receiver is constructed by a customized RF

front-end, a fast data acquisition board FMC108 and a signal processing platform.
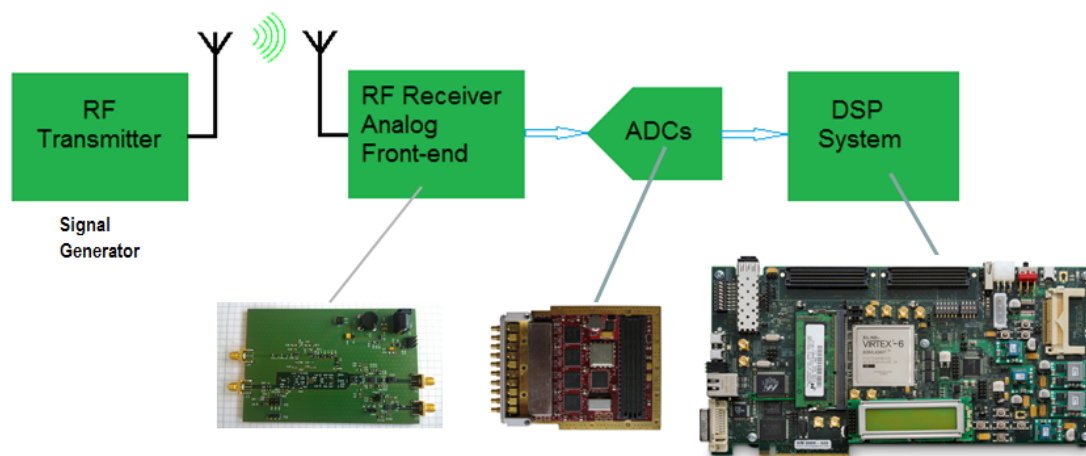


**Figure 3.9:** Block diagram of the signal chain components.

The developed RF front-end is dedicated to sub-sample the UHF radio signal, enabling the data acquisition board to sample the signal with high equivalent time resolution. The acquisition ADC board supports maximum 8 channels, 14 bits resolution at max. 250 Msps. Data is forwarded to the signal processing platform ML605 via FMC interface. The algorithms can be either implemented on the ML605 FPGA evaluation kit or on a work station.

**Developing Tools**
The tools invoked in this work are intended to accomplish these developing tasks: circuit simulation, high frequency component simulation and PCB design. Simulations are carried out separately for the high frequency part and the low frequency circuit. The sub-sampling mixer is simulated in Advance Design System (ADS), the lowpass filter and Op-amps circuit are simulated using LTspice and the high frequency component is simulated in HFSS. For the circuit fabrication, the Altium Designer is involved to develop the PCB layout.

### 3.2.1. RF transmitter

Based on the consideration of system verification and design flexibility, the signal generation for the developed prototype system involves two instruments instead of a customized transmitter design. One is an arbitrary waveform generator M8190A, used to generate the baseband signal. The other is the RF signal generator N5181B intended to modulate the baseband signal with a specific UHF carrier.

**Arbitrary Waveform Generator M8190A**
It benefits from the flexibility in baseband signal generation as to evaluate different signalling strategies. The Keysight M8190A is a powerful instrument, ensuring accuracy and repeatability with 14-bit resolution, up to 8 GSa/s sampling rate and up to 90 dBc Spurious Free Dynamic range (SFDR). It provides digital and analog outputs, either single-ended or differential. The remarkable bandwidth enables a frequency resolution of 100 mHz. In addition to the baseband signal generation, this instrument is also

used to generate the clocks, which drives the pulse strobe signal for the customized RF front-end board.

**RF Analog Signal Generator N5181B**

The RF analog signal generator N5181B MXG X-Series is used as the transmitter. It is working in frequency range from 9 kHz to 6 GHz, with the output power scalable from -144 dBm to +26 dBm at 1 GHz. Many modulation schemes are supported, e.g. AM, FM and PM. External baseband signal input can be used, which is provided by the M8190A.

**Signal Pattern**

The transmitter is supposed to continuously emit a periodic positioning signal. A simple modulation scheme on-off keying (OOK) is proposed in our prototype system for verification purpose (Figure 3.10).
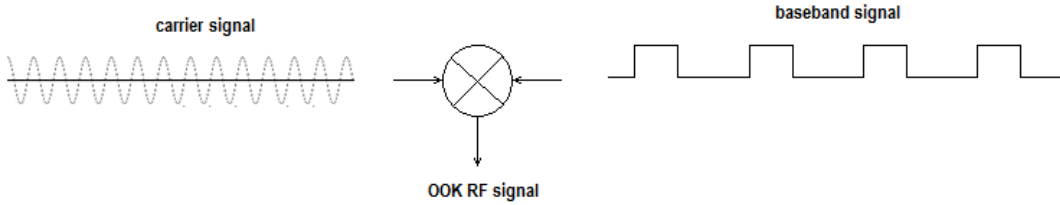


**Figure 3.10:** The transmitter emits periodic OOK modulated signal.

### 3.2.2. Sampling ADC

The component interfacing the RF front-ends and the digital signal processing unit is the FMC108.

The FMC108 is an eight channel ADC FMC daughter card. It provides eight 14-bit 250Msps ADC channels which can be clocked by an internal clock source (optionally locked to an external reference) or an externally supplied sample clock. There is one trigger input for customized sampling control. The FMC108 is mechanically and electrically compliant to FMC standard (ANSI/VITA 57.1). The card has a high-pin count connector and front panel I/O. It can be used in a conduction-cooled environment.

The design is based on TIs ADS62P49 dual-channel 14-bit 250Msps ADC with programmable DDR LVDS or parallel CMOS outputs. The analog signal input can be either AC- or DC-coupled, connecting to SSMC coax connectors on the front panel. The AC- or DC-coupling is a build option that must be specified at the time of order.

The FMC108 allows flexible control of sampling frequency, analog input gain, and offset correction through serial communication busses. The card is also equipped with power supply and temperature monitoring and offers several power-down modes to switch off unused functions or protect the card from overheating.

### 3.2.3. DSP Platform

The positioning computation is carried out on a digital signal processing platform. There are minimum 4 channels signals (corresponding to receivers) are involved in this system for 3D positioning, with the sample rate in range of megahertz. A FPGA platform is preferred to the DSP or MCU solutions, as it has a higher processing speed and more I/O resources. What's more, as the algorithms are modeled and simulated in MAT-LAB/Simulink, the implementation can be accelerated with the usage of the HDL Coder.

The Virtex-6 FPGA ML605 Evaluation Kit includes all the basic components of hardware, design tools, IP, and a pre-verified reference design for system designs that demand high-performance, serial connectivity and advanced memory interfacing. The included pre-verified reference designs and industry-standard FPGA Mezzanine Connectors (FMC) allow scaling and customization with daughter cards.

This Kit collect the digitized signal from ADCs daughter board FMC108 via FMC connector. Positioning algorithms can be implemented either locally or on a work station.

### 3.2.4. RF receiver

This section presents the development of customized receiver front-end. Components are individually discussed.

Data acquisition of high speed signal is a major challenge in developing a high accuracy Indoor Position System (IPS) based on Ultra High Frequency (UHF) Radio. The proposed front-end is developed to achieve a high time resolution for Time Difference of Arrival (TDoA) estimation in a hyperbolic position fix IPS. This component works as the interface component embedded in the distributed receiver nodes of the IPS and is dedicated to convert the incoming UHF signal down to low frequency typically less than 1 MHz that enables the use of conventional relative low speed ADCs. The output low speed analog signal is fed into the ADCs card FMC108.
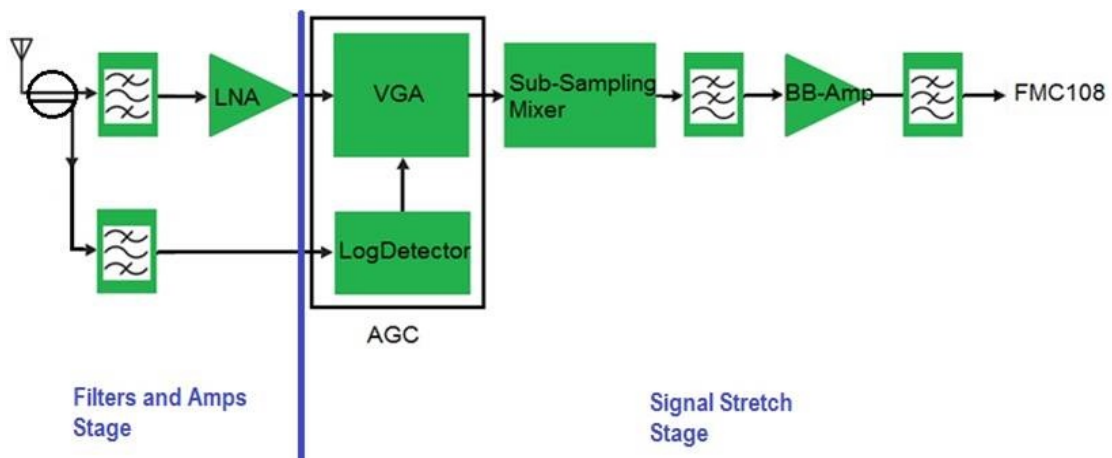


**Figure 3.11:** The proposed front-end block diagram, stretching and forwarding the low speed signal to ADCs acquisition board.

The block diagram in Figure 3.11 shows the architecture of the customized front-end. Two antenna channels detect two separate frequencies. One of the frequency is used for positioning, the other is power correlated with the positioning frequency and is intended to build up the Automatic Gain Controller (AGC).

The developed receiver front-end is splitted into two functional stages, i.e. the Filters&LNAs stage and the Signal Stretch stage. The incoming RF signal is filtered and amplified in the Filters&LNAs stage. The proposed Signal Stretch stage further amplifies the filtered signal with a AGC loop and stretches it down to a desired low frequency range for data acquisition.

**Signal filtering and amplifying**

The basic functionality of this stage is to filter and amplify the incoming RF signal, which consists of two frequency tones. One is the positioning frequency (modulated UHF signal) used for target positioning, while the other is an Continuous Wave (CW) signal dedicated for the power sensing in the AGC loop. A wide-band directional coupler with less than 0.30 dB insertion loss in the bandwidth (698 MHz to 2700 MHz) is placed next to the antenna output. It feeds a portion of the received signal into the power detector in the AGC for detecting the signal strength. The LNA stage for the positioning tone is constructed by 3 stages Infineon BGA825L6S and has an overall gain of 45 dB and a noise figure of less than 0.7 dB. Two surface acoustic wave (SAW) band-pass filters are connected to both output of the directional coupler for filtering. Meanwhile, the power sensing route following the coupler is connected to another SAW filter centering at 869MHZ.
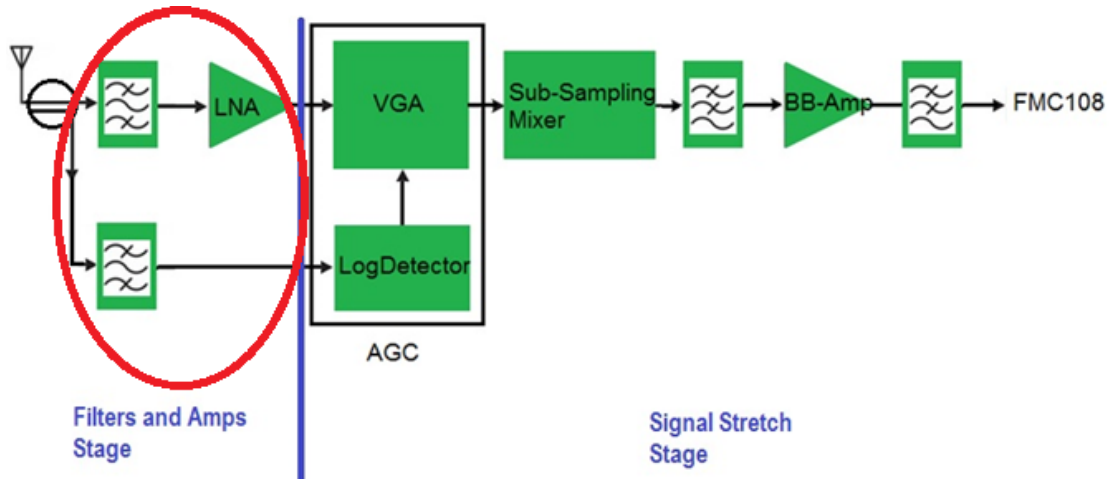


**Figure 3.12:** The filter and amplifer stage is constructed by SAW filters and low noise amplifers.

**Automatic Gain Controlling**

In a RF system, the transmitted signal is attenuated in propagation distance and influenced by the channel. In order to achieve a large dynamic range, an automatic gain controller (AGC) is implemented. The proposed AGC loop introduces the wideband variable gain amplifier from Analog Devices ADL5330. It is a high performance, voltage-controlled variable gain amplifier/attenuator for use in applications with frequencies up to 3 GHz. A wide gain control range from -34 dB to 22 dB at 900 MHz can be reached. The variable gain amplifier (VGA) collaborates with the logarithmic power detector AD8318, which is a demodulating logarithmic amplifier, capable of accurately convert-

ing an RF input signal to a corresponding decibel-scaled output voltage. It has a high detection input range of typically 60 dB with an error of less than $\pm 1$ dB.
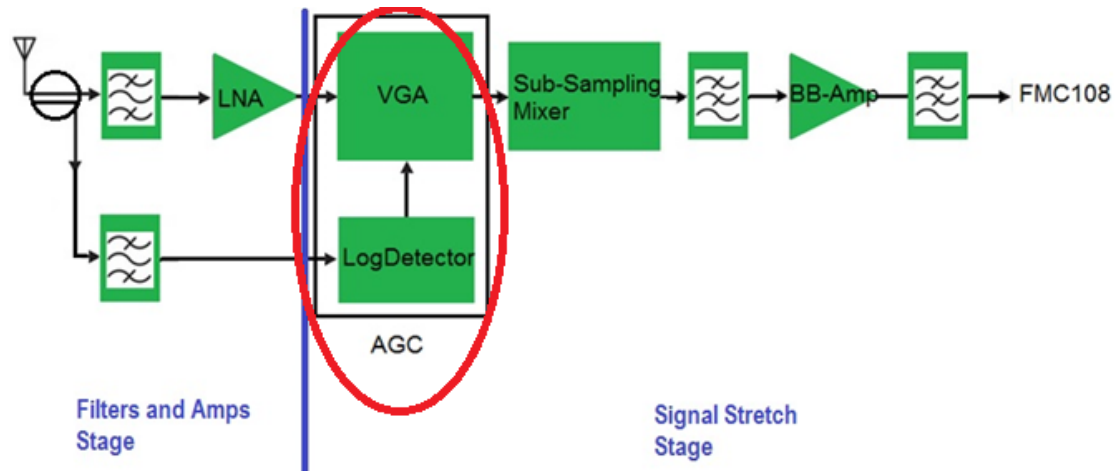


**Figure 3.13:** The AGC loop is constructed by the power detector AD8318 and the variable gain amplifier ADL5330, increasing the dynamic range.

Figure 3.13 shows the location of the AGC module. It increases the dynamic range of the system by 40 dB (Figure 3.14). The frequency for power sensing is in range of 869.7~870 MHz and is generated as continuous wave.
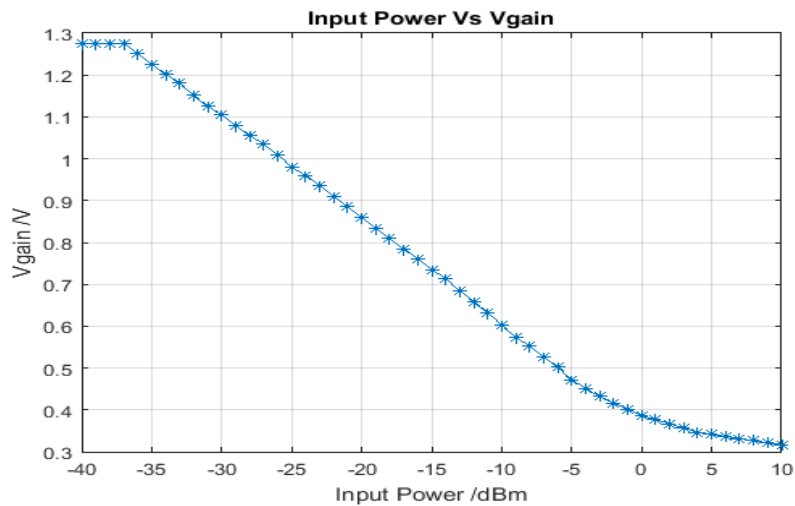


**Figure 3.14:** The measured linear range of the AGC is about 40dB .

**Quasi Time Stretching**
This subsection describes the circuit which follows the AGC. It is constructed by a sub-sampling mixer and a baseband filtering & amplification circuit (Figure 3.15).

In order to develop a high precise IPS based on time measurement methods, a high time resolution is required. For instance, a positioning precision of 1 mm needs a time resolution of 3 picoseconds. This can be realized by direct sampling of the UHF radio signal, which in return requires high speed Analog-to-Digital Converters (ADC) device
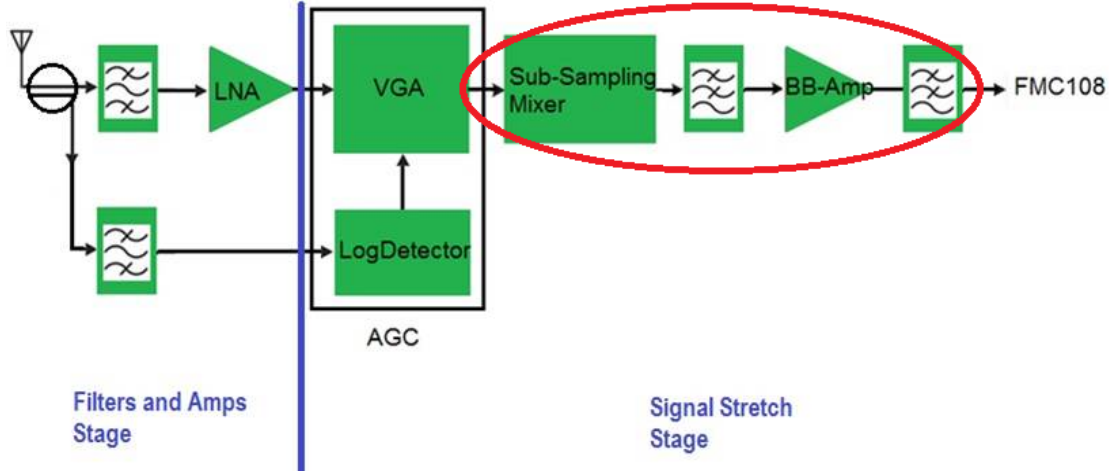
**Figure 3.15:** The proposed signal stretch circuit is constructed by a sub-sampling mixer and a baseband filtering & amplification circuit

that are capable of 330 GSPS conversion rate. A photonic time-stretched ADC concept was proposed by Yan Han and Bahram Jalali [143], but it requires a complicated optical front-end design and a large bank of electronic ADCs. I.e. 330 ADCs at 100 MSPS are required to accomplish an effective sampling rate of 33 GSPS. That number would be increased by 4 times if implemented into the depicted 4 sensors system (Figure 3.16). Another limitation of a conventional ADC is that the ADC should avoid directly sampling the UHF signal due to the signal distortion [144], as the typical aperture time of a relatively low speed ADC is in order of ns. The proposed technology is developed to achieve an effective sampling bandwidth that is broad enough for sampling UHF signals using only one conventional ADC for each sensor. It converts the pulse modulated UHF ($\sim GHz$) signal down to low frequency ($\sim MHz$) signal, meanwhile keeping the timing information. The high time resolution is achieved by stretching the pulse modulated UHF signal, with a factor of $N(\sim O(10^3))$. Specifically, the time resolution is the result of ADC sampling interval divided by stretch factor N, without any interpolation process.

The intuitive view of the developed component is probing the pulse modulated radio signal periodically and rebuilding a single period signal from the continuous N periods (Figure 3.17).

The receiver receives periodic pulse modulated UHF signal $S(t)$, with a signal period of T. It is sampled by the sub-sampling mixer with sampling interval $T_s = T + \Delta T$. $X(n)$ is the resulted set of samples:

$$X(n) = S(n * Ts) = S(n * (T + \Delta T)) = S(n * \Delta T) \tag{3.6}$$

where $n = 0, 1, 2, \cdots$. As the period of $S(t)$ is T, the repetition rate of $X(n)$ is the ratio $N = T/\Delta T$, which leads to a period of $N * T_s$. Formula 3.6 can be rewritten to:

$$X(n) = S(n * Ts) = S(n * (T + \Delta T)) = S(n * (N + 1) * \Delta T) \tag{3.7}$$
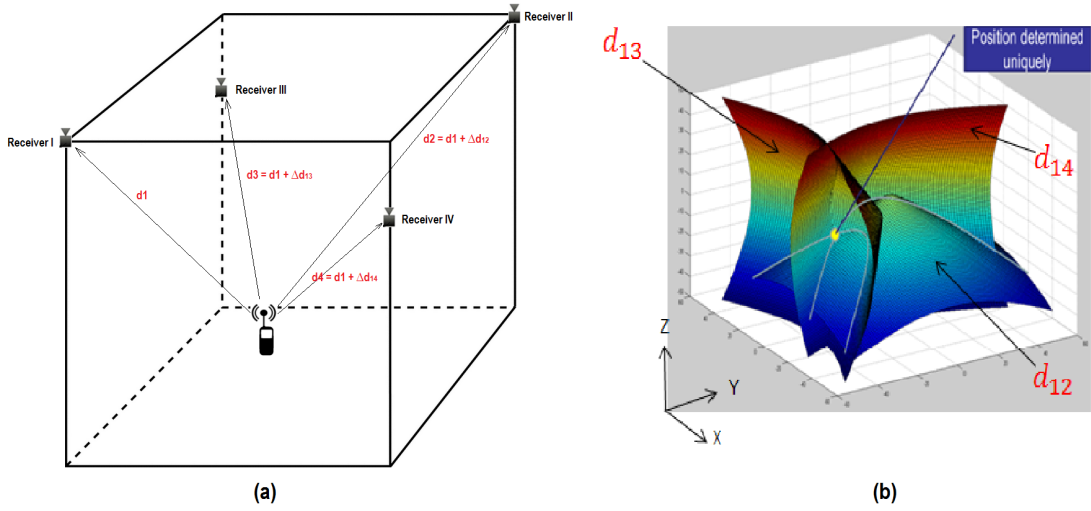
**Figure 3.16:** Example sensor network for a hyperbolic position fix indoor positioning system. RF receivers are placed at known positions (left). The target emitter is located by TDoA information of pairwise receivers (right).
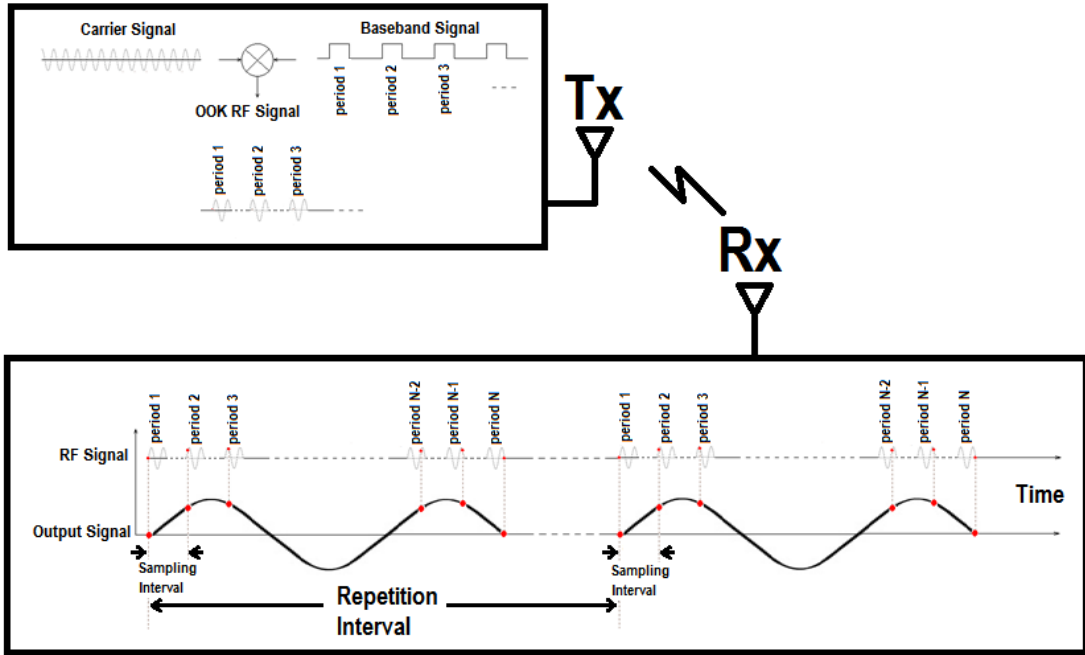


**Figure 3.17:** Reconstruction of one wavelet from N signal periods. The transmitter emits OOK modulated signal. The receiver reconstructs one period signal from sampling N periods (in analog domain).

Formula 3.7 implies that the signal $X(t)$ is a time scaled version of $S(t)$, with the scaling factor of $N + 1$. Feeding $X(n)$ to an appropriate low pass filter results in the stretched signal $X(t)$:

$$X(t) = \alpha(t) * S[(N + 1) * t] \qquad (3.8)$$

Where $\alpha(t)$ is the attenuation function due to filtering. According to the scaling property of the Fourier transform, the frequency of the signal is compressed by $N + 1$ times.

This stretched signal can be sampled by a conventional low speed ADC. The following chapters outline the circuit design, present the simulation results and close with conclusion.

**Circuit Design**
The key requirement of a high precision time-based IPS is the high time resolution. In order to meet the positioning requirement, a dedicated front-end circuit is expected to capture the high speed signal. But it is difficult or costly to accomplish this task with conventional techniques. An alternative solution is to reconstruct the signal pattern rather than the signal itself. The basic idea is implementing a sampling interval close to the signal period. Consequently, one period signal (signal pattern) can be reconstructed by sampling multiple period signals.

The aperture time of low speed ADCs is in range of ns, which means the ADCs are too slow to sample high speed positioning signal (UHF). The signal samples are distorted due to the mismatch. The proposed solution is sampling the incoming signal by the sampling bridge, which is widely used in oscilloscopes. The sampling bridge works as a *track and hold* module. Charge is stored by a fast RC loop and discharged by a slow RC loop. Filtering the output of the sampling bridge with a low pass filter, a stretched signal is obtained. It can be sampled by conventional low speed ADC directly.

The underlying circuit consists of four functional blocks (Figure 3.18). They are a sub-nanosecond pulse generator, a sampling bridge, a solid arc shape Wilkinson power combiner and a wave former which consists of low pass filter and amplifiers. The output is a rebuilt signal which is equivalently time stretched by a factor of N. The factor N is determined by the difference of the probing clock rate and the signal repetition rate.

The pulse generator is designed to generate a pulse sequence with the pulse width of around 100 ps. It introduces the SRD (Step Recovery Diode) SMMD837 and two transmission lines to generate a pair of oppositely polarized pulses. The Wilkinson power combiner is used to minimize the energy loss of the intermediate frequency signal by matching impedance of the IF output to the IF amplifier input. The low pass filter and op-amps then produce a quasi time stretched pulse modulated signal.

**A. Sub-nanosecond Pulse Generator**
Ultra short pulse generators in order of sub-nanosecond have long been researched. A number of reports documenting technologies using tunnel diodes [145], field effect transistors [146], bipolar transistors [147], or step recovery diode [148] have been presented, among which the generator based on the step recovery diode is capable of achieving a fast transition time while consuming moderate power [149]. The pulse generator described in this work introduces the step recovery diode SMMD837 to generate oppositely polarized pulses with pulse width of 100ps and amplitude of 5 V (Figure 3.19). Instead of implementing large area HF transition structure, this component invokes two short microstrip delay lines, simplifying the generator design and producing strong and clean pulses.

The circuit comprises three functional blocks. The driver circuit generates a sharp falling edge by switching the transistor BJT1 and the differential element C3. C1 works as an acceleration capacitor and R1 limit the transistor base current. RC circuit elements R2 and C2 configure the conducting duration of the transistors. The negative driving pulse
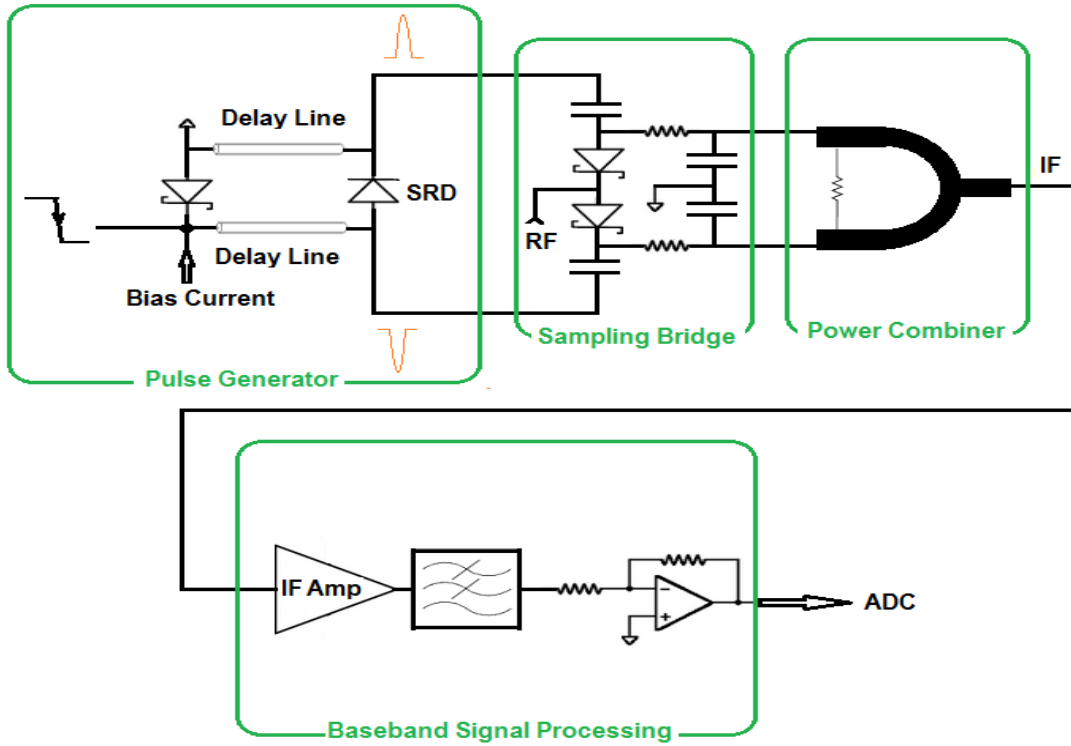
**Figure 3.18:** Simplified block diagram of the proposed system, including pulse generator, sampling bridge, power combiner and baseband Signal Processing module.

turns on the Schottky diode DIODE1, meanwhile the SRD diode DIODE2 is turned off which is previously forward biased by the bias current sourced from circuit R9 and L1. The SRD will keep low impedance until the stored charge is removed. During the storage time, the current through the SRD will keep almost constant but reversely flow away from the diode. The falling edge on the anode traveling back through the transmission line TL1 and is inverted to rising edge by reflecting from the ground. The combination of the edges thus generates a negative Gaussian-like pulse. Analogously, the reversed current flows via TL2 generating another Gaussian-like pulse but positively polarized. Diodes in the pulse shaper unit suppress the unwanted ringing. Capacitors C7, C8 and resistors R11 and R12 block the DC offset and match the circuit to decrease the insertion loss and pulse distortion. The lengths of the implemented microstrip delay lines determine the pulse width. Delay lines of 4 mm are implemented in the example design. The resultant pulses have amplitude of 1.2 V and width of 100 ps, with desirably small ringing (Fig. 3.20). The generated pulse sequence is used as the sampling switch control signal for the sampling bridge.

**B. Sampling Bridge**
The sampling bridge employed in this design implements a symmetric structure which consists of two sampling diodes [150] (Figure 3.21).

In order to accomplish a broad bandwidth and low conversion loss, the sample and hold capacitor should be of appropriate value that is small enough for wide band frequency and big enough for charge storage. Here capacitors of 0.5 pF are used referring to simulation results to achieve a small conversion loss and charging time. Input strobe pulses are fed from the SRD pulse generator. The trigger pulses will forward-bias the
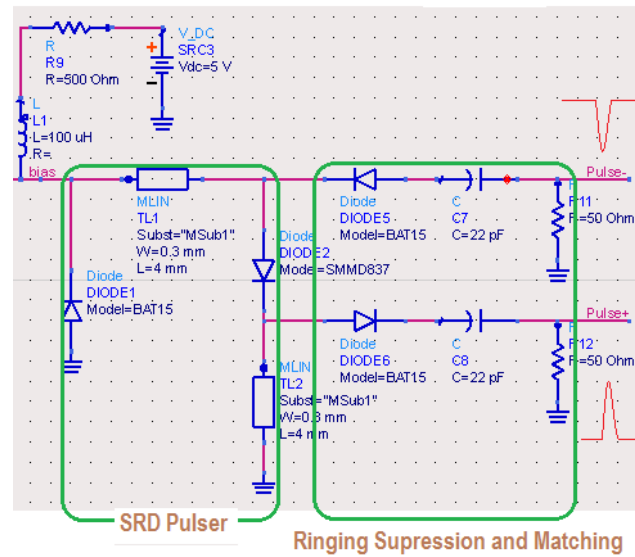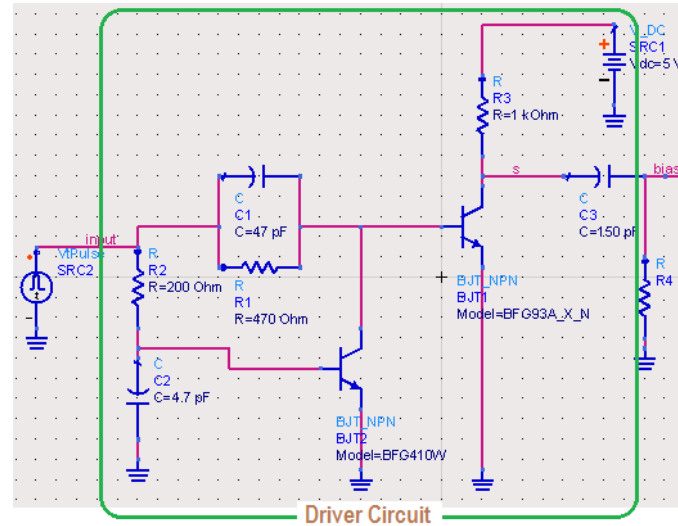
**(a)**
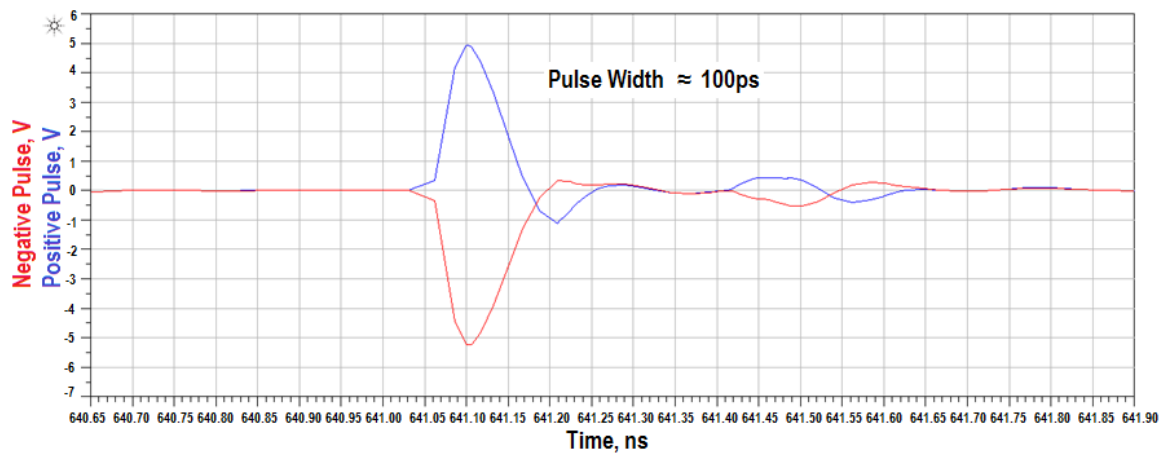


**(b)**

**Figure 3.19:** Circuit diagram of sub-nanosecond pulse generator, which is modeled and simulated in Advance Design System (ADS) (a). Simulation result of generated oppositely polarized pulses of small ringing and high amplitude (b).
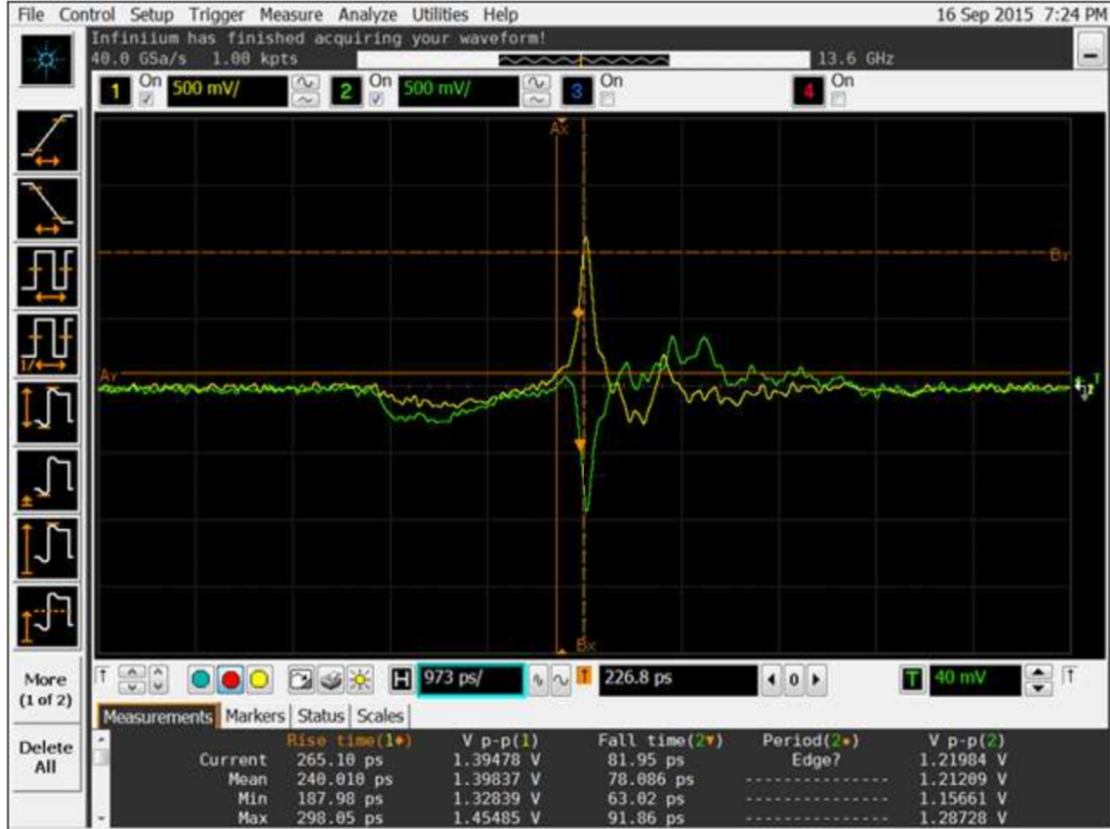
**Figure 3.20:** Measured pulses, with Vp-p of 1.2V and gating window of less than 100 ps, assuming a threshold of 0.6V.

Schottky diodes and start charging the two signal capturing capacitances C1 and C2 by sampling the RF signal. Detector Schottky diode SMS7261 from Skyworks Solutions, Inc. is introduced to build up the sampler. It has a junction capacitor of 0.1 pF and a series resistor of 12 Ohm. This capacitance is sufficiently small compared to C1 and C2, resulting fast charging process and less conversion loss.

**C. Wilkinson Power Combiner**
Because of the symmetric structure of the sampling bridge, there are two identical IF outputs, which are further converged at the Wilkinson power combiner [151] to minimize the power loss. Due to the routing restriction of the PCB design, the employed power combiner spans over four layers (Figure 3.22b), with the matching resistor on the top layer and a solid arc shape input branches on the bottom layer (Figure 3.22a). The arc shape combiner arms make it flexible to adjust the phases of the two input IF signals.

The proposed power combiner obtains an insertion loss of $1 \sim 3$ dB in frequency range of 800 MHz to 1.8 GHz (Figure 3.23a) and a phase difference between two arms is less than 2 degree (Figure 3.23b).

**D. Low Pass Filter and Amplifiers**
A 3rd order Chebychev low pass filter is employed to filter out the unwanted harmonics and high frequency components. It is constructed by three capacitors and two inductors. The simulated result shows a 3 dB bandwidth of 1.1 MHz and ripple of 0.05 dB in pass band. A baseband amplifier is required to amplify the quasi time stretched pulse
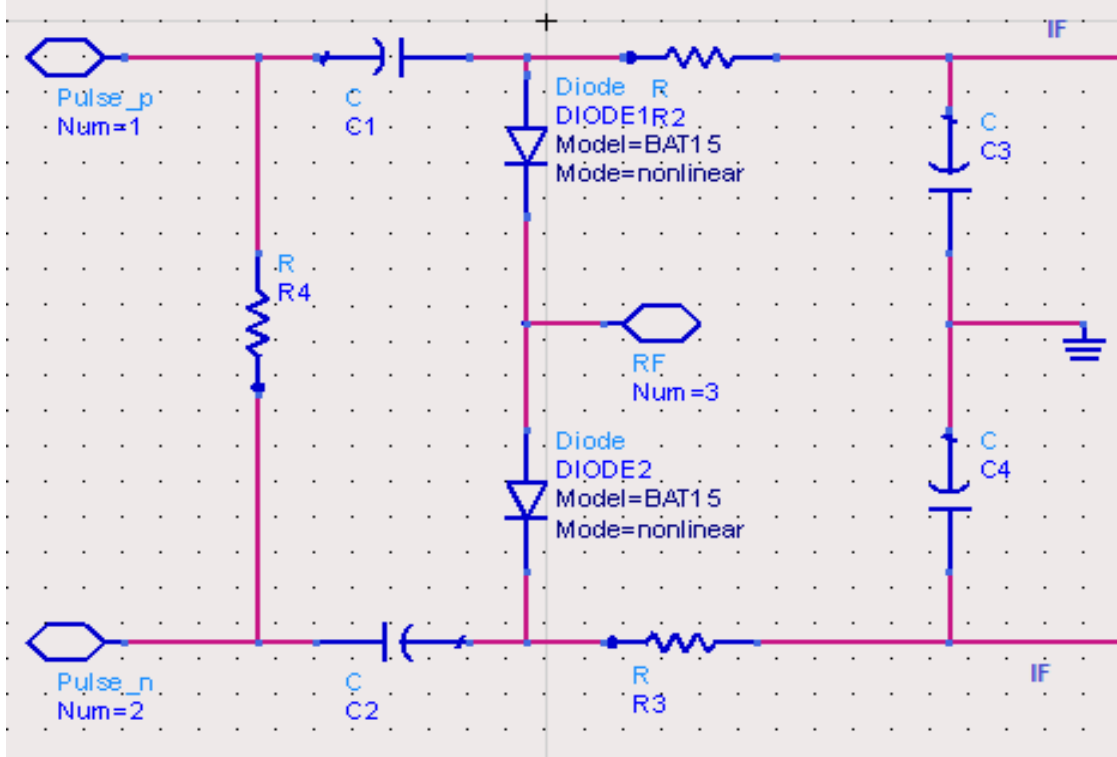
**Figure 3.21:** Sampling bridge consists of two sampling diodes. It samples and holds the incoming RF signal.

modulated signal. Two Op-amps (LT6230) are cascaded as the baseband amplifier. The amplification gain is configured to 59 dB.

**Simulation**

The simulation involves a diode model BAT15 based on the Schottky diode SMS7261. A continuous wave of 1575 MHz is used as the carrier frequency. The modulation pulse repetition rate is 3 MHz, deriving a period T = 333.33 ns. The modulation pulse width is set to 5 ns. The modulated signal is fed into the RF signal input of the sampling bridge and output an intermediate signal from the IF ports of the sampling bridge. By setting the strobe pulse repetition period offset with respect to the signal period to be $\delta t = 0.05$ ns, the stretch rate will be $T/\delta t + 1 = 6667.67$, i.e. 6667.67 times stretched to be smaller than 1 MHz (Figure 3.24). Figure 3.24(a) refers to one segment of the received periodic RF signal Figure 3.24(b). Figure 3.24(c) is the stretched signal by sub-sampling the received signal Figure 3.24(b). An equivalent time resolution of 1.5 ps can be achieved by sampling the baseband signal with ADC at 100 MSPS. This means a better performance than expected can be realized.

The presented design is embedded in an IPS receiver analog front-end. It is fabricated on a 4 layers stack (Figure 3.22b) of 1.6mm thick (refer to appendix for stacks detail).

**Example measurement**

RF input is sourced from a signal generator with a frequency of 1.575GHz and amplitude of -10dBm. AGC gain is fixed to 20 dB. The stretch rate $K$ can be determined:

**(a)**



**(b)**
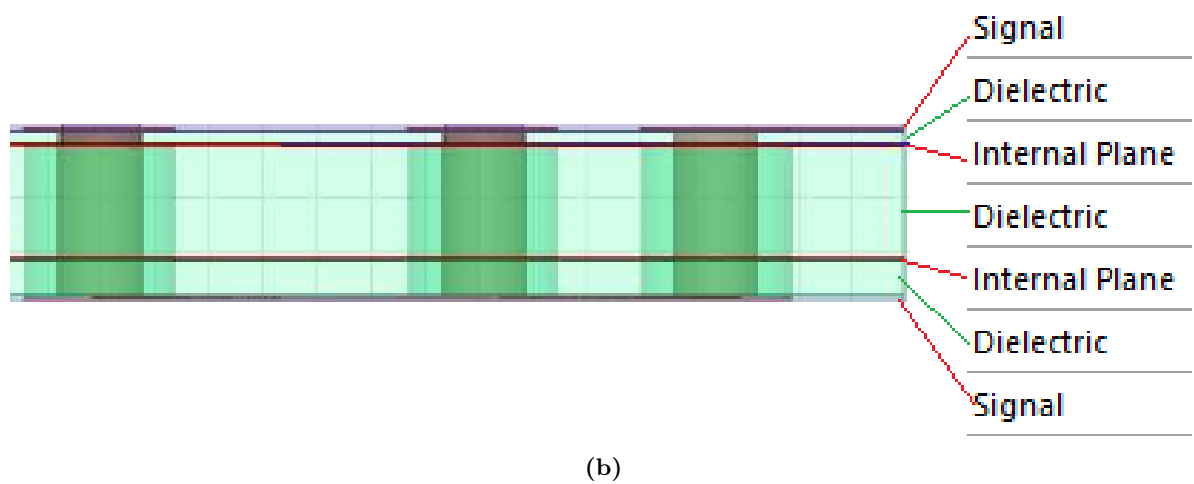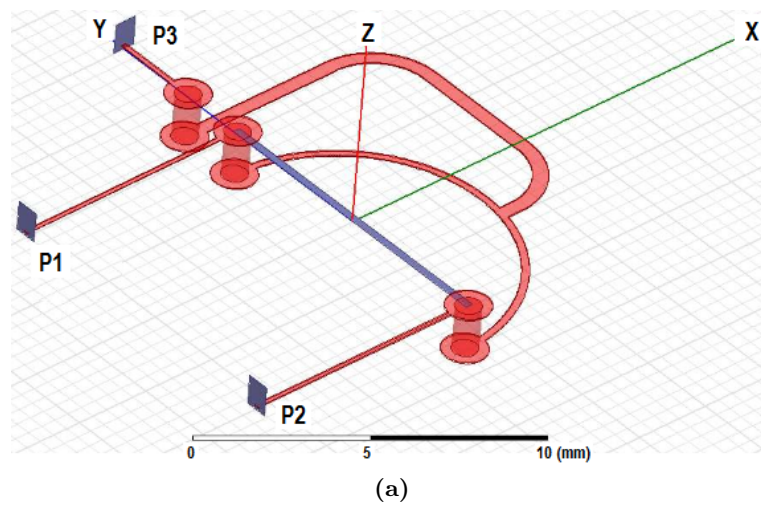
**Figure 3.22:** (a) Employed power combiner with signals input from p1 and p2 then output from p3. (b) PCB layers stack structure with conductor of copper and dielectric material of FR-4.
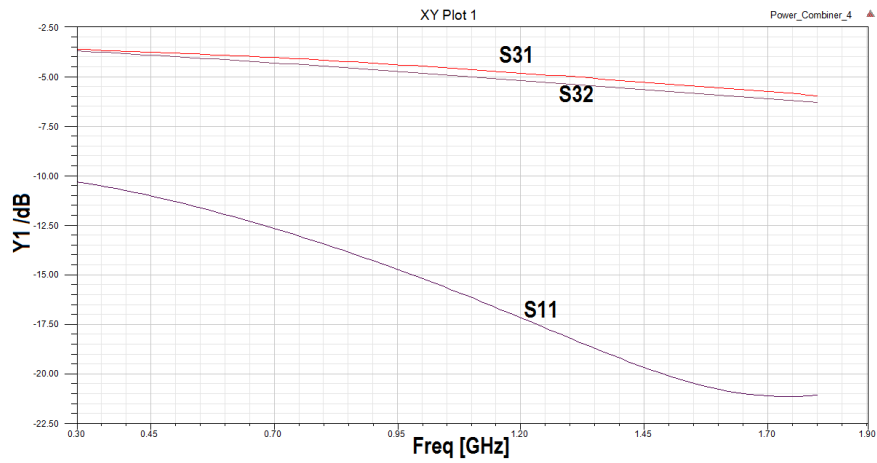
(a)
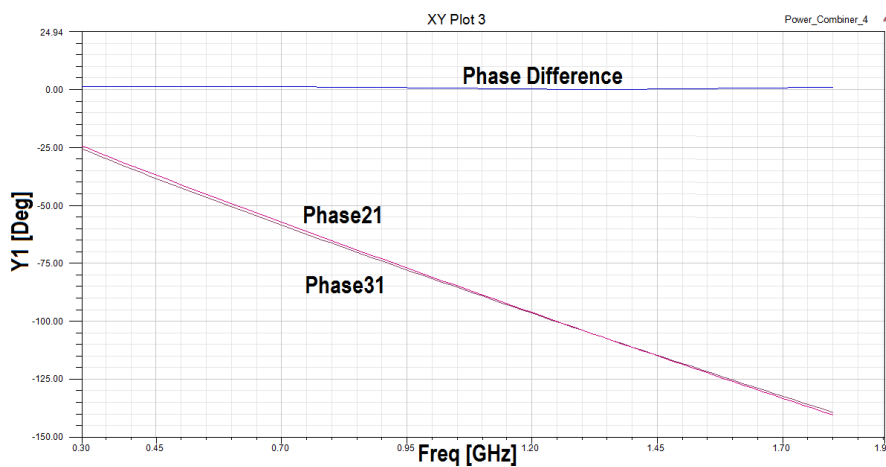


(b)

**Figure 3.23:** Simulation results of scattering parameters (a) and phase characteristics (b) of proposed power combiner. Result shows a 1~3 dB loss within range of 800 MHz to 1.8 GHz and a phase offset of less than 2 degree.
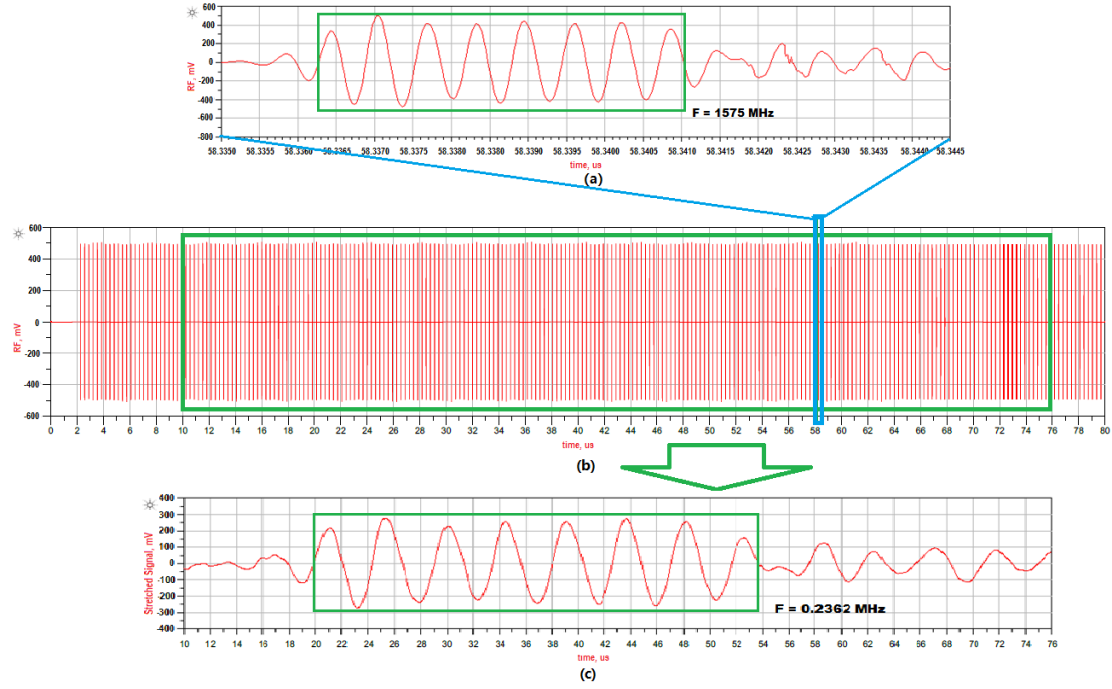
**Figure 3.24:** Example simulation result of the signal stretching. (a) refers to one segment of the received periodic RF signal (b). (c) is the stretched signal by sub-sampling the received signal (b).

$$K = T_s/(Ts - T) \tag{3.9}$$

where, $T_s$ is the sub-sampling interval. $T$ refers to the repetition interval of the periodic RF signal. Formula 3.9 can be rewritten by replacing the time information with frequencies:

$$K = f/(f - f_s) \tag{3.10}$$

where $f_s$ is the sub-sampling frequency and $f$ represents the signal repetition rate. The example measurement involves a signal repetition rate $f$ of 5MHz. A clock of $5MHz - \delta f$ is used to generate the sub-nanosecond sampling pulses, i.e. $f_s = 5MHz - \delta f$, where the difference $\delta f = f - f_s$. Figure 3.25 demonstrates the measurements with different stretched rates. These rates are obtained by setting different pulse repetition period offsets. The carrier signal (1.575GHz) is stretched by 50000 times to 31KHz by setting the offset to 100Hz (Fig. 3.25a). Likewise, 200Hz and 300Hz offset lead to 63KHz and 93KHz respectively. Figure 3.26 shows the relation between the frequency offsets and resulted frequencies. The measurements match well with the calculations.

**Summary**

The developed conversion system is composed of a SRD based sub-nanosecond pulse generator, a broadband sampling bridge, a two layer Wilkinson power combiner and a baseband wave former. It is suitable for application of periodic pulse modulated UHF radio. A simple implementation of strobe pulse generator is presented. It introduces standard discrete elements and microstrips to generate oppositely polarized pulses with
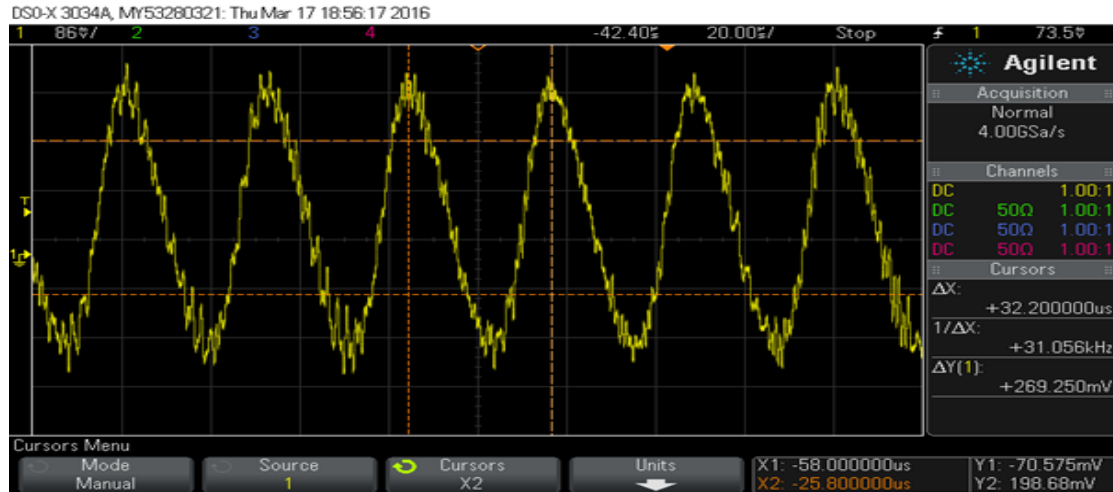
**(a)**
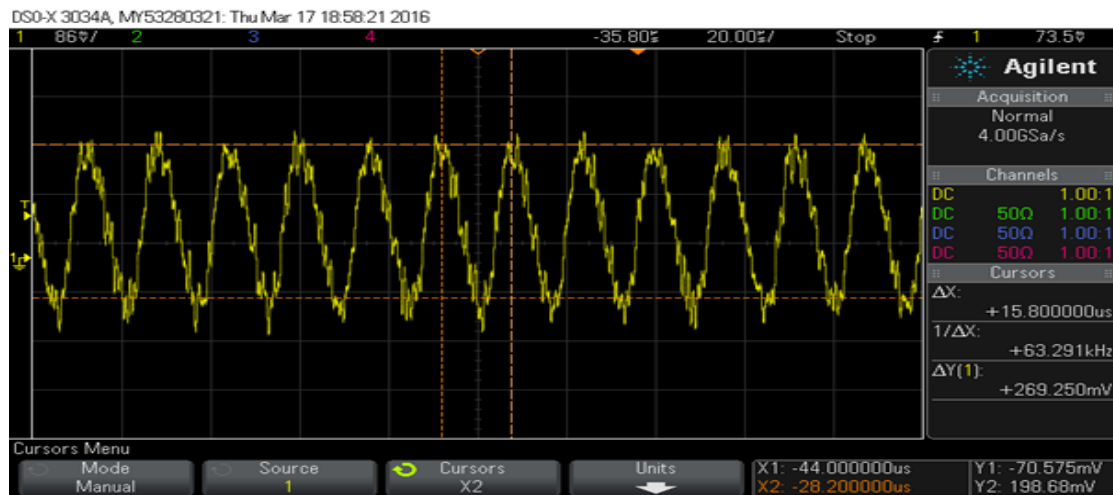


**(b)**



**(c)**

**Figure 3.25:** (a)Measurement result with factor of 49999, corresponding to 100 Hz offset, output frequency at 31 KHz. (b)Measurement result with factor of 24999, corresponding to 200 Hz offset, output frequency at 63 KHz. (c)Measurement result with factor of 16666, corresponding to 200 Hz offset, output frequency at 94 KHz.
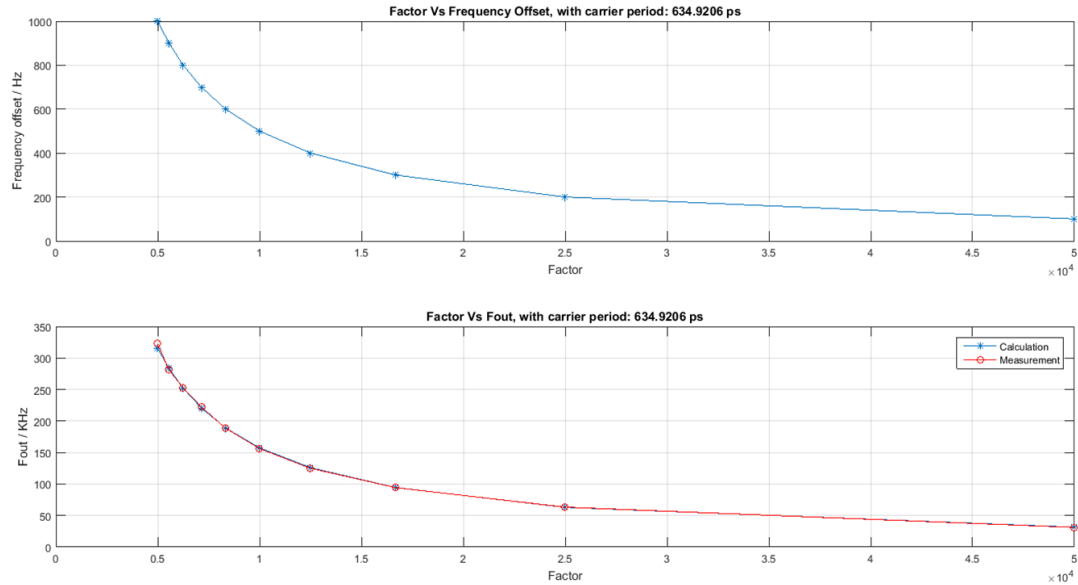
**Figure 3.26:** Relation of stretch factor with clock offset $\delta f$ (up) and with output frequency (down). Measured output frequencies match quite well with the computed result (down).

width of 100 ps, resulting in a corresponding small sampling aperture. The broadband sampling bridge is capable of sampling UHF signal due to its fast charging RC circuit. The power combiner achieves a low conversion loss of 2 dB in the interested frequency range. The baseband wave former consists of low pass filter and Opamp, producing an equivalently stretched signal. This circuit can be applied to a TDoA based positioning system using low speed data acquisition device only to obtain a high time resolution.

## 3.3. Signal Processing System

This section focuses on the digital signal processing. Key modules of the signal processing system include raw data filtering, baseline estimation, event arbitrator, TDoA estimation and hyperbolic equations solver. Each of these is individually discussed and evaluated in the following subsections.

The proposed algorithms are developed and evaluated in MATLAB/Simulink environment. In the complete signal processing chain, some fundamental processes are discussed from the raw data aspect to the non-linear equations solver for coordinate determination. The raw signal is sampled by ADCs with 14 bits resolution, using two's complement data representation. A dynamic baseline estimator is required to compensate the level shifting due to thermal effect and non-identical hardware of receivers. As the signal is continuously fed into the data acquisition system, an arbitrator is needed to determine the event and trigger a data storage enable signal, which also starts up the core positioning algorithms. Because the receivers together construct a synchronized network, the trigger signals are also synchronized. The very first trigger signal established by the network is recognized as the highest priority and is broadcasted to all receivers for controlling. The core positioning process in context consists of two modules. These are TDoA estimator and non-linear equation solver respectively. The accuracy of the TDoAs estimation will directly effect the positioning precision. Minimum 4 pairwise TDoA estimations are required to uniquely determine a 3D coordinate of a target, according to the hyperbolic positioning principle. Each of the TDoA quantity define a hyperbolic equation. In order to resolve the generated non-linear equations, a numerical Newton-Raphson algorithm is introduced, which will be discussed in the following sections.

The last but not the least task desired to be accomplished is the event arbitrator. An event detection system proposed to monitor the received signal and to issue a trigger at the moment of detecting a symbol start. The very first trigger is taken as a control signal to enable the core hyperbolic positioning algorithm, the TDoA estimation and non-linear equation solver.

Initiative position estimation converges within 7 iterations, with an error of less than 100 ppm. Subsequent estimations require only 3 iterations to achieve the similar accuracy by substituting the initial guess with previous estimation. This dissertation presents a Simulink model where the iteration length can be dynamically configured during processing, reducing the computation complexity on demand.

The positioning algorithms presented in this work accomplish two fundamental functions: TDoA Estimation, Hyperbolic Positioning (Figure 1.1).

**Softwares/Tools**
As previously mentioned, the complete processing system is firstly modeled in MATLAB/Simulink environment. The high level synthesis tool HDL Coder is involved in HDL code generation from the Simulink model. Simulation results are provided, including the co-simulation which concludes the identical functionality of the algorithm model and the firmware model. Additionally, the toolbox HDL verifier is necessary to carry out the co-simulation. The involved HDL Simulator ModelSim is used for co-simulation.

The final firmware is synthesized in Xilinx ISE environment.

### 3.3.1. TDoA Estimator

The algorithms development starts with the TDoA estimation. The TDoA estimator contains a set of algorithms, including the baseline compensation, normalizer, filter, thresholding, first peak detection, ambiguity eliminator, etc. (Figure 3.27)
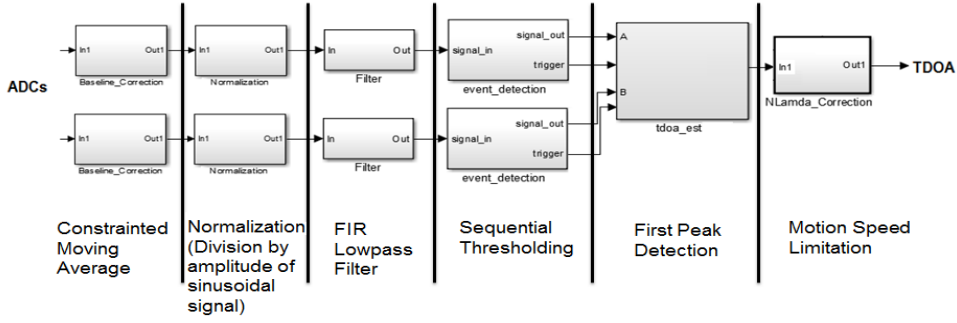


**Figure 3.27:** Simplified signal processing chain

The first step is baseline compensation. The existence of noise along with the level shift on the ADC board requires an approach to suppress its influence on actuating baseline estimation. To deal with this issue, a threshold Restricted Moving Average mechanism (RMA) is implemented for the baseline computing. The baseline of each time point can be derived by averaging the samples which are within certain threshold (Offset) away from former baseline, e.g. the standard deviation. This method could exclude the contribution from signal pulses almost entirely. The second step is to normalize the received OOK signal. Taking advantage of the sinusoidal nature of the signal, the squared amplitude of the signal can be computed by summation of square of two quarter period spaced samples: $A^2 = (S_t{}^2 + S_{t+\frac{T}{4}}{}^2)$. A low pass filter is implemented after the normalization step to reshape the modulated signal. The next step is to estimate the TDoA by subtracting the arriving time of the first period peak with thresholding at pairwise receivers. The last step is to adjust the TDoA estimation, based on the assumption that the target moves within a periods range during the update interval.

This section presents the detail of each step with the mathematical backgrounds, the modeling and the related simulation results for each sub-system.

**Step. 1: Baseline Compensation**
The raw data in context refers to the digitized signal from the underlying data acquisition ADC board. Besides the quantization error caused by the sampling devices, some other sources also introduce noise to the analog signal before sampling. For instance, the additive Gaussian white noise (AGWN), the interference from the neighboring signal routes, and unwanted harmonic components. Together with the analog filters implemented in the circuit board, digital filters are highly recommended for further filtering out the disturbing interference. The estimated baseline is subtracted from

the signal for compensation. An efficient baseline estimator is demonstrated in this work.

The noise sources consist of the random inherent noise from the electrical elements and the interference noise from the unwanted interaction between different routing signals. In this project we only deal with random noise that has a probability density function as the Gaussian distribution [152]. E.g. the Gaussian probability distribution function in a variable x with mean $\mu$ and variance $\sigma^2$:

$$f(x; \mu, \sigma) = \frac{1}{\sigma\sqrt{2\pi}} e^{-\frac{1}{2}(\frac{x-\mu}{\sigma})^2}$$

The threshold Restricted Moving Average (RMA) is a simple mechanism to suppress the influence of the noise on baseline estimation. The following example shows an implementation of this strategy. The current baseline is derived from the mean of the former N samples, which are located in the restricted region. The threshold can be determined dynamically or fixed.

$$Baseline = \frac{1}{N} \sum_{k=i}^{i+N} X_k$$

where $X_k \in [Baseline_- - Offset, Baseline_- + Offset]$ and $Offset \in [\sigma, 4\sigma]$

The implementation of this baseline estimation algorithm in Simulink is displayed in Figure 3.28. The first 256 samples (number of sum elements) are all counted to initialize the baseline. Subsequent samples within the restricted region make effort to the baseline update, using the threshold of 0.05 from the training data. The enable signal of evaluating a new baseline is determined by the comparison result. This baseline estimation is activated if the new signal sample is located within the restricted region. Instead of being divided by 256, the arithmetic shift right operator is introduced to reduce resource cost.

Figure 3.29 shows an example baseline compensation result. The blue signal represents the original signal, the red signal is the the compensated result by subtracting the baseline (black curve).

**Step. 2: Normalization**
In a RF-based indoor positioning system, the propagation of the signal causes attenuation according to the inverse square law. The receiver closer to the transmitter will receive more power. Moreover, the reflection and scattering increase the difference and uncertainty of the signals' amplitude arrives at the reference receivers. A practical method to decrease this difference is implementing an automatic gain controller (AGC) circuit, which is constructed by a power detector and a variable gain amplifier. A section in the hardware development part presents an AGC design and the performance analysis. In addition to the AGC, a digital gain controller is proposed to further suppress this amplitude imbalance. The solution presented here is a digital normalizer, which normalizes the received signal by dynamically dividing its amplitude.

As the signal to be processed is an amplitude-modulated sinusoidal signal, it is important to estimate its amplitude. There are many techniques available for amplitude estimation, including the least square method [153, 154], the adaptive state observers [155, 156], and the well-known fast Fourier transform (FFT). The frequency of the signal is accurately known. A simple algorithm for the amplitude estimation of sinusoidal
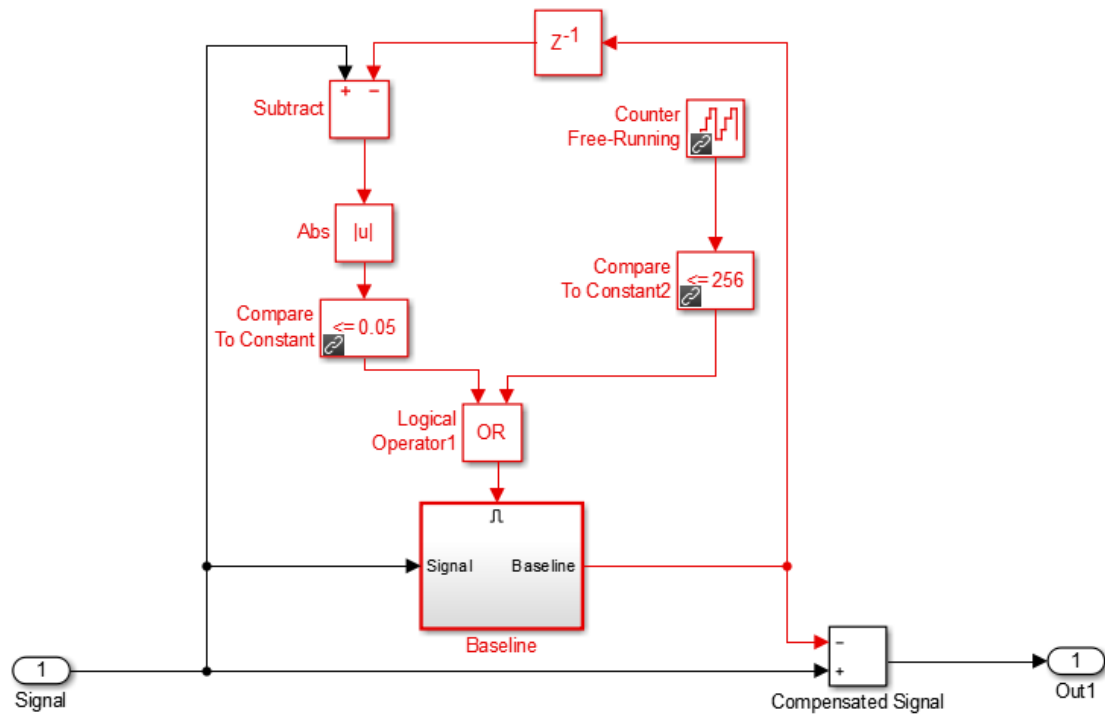
**Figure 3.28:** Baseline Estimation Subsystem, average 64 restricted samples
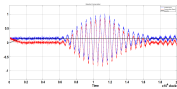


**Figure 3.29:** Baseline estimation with noise influence, the blue signal represents the original signal, the red signal is the baseline compensated one and the black line refer to the estimated baseline.

signals is proposed where two samples are enough to calculate the amplitude.

Consider a sinusoidal signal $y(t)$ with amplitude $A$, frequency $f_c$, arbitrary phase $\phi$ and DC offset $A_0$ denoted by:

$$y(t) = Asin(2\pi f_c t + \phi) + A_0 \tag{3.11}$$

With an ideal baseline compensation, the DC offset $A_0 = 0$, we get:

$$y(t) = Asin(2\pi f_c t + \phi) \tag{3.12}$$

define two points:

$$y_1 = y(t_0) \tag{3.13}$$

$$y_2 = y(t_0 + \frac{1}{4f_c}) \tag{3.14}$$

based on (3.7)-(3.9), $y_1$, $y_2$ can be expressed as:

$$y_1 = Asin(2\pi f_c t_0 + \phi) \tag{3.15}$$

$$y_2 = Asin(2\pi f_c(t_0 + \frac{1}{4f_c}) + \phi) \tag{3.16}$$

denote $\Phi = 2\pi f_c t_0 + \phi$, $y_1$, $y_2$ can be expressed as:

$$y_1 = Asin(\Phi) \tag{3.17}$$

$$y_2 = Acos(\Phi) \tag{3.18}$$

Summing squared $y_i$ yields:

$$y_1^2 + y_2^2 = A^2 sin^2(\Phi) + A^2 sin^2(\Phi + \frac{\pi}{2}) = A^2 \tag{3.19}$$

Then we get the squared amplitude:

$$A^2 = y_1^2 + y_2^2 = y^2(t_0) + y^2(t_0 + \frac{1}{4f_c}) \tag{3.20}$$

$$= y^2(t_0) + y^2(t_0 + \frac{T}{4}) \tag{3.21}$$

where $T$ denotes the signal period.
As the estimation is based on digitized signals, thus the equation (3.16) has to be rewritten as:

$$A^2 = y^2(N_0) + y^2(N_0 + \frac{N}{4} + \Delta) \tag{3.22}$$

where $N_0$ is the first sample index, $N$ refers to the integer samples of a period calculated by $N = fix(f_s/f_c)$. $f_s$ denotes the sampling frequency and correspondingly $T_s$ refers to

the sampling interval. $\Delta$ is the error caused by the "$fix$" operation which rounds to the closest integer, i.e. $\Delta = T_c - NT_s$, where $T_c$ is the carrier's period. With a large the oversampling rate, the error caused by the difference is neglectable, thus:

$$A^2 \approx y^2(N_0) + y^2(N_0 + \frac{N}{4}) \tag{3.23}$$

Referring to the algorithms strategy explained in the scenarios section, the TDoA estimation in our system deploys a threshold and peak detection approach. Peak searching is applied to the squared signal, avoiding computing the square root of the $A^2$. Thus, the normalization process actually involves the squared samples:

$$s(n) = sign(y(n))\frac{y^2(n)}{A^2} = sign(y(n))\frac{y^2(n)}{y^2(n) + y^2(n + \frac{N}{4})} \tag{3.24}$$

where the new signal $s(n)$ will keep the sign of the instant sample $y(n)$. A Simulink model for the normalization sub-system is depicted in the Figure 3.30. And the Figure 3.31 displays an example normalization result. As can be seen in this figure, in the region where there is smaller SNR, the result saturates due to the noisy and small amplitude estimation. A low pass filter is proposed in the next step for filtering the normalized signal.
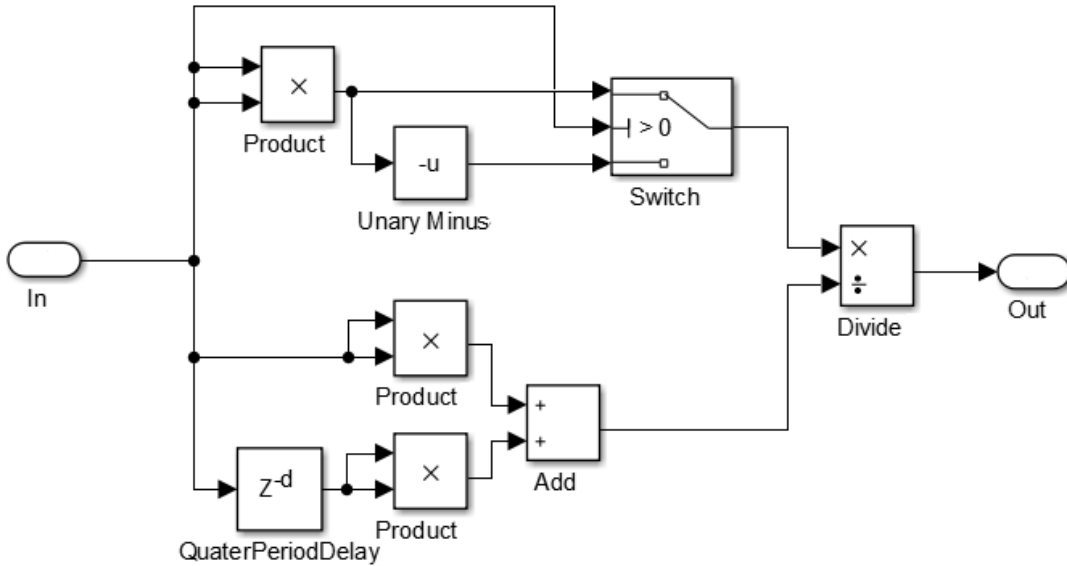


**Figure 3.30:** Simulink model for the proposed normalization sub-system.

**Step. 3: Low Pass Filter**
The normalization process produces the result is depicted in Figure 3.31. It is a noisy signal. In order to precisely determine the time of arrival, a low pass filter is required to filter out the high frequency components. As the temporal information is critical to estimate the TDoA, the phase response of the filter should be linear. Hence, deployment of a FIR filter is proposed for this purpose. The mathematical filter background is
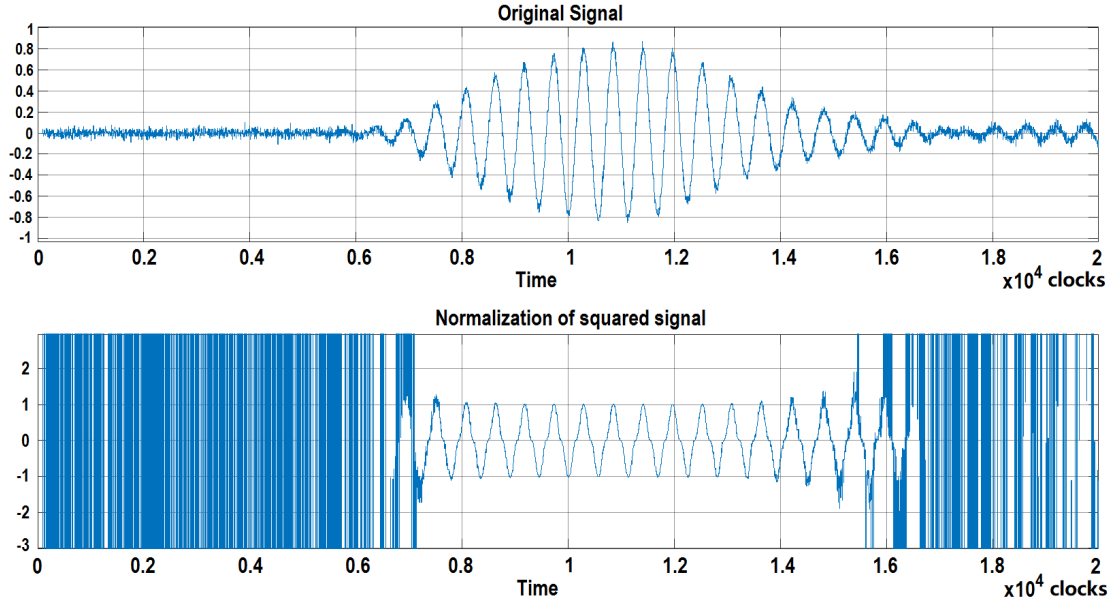
**Figure 3.31:** Example result of the normalization sub-system. Original signal (up) and the normalization of the squared signal (down).

demonstrated in the appendix. The Filter Design & Analysis Tool from MathWorks is used to design the FIR filter. It provides plenty of options to optimize the requirements, referring to the resource and performance. A detailed design process is described in the appendix as well.

Here we only present some key setting for the filter design. The oversampling rate in our system is set by the ADC sampling rate. To give an example setting for the process, we implement a 2 Msps sampling rate and our signal is the sub-sampled signal at 17.42 KHz. There are three frequency parameters need to be set in MATLAB FDATool: sampling frequency, pass frequency and stop frequency.

Frequencies:
1. ADC sampling rate $f_s = 2MSPS(MHz)$
2. Analog front end outputs signal frequency $f_{signal} = 17.42KHz$
3. pass band frequency $f_{pass} = 3 * f_{signal}$
4. stop band frequency $f_{stop} = 10 * f_{signal}$

In digital domain, if we define the signals frequency as 1 (17.42KHz ), then the sampling rate is $f_s/f_{signal}$, which is round to 114. The pass band and the stop band are 3 and 10 respectively. Figure 3.32 is generated in FDATool. The unit displayed in Figure 3.32 refers to the basis of 17.42KHz.

The magnitude response is set to be 0.5 dB at passband and 80 dB attenuation for the stop band. A low pass FIR filter type is selected. The filter result is shown in Figure 3.32. It has a very good magnitude response for suppressing the noise to very low level and a linear phase response within the pass band for keeping the timing information.
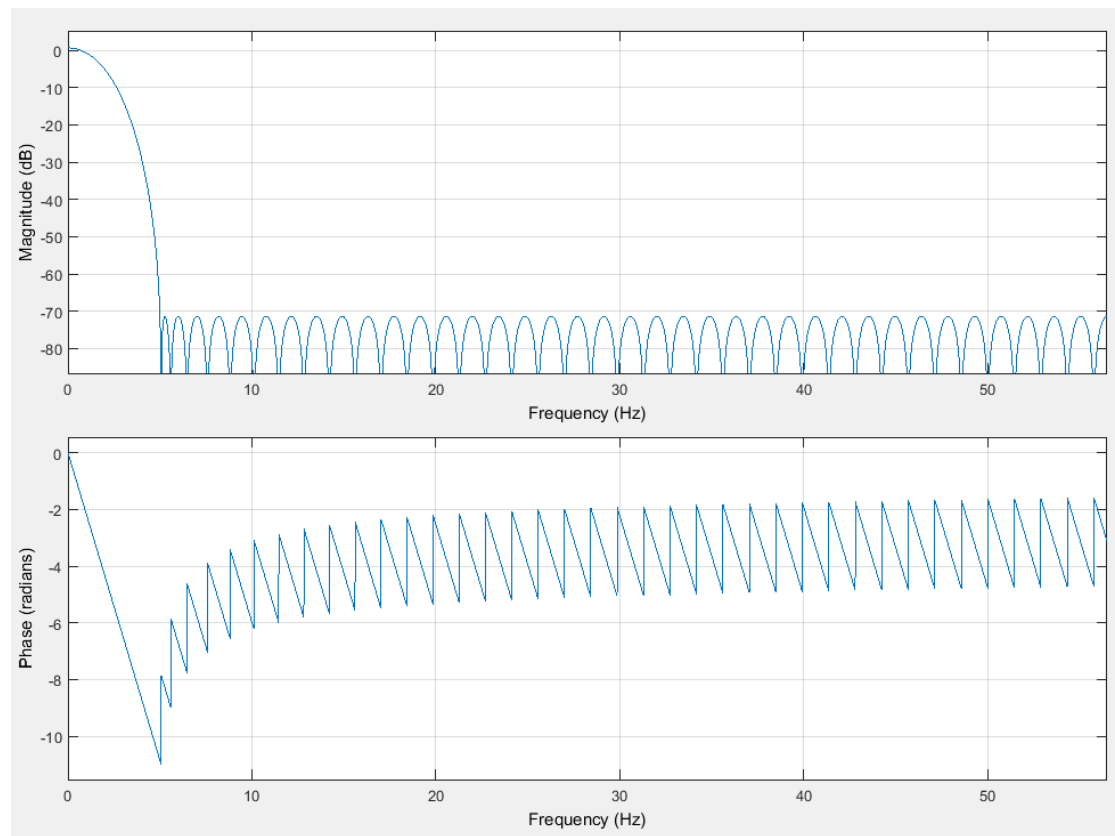
**Figure 3.32:** The designed filter response for our TDoA estimator. Magnitude response (up) and phase response (down).

Apply this filter to the system after normalization. A filtering result is demonstrated in the Figure 3.33.
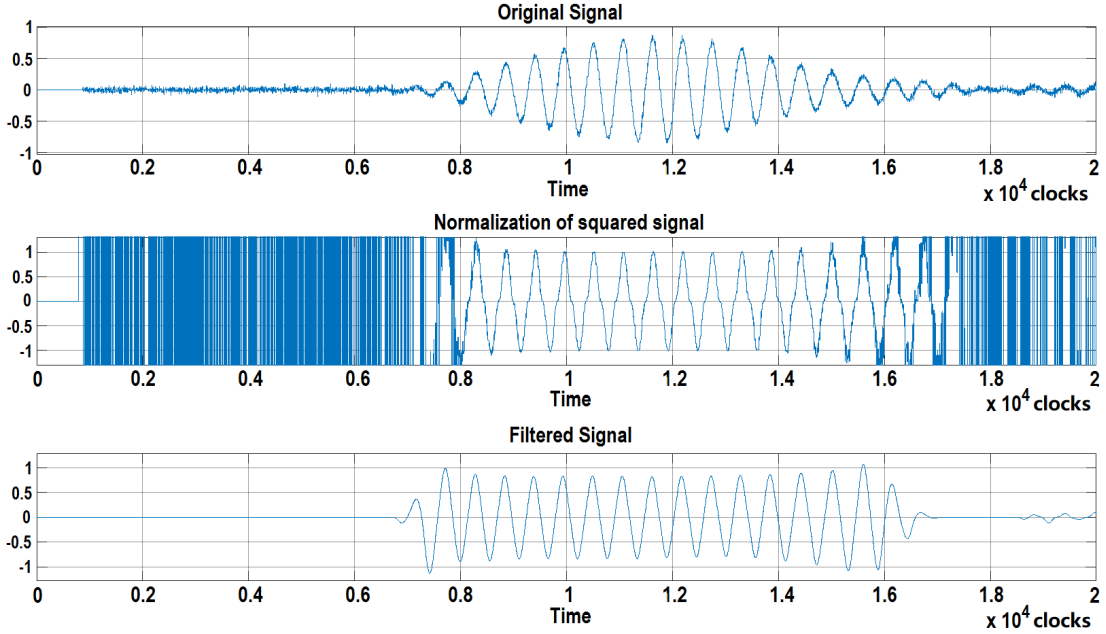


**Figure 3.33:** The normalized signal is filtered by the designed FIR low pass filter. Original signal (up), normalized squared signal (middle) and filtered signal (down)

**Step. 4: Thresholding (edge detection)**

The proposed system is designed to continuously update the position of the target. It means that the target which is designed as a RF transmitter is correspondingly continuously broadcasting the patterned radio signal. As there is no synchronization between transmitter and receivers, an event detection mechanism is required to determine the incoming of a new positioning event, named event arbitrator. In the case of OOK modulation radio system, an arbitration process can be simplified by setting an appropriate threshold. An event of threshold overshooting can be recognized as a positioning alert and issue a trigger. The next arbitration process can only be restarted after the position fix.

An efficient method is necessary for the threshold over cross detection. it should avoid false event detection due to amplitude disturbance. The proposed method recognizes a valid arrival of signal as sequentially crossover the thresholds, where two different threshold levels are used. The procedure is illustrated in the **Algorithm 3.1**, where k denotes the time index of the samples. $s_i$ are the samples used for comparisons, with length I. $N$ is the length of each carrier period. Two threshold levels are predefined: $Th_1$ and $Th_2$, where $Th_1 > Th_2$ to set a tolerance for amplitude fluctuation caused by noise, filter etc.

Algorithm 3.1:

**begin**
   **Initiation**: $k := 0$;
   **Condition**: **if** $s_I > Th_1$
          and $s_i > Th_2$, for even i
          and $s_i < -Th_2$, for odd i
       **then** Arrival Detected, go to **HIT**
       **else** go to **Update**
   **Update**:    $k := k + 1$;
          $\mathbf{s}_i := \mathbf{x}(k + \frac{(I-i)}{2} * N)$;
      go to **Condition**
   **HIT**: wait $(duration < period)$
      go to **Initiation**

In the test, the values are set to 0.7 and 0.2 respectively. The example result is displayed in the Figure 3.34.
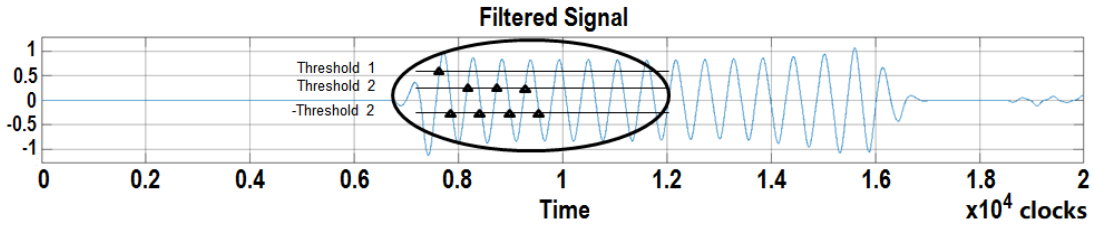


**Figure 3.34:** The normalized signal is filtered by the designed FIR low pass filter. Original signal (up), normalized squared signal (middle) and filtered signal (down), two thresholds are introduced to determine a event.

Sequential threshold crossover detection of the signal with strong sinusoidal pattern avoids the false detection of an amplitude disturbance as shown in the example in Figure 3.35.
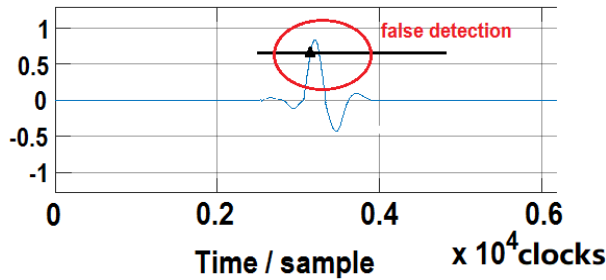


**Figure 3.35:** A simple threshold crossover detection could result in false detection, due to the amplitude disturbance.

**Step. 5: First Peak Detection**
Once the rough catch (step 4) is accomplished, the first peak can be found with multiple comparisons. The TDoA is estimated as the time delay between first peaks received by

two receivers.
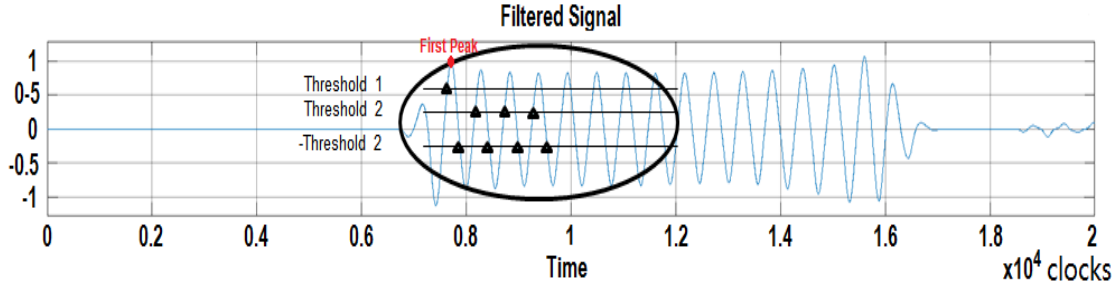


**Figure 3.36:** First peak is located after the threshold crossover detection.

**Step. 6: Ambiguity Eliminator**
The disadvantage of first peak detection of an OOK signal is the potential peak ambiguity due to the selection of the first threshold. A smaller first threshold might result in an earlier first peak and vice versa. The ambiguity $\Delta_t$ is a multiple of the carrier period plus a quantization uncertainty:

$$\Delta_t = n * T_{carrier} + n_q * T_{adc} \tag{3.25}$$

where $n = 0, 1, 2, 3, ...,$ and $T_{carrier}$ denotes the carrier period, the quantization uncertainty $n_q = 0, 1, -1$, and $T_{ADC}$ represents the equivalent ADC sampling interval (sampling interval divided by stretch factor).

The proposed approach to avoid the ambiguity is adjusting the TDoAs based on the motion speed limitation, i.e. the position change within a update interval is limited by the object moving speed:

$$\|p_{new} - p_{old}\| < \Delta_{max} \tag{3.26}$$

Estimated TDoAs should meet the condition (3.21), otherwise, they should be adjusted by adding or subtracting integer multiple of $T_{carrier}$ to meet the requirement (3.21).

### 3.3.2. Hyperbolic Equations Solver

A position represented in three dimensional Cartesian coordinate system (x,y,z) is required for many IPS applications. It can be obtained by solving the non-linear equations (3.5). Chapter 2 has discussed about solving the positioning model analytically and numerically. The Newton-Raphson method is proposed in this work to estimate the position from the TDoAs iteratively. Assume a system of 4 reference nodes, i.e. 4 RF receivers. And the pair-wise time difference of arrival are estimated $TDoA_{ij}$ for $i, j = 1, 2, 3, 4$ and $i \neq j$. Let $RD_{ij}$ be the range difference from the target device to the pair-wise receivers. The relation holds: $RD_{ij} = TDoA_{ij} * v + e_{ij}$ where $e_{ij}$ denotes the estimation error. With a sufficient accurate TDoA estimation, the error $e_{ij}$ can be neglected: $RD_{ij} = TDoA_{ij} * v$. Recall the equation (3.5):

$$\sqrt{(x-x_i)^2+(y-y_i)^2+(z-z_i)^2} - \sqrt{(x-x_j)^2+(y-y_j)^2+(z-z_j)^2} = TDoA_{ij} \times v$$
(3.27)

substitute the time difference terms with the range differences:

$$\sqrt{(x-x_i)^2+(y-y_i)^2+(z-z_i)^2} - \sqrt{(x-x_j)^2+(y-y_j)^2+(z-z_j)^2} = RD_{ij}$$
(3.28)

Because the TDoAs are represented by multiples of the equivalent sampling interval (ADC sampling interval divided by stretch factor), an accurate information of this quantity in addition to the accurate signal propagation speed $v$ are required to calculate the range differences. Alternatively, as the linear relationship between these quantities, the range difference can also be computed by calibrating a 1D measurement:

$$RD_{ij} = \alpha * \Delta N_{ij}$$
(3.29)

where the weight $\alpha$ represents the transformation relation. $\Delta N_{ij}$ is identical to $TDoA_{ij}$, but with the unit of '1'. Note that the weight factor $\alpha$ changes with the equivalent sampling interval, which is determined by the ADC sampling rate and the actual stretch factor.

**Newton-Raphson Method**
As discussed previously, we propose the Newton-Raphson algorithm to solve the hyperbolic non-linear equations. With accurate TDoA measurements, the range difference from the target device to the pair-wise receivers can be obtained. Given the priori knowledge of the reference receivers' location, the target device's position can be estimated by solving the equations (3.23). This section is intended to derive the mathematical solution based on the Newton-Raphson method for our indoor positioning system, i.e. a TDoA-based IPS using UHF frequency in ISM band.

The basic setup of the proposed indoor positioning system is depicted in Figure (3.16), composed of 4 receivers located at the known positions and the transmitter as the target device. Assume the coordinates of the receivers: $(x_i, y_i, z_i)$ $(i = 1, 2, 3, 4)$. Distances from the receivers to the target transmitter: $d_i$ $(i = 1, 2, 3, 4)$. And the range differences referring to the receiver 1 are estimated: $RD_{1j}$ $(j = 2, 3, 4)$.

Rewrite equation (3.23) by moving the right item to the left:

$$\begin{aligned} f(x,y,z) &= \sqrt{(x-x_i)^2+(y-y_i)^2+(z-z_i)^2} \\ &\quad - \sqrt{(x-x_j)^2+(y-y_j)^2+(z-z_j)^2} - RD_{ij} \\ &= 0 \end{aligned}$$
(3.30)

Applying three range differences to the equation (3.25) yields to:

$$\mathbf{F}(x, y, z) = \begin{bmatrix} f_1 \\ f_2 \\ f_3 \end{bmatrix} = 0 \tag{3.31}$$

with

$$f_1 = \sqrt{(x - x_1)^2 + (y - y_1)^2 + (z - z_1)^2} - \sqrt{(x - x_2)^2 + (y - y_2)^2 + (z - z_2)^2} - RD_{12} \tag{3.32}$$

$$f_2 = \sqrt{(x - x_1)^2 + (y - y_1)^2 + (z - z_1)^2} - \sqrt{(x - x_3)^2 + (y - y_3)^2 + (z - z_3)^2} - RD_{13} \tag{3.33}$$

$$f_3 = \sqrt{(x - x_1)^2 + (y - y_1)^2 + (z - z_1)^2} - \sqrt{(x - x_4)^2 + (y - y_4)^2 + (z - z_4)^2} - RD_{14} \tag{3.34}$$

The Newton-Raphson method update the position estimation by:

$$\hat{p}(x_{k+1}, y_{k+1}, z_{k+1}) = \hat{p}(x_k, y_k, z_k) - \mathbf{J}^{-1}(\mathbf{F}(x_k, y_k, z_k)) * \mathbf{F}(x_k, y_k, z_k) \tag{3.35}$$

Where, $\mathbf{J}$ is the Jacobean matrix of size $3 \times 3$ holding the partial derivatives of hyperbolic equation $\mathbf{F}$, $\hat{p}(x_{k+1}, y_{k+1}, z_{k+1})$ is the solution after $k$ iterations, updated from $\hat{p}(x_k, y_k, z_k)$. The Jacobean matrix is defined as:

$$\mathbf{J} = \begin{bmatrix} \frac{\partial f_1}{\partial x} & \frac{\partial f_1}{\partial y} & \frac{\partial f_1}{\partial z} \\ \frac{\partial f_2}{\partial x} & \frac{\partial f_2}{\partial y} & \frac{\partial f_2}{\partial z} \\ \frac{\partial f_3}{\partial x} & \frac{\partial f_3}{\partial y} & \frac{\partial f_3}{\partial z} \end{bmatrix} \tag{3.36}$$

The equations ($3.27 \sim 3.31$) are the complete set for the position estimation from range difference measurements, with the priori knowledge of the receivers' locations (refer to the appendix for more details). As this positioning method is iterative we need to set a certain criteria to break iteration. If this criteria is fulfilled, the iteration will break and the current result is the estimated position. At this point, the value of the error, which is $\Delta$ in our case, is so small that it does not have significant impact on the estimated position. If criteria is not met, the loop will continue till the maximum number of iterations are reached. The iterative process is shown in Figure 3.37.

### 3.3.3. Kalman Filter

The unpredictable indoor environment and the limitation of the measuring system contribute to the estimation error as process noise and measurement noise. The Kalman filter (KF) for object tracking is widely used in positioning and navigation systems. A thorough introduction of this filter can be found in [157].

The KF is applied in our system as the last stage of the TDoA estimation to improve the performance in dynamic state estimation. Instead of the position, the range differences $RDs$ are the states this filter is working on. It implements a feedback loop, constructed by two fundamental elements: position estimation and feedback from TDoA measurements (or range differences $RDs$). Correspondingly, there are two basic pro-
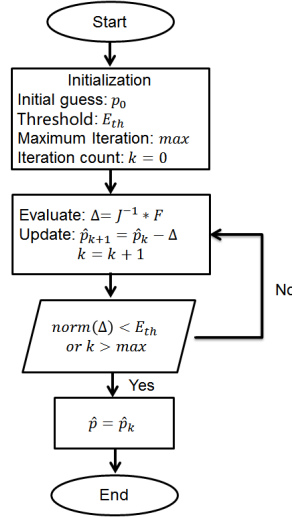
**Figure 3.37:** Flow chart of the proposed iterative estimation process.

cesses involved in the KF: time update and measurement update. The time update process computes both a priori $RD$ estimation $\hat{X}_k^-$ and a priori estimation error covariance $P_k^-$ from the old $RD$ estimation and old error covariance. They together with the new TDoA measurements are used in the measurement update process for a posteriori improved $RD$ estimation $\hat{X}_k$ and update the error covariance $P_k$ as well. They are lately involved in the next time update. This procedure goes round and round again. In another words, the time update is responsible for prediction and the measurement update is used to correct that prediction to obtain a better estimation.

Where the estimation $\hat{X}_k$ has two elements: the new range difference estimation $\hat{RD}_k$ and the old one $\hat{RD}_{k-1}$:

$$\hat{X}_k = \begin{pmatrix} \hat{RD}_k \\ \hat{RD}_{k-1} \end{pmatrix} \tag{3.37}$$

The matrix $A$ reflects the relation between the new estimation and the old estimation. As we have a high update rate, any movement within a short interval is assumed to have a constant speed, thus a linear model is assumed. Based on that consideration, the linear extrapolation is involved in our system to update the estimation. That yields to:

$$A = \begin{pmatrix} 2 & -1 \\ 1 & 0 \end{pmatrix} \tag{3.38}$$

The measurements used in the filter refer to the range differences:

$$Z_k = \begin{pmatrix} RD_k \\ RD_{k-1} \end{pmatrix} \tag{3.39}$$

As matrix $H$ relates the state $\hat{X}_k^-$ to the measurement $Z_k$ for error computation. It yields to:

$$H = \begin{pmatrix} 1 & 0 \\ 0 & 1 \end{pmatrix} \tag{3.40}$$

83
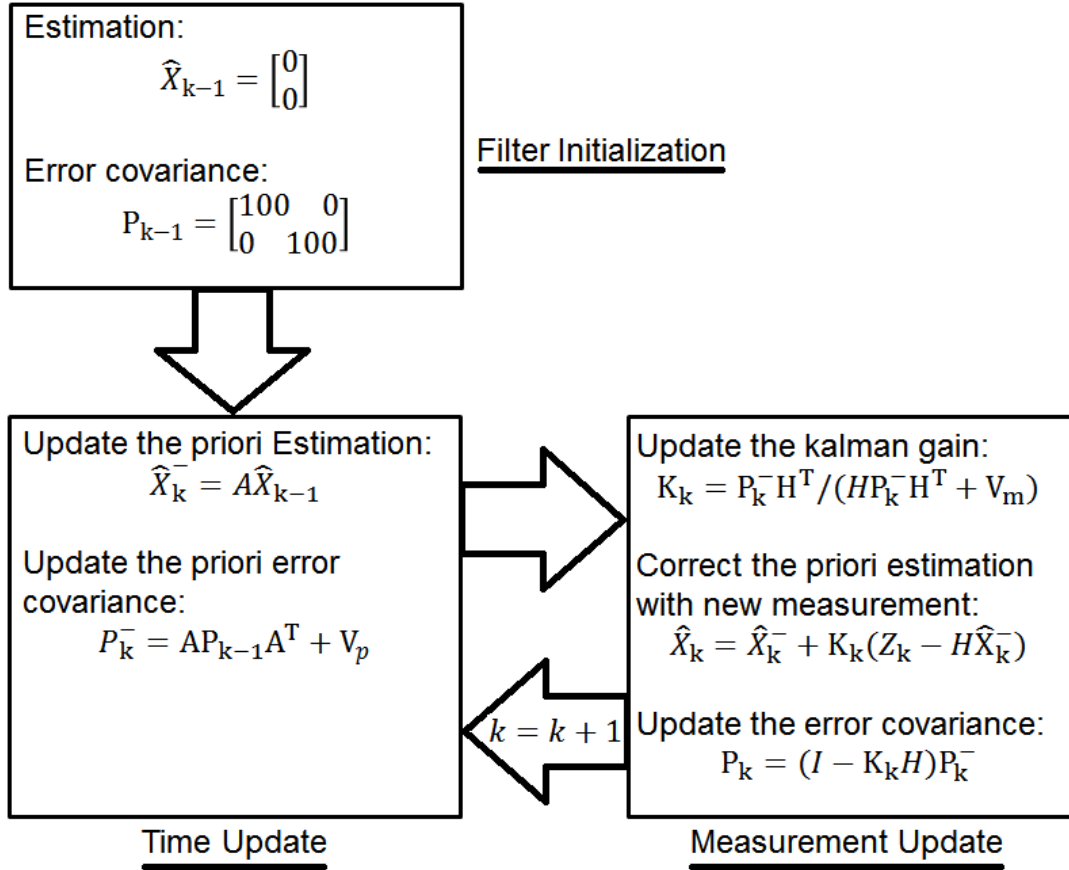
**Figure 3.38:** The Kalman filter improves the estimation by two processes: time update and measurement update.

$V_m$ represents the variance of the measurement noise and $V_p$ is the variance of the process noise.

In the initialization phase, both historic states of $\hat{X}_{k-1}$ were set to 0. (zero range differences assumed). A non-zero covariance $P_{k-1}$ is reasonable, because we are not sure about our state assumptions. We will start with an error covariance of 100, which corresponds to an identity matrix to evaluate two historic states in $\hat{X}_k$.

By tuning the parameters $V_p$ and $V_m$, different filter performance can be obtained. A smaller parameter setting results in an increasing dependency on the related criteria, process noise or measurement noise. A bigger $V_m$ makes the filter react slower to the measurement, i.e. it takes longer to approach the real state. According to our measurements, an error variance of $18.5mm^2$ was observed. Set $V_p = 12mm^2$ and $V_m = 200mm^2$. For an update rate of 100 Hz, the simulation result is depicted in the Figure 3.39. The error variance is decreased by the filtering, reduced from 19 $mm^2$ down to 12 $mm^2$. As the implemented filter is based on linear model, it performs better in situations of slower motion. Based on the current configuration, it has already shown a good performance when maximum speed doesn't exceed 100 km/h.
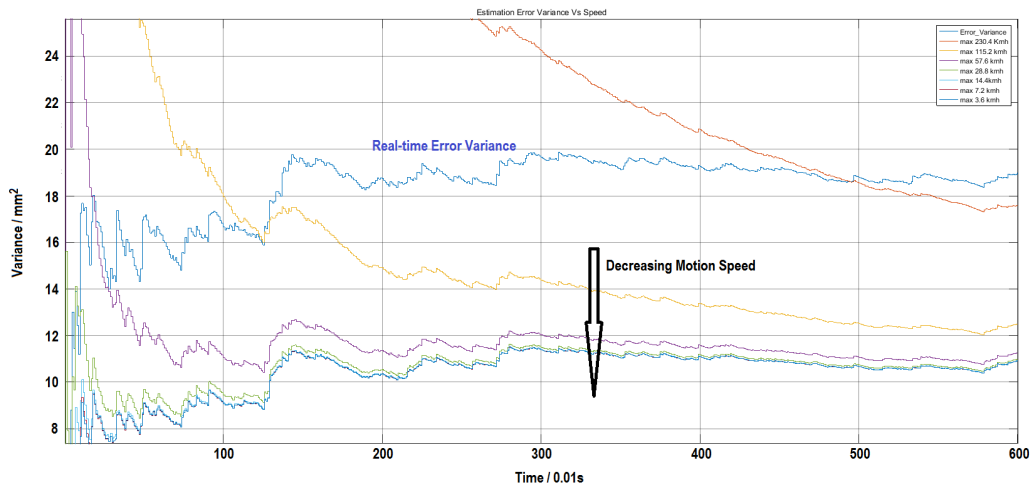
**Figure 3.39:** The filtering performance is improved with a slower motion.

# 4. Prototyping and Evaluation

The previous chapter presents the design procedure of the system by demonstrating the hardware development and the underlying signal processing algorithms. In order to verify the functionality and evaluate the performance, a prototype is developed. This chapter describes the implementation and evaluation of the proposed indoor positioning system. Section 4.1 presents the implementation of the complete system by describing the hardware fabrication and configuration, designing the complete signal processing model and the generation of the corresponding firmware, integrating all modules to a function-ready prototype system. Section 4.2 and section 4.3 show the measurements of 1D and 3D respectively, including the test setup and detailed result analysis.

## 4.1. Implementation of the Prototype System

This is a TDoA-based RF system, with the usage of UHF frequency in ISM band. It consists of minimum 4 receivers that are placed at known positions for 3D positioning, and the mobile RF transmitter as the object to be located.
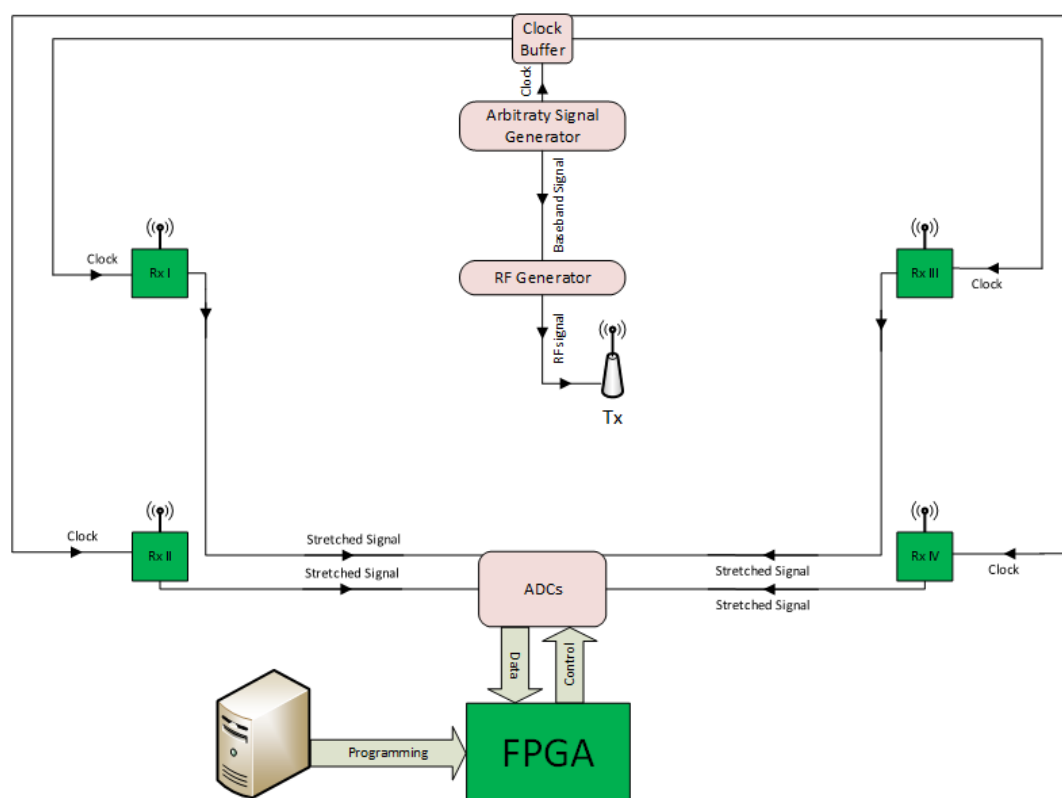


**Figure 4.1:** Prototype system implementation, consisting of 4 RF receivers and 1 RF transmitter.

Figure 4.1 shows the basic architecture of the prototype system. All receivers are driven by the clocks from the clock buffer (eval module for CDCLVC1112 from TI). The clock input for this buffer is generated by an arbitrary signal generator (M8190A), which also generates the baseband signal for the RF signal generator (N5181B). The OOK RF signal from this generator is transmitted to an antenna for broadcasting. It is

continuously broadcasting a periodic OOK-modulated signal. The receiver involves a quasi time stretch technology to achieve high temporal resolution. The stretched signals are transmitted to an ADCs board (FMC108) for digitization. Digital signal processing is carried out on the FPGA platform. By estimating the time difference of arrival of the RF signal at the pair-wise receivers, a hyperbolic positioning model is obtained. The developed signal processing implemented on FPGA is capable of computing the transmitter's position with high precision, high update rate and low latency.

### 4.1.1. Hardware System Implementation

The hardware implementation of the prototype system refers to the receiver board fabrication. The block diagram and fabricated PCB is displayed in Figure 4.2.

This board includes 3 voltage regulators, supplying +7V, +5V, and -5V respectively (F). The AGC loop is constructed by a power detector (AD8318) (H) and a variable gain amplifier (ADL5330) (G), increasing the dynamic range by 40 dB. The pulse generator circuit (D) generates 100 ps width pulses, driving the sampling bridge (E) module to probe the RF signal. Two branches signals are combined by a power combiner and fed into the lowpass filter (A, C). Two lowpass filters are identical, both are 3rd order Chebychev filters, with 3dB frequency at 1.1MHz and a ripple of 0.05dB. The two stages Op-amps circuit (B) is built using LT6230, configured to 59 dB amplification gain. This circuit is fabricated on a 4 layers PCB with dimension of 15cm×8cm×1.6 mm. The complete schematics and PCB layout design can be found in the Appendix A and the Appendix B respectively.

### 4.1.2. Signal Processing System Implementation

The underlying signal processing algorithms have been thoroughly explained in the section 3.3. This section aims to develop a complete processing system ready for run on a FPGA platform. Beside the key algorithms presented previously, the internal communication and controlling sub-systems will be discussed. A demonstration of the processing model from the top layer down to the individual modules and their interconnections is provided. In addition to the signal processing system, some external HDL modules are necessary for the final implementation, including the ADC controlling module and the LCD display module.

**System Architecture**
The functionality of this positioning system is accomplished by three operations: data acquisition, position computing and result output. The architecture, correspondingly, is constructed by three top layer modules as the simplified block diagram depicts in Figure 4.3.

The data acquisition refers to the digitization of the analog signals. The sampling module FMC108 has 4 duo-channel ADC (ADS62P49 from Analog Devices), with 14 bits resolution and maximum 250 Msps speed. Clocks are synthesized using the PLL AD9510. The configuration of this sampling module can be done on-demand via Ethernet with a vendor provided API. 4 channels data are fed into the signal processing core. These are digitized RF receiver output signals, packed to 16 bits width with sign bit. The position computation outputs three 24 bits signals, which carry the estimation
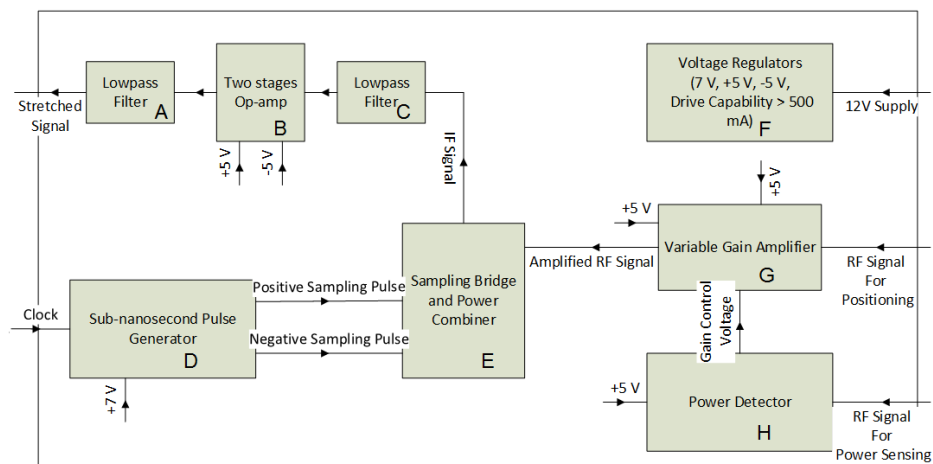
(a)
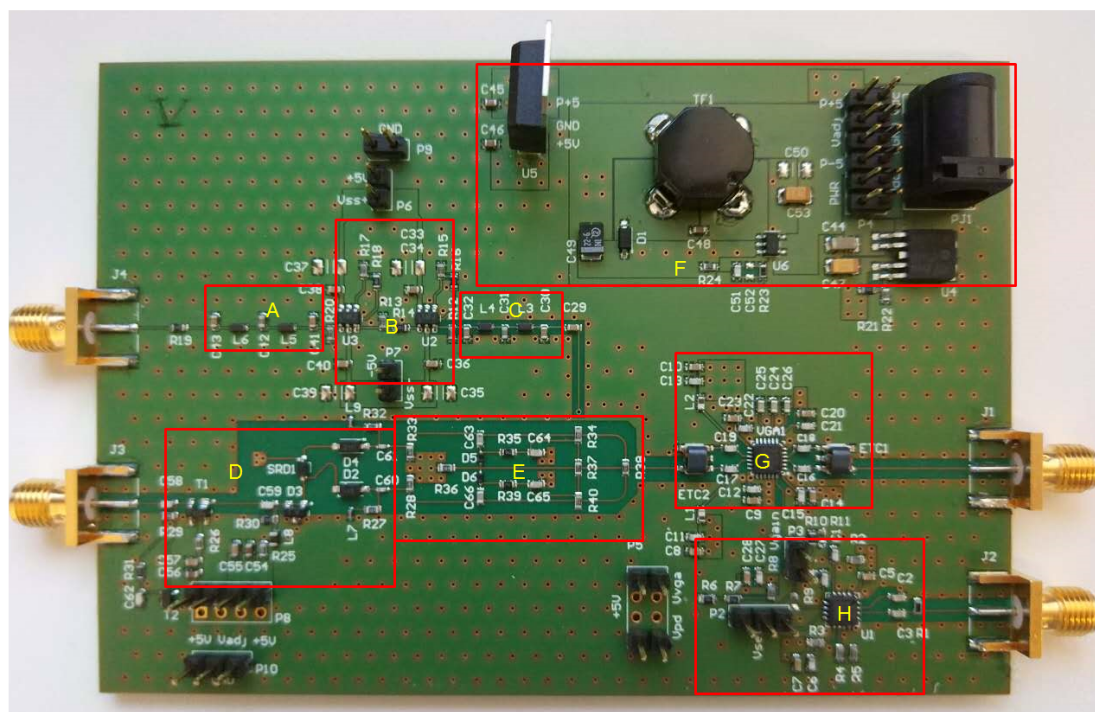


(b)

**Figure 4.2:** Block diagram of the receiver board (a) and fabricated PCB (b) . Blocks are mapped by labels.

coordinate $(\hat{x}, \hat{y}, \hat{z})$ ready for the LCD to display. The data is formatted as in Table 4.1:

**Table 4.1:** Output data format

| bits $23 \sim 20$ | bits $19 \sim 16$ | bits $15 \sim 12$ | bits $11 \sim 8$ | bits $7 \sim 4$ | bits $3 \sim 0$ |
|---|---|---|---|---|---|
| thousands | hundreds | tens | digits | fractions | sign |

The involved LCD module is a $2 \times 16$ character display HD44780U. Resolution of the displayed coordinates with unit $cm$, e.g. 113.3 cm. Driving signals for the display
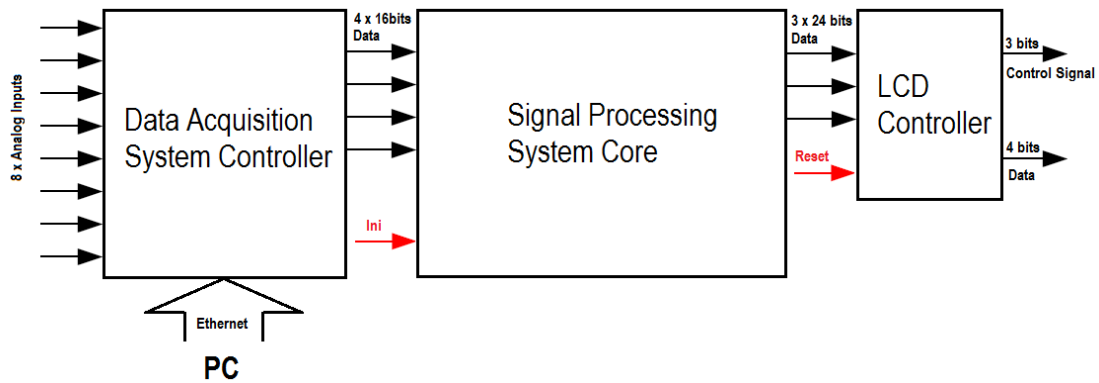
**Figure 4.3:** Simplified block diagram of the processing system, including three modules: Data Acquisition System Controller, Signal Processing System Core and LCD Controller.

include a 3 bits control signal and a 4 bits data signal.

The signal processing system core is modelled in Simulink environment. Besides the key algorithms discussed in the previous chapter, the interconnections and particularly the signal timing is the focus of this section.

**Signal Processing System Core**
The top layer model consists of 3 sub-systems. They are the Interfacing sub-system, the Positioning Core sub-system and the Hex2Dec sub-system (Figure 4.4). Functionality and realization of each sub-system will be demonstrated in this section.
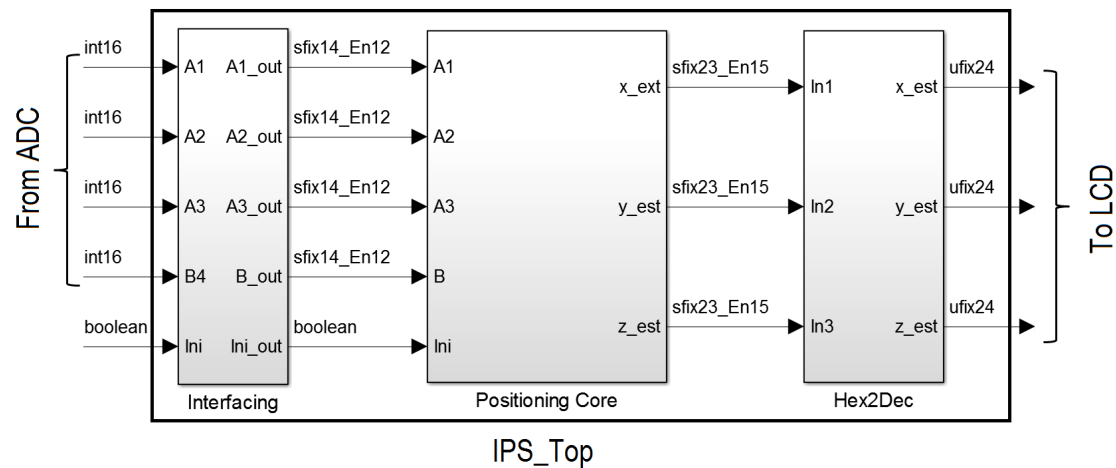


**Figure 4.4:** The processing system model includes three sub-system: Interfacing, Positioning Core and Hex2Dec.

The purpose of each sub-system is summarized:

- Interfacing sub-system
  - Data rate conversion: interface the ADC data rate to the data processing rate.
  - Data type conversion: keep the useful bits.

- Positiong Core sub-system
  - Implement the proposed positioning algorithms.

- Hex2Dec sub-system
  - Convert the estimation result to the data type that could be displayed on the dedicated LCD.

**Interfacing Sub-system**
Due to the limitation of synthesizable clock frequencies of the sampling module FMC108, the minimum samping clock rate feasible on this board is around 40 MSPS. But the demonstration of this prototype system is to utilize a data sampling at 2 Msps. For bridging this data rate differences, a data buffer memory can be used. Alternatively, we convert the date rate down to 2 Msps by undersampling, avoiding the usage of large memory resource and meanwhile process the signal in real-time. Additionally, the data type from the acquisition system is of 16 bits width, of which only the lower 14 bits are the ADC conversion output. Thus, only the lower 14 bits of the incoming data will be kept for further processing. Figure 4.5 depicts an example interfacing process, including two basic operations: rate transition and data type conversion.
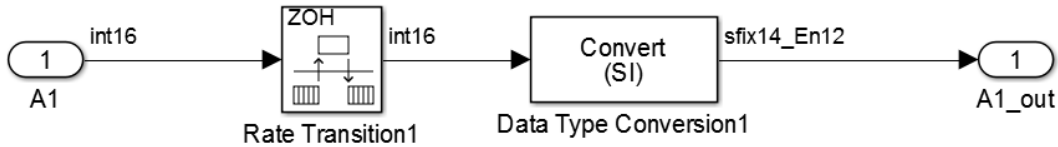


**Figure 4.5:** An example process in the interfacing module. Two basic operations are involved: rate transition and data type conversion.

**Positioning Core Sub-system**
The main processing module performs the underlying algorithms and some necessary controlling and routing operations. Figure 4.6 shows the block diagram of this model, where the black arrows refer to data signals and the red arrows to control signals. The Kalman filter is implemented within the Range Difference Estimator module to improve the range difference estimation. Descriptions of the highlighted signals are summarized in Table 4.2.
The modelling of Baseline Compensation, Normalization and FIR Lowpass Filter have been described in the section 3.3. Considering the Thresholding module, some extra information need to be illustrated that the arrival status signals (A1_en, A2_en, A3_en, B_en) are set high if corresponding signal's arrival was detected. These signals are reset after certain duration (e.g. a measurement interval or shorter period). The TDoA estimation indicator signals (tdoa1_ready, tdoa2_ready, tdoa3_ready) are set high when the computation of range differences is accomplished, and this will trigger an enable signal to start the Newton-Raphson optimization process to estimate the coordinate of the target device in (X,Y,Z). The purpose of the Iteration Controller is to count the iterations. Once the maximum number of iterations is reached, a positioning status signal (pos_ready) is set high for one clock cycle. It is detected by the Range Difference Estimator module to reset all TDoA estimation indicator signals. Meanwhile, this signal enables the output of the estimation result. The Signal Routing module controls the data inputs to the Newton-Raphson Optimization engine. Within one complete iterative process, the range differences (RD) will be kept unchanged and the previous estimation
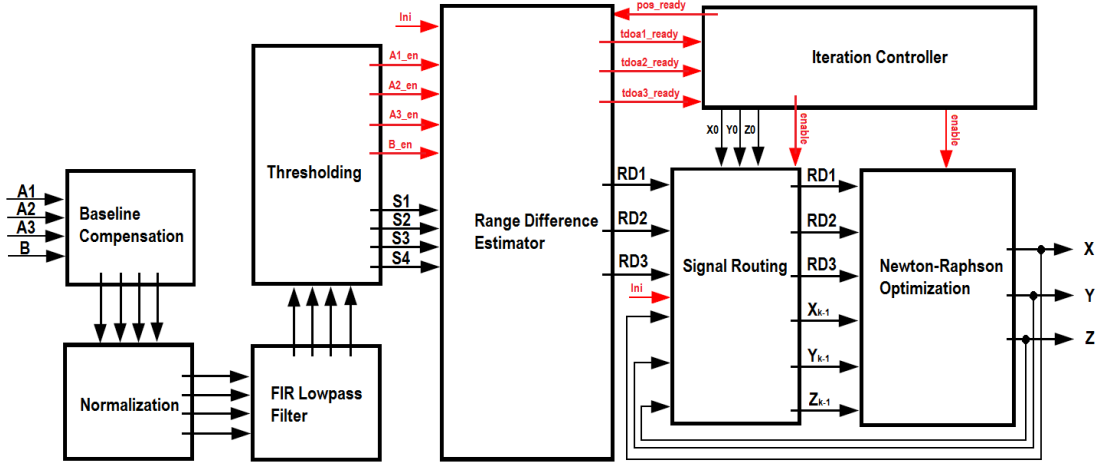
**Figure 4.6:** Block diagram of the processing core sub-system.

**Table 4.2:** List of the interconnections in the processing core sub-system.

| signals | description | signals | description |
|---|---|---|---|
| A1,A2,A3,B | digitized signals | S1,S2,S3,S4 | data forwarded from FIR filters |
| RD1, RD2, RD3 | range differences | X0, Y0, Z0 | initial guess for the iteration process |
| $X_{k-1}$, $Y_{k-1}$, $Z_{k-1}$ | last state estimation | X, Y, Z | position estimation |
| A1_en, A2_en, A3_en, B_en | threshold crossover detection indicator | tdoa1_ready, tdoa2_ready, tdoa3_ready | status of individual TDoA estimation |
| pos_ready | status of the position estimation | enable | enable signal for iterative process |
| Ini | set the computation to initial state | | |

is fed into the iterative engine for position update. The external initialization signal (Ini) is used to start the iterative estimation from the initial guess (X0,Y0,Z0), which we set to the middle of all receivers.

**Hex2Dec Sub-system**

The invoked LCD displays the content by characters, e.g. display the number 1235 as "1235", which contains 4 characters: '1', '2', '3', '5'. The LCD Contoller module is in charge of controlling the LCD and converts the individual element to corresponding ASCII symbols. Before sending the data to the LCD Controller module, it should be converted to the Hexdecimal data type that each nibble represents a decimal number, e.g. $1235_{10} => 1235_{16}$. As with all bases there is a simple algorithm for converting a representation of a decimal number to strings in hexadecimal by doing integer division and remainder operations in the source base. Let d be the decimal number to be display, and the series $h_i h_{i-1}...h_2 h_1$ be the hexadecimal digits representing the number strings. (note that each digit is less than 10)

The Hex2Dec Sub-system firstly converts the signed fixed-point data to unsigned fixed-point data and extracts the sign. The sign nibble is either "0" for positive numbers

or "1" for negative numbers. It outputs the coordinate in 24 bits data format (Table 4.1).

**LCD Controller**

This module is programmed in ISE to interface the $2 \times 16$ characters LCD display. The data from the Hex2Dec module is converted to ASCII symbols that can be displayed by the LCD hardware. The 3D position estimation is shown on the screen in the manner as:

| X | sign | * | * | * | * | . | * | Y | sign | * | * | * | * | . | * |
|---|------|---|---|---|---|---|---|---|------|---|---|---|---|---|---|
| Z | sign | * | * | * | * | . | * |   |      | c | m |   |   |   |   |

Three control signals RS, $R/\bar{W}$ and E are generated for the hardware controlling. Refer to the data sheet of the LCD controller "HD44780U" for detailed programming information.

### 4.1.3. Firmware Architecture

The complete processing system implementation (Figure 4.7) involves the reference design for controlling the data acquisition board FMC108 from the vendor 4DSP. An API is provided to access this module. Communication is done via Ethernet, providing the possibilities to remotely perform: ADC sampling rate control, ADC signalling pattern contrl, data transfer, etc. The positioning module (IPS_Top) reads 4 channels from the module "FMC10x_Ctrl". Displaying the final estimated position result is managed by the LCD Controller module.
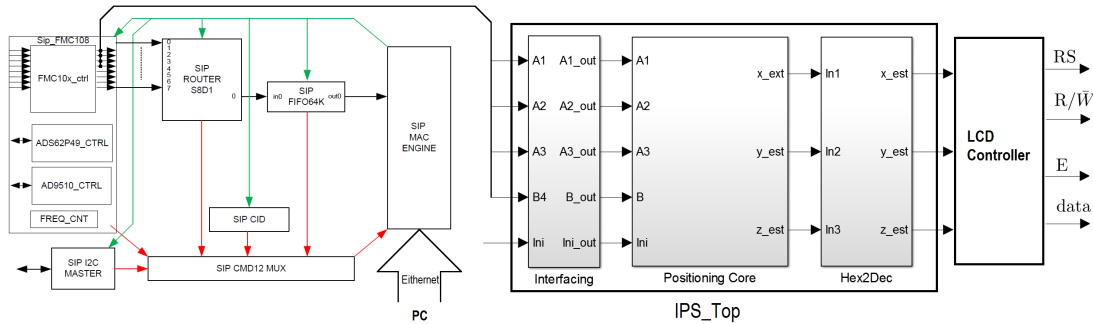


**Figure 4.7:** Firmware architecture, including the data acquisition board controlling, interfacing and the positioning core, etc.

The firmware is synthesized in ISE environment and downloaded to the ML605 platform for system evaluation. The rest of this chapter demonstrates the measurements, including the 1D ranging test and the 3D positioning test.

## 4.2. 1D Ranging Measurement

The proposed system estimates the position based on the measurement of TDoAs. Therefore, the positioning accuracy depends on the measurement quality. In order to evaluate the accuracy of the TDoA estimation, 1D ranging test is performed. The implemented firmware is a simplified version of the complete positioning system, excluding the components for 3D positioning.

### 4.2.1. Test Setup

The measurement of a single TDoA involves a basic system constructed by two RF receivers and a target RF transmitter to be located (Figure 4.8). The receivers are placed in a line at known position and the transmitter moves in between. TDoA is estimated and converted to range difference and further the transmitter's position on the line.



**Figure 4.8:** The range difference from the transmitter to the pairwise receivers is to be determined.

The setup of the measurement system based on the configuration:

- Linear track from -350 mm to +350 mm

- Two receivers located at -500 mm and +500 mm respectively

- Static position estimation

- 50 samples captured at each position with space of 50 mm, i.e. -350 mm, -300 mm, -250 mm, etc.

- $\frac{1}{2}$ wavelength ($\frac{\lambda}{2}$) narrowband dipole antennas are used (centerring at 868 MHz).

- Data acquisition rate of 2 Msps.

- 5MHz OOK, with carrier of 870 MHz.

- Transmission power of 0 dBm.

- Sampling pulse rate at 4.9999 MHz.

The measurement setup in the Lab is depicted in Figure 4.9. Two receivers are located on both sides and one transmitter moves in between. The 870 MHz carrier frequency is modulated by a 5 MHz baseband signal. The repetition rate of sampling pulses on the receiver is 4.9999 MHz. The offset of 100 Hz to the baseband repetition rate results in a signal stretch factor of 49999, generating an output signal with a repetition rate of 100 Hz and a carrier of 17.42 KHz. The stretched signal is further digitized by the data acquisition system. A firmware is implemented to estimate the range difference between the transmitter to the pairwise receivers, which is used to compute the 1D position on the line.

### 4.2.2. Result and Analysis

The transmitter is moved from the left side towards receiver I, in 50 mm. In total 15 positions are estimated. 50 estimations of each position are obtained. The histogram in Figure 4.10 shows the statistic results of these estimations, i.e. the error distributions and the respective counters. As can be seen on this chart, the error distribution is biased, i.e. it doesn't center at 0. The phase center variation (PCV) of
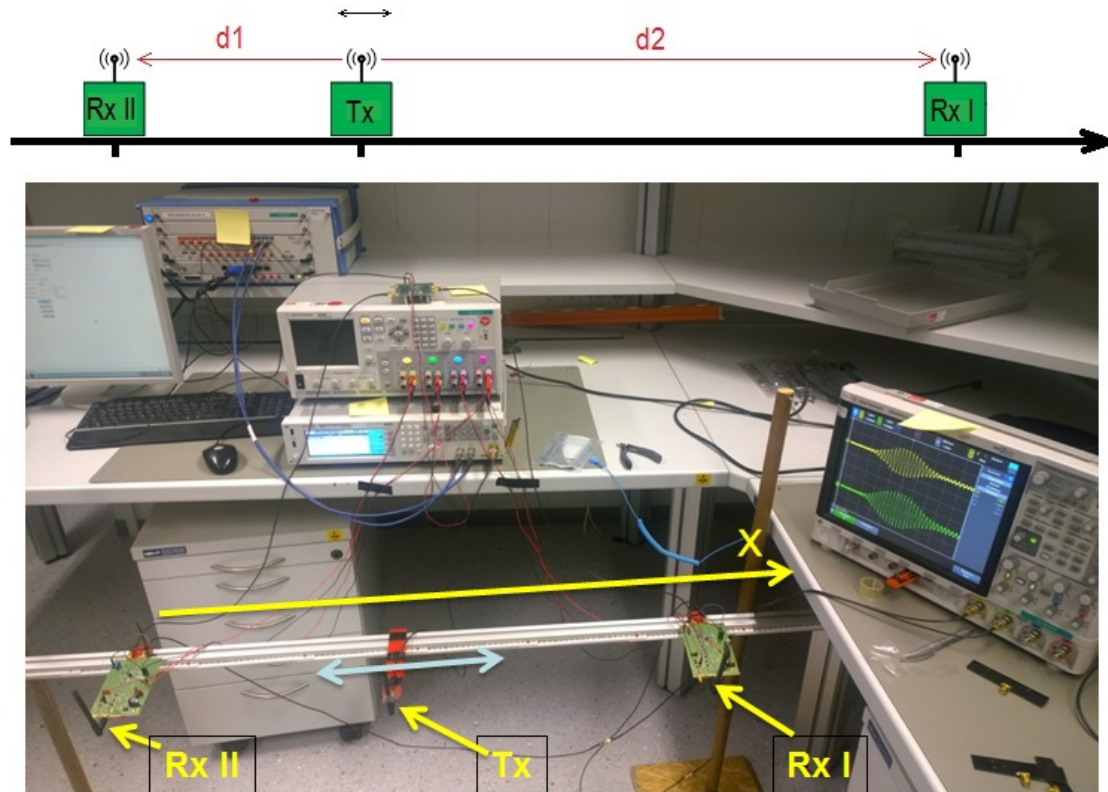
**Figure 4.9:** 1D test in a Lab environment, consisting of two receivers and one transmitter.

the receiver antenna causes the bias, which is the key contributor to the estimation error.
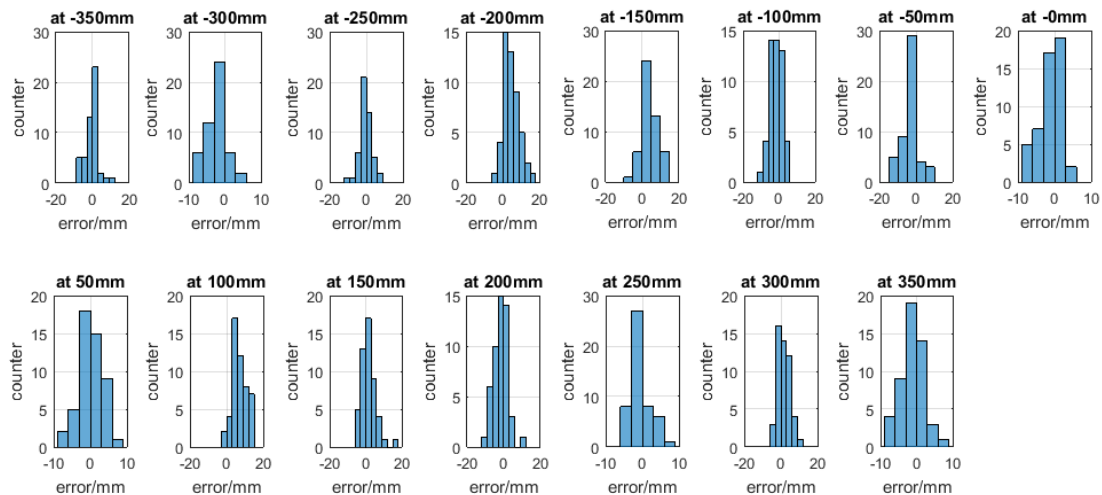


**Figure 4.10:** Estimation error histogram from position -350 mm to position +350 mm.

Figure 4.11(a) displays the RMSE of the estimations along the track. The green curve on the first chart is the estimated locations and the red one on represents the real track. The estimation error is plotted on the second chart. A RMSE of 4.3 mm is obtained. Figure 4.11(b) shows the corresponding estimation variances.
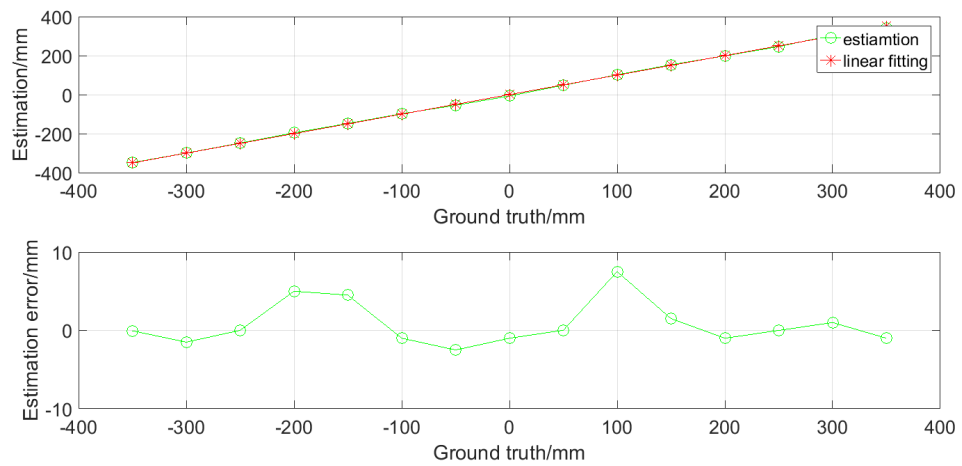
(a)
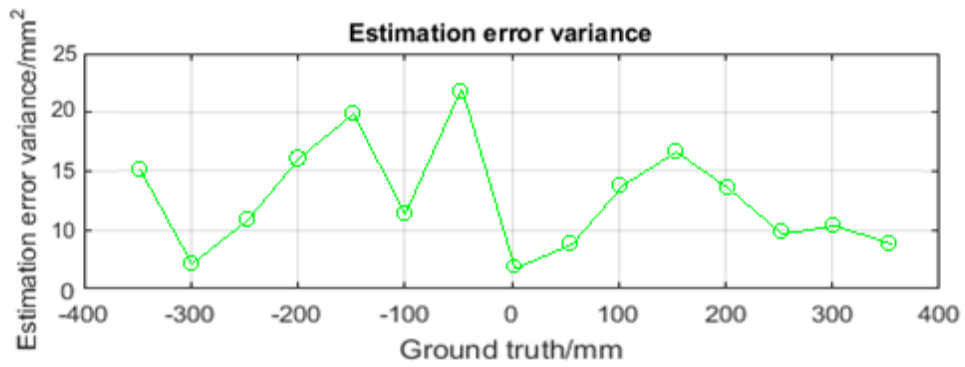


(b)

**Figure 4.11:** 1D position estimation (up, green), linear fitting (up, red), estimation error (down) (a). Variance of estimation error at different positions (b).

The estimation error shown in Figure 4.11(a) shows a strong sinusoidal pattern. The reason for this phenomenon is the PCV of the involved receiver antennas.

**Phase Center Variation (PCV)**
In practice, the antenna is not an ideal point where the signal is received. Instead, the effective point so called phase center will change, depending on many factors, e.g. the arrival angle of the signal, the phase of the arrival signal, the frequency, etc.. For millimeter (mm) ranging applications, this shift has to be compensated, in order to achieve precise (sub-millimeter) position of the antenna. Antenna phase center variation (PCV) is a parameter to describe the deviation of the antenna phase center beyond the antenna offset. The PCV problem is significant for applications requiring the highest attainable precision. Figure 4.12 depicts the phenomenon of antenna phase center variation. The antenna reference point (ARP) is the ideal point where all signals are transmitted or received. All signal sources from the ideal equal phase sphere (EPS) have the same propagation distance to the ARP. But in reality, this real measured phase sphere ($EPS_{real}$) will have deviations from an ideal phase sphere ($EPS_{ideal}$) centered on ARP as shown in Figure 4.12. For example, the phase center for signal from source $S_2$ is located at coincidentally at the ARP, but the signals from $S_1$ and $S_3$ have the same propagation range as $S_2$, because the corresponding phase center offsets ($PC_1$, $PC_2$, $PC_3$) are counteracted (Figure 4.12(a)).
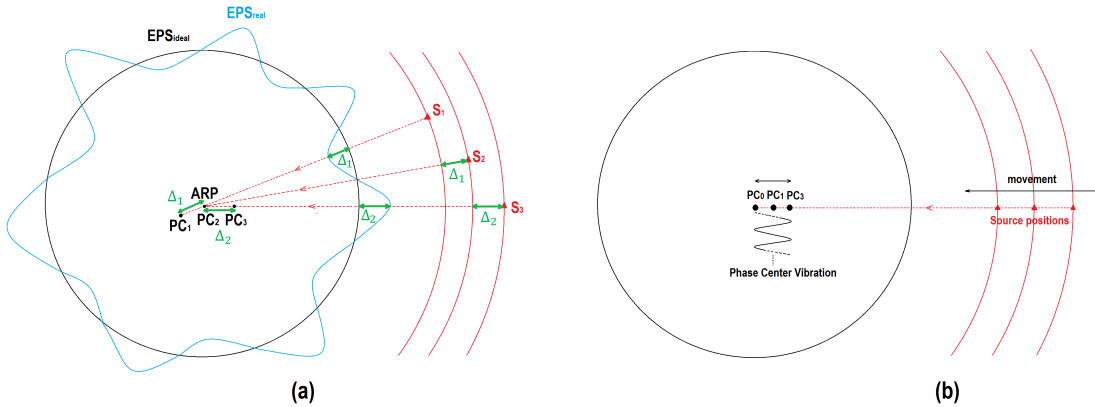


**Figure 4.12:** Antenna phase center variation, dependency on angle of arrival (a), dependency on signal phases (b).

There is no real isotropic antenna. The RF field is radiated from the source and only a portion of the power is detected by the receiver antenna. From the receiver's point of view, only the signals passing through the antenna aperture can be detected and generate a current. Furthermore, a RF signal reception refers to the detection of field superposition of the signals passing through the antenna aperture (Figure 4.13(a)). And the different gains for signals from different angles contribute to the variance. The signal superposition detection causes another parameter effecting the phase center: signal phases. As illustrated in Figure 4.12(b), the phase center vibrates on a line as the signal moves on the same line. This phenomenon is observed in the 1D measurement, referring to the result shown in Figure 4.11(a). The prototype system use half wave dipole antenna with the aperture of approximately $\frac{\lambda}{2} \times \frac{\lambda}{4}$ (as $1.64\lambda^2/4\pi$ in [158]) along the antenna axis. Figure 4.13(b) illustrates the behavior the phase center variation due to range change from the transmitter to the receiver in one dimension.
The antenna PCV can be modeled as:
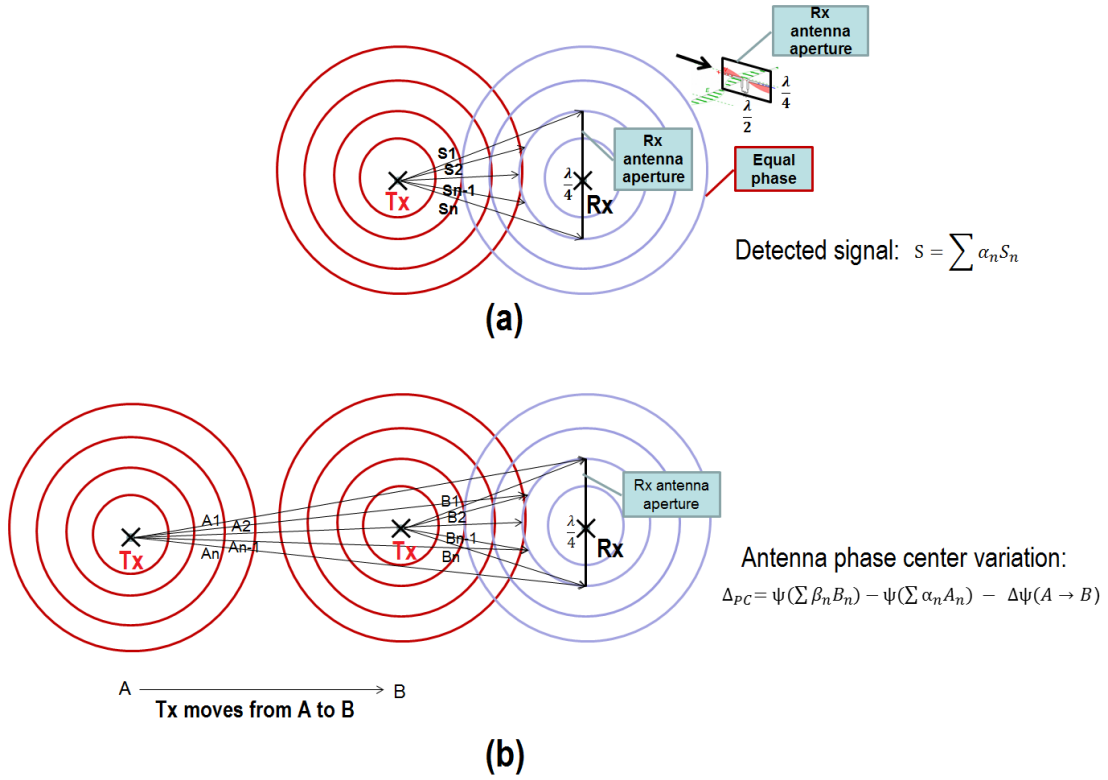
**Figure 4.13:** Detection of RF field (a). PCV dependency on movement.

$$\Delta_{PC} = \Psi\left(\sum(\beta_n)B_n\right) - \Psi\left(\sum(\alpha_n A_n)\right) - \Delta\Psi(A \to B) \tag{4.1}$$

$\Delta_{PC}$: phase center variation (PCV).
$\Psi(\sum(\beta_n)B_n)$: phase of the superposition signal of all $B_i$.
$\Psi(\sum(\beta_n)A_n)$: phase of the superposition signal of all $A_i$.
$\Delta\Psi(A \to B)$: phase change of the corresponding movement from point A to point B.

To demonstrate the effect on 1D ranging measurement, we assume the RF field propagation is decomposed into components and all components arrive at the aperture region have the same gain. A simulation result is illustrated in Figure 4.14(a). The green line represents the linear behavior assuming no phase variation. The red curve is the simulated result, with 2 margin signal components and 1 direct component taken into account. A RMSE of 10.9 mm is computed. For more accurate simulation, usage of physical field simulator is suggested. However in reality, the situation is much more complex, due to complex antenna radiation pattern. Figure 4.14(b) is the 1D ranging measurement in an anechoic chamber where no multi-path interference exists. The red curve on the first chart is the measured position and the phase fluctuation is depicted as the green curve on the second chart. A RMSE of 7.5 mm is observed. It also indicates that the PCV effect on 1D ranging is suppressed in the Lab environment, referring to the RMSE of 4.3 mm. The possible reason is the complicated indoor environment result in a complex EM field propagation, which weakens the phase center vibration pattern by receiving reflected RF signals.
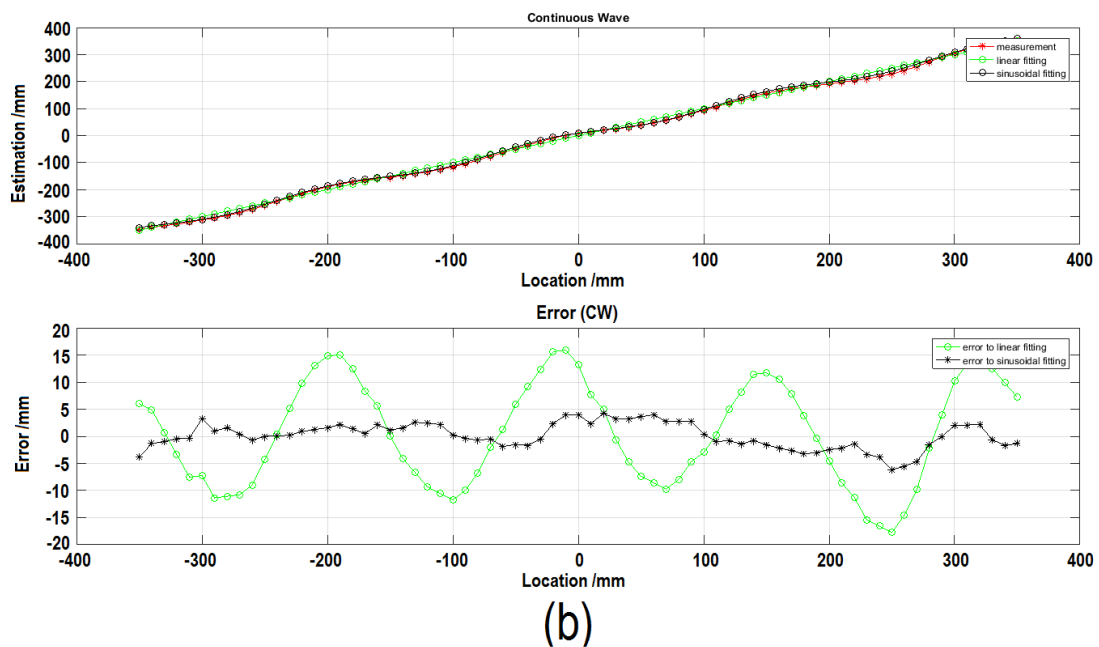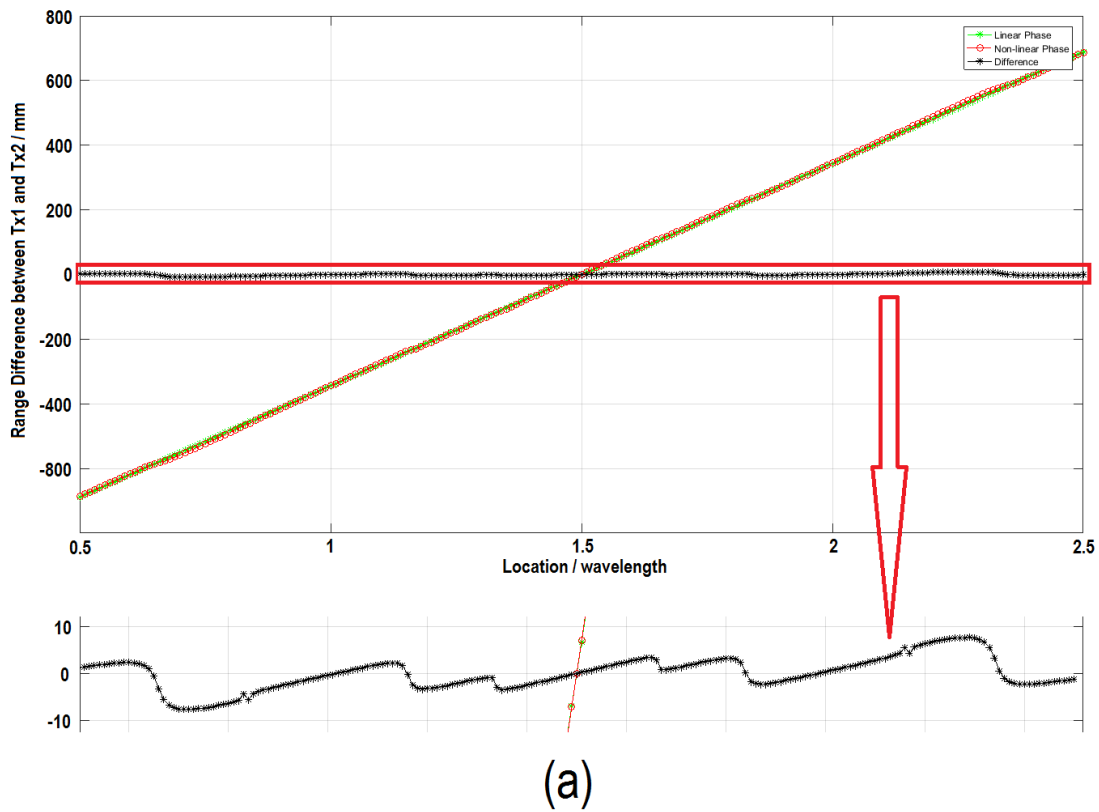
**Figure 4.14:** The simulated result shows a 1D ranging fluctuation due to the antenna phase center vibration (a). The measurement result in an anechoic chamber (b).

## RMSE vs ADC Sampling Frequency

Because the equivalent temporal resolution depends on the stretch factor and the ADC

sampling frequency, i.e. $T_{sampling}/N$, the performance of 1D ranging is also influenced by the ADC sampling frequency. Figure 4.15 shows the 1D ranging measurement result of configuring the sampling rate from 1MHz to 10MHz. It was carried out in an anechoic chamber. The RMSE is approaching a limit after 3MHz at around 7mm. The error variance is approaching at around 25 $mm^2$. As increasing the ADC rate requires more computation effort in the digital signal processing system, the selection of the sampling rate should be considered carefully. In the demonstrator system, 2MHz sampling frequency is implemented.



(a)



(b)
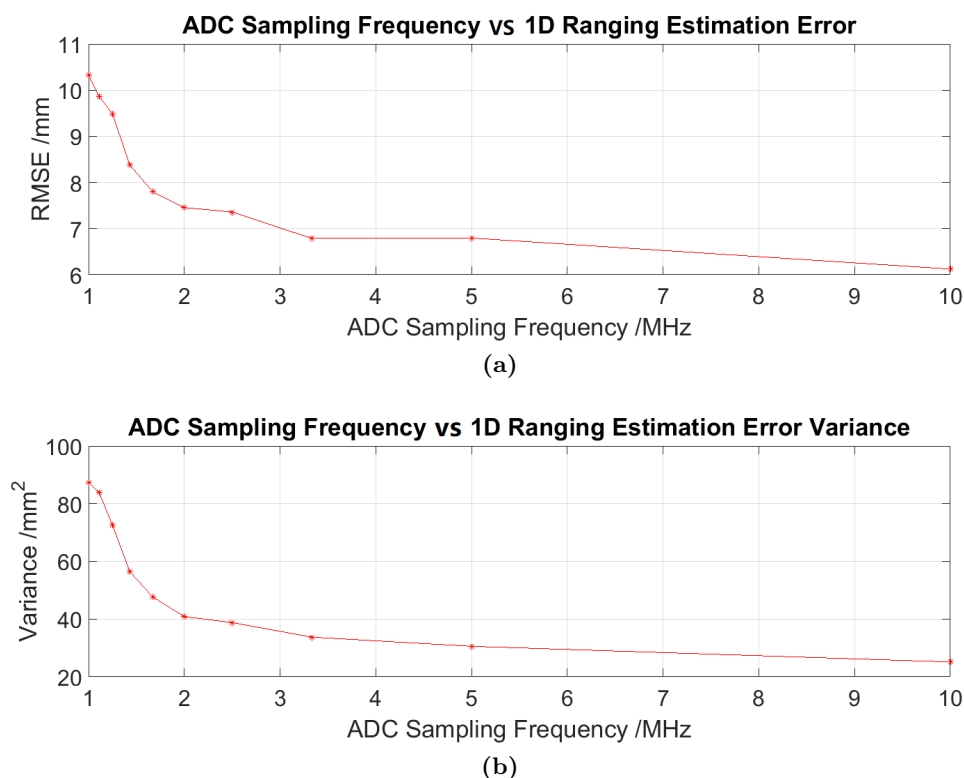
**Figure 4.15:** The 1D ranging performance in an anechoic chamber is improved by increasing the ADC sampling rate, but tend to be limited after 3MHz.

## 4.3. 3D Positioning Measurement

Compared to 1D ranging, the 3D positioning is more useful, considering applications. Because most IPS applications require location information in 3D format, e.g. (x,y,z). For instance, a set of coordinates with index in time domain defines an object tracking system. This section shows the 3D positioning measurement of the prototype system in a Lab environment.

### 4.3.1. Test Setup

A TDoA-based 3D positioning system requires minimum 4 reference nodes, i.e. 4 receivers in the prototype system. A RF transmitter is the target to be located. All the receivers are placed at known locations with the measured coordinates. The signal generation and other settings are identical to the condition in 1D test. The setup of the measurement system is based on the following configuration:

- Four receivers located at (1.443 m, 0.435 m, 2.405 m), (3.083 m, 4.925 m, 2.405 m), (1.433 m, 4.925 m, 1.45 m), (3.083 m, 0.435 m, 1.45 m) respectively (with unknown measurement error), referring to the ground corner of the lab (see setup pictures on the next page).

- 1 Transmitter moves in a space of $60cm \times 90cm \times 60cm$.

- 64 Static potion estimation.

- 10 measurement at each position, with spaced by 20cm/30cm/20cm (X/Y/Z).

- Update rate of 100 Hz.

- $\frac{1}{2}$ wavelength narrowband dipole antennas are used (centering at 868 MHz).

- Data acquisition rate of 2 Msps.

- 5MHz OOK, with carrier of 870 MHz.

- Transmission power of -3 dBm.

- Sampling pulse rate at 4.9999 MHz.

Figure 4.16 depicts the experiment setup for the 3D positioning test. The connections between different modules are shown in Figure 4.1. Receivers' locations are fixed and the transmitter can move in 3 directions. The position change of the transmitter can be read from the rule marks printed on the wood framework, with millimeter resolution. The signal processing system firmware involves the complete design discussed in the subsection 3.3. It is able to estimate the real-time position.

### 4.3.2. Result and Analysis

The experiment demonstrates the measurement result of placing the transmitter on a grid of 64 positions (Figure 4.17). 10 estimations are obtained for each position. An estimation RMSE of 0.807 cm and variance of 0.197 $cm^2$ are observed. Figure 4.18 shows the statistics of the estimation error. Around 82% of the estimation error is smaller than 1 cm (Figure 4.19).

**Figure 4.16:** 3D test in a Lab environment, 4 receivers and 1 target transmitter.

In order to investigate the influence of the geometry of the receivers' locations to the positioning performance, the estimation in 3 dimensions are separately studied. Figure 4.20 shows the estimation error distribution along three directions. RMSE of 0.386cm, 0.224 cm, 0.672 cm respectively are observed. And the variance of the estimation errors are 0.149 $cm^2$, 0.050 $cm^2$, 0.453 $cm^2$ respectively. It can be seen that the system performs the best in Y axis, but worst in Z axis. The reason for this difference is the geometric dilution of precision (GDOP) effect.

**Geometric Dilution of Precision (GDOP)**
The TDoA measurements used to compute target device's coordinate always have some error. These measurement errors are reflected as errors in the computed coordinates. The magnitude of the final error depends on both the magnitude of the measurement error and the geometry of the structure induced by the receiver nodes. The contribution due to geometry is called the geometric dilution of precision (GDOP) [159]. It is defined as:

$$GDOP = \frac{\sqrt{\rho_x^2 + \rho_y^2 + \rho_z^2}}{\rho} \tag{4.2}$$

And the contribution of GDOP on the position dilution of precision (PDOP) can be expressed as [160, 161]:

$$PDOP_{TDoA} = \sqrt{((H^T H)^{-1})_{1,1} + ((H^T H)^{-1})_{2,2} + ((H^T H)^{-1})_{3,3}} \tag{4.3}$$

where H refers to the TDoA-based geometry matrix. It can be computed by applying the receivers coordinates:
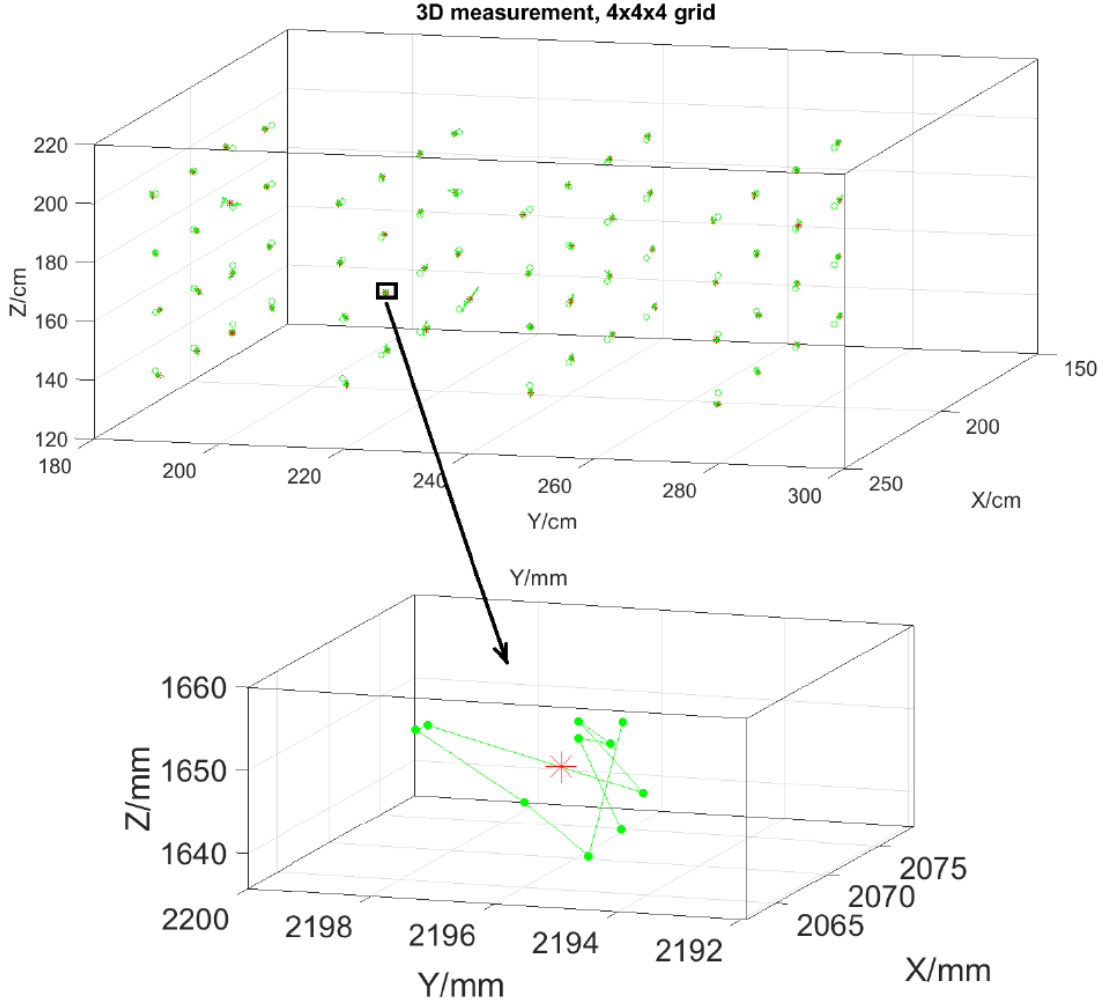
**Figure 4.17:** 10 measurements for each positions (green dots), mean positions (red stars), reference positions (green circles).

$$
H = \begin{bmatrix} x_2 - x_1 & y_2 - y_1 & z_2 - z_1 \\ x_3 - x_1 & y_3 - y_1 & z_3 - z_1 \\ x_4 - x_1 & y_4 - y_1 & z_4 - z_1 \end{bmatrix} = \begin{bmatrix} 1.64 & 4.49 & 0 \\ 0 & 4.49 & 0.955 \\ 1.64 & 0 & 0.955 \end{bmatrix} \tag{4.4}
$$

we compute $((H^T H)^{-1})_{1,1} = 0.279$, $((H^T H)^{-1})_{2,2} = 0.037$, $((H^T H)^{-1})_{3,3} = 0.822$. Assuming the measurement is sufficient accurate (GDOP=PDOP), the estimation error variance in respective axis $(\rho_x^2, \rho_y^2, \rho_z^2)$ is proportional to $((H^T H)^{-1})_{1,1}$, $((H^T H)^{-1})_{2,2}$, $((H^T H)^{-1})_{3,3}$ respectively [162]. The computation result explains the estimation performance difference shown in Figure 4.20. It concludes that the estimation is more accurate in the dimension that the reference nodes are farther apart from each other.
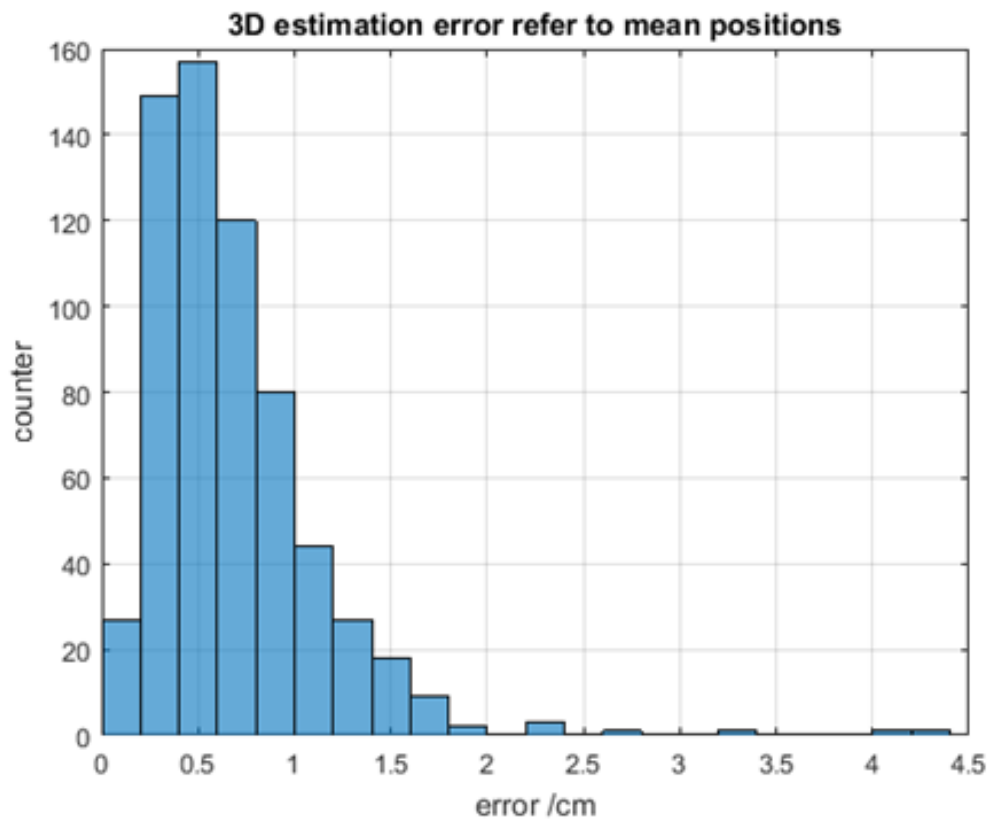
**Figure 4.18:** 3D estimation error statistics, absolute error distribution.
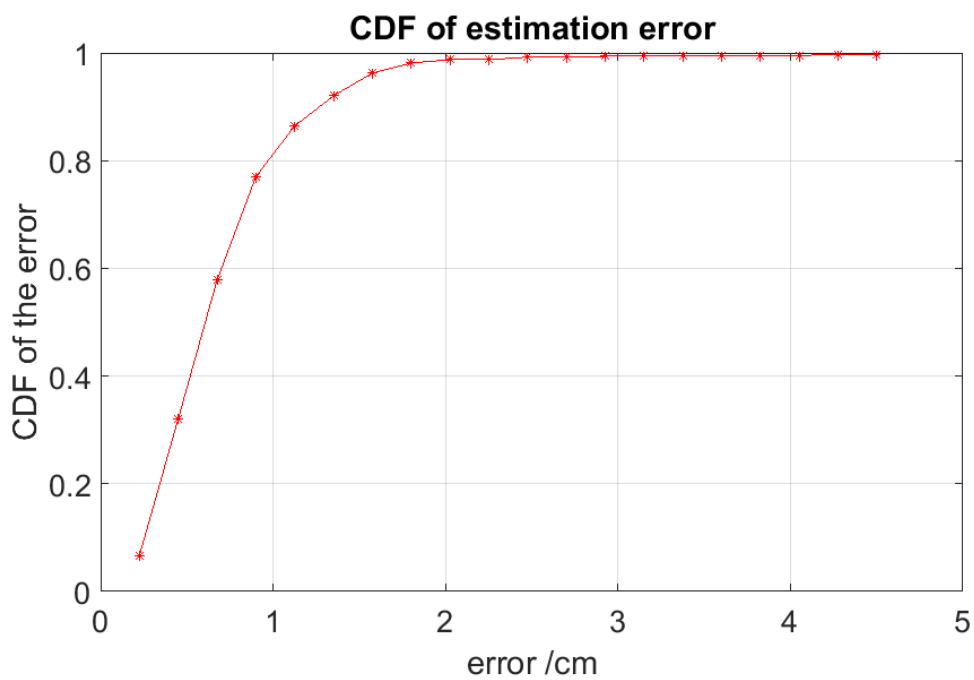


**Figure 4.19:** Cumulative distribution function of the estimation error.
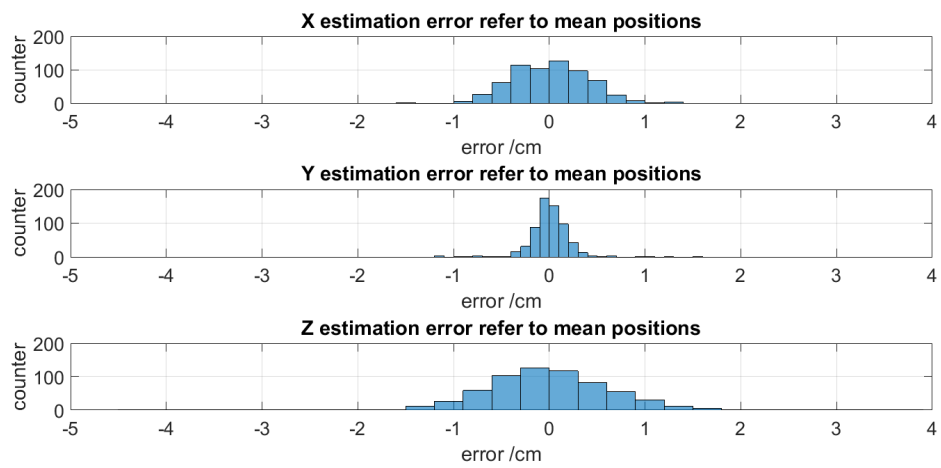
**Figure 4.20:** Estimation error statistics in 3 directions (X,Y,Z).

# 5. Conclusion

This work presents a guideline for developing an indoor positioning system, in aspect of positioning signal, principle and algorithm. A complete development of a high precision indoor positioning system is described. The design, implementation and evaluation of the proposed mm-precision indoor positioning based on TDoA measurements are demonstrated. Underlying hardware, algorithms and system integration are explained. The proposed system is an accurate real-time positioning with high update rate, and provide flexibility in frequency usage.

This chapter concludes the contributions achieved in this work. The challenges and the possible error sources encountered when developing the proposed system are summarized.

## 5.1. Contributions

The complete developing procedure of a sub-centimeter indoor positioning system is described in this work, including the design, implementation and evaluation of the system. A basic system for 3D positioning consists of 4 receivers placed at known locations and a transmitter to be located. It realized positioning based on TDoA measurements. The transmitter emits periodic on-off keying modulated radio frequency signal. This system measures the time difference of arrival of the signal arriving at pairwise receivers, and computes the coordinate of the transmitter.

The following contributions are made to achieve the expected performance.

### Hardware System
The proposed hardwares include RF transmitters, RF receivers and a DSP platform. The developed receiver introduces a narrowband architecture and provides the flexibility in frequency usage. A customized front-end is implemented on the receiver to stretch the received OOK signal with a specific stretch factor configured by manipulating the signal's and the sampling pulse's repetition rate, realizing a temporal resolution in range of pico seconds. It enables the accurate TDoA measurements.

### Signal Processing System
The signal processing includes two key process: TDoA Estimation, Hyperbolic Positioning Algorithm.

The TDoA estimator involves the sequential thresholding and first peak detection approach. A Kalman filter is used as the last stage to improve the estimation performance.

A numerical algorithm based on the Newton-Raphson method is proposed for solving hyperbolic non-linear equations to determine the 3D coordinate of the transmitter.

The firmware development is accelerated with the usage of HDL Coder. Its functionality is tested in the prototype system.

### Prototype Sytem Evaluation
A prototype system is fabricated for concept verification. The system is installed and tested in a lab environment. A positioning RMSE of 0.807cm is achieved in a standard,

fully equipped office/Lab environment, with a variance of $0.197cm^2$. Table 5.1 presents a comparison of the various research and commercial RF-based indoor positioning systems which achieve sub-meter level accuracy. Time-based systems using higher frequencies have shown the potential of better accuracy.

Table 5.1: Comparisons of RF-based IPS techniques

| Indoor Positioning Systems | Positioning Technique | Positioning Signal | Accuracy | Test Environment |
|---|---|---|---|---|
| Horus [122] | RSSI | WLAN | 60cm | Office space |
| Ubicarse [123] | AoA | WLAN | 39cm | Indoor library |
| PAL650 [124] | TDoA | UWB | 30cm | Indoor |
| Ubisense [125] | TDoA and AoA | UWB | 15cm | Indoor |
| Pozyx [127] | ToF | UWB | 10cm | Office room |
| Cricket [95] | ToA | 418MHz RF and 40kHz Ultrasonic | 2cm | Office space |
| This work [42] | TDoA | 870MHz RF | 0.807cm | Indoor laboratory |
| KINETIQ [163] | TDoA | UWB | 1mm~2cm | Indoor |

## 5.2. Challenges

Challenges encountered in development of the proposed system includes:

**Multipath Interference**
The receiving antenna collects many different rays from different directions, producing a rapidly fluctuating RF environment. The multi-path effect makes it hard to achieve high accuracy.

**Antenna Phase Center Variation**
The positioning performance depends on the reliability of the references' locations. An unstable antenna phase center degrades the accuracy of TDoA measurements.

**High Frequency Circuit Design**
The front-end processes high frequencies, including the RF signal and the sub-nanosecond sampling pulse. Design of high frequency components is a difficult task. The signal paths for the pair pulses must be balanced. The phase difference between two branches of the through layer power combiner must as small as possible. Current noise should be carefully considered during PCB development. Individual modules should be fabricated and tested separately before being integrated into a complete system.

**Limited Computation Resources**
Accurate estimation of the position requires a large amount of computation. A compromise between computation resource and processing speed needs to be made when developing the signal processing system. The firmware implements a fixed-point system, and the data types of the interconnections are automatically inherited via internal rule in the Simulink model. But inspection on these signals' range is necessary to decrease the low level resource utilization by setting appropriate data types. Redundant fraction

bits for the dividend is usually required for precise division operation.

**Higher Precision Requirement**
Accurate position measurement is a critical requirement for indoor positioning techniques. This requires the configuration of the system should be as precise as possible, including the measurement of the references' coordinates, calibration of the time to range coefficient, timing within the digital processing system, etc..

## 5.3. Error Sources

Many sources contribute to the overall positioning error. Identifying these issues could help improving the performance in future development. This section discusses some major error sources arising from the signal generation to the final signal processing stage.

**Clocks**
The clocks refer to three different signals: pulse generator driver clocks ($clk_1$), baseband signal ($clk_2$) and ADC sampling clocks ($clk_3$). A stable stretched signal is ensured by stable $clk_1$ and $clk_2$, the repetition offset of which determined the signal stretch rate. Together with ADC sampling clock it effects the accuracy of the TDoA measurement.

**Signal Repetition Rate**
The reason of invoking the OOK modulation scheme is to minimize the influence of the short delayed multi-path components. But it couldn't avoid the effect of long term delayed components. Increasing the symbol interval or decreasing the duty cycle may suppress this effect. However, lower repetition rate results in lower position update frequency.

**Receivers' Locations**
Two folds influences of the receivers' locations on the positioning error need to be considered. First, the accuracy of the receivers' coordinates, which are used for 3D position computation in non-linear model solver. Second, the geometry of the receivers' placement. A specific arrangement could reduce the GDOP contribution.

**Antenna Phase Center Variation (PCV)**
The PCV phenomenon is difficult to model. The uncertainty of the antenna phase center cause the same problem as inaccurate receivers' coordinates. What's worse, it depends on many factors, such as signal arriving angle, frequency and phases.

# 6. Future Work

**Improvement Methods**
The measurements of the prototype system have shown a promising performance. But there are multiple conditions that can be considered for further improvement: frequency, repetition rate, ADC sampling rate, ADC resolution, new antenna, etc. Higher frequency results in better temporal resolution by giving earlier peaks. It results in less effect due to short multipath components. The repetition rate in context refers to the signal and the probing pulse as well. Manipulation of these repetition rates results in different update rate and stretch factor. The trade off of a higher update rate is smaller positioning area. A bigger stretch factor leads to a higher temporal resolution but requires a longer measurement duration. With a fixed stretch factor, increasing the ADC sampling frequency could also achieve a better temporal resolution. An antenna with more stable phase center is preferable. Deployment of antenna arrays is a possibility to eliminate or supress the PCV effect. A more precise receivers placement will improve the estimation. Furthermore, an investigation on geometry of the placement is worthy to improve the precision.

**Transmitter**
The signal in the prototype system is generated by the usage of signal generator instruments. In order to apply the proposed technology to an application, a stand alone transmitter is necessary. As the signal pattern is simple, the development can be accomplished with low cost commercial components. A key consideration is selection of a frequency synthesiser with low phase noise.

**Multiple Access**
Implementation of multiple access is necessary for many applications that multiple objects are tracked simultaneously. Possible options include time division multiple access (TDMA), frequency division multiple access (FDMA), carrier sense multiple access CSMA, etc. The final decision is up to the user requirement on update rate and capacity.

**Wireless Synchronization**
Synchronization in the prototype system is accomplished by deploying cable connections. It refers to two separate tasks. Firstly, the clocks for pulse generation on receivers. The requirement is that they should have the same frequency, phase offset between clocks is not critical. Secondly, the clocks for ADC sampling on receivers. Their frequency is in range from hundreds of kHz to multiple MHz. Offset between these clocks is important, as the time index represent the time of arrival. But due to the low frequency, synchronization between these clocks is not a difficult task. Based on the previous discussions, the implementation of a wireless synchronization can be realized by identical clock generation components and self-calibration processes.

**Development of an Inversed Architecture**
Another possibility for future improvement is deploying an inversed architecture, i.e. transmitters as reference nodes and receivers as the mobile device to be located. It is similar to a pseudolite system but with different signal pattern and positioning scenario. The advantage of this change is that the number of mobile devices would be, in principle, unlimited.

# Appendices

## A. Schematic

Pulse-

Pulse+

GND    R28    50
C60    2pF
L7  36nH  50    R27
GND
Schottky Diode    D2
SRD1
D3    BAW56
GND

Pulse+    50    R33    GND
C61    2pF
50    R32    L9  36nH    GND
Schottky Diode    D4
GND

0.1μF    C55
C54    0.47μF
GND

Vbias    R25    L8  100nH    R30    GND
475
C59    150pF

Vdriver    R26    1K    T1    NPN    GND
0.1μF    C57
C56    0.47μF    GND
T2    NPN    GND

P10    Header 3    GND

C58    470pF    R29    Resistor  50
R31    Resistor  500    470pF    C62    GND

Drive

Receiver Analog Front-end
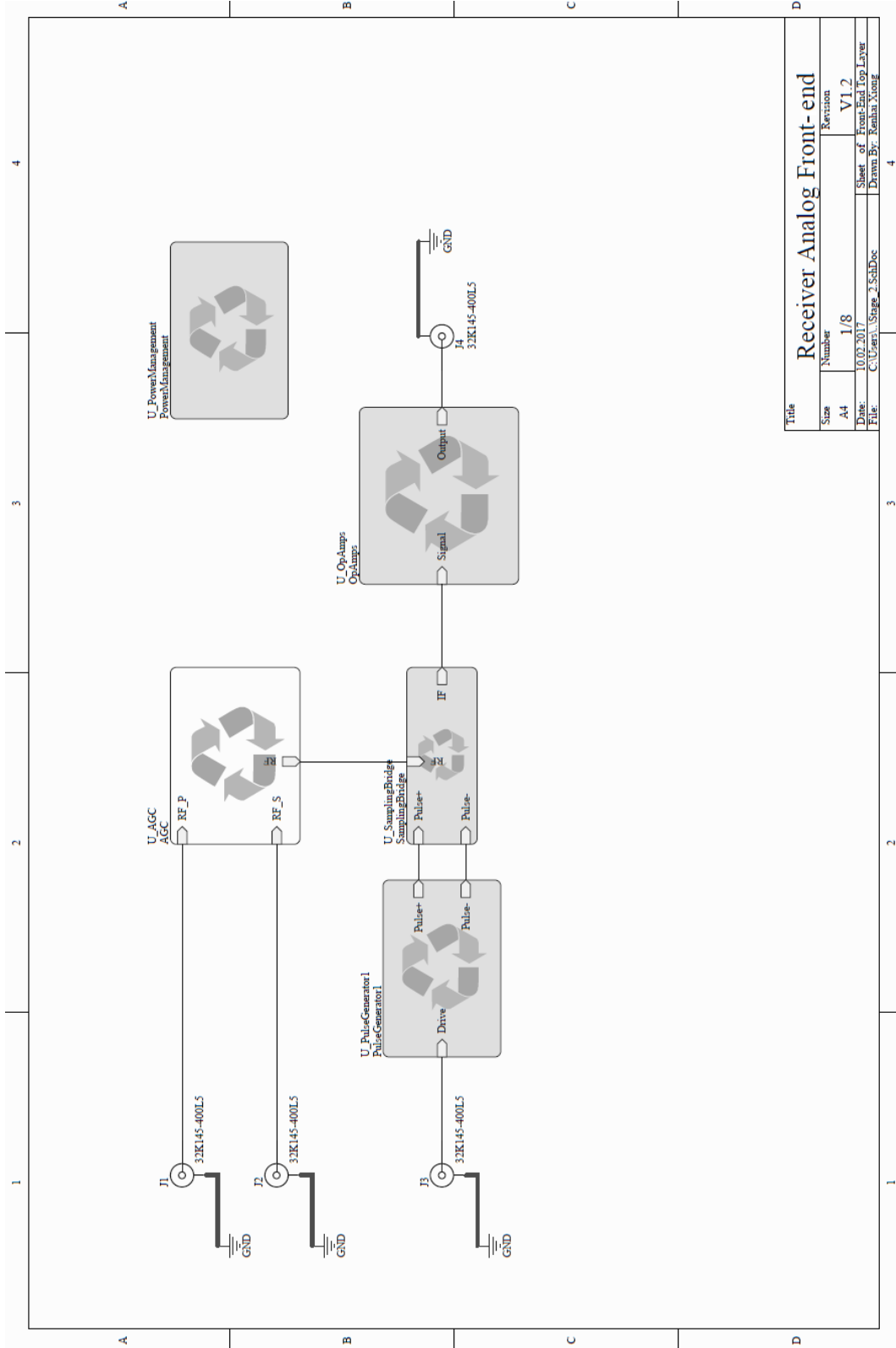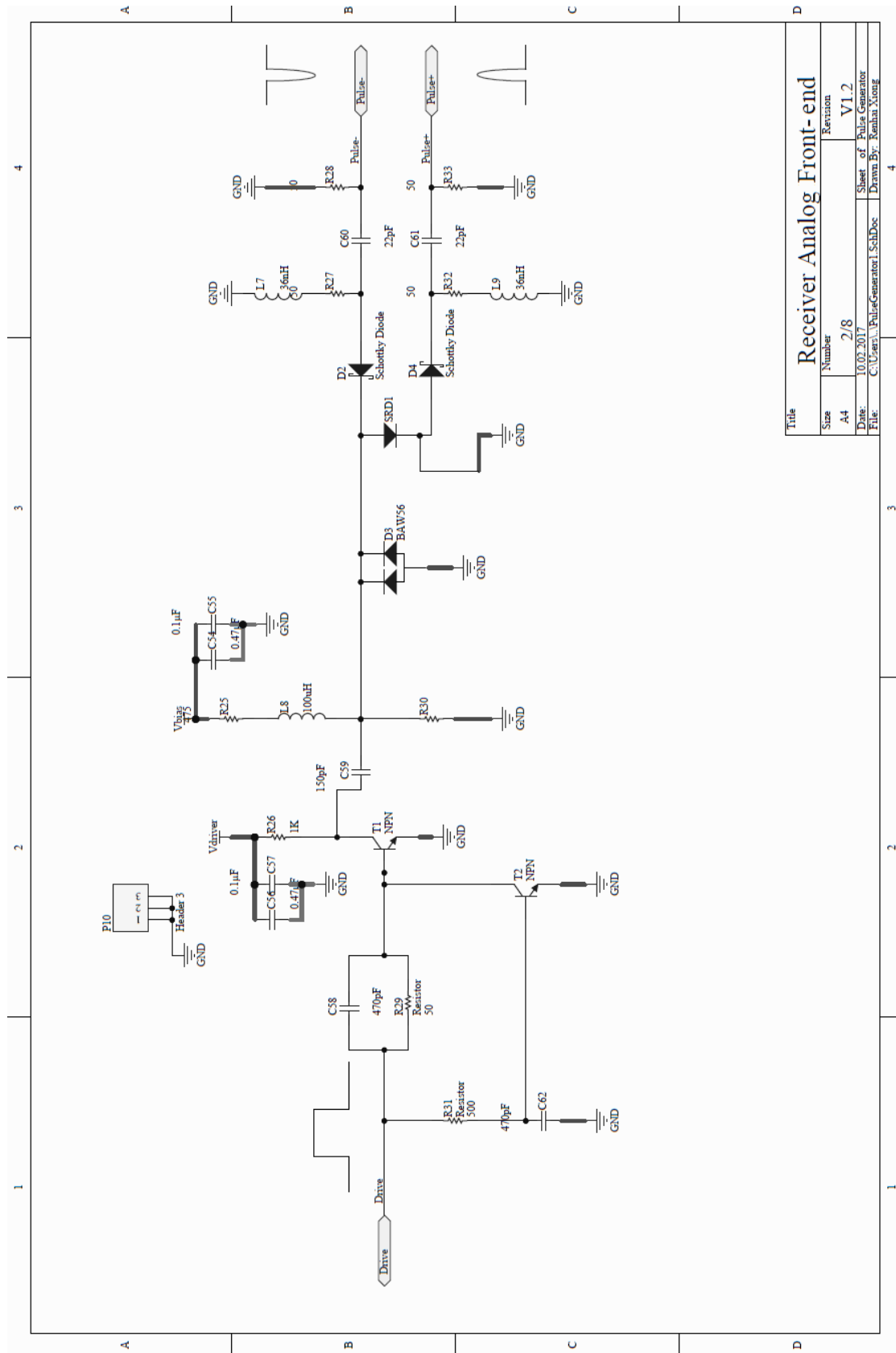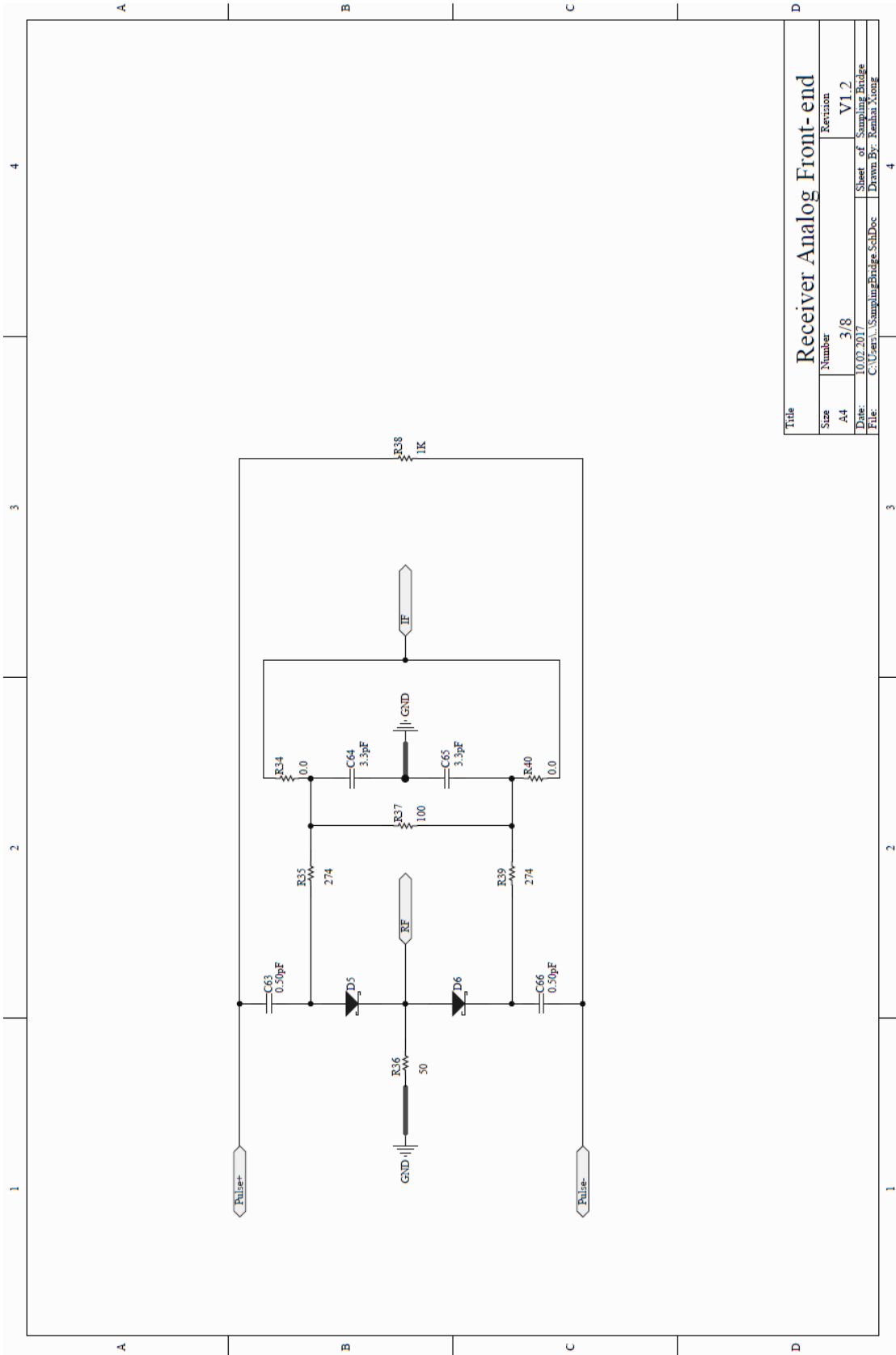
| Title | Receiver Analog Front-end | | |
|---|---|---|---|
| Size | Number | | Revision |
| A4 | 3/8 | | V1.2 |
| Date: | 10.02.2017 | Sheet of | Sampling Bridge |
| File: | C:\Users\..\SamplingBridge.SchDoc | Drawn By: | Renhai Xiong |

Receiver Analog Front-end

RF_P

U ADL5330
ADL5330

RF
RFgain
RF_P

RF

P3
1
2
Header 2

R10
Resistor
207

R11
Resistor
0

GND

VPD

C27
100pF

C28
0.1µF

GND

GND

R8
10k

R9
1K

P2
1
2
3
Header 3

U AD3818
AD3818

Vout

Vset

RF_S

RF S

R7
2.5K

R6
0

GND

RF_P

RF_S

RF

Title
Receiver Analog Front- end

Size
A4

Number

Revision
V1.2

Date: 10.02.2017
File: C:\Users\...\AGC.SchDoc

5/8

Sheet of Automatic Gain Controller
Drawn By: Renhai Xiong

A
B
C
D

4
3
2
1

113

Receiver Analog Front-end

| Title | | |
|---|---|---|
| Size A4 | Number | Revision V1.2 |
| Date: 10.02.2017 | Sheet of Variable Gain Amplifier | |
| File: C:\Users\..\AD3818.SchDoc | Drawn By: Renhai Xiong | |

U1 LT8318

EP ENBL INLO INHI TEMP CMIP CMIP TADJ VPSO

CMIP CMIP VPSI VPSI CLPF VOUT VSET CMOP

RF_S
Vpd
GND

R1 52.3
C2
C3 1000pF
C6 100pF
C7 0.1µF
R3 10.0
R4 1K
R5 1K

C1 100pF
R2 0.0
C4 220pF
C5 0.1µF

Vout
Vset
RF_S

Receiver Analog Front-end

Title

Size: A4
Number
Revision: V1.2

Date: 10.02.2017
Sheet of Power Detector
File: C:\Users\...ADL5330.SchDoc
Drawn By: Renhai Xiong

7/8

U5
L7805CV-DG
INPUT
OUTPUT
GND
+5V
C46 0.1μF
C45 0.33μF
PWR2-5
GND

U4
LD29150
INPUT
INH*
OUTPUT
ADJ
GND
Vadj
C47 10μF
GND
R21 4.69k
R22 1k
GND
PWR
C44 0.33μF
GND

C48 1μF
TF1
SCX147 10n
MBR0520
D1
C49 22μF
GND
GND
-5V
PWR2-5
C50 0μF
GND
C53 4.7μF
GND
U6
LT1931
SW
GND
VIN
*SHDN
NFB
R23 29.4k
R24 10k
GND
C51 220pF
C52 0pF
-5V

Voltage Regulators
12V→-5V
12V→-5V

PJ1
Power Jack-2
VDC
GND

P4
Header 6X2
PWR
PWR2-5
Vadj
PWR2-5
VDC
GND

P5
Header 4X2
Vvga
Vpd
+5V

P6
Header 2
-5V
Vss+
+5V

P7
Header 2
-5V
Vss-

P8
Header 4X2
Vdriver
Vadj
Vbias
+5V
Vadj
+5V

P9
Header 2
GND

# B. PCB Layout

| Symbol | Hit Count | Finished Hole Size | Plated | Hole Type | Physical Length | Rout Path Length |
|---|---|---|---|---|---|---|
| ✿ | 2 | 1,000mm (39,37mil) | PTH | Slot | 3,000mm (118,11mil) | 2,000mm (78,74mil) |
| ○ | 3 | 0,762mm (30,00mil) | PTH | Round | | |
| ▽ | 42 | 0,900mm (35,43mil) | PTH | Round | | |
| □ | 659 | 0,400mm (15,75mil) | PTH | Round | | |
| | 706 Total | | | | | |

Slot definitions : Rout Path Length = Calculated from tool start centre position to tool end centre position.
Physical Length = Rout Path Length + Tool Size = Slot length as defined in the PCB layout
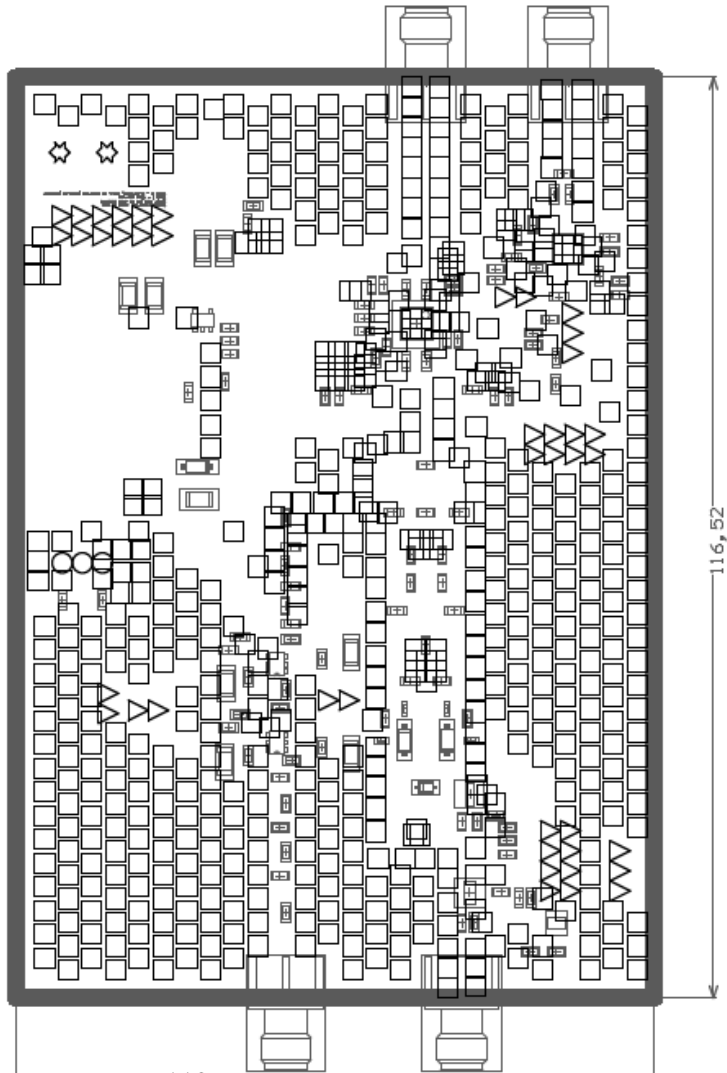
| Layer | Name | Material | Thickness | Constant |
|---|---|---|---|---|
| 1 | Top Overlay | | | |
| 2 | Top Solder | Solder Resist | 0,40mil | 3,5 |
| 3 | Top Layer | Copper | 1,40mil | |
| 4 | Dielectric 1 | FR4 | 6,85mil | 4,5 |
| 5 | Internal Plane 1 | Copper | 0,71mil | |
| 6 | Dielectric 3 | FR4 | 47,24mil | 4,7 |
| 7 | Internal Plane 2 | Copper | 0,71mil | |
| 8 | Dielectric 2 | FR4 | 6,85mil | 4,5 |
| 9 | Bottom Layer | Copper | 1,40mil | |
| 10 | Bottom Solder | Solder Resist | 0,40mil | 3,5 |
| 11 | Bottom Overlay | | | |

116,52

| Layer Name | Type | Material | Thickness (mm) | Dielectric Material | Dielectric Constant | Pullback (mm) | Orientation |
|---|---|---|---|---|---|---|---|
| Top Overlay | Overlay | | | | | | |
| Top Solder | Solder Mask/Co... | Surface Material | 0.01016 | Solder Resist | 3.5 | | |
| Top Layer | Signal | Copper | 0.03556 | | | | Top |
| Dielectric 1 | Dielectric | Core | 0.174 | FR4 | 4.5 | | |
| Internal Plane 1 | Internal Plane | Copper | 0.018 | | | 0.508 | |
| Dielectric 3 | Dielectric | Prepreg | 1.2 | FR4 | 4.7 | | |
| Internal Plane 2 | Internal Plane | Copper | 0.018 | | | 0.508 | |
| Dielectric 2 | Dielectric | Core | 0.174 | FR4 | 4.5 | | |
| Bottom Layer | Signal | Copper | 0.03556 | | | | Bottom |
| Bottom Solder | Solder Mask/Co... | Surface Material | 0.01016 | Solder Resist | 3.5 | | |
| Bottom Overlay | Overlay | | | | | | |
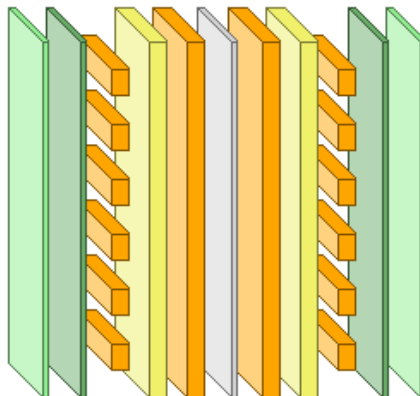
# C. Bill of Material

| Comment | Description | Designator | Footprint | LibRef | Quantity |
|---|---|---|---|---|---|
| 100pF | CAP CER 100PF 50V 5% NP0 0603 | C1, C6, C11, C12, C13, C15, C16, C17, C18, C19, C21, C22, C27 | 0603[1608Metric] | Capacitor | 13 |
| 1000pF | CAP CER 1000PF 50V 10% 0603 | C2, C3, C24, C25, C26 | 0603[1608Metric] | Capacitor | 5 |
| 220pF | CAP CER 220PF 50V 1% NP0 0603 | C4, C51, (C52) leave open | 0603[1608Metric] | Capacitor | 3 |
| 0.1µF | CAP CER 0.1UF 25V 10% X5R 0603 | C5, C7, C8, C9, C10, C14, C20, C23, C28, C34, C36, C38, C40, C55, C57 | 0603[1608Metric] | Capacitor | 15 |
| 0.033µF | CAP CER 0.033UF 25V 5% X7R 0603 | C29 | 0603[1608Metric] | Capacitor | 1 |
| 3.6nF    or 3.3nF | CAP CER 3600PF 50V 5% NP0 0603 | C30, C32, C41, C43 | 0603[1608Metric] | Capacitor | 4 |
| 6.2nF | CAP CER 6200PF 50V 5% NP0 0603 | C31, C42 | 0603[1608Metric] | Capacitor | 2 |
| 47uF | CAP CER 47UF 10V 20% X5R 1206 | leave open C33, C35, C37, C39 | 1206[3216 Metric] | Capacitor | 4 |
| Capacitor    0.33 uF | | C44 | 1206[3216 Metric] | Capacitor | 1 |
| Capacitor  0.33uF, 0.1uF | | C45, C46 | 0603[1608Metric] | Capacitor | 2 |
| 10uF | CAP CER 10UF 10V 10% X5R 1206 | C47 | 1206[3216 Metric] | Capacitor | 1 |
| 1µF | CAP CER 1UF 10V 10% X7R 0603 | C48 | 0603[1608Metric] | Capacitor | 1 |
| 22µF | CAP CER 22UF 6.3V 20% X7R 1206 | C49 | 1410[3524 metric] | Capacitor | 1 |
| 4.7µF | CAP CER 4.7UF 50V 10% X7R 1206 | C50, (C53) leave open | 1206[3216 Metric] | Capacitor | 2 |
| 0.47µF | CAP CER 0.47UF 16V 10% X7R 0603 | C54, C56 | 0603[1608Metric] | Capacitor | 2 |
| 470pF | CAP CER 47PF 50V 1% NP0 0603, CAP CER 4.7PF 250V NP0 0603 | C58, C62 | 0603[1608Metric] | Capacitor | 2 |
| 150pF | CAP CER 150PF 50V 1% NP0 0603 | C59 | 0603[1608Metric] | Capacitor | 1 |
| Capacitor | | C60, C61 | 0402[1005Metric] | Capacitor | 2 |
| 0.50pF | CAP CER 0.5PF 250V NP0 0603 | C63, C66 | 0603[1608Metric] | Capacitor | 2 |
| 3pF      or 3.3pF | CAP CER 3.3PF 50V NP0 0603 | C64, C65 | 0603[1608Metric] | Capacitor | 2 |
| MBR0520 | DIODE SCHOTTKY 20V 500MA SOD123 | D1 | SOD123 | MBR0520 | 1 |
| Schottky Diode | DIODE SCHOTTKY 40V 350MA SOD123 | D2, D4 | SOD123 | Schottky Diode | 2 |
| BAW56 | DIODE ARRAY GP 75V 250MA SOT23 | D3 | SOT-23 | BAW56 | 1 |
| Mixer Diode SMS7621 | DIODE SCHOTTKY MIXER 2V SC-79 | D5, D6 | SC79 | SMS7621 | 2 |
| ETC1-1-13 | E-Series RF 1:1 Transmissions Line Transformer, 4.5 - 3000 MHz | ETC1, ETC2 | 5-SMD | ETC1-1-13 | 2 |
| or 6.8nF 32K145-400L5 | SMA Right Angle Jack, Edge Mount, Up to 18 GHz, -55 to 155 degC | J1, J2, J3, J4 | SMA_FJ_EL | 32K145-400L5 | 4 |
| 120nH | FIXED IND 120NH 300MA 1.2 OHM | L1, L2 | 0603[1608Metric] | Inductor | 2 |
| 10uH | FIXED IND 10UH 80MA 468 MOHM SMD | L3, L4, L5, L6 | 0603[1608Metric] | Inductor | 4 |
| Inductor    40nH | | L7, L9 | 0402[1005Metric] | Inductor | 2 |
| 100uH | FIXED IND 100UH 80MA 5.5 OHM SMD | L8 | 0603[1608Metric] | Inductor | 1 |
| Header 3 | Header, 3-Pin | P2, P10 | HDR1X3 | Header 3 | 2 |
| Header 2 | Header, 2-Pin | P3, P6, P7, P9 | HDR1X2 | Header 2 | 4 |
| Header 6X2 | Header, 6-Pin, Dual row | P4 | HDR2X6 | Header 6X2 | 1 |
| Header 4X2 | Header, 4-Pin, Dual row | P5, P8 | HDR2X4 | Header 4X2 | 2 |
| Power Jack-2 | CON PWR JCK 2.0 X 6.5MM HIGH CUR | PJ1 | P-J-2 | P-J | 1 |

| | | | | | |
|---|---|---|---|---|---|
| 52.3 | RES SMD 52.3 OHM 0.1% 1/10W 0603 | R1 | 0603[1608Metric] | Resistor | 1 |
| 0.0 | RES SMD 0.0 OHM JUMPER 1/10W | R2, R3, R34, R40 | 0603[1608Metric] | Resistor | 4 |
| 1K | RES SMD 1K OHM 5% 1/10W 0603, RES SMD 1K OHM 5% 1/10W 0603, RES SMD 1K OHM 5% 1/10W 0603, RES SMD 1K OHM 5% 1/10W 0603, RES SMD 1K OHM 5% 1/10W 0603, RES SMD 1K OHM 5% 1/10W 0603, RES SMD 1K OHM 5% 1/10W 0603, RES SMD 1K OHM 5% 1/10W 0603, RES SMD 1K OHM 5% 1/10W 0603, RES SMD 10K OHM 1% 1/10W 0603, RES SMD 1K OHM 5% 1/10W 0603, RES SMD 1K OHM 5% 1/10W 0603 | R4, R5, R9, R12, R13, R15, R17, R20, R22, R26, R38 | 0603[1608Metric] | Resistor | 11 |
| 0, 2.43K, 332,22, 51, 511 | | R6, R7, R10, R11, R29, R31 | 0603[1608Metric] | Resistor | 6 |
| 10k | RES SMD 10K OHM 1% 1/10W 0603 | R8, R24 | 0603[1608Metric] | Resistor | 2 |
| 0 | RES SMD 1K OHM 5% 1/10W 0603 | R14, R19 | 0603[1608Metric] | Resistor | 2 |
| 30k    or 30.1k | RES SMD 30K OHM 0.1% 1/10W 0603 | R16, R18 | 0603[1608Metric] | Resistor | 2 |
| 4.69k    or 4.75k | RES SMD 10K OHM 1% 1/10W 0603 | R21 | 0603[1608Metric] | Resistor | 1 |
| 29.4k | RES SMD 29.4K OHM 1% 1/10W 0603 | R23 | 0603[1608Metric] | Resistor | 1 |
| 475 | RES SMD 475 OHM 1% 1/10W 0603 | R25 | 0603[1608Metric] | Resistor | 1 |
| 50 | RES SMD 50 OHM 0.1% 1/8W 0603 | R27, R28, R32, R33, R36 | 0603[1608Metric] | Resistor | 5 |
| 332 | RES SMD 332 OHM 1% 1/10W 0603 | R30 | 0603[1608Metric] | Resistor | 1 |
| 274 | RES SMD 274 OHM 1% 1/10W 0603 | R35, R39 | 0603[1608Metric] | Resistor | 2 |
| 100 | RES SMD 100 OHM 0.1% 1/10W 0603 | R37 | 0603[1608Metric] | Resistor | 1 |
| SMMD837 | SURFACE MOUNT SMMD SILICON MULTIPLIER SERIES (SRD) DIODES IN SOD 323 PACKAGE | SRD1 | SOD323 | SMMD837 | 1 |
| NPN | TRANS NPN 12V 35MA SOT143B | T1 | SOT-143B | BFG93A_X_N | 1 |
| NPN | TRANS NPN 4.5V 21GHZ SOT343R | T2 | SOT-343R | BFG480W | 1 |
| SCX147 | INDUCT ARRAY 2 COIL 10UH SMD | TF1 | TF-4 | SCX147 | 1 |
| LT8318 | IC LOG DETECTOR/CTRLR 16-LFCSP | U1 | CP_16_4 | AD8318ACPZ-REEL7 | 1 |
| LT6230CS6#TRMPBF | IC OPAMP GP 215MHZ RRO TSOT23-6 | U2, U3 | SOT_6-S | LT6230CS6#TRMPBF | 2 |
| LD29150 | IC REG LDO ADJ 1.5A PPAK | U4 | TO-252-5 | LD29150 | 1 |
| L7805CV-DG | IC REG LDO 5V 1.5A TO220 | U5 | TO-220-3 | L7805CV-DG | 1 |
| LT1931 | IC REG INV 1A TSOT23-5 | U6 | SOT_5-S | LT1931AES5#TRMPB | 1 |
| ADL5330 | IC AMP/ATTENUATOR RF | VGA1 | RGE24_M | ADL5330 | 1 |
| | | | | | |

# D. Lowpass Filter Design

For electronic applications, digital filters [164] are broadly involved components of signal processing systems. In contrast to analog filters, digital filters are electronic circuits operating on discrete-time signals. Due to different topologies of the digital filter, there are two categories of digital filters: the recursive filter and the nonrecursive filter, referring to infinite impulse response (IIR) filters and finite impulse response (FIR) filters, respectively. Both are well known for their pros and cons. Comparing to FIR filters, IIR filters cost less hardware but can be unstable and suffer from nonlinear phase response, which is challenging to predict and compensate. This disadvantage induces unexpected delays in time domain to the signal, whereas the linear phase response property of FIR filter makes the algorithm selection obvious, because the allowable tolerance for timing discriminators are expected be as small as possible. Four types of FIR filter have the ability to achieve linear phase response [164] :

| Impulse Response | Number of Coefficients | $H(\omega)$ | Type |
|---|---|---|---|
| $h(n) = h(M-1-n)$ | Odd | $e^{\frac{-j\omega(M-1)}{2}}(h(\frac{M-1}{2}) + 2\sum_{k=1}^{(M-3)/2} h(\frac{M-1}{2} - k)\cos(\omega k)$ | I |
| $h(n) = h(M-1-n)$ | Even | $e^{\frac{-j\omega(M-1)}{2}} 2\sum_{k=1}^{(M-3)/2} h(\frac{M}{2} - k)\cos(\omega(k - \frac{1}{2}))$ | II |
| $h(n) = -h(M-1-n)$ | Odd | $e^{\frac{-j\omega(M-1)}{2} - \pi/2} 2\sum_{k=1}^{(M-1)/2} h(\frac{M-1}{2} - k)\sin(\omega k)$ | III |
| $h(n) = -h(M-1-n)$ | Even | $e^{\frac{-j\omega(M-1)}{2} - \pi/2} 2\sum_{k=1}^{(M-1)/2} h(\frac{M}{2} - k)\sin(\omega(k - \frac{1}{2}))$ | IV |

**Table D.1:** Four types of FIR filters, with linear phase response

Type II in D.1 is implemented in this project, because of its versatile usage [164]. The even symmetric impulse response reduces the usage of multiplications by half which will significantly save the resource cost, as each multiplier can be shared by two product operations in the FIR filter algorithm.

There are currently pretty various references available for designing digital filter. Analogical to the Laplace transformation in continues domain, the Z-transform is introduced to characterize transfer functions for discrete systems. Each Z-domain function is equivalent to a difference equation in discrete domain. The produced design should have the transfer function that can satisfy the filter property specifications. A general digital filter has a transfer function as:

$$Y(z) = -\sum_{k=1}^{N} a_k Y(z) z^{-k} + \sum_{k=0}^{M} b_k X(z) z^{-k}$$

Filter input $x(n)$, output $y(n)$. $Y(z)$ and $X(z)$ are their $Z$ transformation respectively. $a_k$ and $b_k$ are the filter coefficients, $N$ is the feedback filter order, $M$ is the feed forward filter order.
As FIR filters do not have the recursive network, $N = 0$:

$$Y(z) = \sum_{k=0}^{M} b_k X(z) z^{-k}$$

The transfer function of FIR filter:

$$H(z) = \frac{Y(z)}{Xz()} = \sum_{k=0}^{M} b_k z^{-k}$$

Converse Z-transform of FIR filter:

$$y(n) = \sum_{k=0}^{M} b_k x(n-k) \tag{D.1}$$

$b_k$ in (D.1) is called filter coefficients. It implies that the dedicated filter system leads to the architecture of summation of delayed samples, weighted by filter coefficients. Figure D.1 diagrams the topology of the FIR filter, with input $x[n]$, output $y[n]$ and filter coefficients $b_k$.
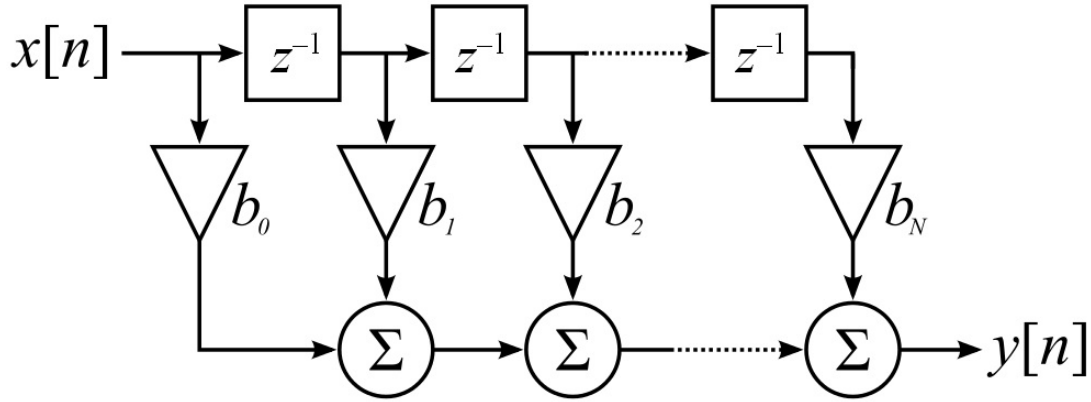


**Figure D.1:** FIR filter direct form diagram

Assume an impulse input signal $x(n) = \delta(n)$. The impulse response is derived:

$$h(n) = y(n) = \sum_{k=0}^{M} b_k \delta(n-k) = b_n$$

Firstly, we need to know how the detector signal looks like both in time-domain and in frequency domain.

Secondly, approximate the frequency range of the pulses which we are interested in. The related frequency is referred to the digital frequency defined as:

$$\omega = 2\pi \frac{f_{carrier}}{f_{sample}} = 2\pi \frac{T_{sample}}{T_{carrier}}$$

The period of pulse can be approximated by the pulse width. In the condition of N oversampling rate, it derives a digital frequency $\omega$ of $2 * \pi / N$.

In this project, the window based method is introduced for the filter design. Filter coefficients can be computed by the element-wise multiplication of ideal filter coefficients and appropriate window function.

An ideal frequency response with respect to the stop frequency can be formulated as:

| Windows | Transition Region Ca. | Minimum Stop Band Attenuation |
|---|---|---|
| Rectangular | $4\pi/L$ | $-21dB$ |
| Hanning | $8\pi/L$ | $-44dB$ |
| Hamming | $8\pi/L$ | $-53dB$ |
| Blackman | $12\pi/L$ | $-74dB$ |

**Table D.2:** Four types window functions for designing FIR filters.

$$H_{ideal}(\omega) = \begin{cases} 1 & \text{when } |\omega| < \omega_c \\ 0 & \text{otherwise} \end{cases} \tag{D.2}$$

The ideal filter coefficients can be derived from the Inverse Discrete Fourier Transform (IDFT) of (D.2)

$$h_{ideal}(n) = \frac{1}{2\pi} \int_{-\pi}^{\pi} H_{ideal}(\omega) e^{j\omega n} \delta_\omega = \frac{\sin(n\omega_c)}{n\pi} \qquad \text{where} \qquad n \in Z \tag{D.3}$$

The ideal filter has an infinite length, which is not practical realizable, whereupon some special shaped windows [165] (e.g. Rectangular window, Hanning window, Hamming window, Blackman window, etc.) are contrived to restrict the filter length, meanwhile close the delta Dirac mass close to the ideal frequency response $H_{ideal}(\omega)$. The induced window is sampled with finite length $L$. The value $\frac{L-1}{2}$ is called the order of this filter.

As practical filters should also be casual, another restriction is put forward, that the system is delayed by $\frac{L-1}{2}$

$$h_{ideal}(n) = \frac{1}{2\pi} \int_{-\pi}^{\pi} H_{ideal}(\omega) e^{j\omega n} \delta_\omega = \frac{\sin((n - \frac{L-1}{2})\omega_c)}{(n - \frac{L-1}{2})\pi} \qquad \text{where} \qquad n \in Z$$

Desired filter response:

$$H_{ideal}(\omega) = \begin{cases} 1 & \text{when } |\omega| < \omega_c \\ 0 & \text{otherwise} \end{cases} \tag{D.4}$$

Coefficients of the ideal window (L order), derived by IFFT of $H_{ideal}(\omega)$.

$$h_n = \begin{cases} \frac{\sin(\frac{2\pi}{N}(n-L/2))}{\pi(n-L/2)} \\ \frac{\omega_c}{\pi} = \frac{2}{N} \end{cases} \qquad \text{when} \qquad n = L/2$$

Hamming window function:

$$W_n = \begin{cases} 0.54 - 0.46\cos(\frac{2\pi n}{L}) & \text{when } 0 \leqslant n \leqslant L \\ 0 & \text{otherwise} \end{cases}$$

The filter coefficients:

$$b_n = h_n * W_n$$

Result Design can be implemented by applying the coefficients in to filter system function:

$$y(n) = \sum_{k=0}^{N} b_k x(n-k)$$

A convenient way as suggested in this work for designing a filter is with the assistance of a MATLAB tool. The Filter Design & Analysis Tool provided by MathWorks free the algorithm developer from manually modelling (Figure D.2) Part A gives some basic setting about the filter types and design methods. Settings in B specify some preferences. Frequencies and magnitude specifications in C/D define the response of the expected filter. The result filter is summarized in region F and its magnitude/phase response graphs are displayed in zone E. This design tool provides many other options listed in G, including realizing the filter, zeros and poles editor, multirate filter, filter quantization, etc. The filter quantization function is important for further development when generating a HDL code from this filter, where fixed point data is expected.
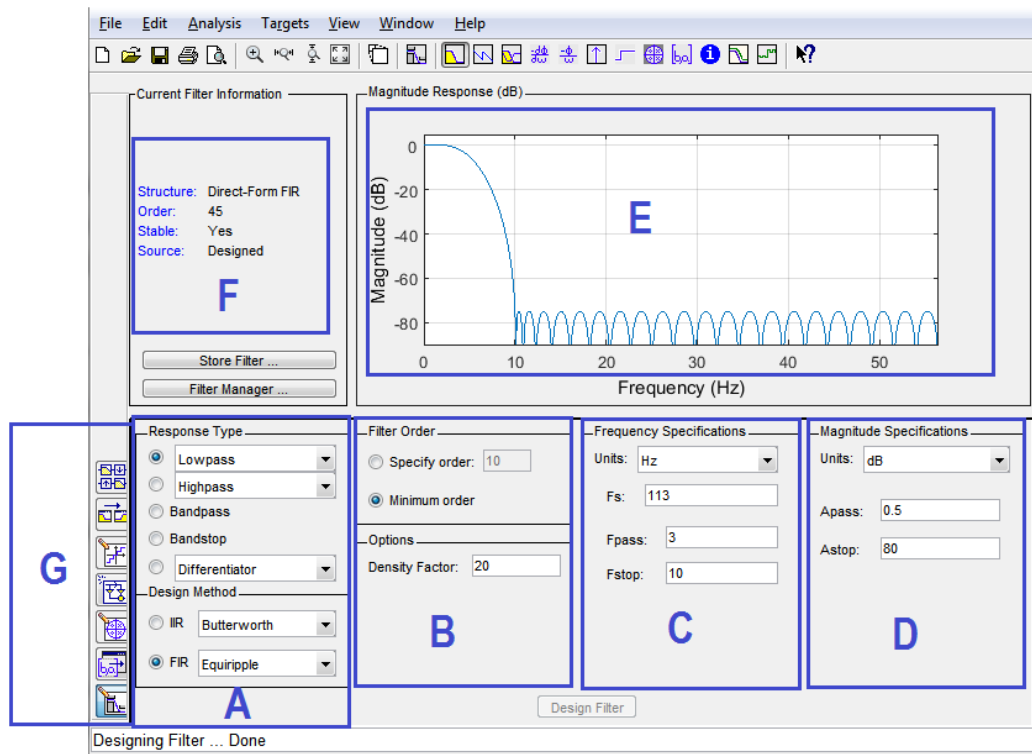


**Figure D.2:** Interface of the Filter Design & Analysis Tool from MathWorks.

Realizing the designed filter in Simulink model is shown in Figure D.3. There are two modules included in this filter module: a filter and a quantizer. The filter designer will automatically quantize the coefficients and adjust the input to the data type that was set previously.
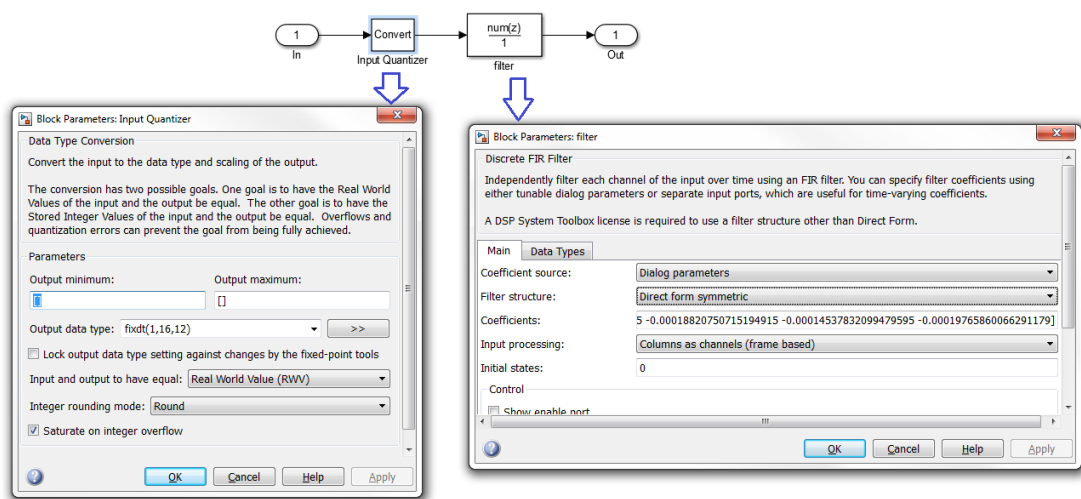
**Figure D.3:** Realize the designed filter in Simulink, including two basic modules: a filter and a quantizer.

## E. Newton-Raphson Equations

Assume the coordinates of the receivers: $(x_i, y_i, z_i)$ $(i = 1, 2, 3, 4)$. Distances from the receivers to the target transmitter: $d_i$ $(i = 1, 2, 3, 4)$. And the range difference referring to the receiver 1 are estimated: $RD_{1j}$ $(j = 2, 3, 4)$.

Rewrite equation (3.23) by moving the right item to the left:

$$
\begin{aligned}
f(x, y, z) &= \sqrt{(x - x_i)^2 + (y - y_i)^2 + (z - z_i)^2} \\
&\quad - \sqrt{(x - x_j)^2 + (y - y_j)^2 + (z - z_j)^2} - RD_{ij} \\
&= 0
\end{aligned}
\tag{E.1}
$$

These range differences are applied to the equation (E.1) yields to:

$$
\mathbf{F}(x, y, z) = \begin{bmatrix} f_1 \\ f_2 \\ f_3 \end{bmatrix} = 0
\tag{E.2}
$$

with

$$
f_1 = \sqrt{(x - x_1)^2 + (y - y_1)^2 + (z - z_1)^2} - \sqrt{(x - x_2)^2 + (y - y_2)^2 + (z - z_2)^2} - RD_{12}
\tag{E.3}
$$

$$
f_2 = \sqrt{(x - x_1)^2 + (y - y_1)^2 + (z - z_1)^2} - \sqrt{(x - x_3)^2 + (y - y_3)^2 + (z - z_3)^2} - RD_{13}
\tag{E.4}
$$

$$
f_3 = \sqrt{(x - x_1)^2 + (y - y_1)^2 + (z - z_1)^2} - \sqrt{(x - x_4)^2 + (y - y_4)^2 + (z - z_4)^2} - RD_{14}
\tag{E.5}
$$

The Newton-Raphson method update the position estimation by:

$$
\hat{p}(x_{k+1}, y_{k+1}, z_{k+1}) = \hat{p}(x_k, y_k, z_k) - \mathbf{J}^{-1}(\mathbf{F}(x_k, y_k, z_k)) * \mathbf{F}(x_k, y_k, z_k)
\tag{E.6}
$$

Where, $\mathbf{J}$ is the Jacobean matrix of size $3 \times 3$ holding the partial derivatives of the hyperbolic equation $\mathbf{F}$, $\hat{p}(x_k, y_k, z_k)$ is the solution after $k$ iterations, updated from $\hat{p}(x_k, y_k, z_k)$. The Jacobean matrix is defined as:

$$
\mathbf{J} = \begin{bmatrix}
\frac{\partial f_1}{\partial x} & \frac{\partial f_1}{\partial y} & \frac{\partial f_1}{\partial z} \\
\frac{\partial f_2}{\partial x} & \frac{\partial f_2}{\partial y} & \frac{\partial f_2}{\partial z} \\
\frac{\partial f_3}{\partial x} & \frac{\partial f_3}{\partial y} & \frac{\partial f_3}{\partial z}
\end{bmatrix}
\tag{E.7}
$$

The partial derivatives of these functions w.r.t x, y and z:

$$\frac{\partial f_1}{\partial x} = \frac{x-x_1}{\sqrt{(x-x_1)^2+(y-y_1)^2+(z-z_1)^2}} - \frac{x-x_2}{\sqrt{(x-x_2)^2+(y-y_2)^2+(z-z_2)^2}} \tag{E.8}$$

$$\frac{\partial f_1}{\partial y} = \frac{y-y_1}{\sqrt{(x-x_1)^2+(y-y_1)^2+(z-z_1)^2}} - \frac{y-y_2}{\sqrt{(x-x_2)^2+(y-y_2)^2+(z-z_2)^2}} \tag{E.9}$$

$$\frac{\partial f_1}{\partial z} = \frac{z-z_1}{\sqrt{(x-x_1)^2+(y-y_1)^2+(z-z_1)^2}} - \frac{z-z_2}{\sqrt{(x-x_2)^2+(y-y_2)^2+(z-z_2)^2}} \tag{E.10}$$

$$\frac{\partial f_2}{\partial x} = \frac{x-x_1}{\sqrt{(x-x_1)^2+(y-y_1)^2+(z-z_1)^2}} - \frac{x-x_3}{\sqrt{(x-x_2)^2+(y-y_2)^2+(z-z_2)^2}} \tag{E.11}$$

$$\frac{\partial f_2}{\partial y} = \frac{y-y_1}{\sqrt{(x-x_1)^2+(y-y_1)^2+(z-z_1)^2}} - \frac{y-y_3}{\sqrt{(x-x_2)^2+(y-y_2)^2+(z-z_2)^2}} \tag{E.12}$$

$$\frac{\partial f_2}{\partial z} = \frac{z-z_1}{\sqrt{(x-x_1)^2+(y-y_1)^2+(z-z_1)^2}} - \frac{z-z_3}{\sqrt{(x-x_2)^2+(y-y_2)^2+(z-z_2)^2}} \tag{E.13}$$

$$\frac{\partial f_3}{\partial x} = \frac{x-x_1}{\sqrt{(x-x_1)^2+(y-y_1)^2+(z-z_1)^2}} - \frac{x-x_4}{\sqrt{(x-x_2)^2+(y-y_2)^2+(z-z_2)^2}} \tag{E.14}$$

$$\frac{\partial f_3}{\partial y} = \frac{y-y_1}{\sqrt{(x-x_1)^2+(y-y_1)^2+(z-z_1)^2}} - \frac{y-y_4}{\sqrt{(x-x_2)^2+(y-y_2)^2+(z-z_2)^2}} \tag{E.15}$$

$$\frac{\partial f_3}{\partial z} = \frac{z-z_1}{\sqrt{(x-x_1)^2+(y-y_1)^2+(z-z_1)^2}} - \frac{z-z_4}{\sqrt{(x-x_2)^2+(y-y_2)^2+(z-z_2)^2}} \tag{E.16}$$

The inverse of the Jacobian matrix $\mathbf{J}$ (eq. E.7):

$$\mathbf{J}^{-1} = \frac{1}{det(\mathbf{J})} adj(\mathbf{J}) \tag{E.17}$$

$det(\mathbf{J})$ is the matrix determinant and the adjugate matrix of $\mathbf{J}$ is represented as $adj(\mathbf{J})$. The computation of these two terms:

$$det(\mathbf{J}) = \frac{\partial f_1}{\partial x}\left(\frac{\partial f_2}{\partial y}\frac{\partial f_3}{\partial z} - \frac{\partial f_3}{\partial y}\frac{\partial f_2}{\partial z}\right) - \frac{\partial f_1}{\partial y}\left(\frac{\partial f_2}{\partial x}\frac{\partial f_3}{\partial z} - \frac{\partial f_3}{\partial x}\frac{\partial f_2}{\partial z}\right) - \frac{\partial f_1}{\partial z}\left(\frac{\partial f_2}{\partial x}\frac{\partial f_3}{\partial y} - \frac{\partial f_3}{\partial x}\frac{\partial f_2}{\partial y}\right)$$
$$\tag{E.18}$$

$$adj(\mathbf{J}) = \begin{bmatrix} \frac{\partial f_1}{\partial x} & \frac{\partial f_2}{\partial x} & \frac{\partial f_3}{\partial x} \\ \frac{\partial f_1}{\partial y} & \frac{\partial f_2}{\partial y} & \frac{\partial f_3}{\partial y} \\ \frac{\partial f_1}{\partial z} & \frac{\partial f_2}{\partial z} & \frac{\partial f_3}{\partial z} \end{bmatrix} \tag{E.19}$$

The equations $(E.3 \sim E.19)$ are the complete set of one iteration for the position estimation from range difference measurements, with the priori knowledge of the receivers' locations.

# References

[1] R. Mautz, "Indoor positioning technologies," 2012.

[2] M. Kuhn, C. Zhang, B. Merkl, D. Yang, Y. Wang, M. Mahfouz, and A. Fathy, "High accuracy uwb localization in dense indoor environments," in *Ultra-Wideband, 2008. ICUWB 2008. IEEE International Conference on*, vol. 2. IEEE, 2008, pp. 129–132.

[3] M. I. Skolnik, "Radar systems," 2001.

[4] W. Dickinson, "Engineering evaluation of the loran-c navigation system," *Final Report by Jansky and Bailey, Inc., Washington, DC, September*, 1959.

[5] H. Sorg, "From serson to drapertwo centuries of gyroscopic development," *Navigation*, vol. 23, no. 4, pp. 313–324, 1976.

[6] I. Getting, "The global positioning system," *IEEE Spectrum*, pp. 30(12):36–47, December 1993.

[7] D. Aufderheide and W. Krybus, "Towards realtime camera egomotion estimation and threedimensional scene acquisition from monocular image streams," *Proceedings of the 2010 International Conference on Indoor Positioning and Indoor Navigation (IPIN)*, September 15-17 2010.

[8] S. R. S. C. M. F. W. H. Boochs, F. and J. Meier, "Increasing the accuracy of untaught robot positions by means of a multi-camera system," *Proceedings of the 2010 International Conference on Indoor Positioning and Indoor Navigation (IPIN)*, September 15-17 2010.

[9] K. Pahlavan, X. Li, and J.-P. Makela, "Indoor geolocation science and technology," *IEEE Communications Magazine*, vol. 40, no. 2, pp. 112–118, 2002.

[10] H. Hile and G. Borriello, "Positioning and orientierung in indoor environments using camera phones," *IEEE Computer Graphics and Applications*, pp. 32–39, July/August 2008.

[11] S. J. Muffert, M. and W. Frstner, "Positioning and orientierung in indoor environments using camera phones," *Proceedings of the 2nd International Conference on Machine Control & Guidance*, pp. 95–104, 2010.

[12] B. G. M. M. Popescu, V. and E. Sacks, *The Modelcamera,*. Graphical Models, 2006, vol. 68.

[13] D. Hauschildt and N. Kirchhof, "Advances in thermal infrared localization: Challenges and solutions," *Proceedings of the 2010 International Conference on Indoor Positioning and Indoor Navigation (IPIN)*, September 15-17 2010.

[14] S. Lee and J. Song, "Mobile robot localization using infrared light reflecting landmarks," *Proceedings of the International Conference on Control, Automation and Systems (ICCAS07)*, pp. 674–677, 2007.

[15] C. Lee, Y. Chang, G. Park, J. Ryu, S.-G. Jeong, S. Park, J. W. Park, H. C. Lee, K.-s. Hong, and M. H. Lee, "Indoor positioning system based on incident angles of infrared emitters," in *Industrial Electronics Society, 2004. IECON 2004. 30th Annual Conference of IEEE*, vol. 3. IEEE, 2004, pp. 2218–2222.

[16] C. Medina, J. C. Segura, and n. De la Torre, "Ultrasound indoor positioning system based on a low-power wireless sensor network providing sub-centimeter accuracy," *Sensors*, vol. 13, no. 3, p. 3501, 2013. [Online]. Available: http://www.mdpi.com/1424-8220/13/3/3501

[17] A. Yazici, U. Yayan, and H. Ycel, "An ultrasonic based indoor positioning system," in *Innovations in Intelligent Systems and Applications (INISTA), 2011 International Symposium on*, June 2011, pp. 585–589.

[18] M. Hazas and A. Hopper, "Broadband ultrasonic location systems for improved indoor positioning," *IEEE Transactions on Mobile Computing*, vol. 5, no. 5, pp. 536–547, May 2006.

[19] C. Randell and H. Muller, *Low Cost Indoor Positioning System*. Berlin, Heidelberg: Springer Berlin Heidelberg, 2001, pp. 42–48. [Online]. Available: http://dx.doi.org/10.1007/3-540-45427-6_5

[20] M. Minami, Y. Fukuju, K. Hirasawa, S. Yokoyama, M. Mizumachi, H. Morikawa, and T. Aoyama, *DOLPHIN: A Practical Approach for Implementing a Fully Distributed Indoor Ultrasonic Positioning System*. Berlin, Heidelberg: Springer Berlin Heidelberg, 2004, pp. 347–365. [Online]. Available: http://dx.doi.org/10.1007/978-3-540-30119-6_21

[21] N. L. Dortz, F. Gain, and P. Zetterberg, "Wifi fingerprint indoor positioning system using probability distribution comparison," in *2012 IEEE International Conference on Acoustics, Speech and Signal Processing (ICASSP)*, March 2012, pp. 2301–2304.

[22] C. Feng, W. S. A. Au, S. Valaee, and Z. Tan, "Received-signal-strength-based indoor positioning using compressive sensing," *IEEE Transactions on Mobile Computing*, vol. 11, no. 12, pp. 1983–1993, Dec 2012.

[23] H.-H. Liu and Y.-N. Yang, "Wifi-based indoor positioning for multi-floor environment," in *TENCON 2011 - 2011 IEEE Region 10 Conference*, Nov 2011, pp. 597–601.

[24] A. H. Lashkari, B. Parhizkar, and M. N. A. Ngan, "Wifi-based indoor positioning system," in *Computer and Network Technology (ICCNT), 2010 Second International Conference on*, April 2010, pp. 76–78.

[25] C. Pei, Y. Cai, and Z. Ma, "An indoor positioning algorithm based on received signal strength of wlan," in *Circuits, Communications and Systems, 2009. PACCS'09. Pacific-Asia Conference on*. IEEE, 2009, pp. 516–519.

[26] M. Cypriani, F. Lassabe, P. Canalda, and F. Spies, "Open wireless positioning system: A wi-fi-based indoor positioning system," in *Vehicular Technology Conference Fall (VTC 2009-Fall), 2009 IEEE 70th*, Sept 2009, pp. 1–5.

[27] M. Ocana, L. Bergasa, M. Sotelo, J. Nuevo, and R. Flores, "Indoor robot localization system using wifi signal measure and minimizing calibration effort," in *Proceedings of the IEEE International Symposium on Industrial Electronics*, vol. 4, 2005, pp. 1545–1550.

[28] H. Zou, H. Wang, L. Xie, and Q.-S. Jia, "An rfid indoor positioning system by using weighted path loss and extreme learning machine," in *Cyber-Physical Systems, Networks, and Applications (CPSNA), 2013 IEEE 1st International Conference on.* IEEE, 2013, pp. 66–71.

[29] S. S. Saab and Z. S. Nakad, "A standalone rfid indoor positioning system using passive tags," *IEEE Transactions on Industrial Electronics*, vol. 58, no. 5, pp. 1961–1970, 2011.

[30] A. Bekkali, H. Sanson, and M. Matsumoto, "Rfid indoor positioning based on probabilistic rfid map and kalman filtering," in *Third IEEE International Conference on Wireless and Mobile Computing, Networking and Communications (WiMob 2007).* IEEE, 2007, pp. 21–21.

[31] J. Na, "The blind interactive guide system using rfid-based indoor positioning system," in *International Conference on Computers for Handicapped Persons.* Springer, 2006, pp. 1298–1305.

[32] L. M. Ni, Y. Liu, Y. C. Lau, and A. P. Patil, "Landmarc: indoor location sensing using active rfid," *Wireless networks*, vol. 10, no. 6, pp. 701–710, 2004.

[33] M. Korona, M. Mandić, V. Pejić, and D. Silađi, "Bluetooth indoor positioning," 2015.

[34] A. Bekkelien, M. Deriaz, and S. Marchand-Maillet, "Bluetooth indoor positioning," *Master's thesis, University of Geneva*, 2012.

[35] L. Pei, R. Chen, J. Liu, T. Tenhunen, H. Kuusniemi, and Y. Chen, "Inquiry-based bluetooth indoor positioning via rssi probability distributions," in *Advances in Satellite and Space Communications (SPACOMM), 2010 Second International Conference on.* IEEE, 2010, pp. 151–156.

[36] S. Feldmann, K. Kyamakya, A. Zapater, and Z. Lue, "An indoor bluetooth-based positioning system: Concept, implementation and experimental evaluation." in *International Conference on Wireless Networks*, 2003, pp. 109–113.

[37] Y. Luo and C. L. Law, "Indoor positioning using uwb-ir signals in the presence of dense multipath with path overlapping," *IEEE Transactions on wireless communications*, vol. 11, no. 10, pp. 3734–3743, 2012.

[38] B. Yan and L. Xiaochun, "Research on uwb indoor positioning based on tdoa technique," in *Electronic Measurement & Instruments, 2009. ICEMI'09. 9th International Conference on.* IEEE, 2009, pp. 1–167.

[39] Z. Sahinoglu, S. Gezici, and I. Guvenc, "Ultra-wideband positioning systems," *Cambridge, New York*, 2008.

[40] Y.-H. Jo, J.-Y. Lee, D.-H. Lee, and S.-H. Kang, "Accuracy enhancement for uwb indoor positioning using ray tracing," *The Journal of Korean Institute of Communications and Information Sciences*, vol. 31, no. 10C, pp. 921–926, 2006.

[41] S. Ingram, D. Harmer, and M. Quinlan, "Ultrawideband indoor positioning systems and their use in emergencies," in *Position Location and Navigation Symposium, 2004. PLANS 2004.* IEEE, 2004, pp. 706–715.

[42] R. Xiong, S. van Waasen, C. Rheinlnder, and N. Wehn, "Development of a novel indoor positioning system with mm-range precision based on rf sensors network," *IEEE Sensors Letters*, vol. 1, no. 5, pp. 1–4, Oct 2017.

[43] R. Xiong, S. van Waasen, J. Schelten, M. Schloesser, C. Rheinländer, and N. Wehn, "Development of a quasi time stretch technology for indoor positioning system based on pulse modulated ultra high frequency radio," in *SENSORS, 2015 IEEE*. IEEE, 2015, pp. 1–4.

[44] J. Hightower and G. Borriello, "A survey and taxonomy of location systems for ubiquitous computing," *IEEE computer*, vol. 34, no. 8, pp. 57–66, 2001.

[45] H. Liu, H. Darabi, P. Banerjee, and J. Liu, "Survey of wireless indoor positioning techniques and systems," *IEEE Transactions on Systems, Man, and Cybernetics, Part C (Applications and Reviews)*, vol. 37, no. 6, pp. 1067–1080, 2007.

[46] A. Bensky, *Wireless positioning technologies and applications*. Artech House, 2016.

[47] F. Seco, A. Jimenez, C. Prieto, J. Roa, and K. Koutsou, "A survey of mathematical methods for indoor localization," *Intelligent Signal Processing*, pp. 9–14, 2009.

[48] R. Mautz, "The challenges of indoor environments and specification on some alternative positioning systems," in *Positioning, Navigation and Communication, 2009. WPNC 2009. 6th Workshop on*. IEEE, 2009, pp. 29–36.

[49] S. Koyama, K. Onozawa, K. Tanaka, and Y. Kato, "A 3d vision 2.1 mpixel image sensor for single-lens camera systems," in *2013 IEEE International Solid-State Circuits Conference Digest of Technical Papers*. IEEE, 2013, pp. 492–493.

[50] A. Payne, A. Daniel, A. Mehta, B. Thompson, C. S. Bamji, D. Snow, H. Oshima, L. Prather, M. Fenton, L. Kordus *et al.*, "7.6 a 512× 424 cmos 3d time-of-flight image sensor with multi-frequency photo-demodulation up to 130mhz and 2gs/s adc," in *2014 IEEE International Solid-State Circuits Conference Digest of Technical Papers (ISSCC)*. IEEE, 2014, pp. 134–135.

[51] R. Mautz and S. Tilch, "Survey of optical indoor positioning systems." in *IPIN*, 2011, pp. 1–7.

[52] F. Boochs, R. Schütze, C. Simon, F. Marzani, H. Wirth, and J. Meier, "Increasing the accuracy of untaught robot positions by means of a multi-camera system," in *Indoor Positioning and Indoor Navigation (IPIN), 2010 International Conference on*. IEEE, 2010, pp. 1–9.

[53] R. Want, A. Hopper, V. Falcao, and J. Gibbons, "The active badge location system," *ACM Transactions on Information Systems (TOIS)*, vol. 10, no. 1, pp. 91–102, 1992.

[54] K. Atsuumi and M. Sano, "Indoor ir azimuth sensor using a linear polarizer," in *Indoor Positioning and Indoor Navigation (IPIN), 2010 International Conference on*. IEEE, 2010, pp. 1–5.

[55] D. Hauschildt and N. Kirchhof, "Advances in thermal infrared localization: Challenges and solutions," in *Indoor Positioning and Indoor Navigation (IPIN), 2010 International Conference on*. IEEE, 2010, pp. 1–8.

[56] S. Widodo, T. Shiigi, N. Hayashi, H. Kikuchi, K. Yanagida, Y. Nakatsuchi, Y. Ogawa, and N. Kondo, "Moving object localization using sound-based positioning system with doppler shift compensation," *Robotics*, vol. 2, no. 2, pp. 36–53, 2013.

[57] S. I. Lopes, J. M. Vieira, J. Reis, D. Albuquerque, and N. B. Carvalho, "Accurate smartphone indoor positioning using a wsn infrastructure and non-invasive audio for tdoa estimation," *Pervasive and Mobile Computing*, vol. 20, pp. 29–46, 2015.

[58] R. Novelline, *Squire's Fundamentals of Radiology*, 5th ed. Harvard University Press, 1997.

[59] G. Ulivieri, E. Marchetti, M. Ripepe, I. Chiambretti, G. De Rosa, and V. Segor, "Monitoring snow avalanches in northwestern italian alps using an infrasound array," *Cold Regions Science and Technology*, vol. 69, no. 2-3, pp. 177–183, 2011.

[60] O. Marcillo, S. Arrowsmith, R. Whitaker, D. Anderson, A. Nippress, D. N. Green, and D. Drob, "Using physics-based priors in a bayesian algorithm to enhance infrasound source location," *Geophysical Journal International*, vol. 196, no. 1, pp. 375–385, 2013.

[61] E. D. Scott, C. T. Hayward, R. F. Kubichek, J. C. Hamann, J. W. Pierre, B. Comey, and T. Mendenhall, "Single and multiple sensor identification of avalanche-generated infrasound," *Cold Regions Science and Technology*, vol. 47, no. 1-2, pp. 159–170, 2007.

[62] C. R. Rowell, D. Fee, C. A. Szuberla, K. Arnoult, R. S. Matoza, P. P. Firstov, K. Kim, and E. Makhmudov, "Three-dimensional volcano-acoustic source localization at karymsky volcano, kamchatka, russia," *Journal of Volcanology and Geothermal Research*, vol. 283, pp. 101–115, 2014.

[63] D. J. Griffiths and R. College, *Introduction to electrodynamics*. prentice Hall Upper Saddle River, NJ, 1999, vol. 3.

[64] G. Binasch, P. Grünberg, F. Saurenbach, and W. Zinn, "Enhanced magnetoresistance in layered magnetic structures with antiferromagnetic interlayer exchange," *Physical review B*, vol. 39, no. 7, p. 4828, 1989.

[65] E. Hirota, H. Sakakima, and K. Inomata, *Giant magneto-resistance devices*. Springer Science & Business Media, 2013, vol. 40.

[66] J. Haverinen and A. Kemppainen, "Global indoor self-localization based on the ambient magnetic field," *Robotics and Autonomous Systems*, vol. 57, no. 10, pp. 1028–1035, 2009.

[67] W. Storms, J. Shockley, and J. Raquet, "Magnetic field navigation in an indoor environment," in *Ubiquitous Positioning Indoor Navigation and Location Based Service (UPINLBS), 2010*. IEEE, 2010, pp. 1–10.

[68] J. Blankenbach and A. Norrdine, "Position estimation using artificial generated magnetic fields," in *Indoor Positioning and Indoor Navigation (IPIN), 2010 International Conference on*. IEEE, 2010, pp. 1–5.

[69] D. Arumugam, J. Griffin, D. Stancil, and D. Ricketts, "Higher order loop corrections for short range magnetoquasistatic position tracking," in *Antennas and Propagation (APSURSI), 2011 IEEE International Symposium on.* IEEE, 2011, pp. 1755–1757.

[70] M. H. Afzal, V. Renaudin, and G. Lachapelle, "Multi-magnetometer based perturbation mitigation for indoor orientation estimation," *Navigation*, vol. 58, no. 4, pp. 279–292, 2011.

[71] H. Hashemi, "The indoor radio propagation channel," *Proceedings of the IEEE*, vol. 81, no. 7, pp. 943–968, 1993.

[72] D. C. Cox, R. R. Murray, and A. Norris, "800-mhz attenuation measured in and around suburban houses," *AT&T Bell Laboratories technical journal*, vol. 63, no. 6, pp. 921–954, 1984.

[73] F. Owen and C. Pudney, "Radio propagation for digital cordless telephones at 1700 mhz and 900 mhz," *Electronics Letters*, vol. 25, no. 1, pp. 52–53, 1989.

[74] D. Howbaker and T. Rappaport, "Erratum: Indoor wideband radiowave propagation measurements at 1.3 ghz and 4.0 ghz," *Electronics Letters*, vol. 27, no. 2, pp. 191–191, 1991.

[75] A. A. Saleh and R. Valenzuela, "A statistical model for indoor multipath propagation," *IEEE Journal on selected areas in communications*, vol. 5, no. 2, pp. 128–137, 1987.

[76] D. Devasirvatham, M. Krain, D. Rappaport, and C. Banerjee, "Radio propagation measurements at 850 mhz, 1.7 ghz and 4 ghz inside two dissimilar office buildings," *Electronics Letters*, vol. 26, no. 7, pp. 445–447, 1990.

[77] T. S. Rappaport, S. Y. Seidel, and K. Takamizawa, "Statistical channel impulse response models for factory and open plan building radio communicate system design," *IEEE Transactions on Communications*, vol. 39, no. 5, pp. 794–807, 1991.

[78] V. Honkavirta, T. Perala, S. Ali-Loytty, and R. Piché, "A comparative survey of wlan location fingerprinting methods," in *Positioning, Navigation and Communication, 2009. WPNC 2009. 6th Workshop on.* IEEE, 2009, pp. 243–251.

[79] P. Bahl and V. N. Padmanabhan, "Radar: An in-building rf-based user location and tracking system," in *INFOCOM 2000. Nineteenth Annual Joint Conference of the IEEE Computer and Communications Societies. Proceedings. IEEE*, vol. 2. Ieee, 2000, pp. 775–784.

[80] M. Ibrahim and M. Youssef, "Cellsense: A probabilistic rssi-based gsm positioning system," in *Global Telecommunications Conference (GLOBECOM 2010), 2010 IEEE.* IEEE, 2010, pp. 1–5.

[81] T. Kitasuka, K. Hisazumi, T. Nakanishi, and A. Fukuda, "Positioning technique of wireless lan terminals using rssi between terminals." in *PSC*, 2005, pp. 47–53.

[82] U. Grossmann, M. Schauch, and S. Hakobyan, "Rssi based wlan indoor positioning with personal digital assistants," in *Intelligent Data Acquisition and Advanced Computing Systems: Technology and Applications, 2007. IDAACS 2007. 4th IEEE Workshop on.* IEEE, 2007, pp. 653–656.

[83] S. Mazuelas, A. Bahillo, R. M. Lorenzo, P. Fernandez, F. A. Lago, E. Garcia, J. Blas, and E. J. Abril, "Robust indoor positioning provided by real-time rssi values in unmodified wlan networks," *IEEE Journal of selected topics in signal processing*, vol. 3, no. 5, pp. 821–831, 2009.

[84] U. Bandara, M. Hasegawa, M. Inoue, H. Morikawa, and T. Aoyama, "Design and implementation of a bluetooth signal strength based location sensing system," in *Radio and Wireless Conference, 2004 IEEE.* IEEE, 2004, pp. 319–322.

[85] S. Zhou and J. K. Pollard, "Position measurement using bluetooth," *IEEE Transactions on Consumer Electronics*, vol. 52, no. 2, pp. 555–558, 2006.

[86] L. Pei, R. Chen, J. Liu, H. Kuusniemi, T. Tenhunen, and Y. Chen, "Using inquiry-based bluetooth rssi probability distributions for indoor positioning," *Journal of Global Positioning Systems*, vol. 9, no. 2, pp. 122–130, 2010.

[87] H.-S. Kim, D.-R. Kim, S.-H. Yang, Y.-H. Son, and S.-K. Han, "An indoor visible light communication positioning system using a rf carrier allocation technique," *Journal of Lightwave Technology*, vol. 31, no. 1, pp. 134–144, 2013.

[88] X. Lv, K. Liu, and P. Hu, "Geometry influence on gdop in toa and aoa positioning systems," in *Networks Security Wireless Communications and Trusted Computing (NSWCTC), 2010 Second International Conference on*, vol. 2. IEEE, 2010, pp. 58–61.

[89] H.-J. Kim and J. Lee, "Stereo aoa system for indoor slam," in *Control, Automation and Systems (ICCAS), 2013 13th International Conference on.* IEEE, 2013, pp. 1164–1169.

[90] N. B. Priyantha, A. K. Miu, H. Balakrishnan, and S. Teller, "The cricket compass for context-aware mobile applications," in *Proceedings of the 7th annual international conference on Mobile computing and networking.* ACM, 2001, pp. 1–14.

[91] J. James and J. Caffery, "Wireless location in cdma cellular radio systems," 2000.

[92] P. Kemppi, T. Rautiainen, V. Ranki, F. Belloni, and J. Pajunen, "Hybrid positioning system combining angle-based localization, pedestrian dead reckoning and map filtering," in *Indoor Positioning and Indoor Navigation (IPIN), 2010 International Conference on.* IEEE, 2010, pp. 1–7.

[93] P. Kułakowski, J. Vales-Alonso, E. Egea-López, W. Ludwin, and J. García-Haro, "Angle-of-arrival localization based on antenna arrays for wireless sensor networks," *Computers & Electrical Engineering*, vol. 36, no. 6, pp. 1181–1186, 2010.

[94] R.-M. Cramer, R. A. Scholtz, and M. Z. Win, "Evaluation of an ultra-wide-band propagation channel," *IEEE Transactions on Antennas and Propagation*, vol. 50, no. 5, pp. 561–570, 2002.

[95] N. B. Priyantha, "The cricket indoor location system," Ph.D. dissertation, Massachusetts Institute of Technology, 2005.

[96] B. Büttgen, T. Oggier, M. Lehmann, R. Kaufmann, and F. Lustenberger, "Ccd/cmos lock-in pixel for range imaging: Challenges, limitations and state-of-the-art," *1st range imaging research day*, pp. 21–32, 2005.

[97] F. Remondino and D. Stoppa, *TOF range-imaging cameras.* Springer, 2013, vol. 68121.

[98] K. Yasutomi, T. Usui, S.-M. Han, T. Takasawa, K. Kagawa, and S. Kawahito, "7.5 a 0.3 mm-resolution time-of-flight cmos range imager with column-gating clock-skew calibration," in *2014 IEEE International Solid-State Circuits Conference Digest of Technical Papers (ISSCC).* IEEE, 2014, pp. 132–133.

[99] L. Gazzah, L. Najjar, and H. Besbes, "Selective hybrid rss/aoa weighting algorithm for nlos intra cell localization," in *2014 IEEE Wireless Communications and Networking Conference (WCNC).* IEEE, 2014, pp. 2546–2551.

[100] H. Kloeden, D. Schwarz, E. M. Biebl, and R. H. Rasshofer, "Vehicle localization using cooperative rf-based landmarks," in *Intelligent Vehicles Symposium (IV), 2011 IEEE.* IEEE, 2011, pp. 387–392.

[101] S. Wang, B. R. Jackson, and R. Inkol, "Hybrid rss/aoa emitter location estimation based on least squares and maximum likelihood criteria," in *2012 26th Biennial Symposium on Communications (QBSC)*, 2012.

[102] S. Venkatraman and J. Caffery, "Hybrid toa/aoa techniques for mobile location in non-line-of-sight environments," in *Wireless Communications and Networking Conference, 2004. WCNC. 2004 IEEE*, vol. 1. IEEE, 2004, pp. 274–278.

[103] H. C. So and E. M. K. Shiu, "Performance of toa-aoa hybrid mobile location," *IEICE TRANSACTIONS on Fundamentals of Electronics, Communications and Computer Sciences*, vol. 86, no. 8, pp. 2136–2138, 2003.

[104] L. Taponecco, A. D'Amico, and U. Mengali, "Joint toa and aoa estimation for uwb localization applications," *IEEE Transactions on Wireless Communications*, vol. 10, no. 7, pp. 2207–2217, 2011.

[105] N. Thomas, D. Cruickshank, and D. Laurenson, "Performance of a tdoa-aoa hybrid mobile location system," in *3G Mobile Communication Technologies, 2001. Second International Conference on (Conf. Publ. No. 477).* IET, 2001, pp. 216–220.

[106] C.-D. Wann, Y.-J. Yeh, and C.-S. Hsueh, "Hybrid tdoa/aoa indoor positioning and tracking using extended kalman filters," in *2006 IEEE 63rd Vehicular Technology Conference*, vol. 3. IEEE, 2006, pp. 1058–1062.

[107] C. Yang, Y. Huang, and X. Zhu, "Hybrid tdoa/aoa method for indoor positioning systems," in *Location Technologies, 2007. The Institution of Engineering and Technology Seminar on.* IET, 2007, pp. 1–5.

[108] J. Rice, *Mathematical statistics and data analysis.* Nelson Education, 2006.

[109] F. Gustafsson and F. Gunnarsson, "Mobile positioning using wireless networks: possibilities and fundamental limitations based on available wireless network measurements," *IEEE Signal processing magazine*, vol. 22, no. 4, pp. 41–53, 2005.

[110] S. M. Kay, "Fundamentals of statistical signal processing, volume i: estimation theory," 1993.

[111] J. S. Abel and J. O. Smith, "Source range and depth estimation from multipath range difference measurements," *IEEE Transactions on Acoustics, Speech, and Signal Processing*, vol. 37, no. 8, pp. 1157–1165, 1989.

[112] W. Hahn and S. Tretter, "Optimum processing for delay-vector estimation in passive signal arrays," *IEEE Transactions on Information Theory*, vol. 19, no. 5, pp. 608–614, 1973.

[113] B. T. Fang, "Simple solutions for hyperbolic and related position fixes," *IEEE transactions on aerospace and electronic systems*, vol. 26, no. 5, pp. 748–753, 1990.

[114] J. Chaffee and J. Abel, "On the exact solutions of pseudorange equations," *IEEE Transactions on Aerospace and Electronic Systems*, vol. 30, no. 4, pp. 1021–1030, 1994.

[115] S. Bancroft, "An algebraic solution of the gps equations," *IEEE Transactions on Aerospace and Electronic Systems*, no. 1, pp. 56–59, 1985.

[116] Y. T. Chan and K. Ho, "A simple and efficient estimator for hyperbolic location," *IEEE Transactions on signal processing*, vol. 42, no. 8, pp. 1905–1915, 1994.

[117] C. G. Broyden, "A class of methods for solving nonlinear simultaneous equations," *Mathematics of computation*, vol. 19, no. 92, pp. 577–593, 1965.

[118] P. E. Frandsen, K. Jonasson, H. B. Nielsen, and O. Tingleff, "Unconstrained optimization," 1999.

[119] P. Teunissen, "Nonlinear least squares," 1990.

[120] G. Zoutendijk, *Methods of feasible directions: a study in linear and non-linear programming.* Elsevier, 1960.

[121] E. Aitenbichler and M. Muhlhauser, "An ir local positioning system for smart items and devices," in *Distributed Computing Systems Workshops, 2003. Proceedings. 23rd International Conference on.* IEEE, 2003, pp. 334–339.

[122] M. Youssef and A. Agrawala, "The horus wlan location determination system," in *Proceedings of the 3rd international conference on Mobile systems, applications, and services.* ACM, 2005, pp. 205–218.

[123] S. Kumar, S. Gil, D. Katabi, and D. Rus, "Accurate indoor localization with zero start-up cost," in *Proceedings of the 20th annual international conference on Mobile computing and networking.* ACM, 2014, pp. 483–494.

[124] R. J. Fontana and S. J. Gunderson, "Ultra-wideband precision asset location system," in *Ultra Wideband Systems and Technologies, 2002. Digest of Papers. 2002 IEEE Conference on.* IEEE, 2002, pp. 147–150.

[125] P. Steggles and S. Gschwind, "The ubisense smart space platform," 2005.

[126] A. R. Jiménez and F. Seco, "Comparing decawave and bespoon uwb location systems: Indoor/outdoor performance analysis," in *2016 International Conference on Indoor Positioning and Indoor Navigation (IPIN).* IEEE, 2016, pp. 1–8.

[127] P. Dabove, V. Di Pietra, M. Piras, A. A. Jabbar, and S. A. Kazim, "Indoor positioning using ultra-wide band (uwb) technologies: Positioning accuracies and sensors' performances," in *2018 IEEE/ION Position, Location and Navigation Symposium (PLANS).* IEEE, 2018, pp. 175–184.

[128] J. Kulmer, S. Hinteregger, B. Growindhager, M. Rath, M. S. Bakr, E. Leitinger, and K. Witrisal, "Using decawave uwb transceivers for high-accuracy multipath-assisted indoor positioning," in *2017 IEEE International Conference on Communications Workshops (ICC Workshops)*, May 2017, pp. 1239–1245.

[129] J. Barnes, C. Rizos, J. Wang, D. Small, G. Voigt, and N. Gambale, "Locata: the positioning technology of the future," in *Proceedings of the 6thIinternational Symposium on Satellite Navigation Technology Including Mobile Positioning & Location Services, Melbourne, Australia July*, 2003.

[130] C. Kee, H. Jun, and D. Yun, "Indoor navigation system using asynchronous pseudolites," *The Journal of Navigation*, vol. 56, no. 3, p. 443, 2003.

[131] H. Niwa, K. Kodaka, Y. Sakamoto, M. Otake, S. Kawaguchi, K. Fujii, Y. Kanemori, and S. Sugano, "Gps-based indoor positioning system with multi-channel pseudolite," in *Robotics and Automation, 2008. ICRA 2008. IEEE International Conference on*. IEEE, 2008, pp. 905–910.

[132] M. O. Kanli *et al.*, "Limitations of pseudolite systems using off-the-shelf gps receivers," *Positioning*, vol. 1, no. 08, 2004.

[133] Website, available online at http://www.ubisense.net/; visited on July 1st 2016.

[134] "Lpr-2d," Website, available online at http://www.symeo.com/; visiteded on July 1st 2016.

[135] "Dart uwb," Website, available online at http://www.zebra.com/; visiteded on July 1st 2016.

[136] Y. Zhao, "Standardization of mobile phone positioning for 3g systems," *IEEE Communications Magazine*, vol. 40, no. 7, pp. 108–116, 2002.

[137] S. Gezici, Z. Tian, G. B. Giannakis, H. Kobayashi, A. F. Molisch, H. V. Poor, and Z. Sahinoglu, "Localization via ultra-wideband radios: a look at positioning aspects for future sensor networks," *IEEE signal processing magazine*, vol. 22, no. 4, pp. 70–84, 2005.

[138] J. Yan, "Algorithms for indoor positioning systems using ultra-wideband signals," Ph.D. dissertation, TU Delft, Delft University of Technology, 2010.

[139] G. Shen, R. Zetik, and R. S. Thoma, "Performance comparison of toa and tdoa based location estimation algorithms in los environment," in *Positioning, Navigation and Communication, 2008. WPNC 2008. 5th Workshop on*. IEEE, 2008, pp. 71–78.

[140] R. Kaune, "Accuracy studies for tdoa and toa localization," in *2012 15th International Conference on Information Fusion*, July 2012, pp. 408–415.

[141] O. H. Woon and S. Krishnan, "Investigation of methods to extract tdoa from uwb-ir waveforms," in *Communication Systems (ICCS), 2010 IEEE International Conference on*. IEEE, 2010, pp. 228–232.

[142] M. Deffenbaugh, J. G. Bellingham, and H. Schmidt, "The relationship between spherical and hyperbolic positioning," in *OCEANS'96. MTS/IEEE. Prospects for the 21st Century. Conference Proceedings*, vol. 2. IEEE, 1996, pp. 590–595.

[143] Y. Han and B. Jalali, "Photonic time-stretched analog-to-digital converter: Fundamental concepts and practical considerations," *Journal of Lightwave Technology*, vol. 21, no. 12, p. 3085, 2003.

[144] W. A. Kester, *Data conversion handbook*. Newnes, 2005.

[145] E. K. Miller, *Time-domain measurements in electromagnetics*. Springer Science & Business Media, 1986.

[146] A. Ouslimani, G. Vernet, H. Hardallah, and R. Adde, "Large amplitude picosecond step generation with fets," *Electronics Letters*, vol. 26, no. 19, pp. 1563–1564, 1990.

[147] M. Gerding, T. Musch, and B. Schiek, "Generation of short electrical pulses based on bipolar transistorsny," *Advances in Radio Science*, vol. 2, no. A. 1, pp. 7–12, 2005.

[148] J. Han and C. Nguyen, "A new ultra-wideband, ultra-short monocycle pulse generator with reduced ringing," *IEEE Microwave and wireless components letters*, vol. 12, no. 6, pp. 206–208, 2002.

[149] P. Protiva, J. Mrkvica, and J. Machac, "Universal generator of ultra-wideband pulses," *Radioengineering*, vol. 17, no. 4, pp. 74–78, 2008.

[150] J. Han and C. Nguyen, "Coupled-slotline-hybrid sampling mixer integrated with step-recovery-diode pulse generator for uwb applications," *IEEE transactions on microwave theory and techniques*, vol. 53, no. 6, pp. 1875–1882, 2005.

[151] D. M. Pozar, "Microwave engineering 3e," *Tramsmission Lines and Waveguides*, pp. 143–149, 2005.

[152] K. Krishnamoorthy, *Handbook of Statistical Distributions with Applications*. Chapman & Hall/CRC, 2006, ISBN 1-58488-635-8.

[153] P. Stoica, H. Li, and J. Li, "Amplitude estimation with application to system identification," in *Acoustics, Speech, and Signal Processing, 1999. Proceedings., 1999 IEEE International Conference on*, vol. 4. IEEE, 1999, pp. 1777–1780.

[154] A. Flammini, D. Marioli, E. Sisinni, and A. Taroni, "Least mean square method for lvdt signal processing," *IEEE Transactions on Instrumentation and Measurement*, vol. 56, no. 6, pp. 2294–2300, 2007.

[155] K. S. Narendra and A. M. Annaswamy, *Stable adaptive systems*. Prentice-Hall Englewood Cliffs, New Jersey, 1989.

[156] M. Hou, "Amplitude and frequency estimator of a sinusoid," *IEEE Transactions on Automatic Control*, vol. 50, no. 6, pp. 855–858, 2005.

[157] G. Welch and G. Bishop, "An introduction to the kalman filter," 1995.

[158] R. C. Johnson and H. Jasik, "Antenna engineering handbook," *New York, McGraw-Hill Book Company, 1984, 1356 p. No individual items are abstracted in this volume.*, vol. 1, 1984.

[159] M. A. Spirito, "Accuracy of hyperbolic mobile station location in cellular networks," *Electronics Letters*, vol. 37, no. 11, pp. 708–710, 2001.

[160] D.-W. Lim, H.-W. Kang, S.-J. Lee, and D.-H. Hwang, "Position dop analysis for sensor placement in the tdoa-based localization system," *Journal of Electrical Engineering and Technology*, vol. 7, no. 6, pp. 1009–1013, 2012.

[161] I. Kim, C. Park, and J. Lee, "Relationships between gdop, condition number and the volume of tetrahedron in gps positioning," in *Proc. of the 3rd GPS Workshop*, 1996, pp. 482–487.

[162] R. B. Langley *et al.*, "Dilution of precision," *GPS world*, vol. 10, no. 5, pp. 52–59, 1999.

[163] "Kinetiq," Website, available online at https://www.humatics.com/products/; visiteded on March 26st 2019.

[164] L. R. Rabiner and B. Gold, *Theory and Application of Digital Signal Processing*. Englewood Cliffs, New Jersey: Prentice-Hall, Inc., 1975, ISBN 0-13-914101-4.

[165] A. H. Nuttal, "Some windows with very good sidelobe behavior," *IEEE Transactions on Acoustics, Speech, and Signal Processing*, February 1981.

## List of Abbreviations

| | |
|---|---|
| *ADC* | Analog to Digital Converter |
| *ADS* | Advance Design System |
| *AGC* | Automatic Gain Controlling |
| *AGWN* | Additive Gaussian White Noise |
| *AMR* | Anisotropic Magnetoresistance |
| *AoA* | Angle of Arrival |
| *AP* | Access Point |
| *APC* | Antenna Phase Center |
| *API* | Application Programming Interface |
| *ARP* | Antenna Reference Point |
| *ASCII* | American Standard Code for Information Interchange |
| *CCD* | Charge-Coupled Device |
| *CMOS* | Complementary Metal-Oxide-Semiconductor |
| *CRLB* | Cramer-Rao Lower Bound |
| *CSMA* | Carrier Sense Multiple Access |
| *CW* | Continuous Wave |
| *DC* | Direct Current |
| *DP* | Direct Path |
| *DSP* | Digital Signal Processing |
| *EKF* | Extended Kalmann Filter |
| *EPS* | Equal Phase Sphere |
| *ERP* | Effective Radiated Power |
| *ETSI* | European Telecommunications Standards Institute |
| *FCC* | Federal Communications Commission |
| *FDMA* | Frequency Division Multiple Access |
| *FFT* | Fast Fourier Transform |
| *FIM* | Fisher Information Matrix |
| *FIR* | Finite Impulse Response |
| *FM* | Frequency Modulation |
| *FMC* | FPGA Mezzanine Card |

| | |
|---|---|
| $FPGA$ | Field Programable Gate Array |
| $GDOP$ | Geometry Dilution of Precision |
| $GML$ | Gaussian Maximum Likelihood |
| $GMR$ | Giant Magnetoresistance |
| $GNSS$ | Global Navitation Satellite Systems |
| $GPS$ | Global Positioning System |
| $HDL$ | Hardware Discription Language |
| $HLS$ | High Level Synthesis |
| $IoT$ | Internet of Things |
| $IPS$ | Indoor Positioning System |
| $IR$ | Infra-Red |
| $IRIS$ | Infrared Indoor Scout |
| $ISM$ | Industrial Scientific Medical |
| $KF$ | Kalmann Filter |
| $LBS$ | Location Based Service |
| $LCD$ | Liquid Crystal Display |
| $LED$ | Light Emitting Diode |
| $LNA$ | Low Noise Amplifier |
| $LORAN$ | Long Range Navigation |
| $LoS$ | Line-of-Sight |
| $LS$ | Least Squares |
| $MD$ | Mobile Device |
| $MEMS$ | Micro Electro Mechanical Systems |
| $MF$ | Matched Filter |
| $ML$ | Maximum Likelihood |
| $MSPS$ | Million Samples Per Second |
| $NLLS$ | Non-Linear Least Squares |
| $NLoS$ | Non-Line-of-Sight |
| $NLS$ | Non-Linear Least Squares |
| $OOK$ | On Off Keying |
| $PC$ | Phase Center |

| | |
|---|---|
| $PCB$ | Printed Circuit Board |
| $PCV$ | Phase Center Variation |
| $PDOP$ | Position Dilution of Precision |
| $RD$ | Range Difference |
| $RF$ | Radio Frequency |
| $RFID$ | Radio Frequency Identification |
| $RMA$ | Restricted Moving Average |
| $RMSE$ | Root Mean Square Error |
| $RMSE$ | Root Mean Square Error |
| $RSS$ | Received Signal Strength |
| $RSSI$ | Received Signal Strength Indicator |
| $RTT$ | Round Trip Time |
| $SAW$ | Surface Acoustic Wave |
| $SFDR$ | Spurious Free Dynamic range |
| $SHF$ | Super High Frequency |
| $SNR$ | Signal-to-Noise Ratio |
| $SRD$ | Step Recovery Diode |
| $TDMA$ | Time Division Multiple Access |
| $TDoA$ | Time Difference of Arrival |
| $ToA$ | Time of Arrival |
| $ToF$ | Time of Flight |
| $TV$ | Television |
| $UHF$ | Ultra High Frequency |
| $UWB$ | Ultra-Wide-Band |
| $VGA$ | Variable Gain Amplifier |
| $WLAN$ | Wireless Local Area Network |
| $WNLS$ | Weighted Non-Linear Least Squares |

# Lebenslauf

## Persöliche Daten

| | |
|---|---|
| Name, Vorname: | Xiong, Renhai |
| Geburtsort: | Fujian, VR China |
| Nationalität: | chinesisch |
| Familienstand: | verheiratet |

## Berufliche Erfahrung

| | |
|---|---|
| 05.2017 - heute | Mitgrüder und CTO. Hangzhou Dreieck Energy Technology Co., Ltd. |
| 04.2013 - 04.2017 | Wissenschaftlicher Mitarbeiter am Zentralinstitut für Engineering, Elektronik und Analytik (ZEA) Systeme der Elektronik (ZEA-2), Jülich Forschungszentrum |
| 08.2012 - 03.2013 | Master Arbeit am Zentralinstitut für Engineering, Elektronik und Analytik (ZEA) Systeme der Elektronik (ZEA-2), Jülich Forschungszentrum |
| 10.2011 - 03.2012 | Praktikum im Fraunhofer-Institut für Mikroelektronische Schaltungen und Systeme (IMS), Duisburg |

## Studium und Ausbildung

| | |
|---|---|
| 04.2013 - heute | Elektrotechnik und Informationstechnik (Doktorand), Universität Kaiserslautern |
| 04.2010 - 03.2013 | Elektrotechnik und Informationstechnik (Master), Universität Kaiserslautern |
| 10.2008 - 03.2010 | Kommunikationstechnik (Gast Program), Universität Bremen |
| 09.2005 - 07.2008 | IC Design, Shandong Universität, ChinaInternationale Wirtschaft, Shandong Universität, China |
| 09.2003 - 07.2005 | Yongan Nr.9 Oberschule der StadtYongan |
| 09.2000 - 07.2003 | Yongan Nr.1 Oberschule der StadtYongan |
| 09.1997 - 07.2000 | Yongan Mingzu Mittelschule der Stadt Yongan |
| 09.1991 - 07.1997 | Yongan Mingzu-Grundschule der Stadt Yongan |